School of Engineering

Single Cell Dynamics in Bacterial Populations for the Production of Heterologous Proteins

Anca Manuela Mitchell

Thesis Submitted for the Degree of Doctor of Philosophy at Newcastle University, Newcastle upon Tyne

November, 2019

Abstract

Rising healthcare costs and increased population longevity have urged research and the development of methods for the production of biopharmaceuticals. A third of the total sale of biopharma are microbial recombinant products. Recently, a central feature of the microbial populations in fermenters is that of heterogeneity at single cell level.

Considering the cellular heterogeneity, population level analysis used for bioprocess optimisation and control is misleading. Individual biological entities, their properties and their interaction with one another and the environment determine the overall behaviour monitored at population level. As far as protein production, the cellular variability is important for industry, because the yield affects the bioprocess' profitability and viability.

To predict cellular behaviour, cells in balanced growth are required. The fermentation methods that give balanced growth are batch and continuous. The present thesis investigates heterologous protein production in *E. coli* at single cell level. Most measurements at single cell level to unravel heterogeneity use fluorescence, hence the expression system includes green fluorescent protein (GFP).

The main areas of this thesis are fermentations characteristics at single cell level in host and recombinant *E. coli* at different growth rates on glucose or glycerol substrate. The techniques used to quantify heterogeneity are flow and image cytometry. This work gives new insights into the cellular heterogeneity that exists in bioreactors and the extent of which it affects the bioprocess. Focusing on cellular physiology and metabolism of cells used for recombinant protein production, this work may further facilitate the use of bacteria as cell factories.

Keywords: *Escherichia coli*, Single Cell, Flow Cytometry, Microscopy

Acknowledgements

I am proud to have completed my research and written this thesis in the School of Engineering at Newcastle University.

This work would have not been possible without the support of the following people:

- Dr Dana Ofiteru for her excellent guidance and supervision, and for giving me the opportunity to conduct this work.
- Professor Anil Wipat for his supervision, guidance and encouragement.
- Andrew Fuller from the Flow Cytometry Core Facility at Newcastle University for help with setting up the flow cytometer.
- Dr Alex Laude from the BioImaging Facility for help with fluorescence microscopy.
- Dr Valentina Gogulancea for the advice and support with Matlab.
- Professor Alan Ward from Centre for Bacterial Cell Biology for his patience and enthusiasm when discussing all things about chemostats.
- My friend, Allan Euerby for proofreading and help with Autodesk graphics.
- My girls, Cassandra and Raluca for their unconditional encouragement and confidence in my abilities.

I would especially like to thank Dr Wendy Smith who, out of the goodness of her heart and academic collegiality, provided me with support, guidance, advice and friendship without which I would not have been able to complete this work. I am forever indebted to her.

I gratefully acknowledge the financial support from Engineering and Physical Sciences Research Council (EPSRC).

Table of Contents

List of Figures

List of Tables

Abbreviations

Absorbance	A
Adenosine triphosphate	ATP
Amino acid	Aa
Arbitrary units	A.U.
Base pair	Bp
Bis-(1,3-dibarbituric acid)-trimethine oxanol	$DIBAC_{4(3)}$
Carbon	C
Carbon catabolite repression	CCR
Carbonyl cyanide 3-chlorophenylhydrazone	CCCP
Cell dry weight (g/L)	CDW
Colony forming units	CFU
Deoxyribonucleic acid	DNA
Dilution (set specific growth rate)	D (μ_{set})
Dulbecco buffered saline	DBS
Ethidium bromide	EB
Fluorescein	FITC
Fluorescence-activated cell sorting	FACS
Fluorescence microscopy	FM
Fluorescence intensity	FI
Fluorescent protein	FP
Flow cytometry	FC
Forward scatter	FSC
Good Manufacturing Practices	cGMP
Green Fluorescent Protein	GFP

High cell density fermentation	HCD
High density polyethylene	HDPE
Hour	H
Inclusion bodies	IBs
Isopropyl β-D-1-thiogalactopyranoside	IPTG
Kilo bases	Kb
Kilo daltons	kD
Lipopolysaccharide	LPS
Maximum growth rate	μ_{max}
Mean fluorescence intensity	MFI
Membrane potential	MP
Messenger RNA	mRNA
Micro-gram	µg
Micro-molar	µM
Microtiter plates	MTP
Nicotinamide adenine dinucleotide hydrogen	NADH
Nanometre	Nm
Optical density	OD
Parts per million	Ppm
Plasmid DNA	pDNA
Propidium iodide	PI
Recombinant proteins	RP
Recombinant protein production	RPP
Ribonucleic acid	RNA
Ribosomal binding site	RBS
Side scatter	SSC

Specific growth rate	μ
Steady state	SS
Stirred tank reactor	STR
Thiazole orange	TO
Total cell count	TCC
Viable but not culturable	VBNC
Volatile fatty acids	VFA
Weight-to-volume	w/v
Weight-to-weight	w/w

CHAPTER 1

GENERAL INTRODUCTION

Chapter 1 Introduction

1.1 Overview

Recombinant proteins (RP) are a class of biological drugs that have revolutionised the treatment of various conditions such as diabetes, cancer, multiple sclerosis, arthritis and many more (Sarpatwari *et al*., 2015, Kelly and Mir, 2009). By definition, biological drugs (biopharmaceuticals) are pharmaceutical products produced through biotechnology methods, using recombinant DNA techniques in living host cells. The hosts can be mammalian, bacteria, yeast, insect or plant cells. While insects, plants and yeasts remain of limited industrial uptake for the large-scale production of RP, there is a clear dominance of mammalian and bacterial systems. Facilities using mammalian cell culture reduced from 81.1% in 2017 to 79.3% in 2018, which was also recorded in 2016. Conversely, there was an increase in facilities using bacteria for protein production from 37.5% in 2016 to 47.8% in 2018 (*Figure 1.1*).

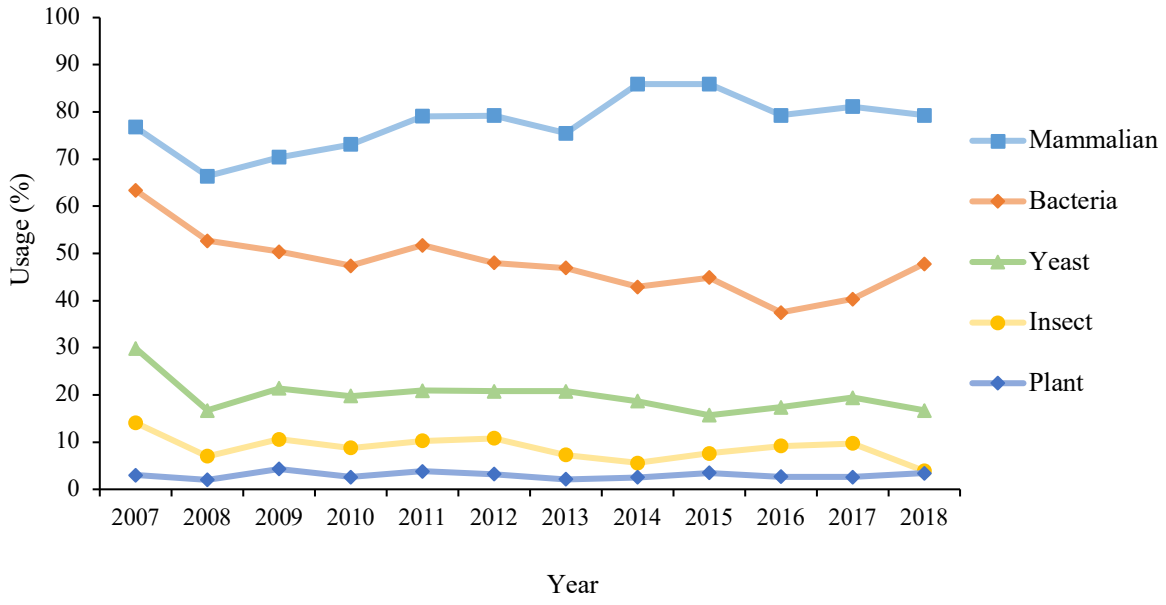

Figure 1.1. Biopharmaceuticals manufacturing system trends 2007-2018 (Langer, 2019).

Recombinant proteins, such as insulin have existed for decades, but newer biologics are becoming available for treating a range of conditions. The cost of newer biologics is enormous, and the demand is high, driven by both doctors and patients seeking to improve

prognosis in incurable diseases. Biologics are the most expensive drugs available on the market, forecast to reach 394 billion sale by 2024 (Langer, 2019). Seeking strategies to reduce the cost has become a key priority. The cost savings for biologics is limited, because they are complex molecules, harder to produce than a chemically synthesised drug. The challenge to cut costs may be large, but not impossible.

This work refers to the production of recombinant proteins, which represent a major class of biopharmaceuticals. Simply structured recombinant proteins that do not require post-translational modifications are produced preferentially in microbial cells (Jagschies, 2018). The most commonly used microbial host in industry is *Escherichia coli*. Manufacturing recombinant proteins is a complex process that starts with the cultivation of the cells, followed by downstream processes (Chirino and Mire-Sluis, 2004). Despite many advances in recombinant microbial cell lines, a central issue in recent years is the **heterogeneity in protein production** (*Figure 1.2*).

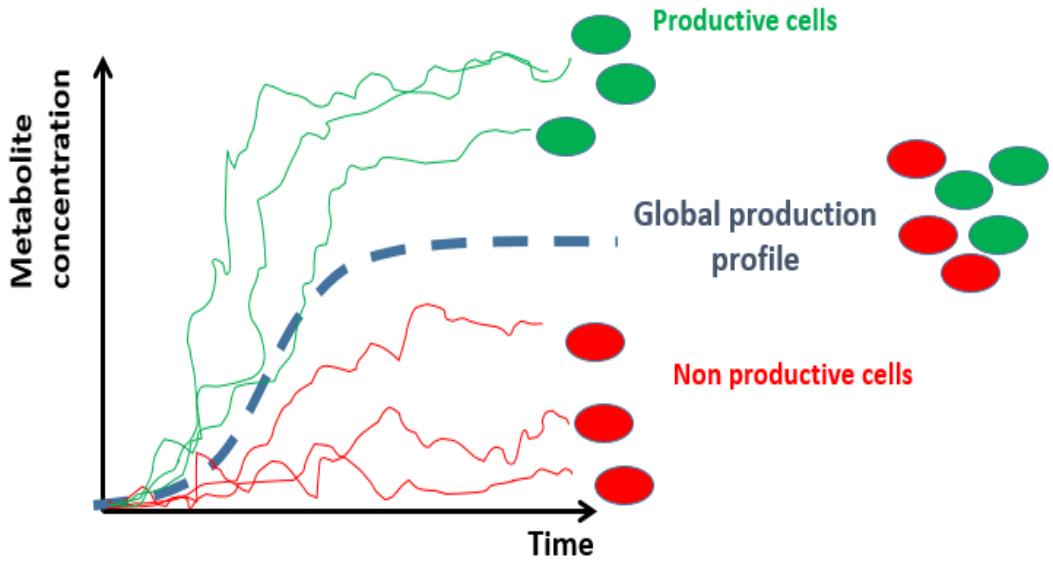

Figure 1.2. Schematic representation of heterogeneity in protein production. A subpopulation of cells with reduced protein synthesis lowers the average yield of bioprocess (Delvigne and Goffin, 2014).

Measurements of heterogeneity in bioreactors are essential for informed decisions regarding bioprocess optimisation and control. Process performance depends largely on the number of metabolically active cells, which becomes visible only through single cell measurements. At

this level, cell physiological state, proliferation and viability help with understanding the cellular variability and the ways by which microbial fermentations may be optimised and controlled.

It has been pointed out that heterogeneity in microbial production cell lines causes lower yields in bioprocess (Baert *et al*., 2015). More recently, reducing heterogeneity and promoting homogeneity seems a strategy for forcing cells into high productivity (Binder *et al*., 2017). However, there is no recorded consensus. There are now indications that the more heterogeneous a system is, the higher the productivity (Fragoso-Jimenez *et al*., 2019).

Whilst heterogeneity affects the bioprocess, current monitoring of process parameters addresses the whole population and does not routinely include measurements of heterogeneity. To address this issue, single cell measurements were made using Flow Cytometry (FC) with Fluorescence Microscopy (FM) to characterise an *E. coli* population grown in a fermenter used for recombinant protein production. A number of fluorescent approaches were used to measure heterogeneity. The expression system allows the production of a high level of intracellular protein, which is a soluble variant of GFP. The system is chemically inducible, mediated by isopropyl β-D-1-thiogalactopyranoside (IPTG), added to induce protein expression.

There have been several reports of applying fluorescent approaches in studies of microbial heterogeneity for bioprocess (Delvigne and Goffin, 2014, Binder *et al*., 2017, Baert *et al*., 2015, Fragoso-Jimenez *et al*., 2019, Delvigne *et al.*, 2009). These reports, however, originate from a nearly identical group, hence the suggestions may be biased, although currently are of opposite stance. Whilst these studies use fed-batch, which remains the gold standard in industry for RP production, it is not the right choice for investigating microbial heterogeneity.

Fed-batch fermentations are highly variable environments, with permanently changing system dynamics. The existence of gradients of different nature creates different cell phenotypes. The most important gradient remains the nutrient concentration. Near the feeding point, at the top of the fermenter, the cells grow at maximum growth rate. In the lower part of the fermenter, accentuated by poor mixing, cells have a lower growth rate, with substrate limitation. This deems fed-batch as a limited technique for investigating heterogeneity, with the observed phenomena dependent on the growth rate and sampling time.

What is needed is a methodology where a culture can grow at a constant growth rate, unaffected by time and gradients. This condition is known as "balanced growth", defined by Campbell as follows: "Growth is balanced over a time interval if, during the interval, every 'extensive' property of the growing system increases by the same factor" (Campbell, 1957). In balanced growth, the cell increases exponentially in size, while maintaining the concentrations of cellular components constant, acquiring a 'steady state' (Hagen, 2017). Two cultivation methods achieve cells in balanced growth: batch at mid-exponential point of growth and continuous. Neither are standards for bioprocess nor cited in research for illustrating heterogeneity, but both provide cells in "balanced growth" which is a basic requirement for investigating heterogeneity in microbial bioreactors. Here the fed-batch limitation as a methodology is addressed by investigating *E. coli* cell dynamics in conditions of excess and limited-nutrient at bioreactor scale using batch and continuous cultivations.

Continuous cultivations in particular add extra motivation to present work. There is a call for continuous bioprocessing for pharmaceuticals, driven by a rising global requirement for biological drugs. Continuous cultivation declined in popularity after the 1970s due to the widespread belief that they are difficult and impracticable. Recently, there has been an increased demand for flexibility with disposable bioprocessing adopted at many scales of manufacturing. The need for cheaper bioprocesses with improved productivity remained a major challenge. Continuous bioprocessing as production strategy has attracted attention in recent years as cost-optimised, but is lagging behind (Konstantinov and Cooney, 2015).

Furthermore, this work used a growth media with a single factor limitation. The media commonly used in research as "minimal media" does not allow balanced growth and is not suitable for physiological studies of bacteria. This is due to multiple nutrient limitations (Appendix A).

1.2 Research Objectives

The aim of this work was to understand how microbial heterogeneity influences the bioprocess for the production of recombinant proteins. As representative for zones of substrate gradients in industrial fed-batch fermentations, this work addresses the heterogeneity in conditions of excess and limited substrate. For excess substrate, the method is **batch** with focus on the mid-exponential point, whilst for limited substrate the method is **chemostat**

growth. Both methods produce **cells in balanced growth**, an important prerequisite for investigating microbial heterogeneity.

To apply continuous cultivations in a meaningful way, two kinetic issues are considered. The first is the nutrient that stoichiometrically limits growth. This is the sole carbon source, all the other components being present in excess. The second is choosing the growth rate for chemostat operation. These two considerations demand preliminary batch cultures, with the same growth medium and conditions. Fermentations in relation with critical process parameters were examined. Operating variables such as pH, dissolved oxygen and temperature, all impact on the physiology and metabolism of bacterial single cells. For this purpose, the population is monitored before addressing the single cell heterogeneity.

Following on, the main experimental part addresses the microbial heterogeneity in conditions of excess nutrient and limited nutrient growth. To study heterogeneity, experiments consist of fermentations in a stirred tank reactor (STR). At single cell level, the process is characterised in terms of membrane integrity, membrane potential and cellular morphology, and the heterologous protein itself in recombinant strain. The production of RP introduces a level of stress to the host cell, as it diverts from the cell's native sources to produce a non-native product: the recombinant protein itself.

The main objectives of this study were:

(a) To study the cellular dynamics in fermentations with host *E. coli* on glucose as the sole carbon source.
(b) To characterise the cellular dynamics in fermentations with recombinant *E. coli* on glucose as sole carbon source.
(c) To investigate the cellular dynamics in fermentations with host *E. coli* on glycerol as the sole carbon source.
(d) To analyse the cellular dynamics in fermentations with recombinant *E. coli* on glycerol as the sole carbon source.

1.3 Outline of thesis

The findings of this study are organised as follows:

Chapter 2 reviews the literature relating to microbial heterogeneity in bioprocess, which highlights the need for single cell analysis and its underpinnings: fluorescence. It outlines the

single cell methods used in this work: Flow Cytometry and Fluorescence Microscopy. Fermentation methods for producing biopharmaceuticals are summarised, focusing on *E. coli* as the current object of study.

Chapter 3 details the experimental set up and methodologies used during this work and, with justification for fluorophores selection.

Chapter 4 describes the detailed experimental work and results on host *E. coli* W3110 grown on glucose minimal media.

Chapter 5 presents the results of experimental work performed on recombinant *E. coli* CLD1301 on glucose minimal media.

Chapter 6 discusses the results from the experimental work on host *E. coli* W3110 on glycerol minimal media.

Chapter 7 presents the results of experimental work on recombinant *E. coli* CLD1301 on glycerol minimal media.

Chapter 8 provides the general conclusions of this thesis and suggests further work.

Each chapter documenting experimental work (chapter IV-VII) contains abstract, introduction, description, discussion and conclusions.

CHAPTER 2

LITERATURE REVIEW

Chapter 2 Literature review

2.1 Heterogeneity – a possible bottleneck in protein production

This section covers the microbial heterogeneity used to produce recombinant proteins in fermenters. Many papers address microbial heterogeneity, but only a handful of contributions show its importance in the field of biotechnology. This may be due in part to the scope of biotechnology, focusing on product rather than the cell producing it.

Protein production in bacteria was investigated in the past using population averages. The expression levels of an inducible gene were blindly accepted as identical to the average and a function of the concentration of the inducer. Contrastingly, single-cell techniques identified the heterogeneous nature of gene expression in bacterial populations. There can be criticism on many fronts, on media, on technique, on limitation, on not investigating cell morphology, but overall it is an opportunity to re-open the discussion for single-cell analysis in the bioprocess.

Msadek's hypothesis is that bacterial heterogeneity is a survival strategy by which cells adapt to changing environments (Msadek, 1999). This is explained for both natural environments and industrial bioreactors. In natural environments, cells experience continuous nutrient fluctuations, adapting from "feast" to "famine" and "hunger". In large industrial bioreactors, the cells circulate through alternating zones of nutrient upshift and downshift. The zones are caused primarily by substrate gradients and are accentuated by poor mixing (Baert *et al*., 2016, Baert *et al*., 2015, Delvigne *et al.*, 2009).

Simulating large scale heterogeneity from an industrial fermenter into a small and well mixed bench reactor has been problematic. All of the current observations on heterogeneity in a bioprocess focussed on batch and fed-batch fermentations and some on agar plates. No approach has so far followed heterogeneity by returning to the old idea of cells in "balanced growth". Furthermore, the lack of consensus concerning the effect of cellular heterogeneity on the bioprocess makes a causal effect hard to establish.

Few other authors brought different reports; nevertheless, Delvigne presented the main contributions. Earlier works suggested that microbial heterogeneity leads to decreased product yields, which affects both the profitability of the bioprocess and the cost of drugs (Delvigne and Goffin, 2014). In a later paper, Delvigne further encouraged strategies for attaining

homogeneity for higher process performance (Binder *et al*., 2017). It might be expected that heterogeneity is detrimental to the bioprocess and thus seek strategies to reduce it.

New research from Delvigne's group has revealed that this is exactly the opposite of what happens, with an emphasis that the more heterogeneous a system is, the higher its performance (Fragoso-Jimenez *et al*., 2019). The author further proposes a re-examination of the widely accepted idea that heterogeneity is unwanted in a bioprocess (Fragoso-Jimenez *et al*., 2019). The persistent activities of Delvigne's group show that the bioprocess industry is breaking away from the traditional averaged values and is re-investigating single cell analysis. This is a necessary movement for understanding the process on a large scale, which would in turn allow process control and optimisation.

By definition, heterogeneity means multiple cell types with an individual specificity. In an isogenic cell line, if cells maintain their genetic makeup, they are a homogenous population from a genetic viewpoint. However, cells from a homogeneous genetic population are different from one another in many, if not all, "non-genetic" ways - this is termed **phenotypic heterogeneity**. It has been described as different cellular states, caused by the cell cycle or the effect of stress on a single cell. Phenotypic heterogeneity has also been related to fluctuations in cellular components, such as RNA and protein levels (Li and You, 2013). The cell history and local environments experienced by the cell, related to cell density and cell-to-cell contact further increase microbial heterogeneity (Snijder *et al.*, 2012).

As research continues to monitor phenotypic heterogeneity, it becomes more obvious that there is much more to it than was originally thought. While the factors promoting cellular heterogeneity are multiple, the understanding and utilisation of bacteria as cell factories necessitates the analysis of heterogeneity. There are many ways to decipher microbial heterogeneity, but this work focuses on two single cell techniques: **Flow Cytometry (FC)** and **Fluorescence Microscopy (FM)** - detailed in Section *2.3 Cytometry – single cell analysis.* At individual cell level, fluorescence and shape descriptors are analysed.

2.2 Fluorescence in biotechnology

For unravelling cell heterogeneity, almost all measurements use fluorescence. By applying fluorescent approaches, one can measure and monitor an increasing number of processes in single cells. Chalfie illustrated gene expression, protein localisation and dynamics, and cell division to name just a few (Chalfie *et al.*, 1994).

The signal measured is fluorescence intensity (Scholz *et al.*, 2000); the signal provides a measure of a certain parameter or property of the cell, for which there is often a linear relationship. This is not normally applicable to viability dyes, where the measured principle is membrane exclusion. The measured parameter is, with some uncertainty intrinsic or extrinsic. Intrinsic fluorescence originates from fluorescent proteins (FP) or cellular components (NADH, tryptophan). The nature of FP as intrinsic parameters is, however, arguable, since they are non-native to the cell. Extrinsic fluorescence refers often to dyes (probes, stains or chemical fluorophores).

2.2.1 Green Fluorescent Protein (GFP) – The Green of Biology

The use of green fluorescent protein (GFP) revolutionised research in biological systems. First isolated from the jellyfish *Aequorea victoria* in 1962, GFP was a companion protein to aequorin (Tsien, 1998, Shimomura, 2005). Morin and Hastings named aequorea GFP as native GFP or wild-type GFP (wt-GFP) (Morin and Hastings, 1971). Green fluorescent proteins exist in many coelenterates, but only GFP from jellyfish has been well characterised (Tsien, 1998). Under UV excitation, the protein fluoresced green, a revelation that facilitated conducting further research with the aim to expand excitation spectrum.

Fluorescence arises from the interaction of light with a molecule that is able to fluoresce, called a fluorophore. The molecule that fluoresces may be a chemical fluorophore (probe), a FP (GFP), or an intrinsic biochemical molecule (NADH, FAD, and tryptophan). The fluorophore absorbs light at one wavelength and re-emits at another. The absorption and emission spectra are usually mirror images of each other, which is a general rule for simple fluorophores, known as Kasha's rule**.** Wild type-GFP is not a good choice for living cells because UV light can damage living cells. Its excitation spectrum has been optimised with a single point mutation S65T (Ser-Thr).

The strength of wt-GFP lies in its small size, formidable stability, with no photo-bleaching (i.e. loss of the ability to emit light) and low toxicity (March *et al*., 2003, Prasher, 1995). The protein, encoded by a single gene is synthesised from moieties from its own polypeptide chain, requiring only oxygen for maturation. Its remarkable properties come from its compact barrel-shaped structure with 238 amino acids (26.9 kDa), comprising of 11 β-strands on the outside, threaded by an α-helix *(Figure 2.1).*

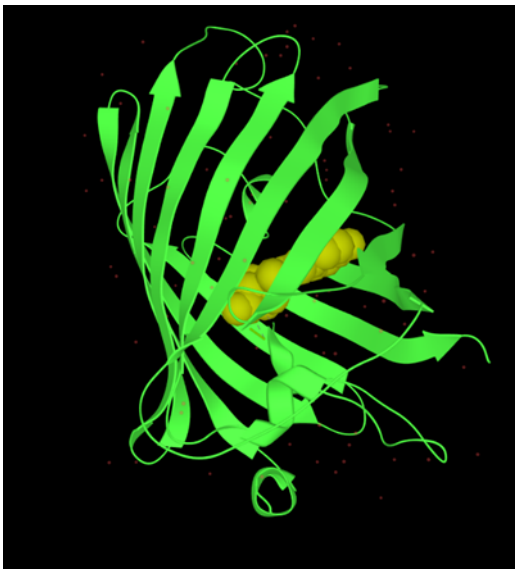

Figure 2.1. Tertiary structure of GFP, displaying can (barrel) shape with 11 β-strands and a threaded α-helix. The chromophore is in the middle of the β-barrel, in yellow (created using Litemol).

The fluorophore is in the α-helix and forms spontaneously from the oxidation of a tri-peptide motif Ser65-Tyr66-Gly67 (Cubitt *et al.*, 1995). As the fluorophore is contained in a constrained β-can environment, the fluorescence of wt-GFP is resistant to environmental changes. Moreover, GFP is non-toxic, hence it can be highly expressed in many hosts, with minor effects on cellular physiology (Chalfie *et al*., 1994).

In spite of its early 1960's discovery, cloning the gene for GFP occurred later. Two articles in 1994 simultaneously cited wt-GFP as a marker for gene expression. Studies by the two groups were conceptually the same; one study produced fluorescence in the worm *Caenorhabditis elegans*, and the other in *E. coli* (Tsuji, 2010). The cloning of GFP in heterologous hosts opened up a new era in biotechnology. In any biological system grown under aerobic conditions, the expression of the GFP gene leads to the appearance of a colour signal, which serves for labelling and detection.

The properties of wt-GFP, although massively useful, were far from ideal. The peak excitation of wt-GFP is 395 nm, while the emission maximum is 509 nm (Ward *et al.*, 1980). An extensive amount of work has been done since to create GFP variants, by changes in the

primary aa sequence. Nowadays, a whole family of related FP with a diversity of features exist (*Figure 2.2*). There is still a long way to go, as most FP are clustered within two regions of the visible spectrum (cyan-green and orange-red).

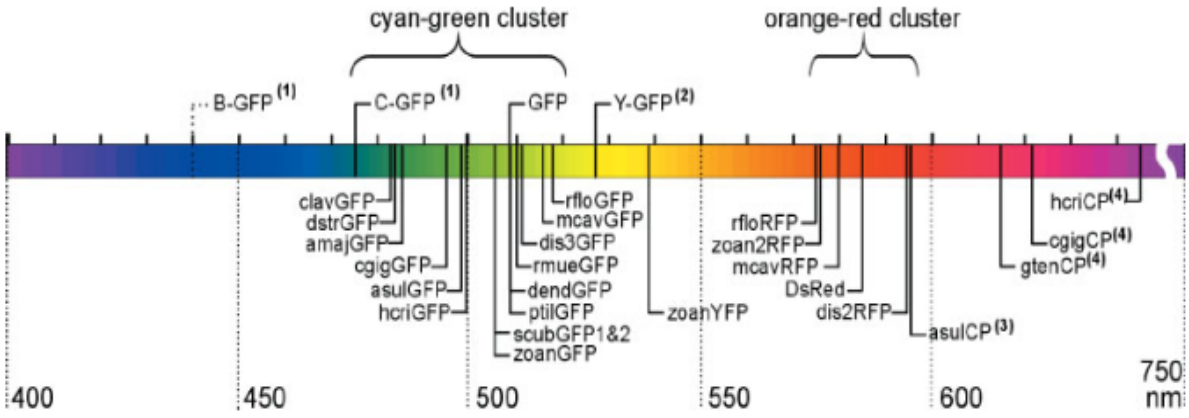

Figure 2.2. Summary of emission maxima in GFP-like proteins family for biotechnology applications. GFP from A. victoria and its mutants are shown above the rainbow bar (Matz *et al*., 2002).

As a host cell, *E. coli* grows at a range of temperatures, as low as 8^0C. Nevertheless, the design of the experiment depends largely on the desired product or the FP used as a marker for monitoring gene expression. It has been established that the oceanic habitat of the jellyfish *Aequorea victoria* dictates the folding temperature of wt-GFP. Below or at room temperature, wt-GFP folding and expression declines at higher temperature. It is beyond dispute that experiments at 37^0C are not suitable for expression studies, where the protein or its chimeric partner is wt-GFP. A temperature higher than the optimum leads to reduced maturation with decreased fluorescence and poor protein quantification.

The applications of GFP for expression studies in mammalian systems require optimal folding at 37°C. Mutations in the fluorophore region and in the surrounding β-barrel have created FP with altered photo-physical properties, better suited for mammalian applications with optimised folding at 37°C. From the array of possible FP, the characteristic of each one of them is crucial for experimental design.

The following should be stressed:

"The desired product is the determinant for experimental design."

2.2.2 Properties of FP for gene expression studies

The use of FP is common to biological systems and there are several biotechnological applications. The most important is for bioprocess monitoring (March *et al*., 2003). Several characteristics of FP have been optimised, that account for the popularity of FP to visualise physiological processes, to report on gene expression or protein localisation at single cell level. However, there is no single best FP for single cell studies of gene expression. To guide decisions about the right FP, brightness, photo-stability and spectrum are primarily considered.

Brightness is an important requirement, in that the signal is "bright" enough for detection above the auto-fluorescence threshold. For measuring protein expression using FP, the FP signal needs to be separated from other fluorescent signals that co-exist in a cell and that of the media components. For this reason, in single colour applications, FP is either highly expressed using a strong promoter or red-shifted on the spectrum.

Photo-stability is important in measuring FP signal, in that the fluorescent signal is imaged for the duration of the experiment. All FP will eventually photo-bleach so choosing the most photo-stable protein is crucial for experiments spread over many hours. Photo-stability of FP may be affected by various external factors (pH, temperature, excitation light intensity), but most GFP variants are resistant to environmental changes because they retain the β-barrel structure. GFP variants are the "molecular laboratory rats" that serve well for gene expression studies, as they are readily expressed in heterologous hosts.

Spectrum is an important consideration for choosing a FP. Each FP has its own excitation and emission (ex/em) peaks, which have been optimised for single cell expression studies. An excitation maximum of 488 nm is desirable as it is detected with a blue 488 nm laser, the gold standard in cytometry. Moreover, the development of GFP variants allowed enough spectral separation for dual-colour labelling. The most important consideration that remains is choosing a GFP protein that the system can detect.

2.3 Cytometry – single cell analysis

Sufficient evidence exists to indicate that microbial populations in fermenters are heterogeneous. The work of Delvigne should be noted here. In his latest work, Delvigne concludes that heterogeneity is beneficial for recombinant protein production (Fragoso-

Jimenez *et al*., 2019). His finding is based on reducing the growth rate of *E. coli* cells grown on glucose minimal medium by gene knock-outs in batch cultivations. He emphasises that reducing the growth rate increases the heterogeneity, which increases the production of GFP as heterologous protein.

While in most papers on heterogeneity, no details of the purpose and significance in a bioprocess are given, there is a common idea that runs through their work: heterogeneity is a complex phenomenon, much more extensive than once thought. To detect and quantify heterogeneity in a bioprocess, the analysis requires single cell techniques. Measurements of single cell properties are readily summarised as cytometry.

Cytometry analyses single cells as they are – individual entities in a heterogeneous culture. For cells found in a flow of fluid, the technique is "cytometry in flow" or flow cytometry (FC). For cells found on slides, single cell cytometry involves a microscope. Both are powerful techniques for examining heterogeneity, but limitations of each method require a combined approach to ensure accuracy. For example, FC has been applied for the assessment of bacterial morphology, but cell morphology is better suited for microscopic analysis. Hence, for quantifying heterogeneity, combining single cell methods is preferred.

Overall, FC and FM quantify the following:

(a) Patterns of gene expression (Miyashiro and Goulian, 2007, Galbusera *et al*., 2019);

(b) The number of cells in a population as an indication of growth (Frossard *et al*., 2016, Muthukrishnan *et al*., 2017);

(c) The analysis of a population into live/dead/injured subpopulations (Stiefel *et al*., 2015, Robertson *et al*., 2019);

(d) The detection of active/inactive cells (Jernaes and Steen, 1994, Goormaghtigh and Van Melderen, 2019);

(e) Cell morphology (Jones *et al.*, 2001, Katz, 2003).

2.3.1 Flow cytometry

Of the techniques available to analyse single cells, few are as widely employed as flow cytometry (FC). For characterising a population in its diversity, FC is rapid, sensitive and high throughput, assaying thousands of cells. In microbial applications, FC provides

information about different sub-populations of cells related by chemical and physical parameters (Vasdekis and Stephanopoulos, 2015). The variability that exists in a microbial population has important consequences for the productivity and stability of industrial fermentations.

Studies made with FC provide single-cell information that is unavailable with traditional bulk methods. In some cases, however, this information may be limiting. For example, FM may be better suited for analysing cell morphology as it allows visualising the cells, however, the amount of data from FM is meagre compared to that from FC. At the same time, FC is better suited for bioprocess optimisation and control, allowing near real-time measurements. No single method, however, can answer an argument, so combined single cell techniques are often used.

In characterising heterogeneous populations, FC is a powerful method. It has advanced understanding of recombinant *E. coli* in fed-batch fermentations (Hewitt and Nebe-Von-Caron, 2001, Lewis *et al.*, 2004). Fed-batch is the gold standard of industrial fermentations, as it allows a high cell density culture with an increased product yield. This cultivation mode, however, is inherently dynamic in nature, with no "steady state". It is important to reiterate that physiological studies require cells in "balanced growth" (see Section *2.6.3 Balanced growth),* found either in mid-exponential batch or in "steady state" continuous cultures.

Nearly all papers published at present addressing physiological questions completely miss two issues: the choice of method and the growth media. This is especially true for work in the field of biotechnology, which also emphasises the general lack of observations for the third issue: cell morphology. Egli systematically considered the first two issues (Egli, 2015). Their disregard was previously observed by Dawson who wrote "regrettably, the fact that growth is indeed basic to the discipline goes largely ignored in the general practice of microbiology and related endeavours. The omission often leads to superficial experimentation and much wasted effort, thus cluttering the literature with a lot of meaningless data" (Dawson, 1985).

(a) Principles of flow cytometry

In FC, cells in suspension "flow" continuously through a detector system one-by-one. To support a single orderly manner and avoid clumping, a prerequisite is sample dilution. A concentration of 10^4 cells/mL is too low, whereas 5 x 10^5 - 10^7 cells/mL is more appropriate (Shapiro, 2002). In all fairness, if cells flow as "single" entities through the interrogation

point is impossible to tell, particularly in the view that a later “gating” stage eliminates the doublets.

A buffer solution (the sheath fluid) introduces the cell suspension into the flow cytometer for analysis. To accurately measure parameters of single cells, cells are “forced” in the centre of a sheath stream of fluid. For precise positioning of cells in a liquid jet, most cytometers use hydrodynamic focusing (Kachel *et al.*, 1990). This way the cells pass from a zone of wide tubing towards a zone of narrow tubing (*Figure 2.3*). An acoustic focusing technology was developed by Drs Kaduchak and Ward (Ward *et al.*, 2009). Acoustic focusing allows samples to be run 10 times faster, while maintaining the operational sensitivity. This principle lies at the basis of the Attune Nxt Acoustic Focusing Cytometer (Life Technologies, Carlsbad, CA, USA).

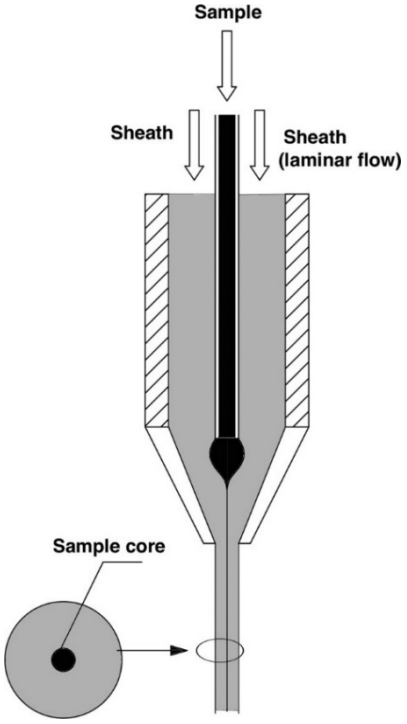

Figure 2.3. Hydrodynamic focusing of a sample in flow cytometry.

The cell suspension flows towards a laser aimed at the suspension’s path. The laser is either blue (488 nm), or in more sophisticated instruments, a combination of lasers, such as red (633 nm) and violet (405 nm). As the cells align one-by-one in front of the laser, an optics system measures parameters of single cells. These are light scattering and fluorescence, detailed below:

(b) Measurements of light scattering

Two detectors measure the light scattered by a cell at different angles. A detector sits opposite the 488 nm laser and collects light scattered at 0.5º to 5º from the incident light beam as FSC (forward scatter). Another detector, known as SSC (side scatter) collects light scattered at right angle to the laser beam (*Figure 2.4*).

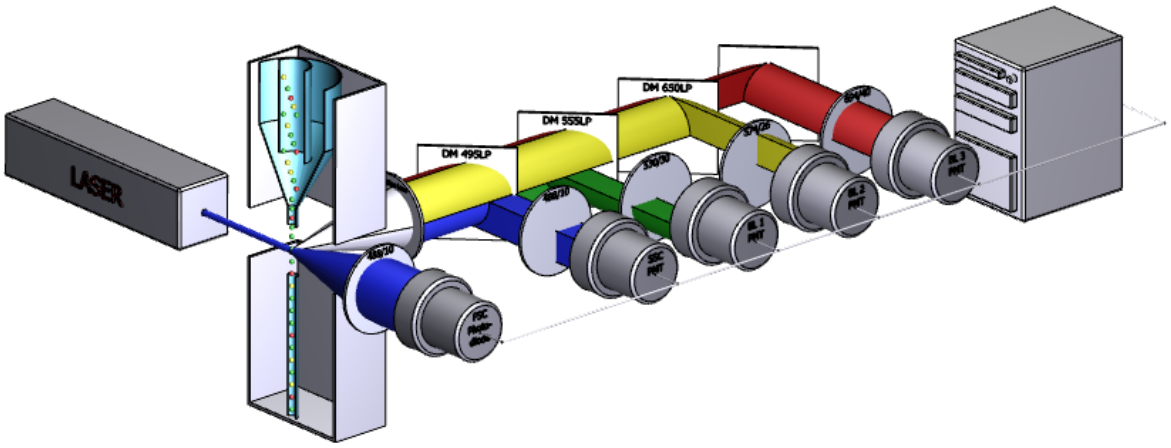

Figure 2.4. Flow Cytometer model (created in Autodesk Inventor). There are four basic components: fluidic system, laser, optics and electronics/external computer system. A laser excites the fluorophores on the cells as cells pass through the flow chamber. Light scatter signals are collected at two angles: FSC (488/10 nm) and SSC (488/10 nm). Light emitted by the cells is directed through three dichroic mirrors (DM) and filtered spectrally on different channels: BL1 (530/30 nm), BL2 (574/26 nm), BL3 (694/40 nm). The 3 DM are DM 495LP, DM 555LP, DM 650LP (see Appendix B).

The most basic way of visualising FC data is a scatter plot. Light scatter signals are collected with the FSC signal on the X-axis and the SSC signal on the Y-axis (*Figure 2.5*). A "gate" placed on a population of interest isolates the respective population. The "gate" separates the population for further analysis (*Figure 2.5*). The gating of a population is ultimately user dependent.

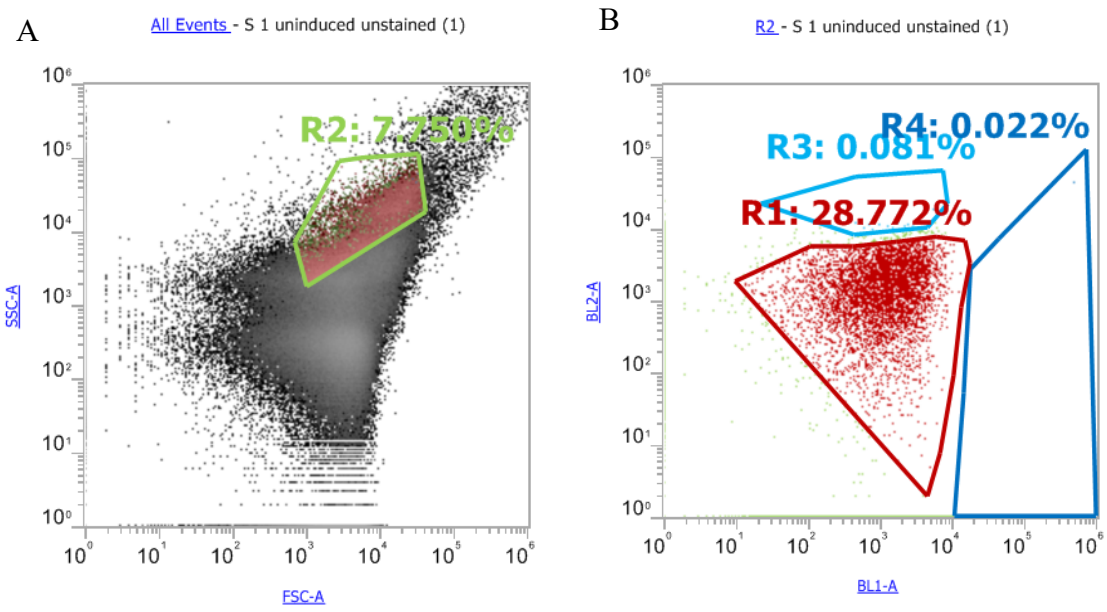

Figure 2.5. Scatter plot of recombinant *E. coli* CLD1301, uninduced and unstained used as control. A: A gate (R2) is applied to the bacterial population. Grey area is debris. B: Fluorescence data from the gated population R2 separates it into three further subpopulations: R1 (un-induced cells), R3 (dead cells) and R4 (induced cells).

It has been widely acknowledged in FC that FCS gives information about the cell size since Melamed has shown that the intensity of scattered light was proportional to its volume (Melamed *et al.*, 1979). A great amount of work investigated bacterial cell size through FCS. Koch established formulae for calculating *E. coli* biomass using FCS signals (Koch *et al.*, 1996). Contrastingly, Shapiro stated that although FSC may give details about the cell size, it will more likely not (Shapiro, 2002). His argument was based on FSC not being a monotonous function of cell size.

The problem with FSC is the minute bacterial size. This could limit the ability to distinguish small cells from a large amount of debris (*Figure 2.5*). A 10 µm cell might give a higher FSC signal than a 2 µm cell. However, when the particles are small rods, such as *E. coli* cells, it may be impossible to tell on which side of the cylinder the laser goes through. Shapiro further suggested that FSC signals may prove more accurate for detecting changes in size in spherical bacteria more than rods (Shapiro, 2005). Given the minute cell size, FSC in small diving bacteria could only show a small signal difference. In all events, FSC represents a signal for

whether or not the particle being analysed fluoresces, triggering the instrument to recognise an “event”.

A vast amount of evidence confirms that many factors influence FSC signals, such as a cell’s refractive index or its internal structure (Shapiro, 1977, Kerker *et al.*, 1979, Loken *et al.*, 1976, Hu *et al.*, 2018, Holme *et al.*, 1988, Sharpless *et al.*, 1977). The cell membrane is partially responsible for maintaining a difference in refractive index between the cell and the media. In the absence of a membrane, no difference in refraction would exist and the cells would not scatter any light. Therefore, cells with damaged membranes (permeable to viability dyes) generally have lower refractive indices, with smaller FSC signals. This may suggest that smaller FSC signals represent cellular death, but discriminating between live and dead subpopulations by FSC signals is not clear-cut since the signal is also dependent on other factors (Novo *et al.*, 2000, Shapiro, 2005). Lower FCS signals may also occur with increased cell volume in osmotic swelling while preserving membrane integrity.

Another widely acknowledged concept in FC is that SSC gives information about granularity. Granularity is a feature of mammalian cells. In bacteria, SSC may be an indicator for dry cell weight and total protein content. Ward pointed out that the information from SSC and FCS signals becomes similar when the analysed particles are small (Ward *et al.*, 2009). This originates from a background interference much higher in FSC than SSC, as cells scatter more light at small angles than at larger ones (Ward *et al.*, 2009). Nevertheless, light scatter measurements are useful, when taken in context.

(c) Measurements of fluorescence

To characterise a population of interest at single cell level, FC uses fluorescence by labelling cells with fluorophores. Fluorescence-based FC has been applied in a variety of studies. It has identified microorganisms that are viable but not culturable (Kramer and Thielmann, 2016). It has been applied for assessments of membrane permeability (O'Brien-Simpson *et al.*, 2016, Marba-Ardebor *et al.*, 2016), membrane potential (Rezaeinejad and Ivanov, 2011, Novo *et al.*, 1999) and heterologous protein expression (Richard *et al.*, 2007, Brognaux *et al.*, 2013). In any bioprocess, the unique advantage of FC remains the rapid near real-time measurements for monitoring and control.

When using multiple fluorophores to stain a cell of interest, ideally the fluorophores have different emission spectra, so that filters and mirrors in the optical bench separate the signal

from one another. Two possible limitations may occur when measuring fluorescence: “spill-over” and “auto-fluorescence”, detailed below.

“Spillover” occurs when simultaneously using two or more fluorophores, and the emission spectra overlap to varying degrees. The detector will see the combined signal of both. To distinguish the signal of a fluorophore from another, the “spill-over” is removed through a further mathematical correction called “compensation”. Compensation depends on the user’s knowledge, and this may represent a limitation.

The auto-fluorescence originating from media and cells may be a problem in itself when fluorescence is an indicator for protein expression. The inherent auto-fluorescence of bacterial cells is the result of fluorescent cell metabolites, such as flavins, NADH/NADPH and lipofuscins (Billinton and Knight, 2001). A high auto-fluorescent signal becomes misleading in cases of low-level protein expression and harder to separate from the real FP signal. For precise measurements of the FP signal, the auto-fluorescence needs to be deducted from the total signal. A strategy to bypass the cellular auto-fluorescence is using a fluorescent protein with a strong signal, detected easily above auto-fluorescence.

(d) Assessing membrane integrity

The most basic question in a bioprocess is whether the bacterial cell is dead or alive. The notion of viability, however, has wide meanings and largely depends on the technique employed. In a bioprocess, the accurate quantification of the viable biomass is essential to enable informed decisions on process control and optimisation. It is clear that a bioprocess is successful if it maintains a high cell viability that supports a high productivity. Otherwise, a high number of dead cells would be counterproductive.

The question of what is “viable” remains unanswered. Traditionally a cell was viable if it was “capable of diving to form one or more live daughter cells” following plating (Postgate, 1969, Davey, 2011). Assessing viability by plating has nil applications in a bioprocess, where there is a need for real-time techniques. Fluorescence-based assays investigating the status of the cell membrane were increasingly applied to assess viability in bioprocess. When labelling cells with fluorophores for evaluating microbial viability, however, a knowledge of the dye itself as well as the physiology of the target cell are required. The assessment of the membrane integrity in bacteria is complicated because of a complex interaction between the fluorophore and the cell, depending on the pores and pumps in the cell membrane and the existence of a cell wall.

A review of fluorophores is required for a critical analysis. Membrane permeability assays are based on the exclusion of a large dye, such as propidium iodide (PI) that does not normally cross the cell membrane. PI has been widely used in research since 1973, to label dead cells based on its fluorescence enhancement after binding to nucleic acids, which are plentiful in bacteria (Hudson *et al.*, 1969). Typically, membrane integrity assays combine the dead cell indicator (PI) with a membrane permeable DNA-counterstain, such as fluorescein (FITC). FITC stains all cells green, but in "dead" cells, the red fluorescence of PI replaces FITC. Based on different emission spectra, the fluorescent signals of PI and FITC are separated with ease, dividing the population into the desired "live" ($FITC^+$) and undesired "dead" (PI^+) subpopulations.

PI staining of bacteria may distinguish apoptotic from necrotic cells (Kramer *et al.*, 2016). Other studies point towards limitations of PI in that it stains viable cells in adherent biofilms (Rosenberg *et al*., 2019). Membrane integrity assays normally show a significant damage to the cell membrane. The loss of the membrane signifies the loss of all associated functions: transport, respiratory activity and permeability barrier. Whilst PI remains a popular dye for assessing membrane integrity, there is no all-encompassing test for assessing viability, so combining a range of viability indicators to characterise the physiological state of the cells in a population is essential. Considerations for each fluorophore used in this work are discussed in Chapter 3.

(e) Assessing membrane potential

No single method identifies all physiological traits (Barer and Harwood, 1999). Membrane potential (MP) assays generate a wider perspective on the cell physiological state (Rezaeinejad and Ivanov, 2011). By assessing the physiological state of individual cells, MP assays are of immense use for industrial process monitoring.

MP is the difference in electrical potential that exists across the membrane. It is a result of the selective permeability of biological membranes to various ions and the activity of various pumps. Key enzymes responsible for metabolism are located on the inner surface of the cytoplasmic membrane, and the difference in MP, typically *100-200* mV often correlates with cell metabolic or functional activity. The inside of the cell is negatively charged, relative to the outside.

MP reflects both an intact cytoplasmic membrane as a viability indicator, and the maintenance of cell metabolism as a physiological indicator (Shapiro, 2000). Primarily all metabolically active cells with intact cytoplasmic membranes maintain MP, hence studies of MP are used to assess viability (Diaz *et al.*, 2010). When MP tends towards zero, there is membrane damage, with ions travelling freely through it. This may not necessarily mean death, but a compromised cell with decreased cellular functions, including biosynthesis of proteins and DNA, efflux pumping and respiration activity (Nebe-von-Caron *et al*., 2000, Bridier *et al.*, 2015).

To analyse heterogeneity in bacterial populations by means of the MP, voltage-sensitive dyes are used. Staining of bacteria is, however far from simple because of the complex structure of the membrane and efficient efflux pumps (Midgley, 1986). *E. coli* are less permeable than Gram-positive cells, with the outer membrane as the least permeable, excluding most lipophilic and hydrophobic substances, such as cyanine dyes. EDTA is used to improve the permeability of the outer membrane, but some argue that EDTA-permeabilised bacteria are not the same with cells in a native state (Shapiro, 2005). However, cyanine dyes, such as $DIBAC_{4(3)}$ are anionic. While they do not stain active cells that maintain an MP, they stain depolarised cells.

The implications of this in a bioprocess are simple. For processes used for producing recombinant proteins, the success depends on the number of cells that maintain MP or are "metabolically active". Hence, the applications of MP assays analysed by FC are most useful for monitoring biotechnological processes.

2.3.2 Microscopy

The first method used for analysing single cells was light microscopy (Nebe-von-Caron *et al.*, 2000). From its beginnings, in the 1600s and for the next 100 years, the information provided was only an observation of the physical characteristics of the cell (Bridson and Gould, 2000). While bacterial cells display colours at population level when grown in colonies, a single cell on a microscopic slide is essentially transparent and difficult to see with regular bright-field optics. Closing the condenser diaphragm would make the cell appear darker, but this introduces fringe artefacts that obscure the cell boundaries and impact on the morphology assessment.

To bypass the cell transparency, advances in microscopy focussed on obtaining contrast. Several methods improve contrast, two of them described below: phase–contrast and fluorescence microscopy.

(a) Phase microscopy

Dutch physicist Fritz Zernicke found that introducing a phase shift by manipulating the light path increases contrast. Since its introduction in the early 20th century, phase contrast microscopy has long been a favourite for visualising bacteria. For this work, Zernicke was awarded the Nobel Prize in 1953. In phase contrast microscopy, individual bacterial cells appear dark against a characteristic grey background. The main advantage of phase microscopy is providing details about cells in their natural state, without the need for labelling or fixation. To aid analysis and avoid the constant swimming and tumbling, cells are immobilised in agarose mounts.

(b) Fluorescence microscopy

By far the most used contrasting technique for visualising single cells is fluorescence microscopy. The technique combines the magnifying properties of optical microscopy with the visualisation of fluorescence. A "dark field" technique, fundamentally different to phase-contrast, FM is a powerful tool for single cell analysis, with fluorescent cells brightly lit surrounded by a dark background.

While in phase microscopy, the light phase shift comes from a light source within the microscope, in fluorescence microscopy the light comes from the cells themselves. Certain molecules within the cell fluoresce in the presence of excitatory light. An intrinsic fluorescence or auto-fluorescence arises from various cell metabolites, but often the cells are labelled with fluorophores to make them visible. An example is PI, an extrinsic label (dye) that passes through compromised membranes, binds to both nucleic acids, fluoresces red and indicates cell "death". Other tagging methods are constructing fusions or chimeric proteins of an FP, such as GFP with structures within the cell.

FM offers a quantitative characterisation of heterogeneity in a population and visualises patterns of protein production at single cell level. A common assay for assessing membrane integrity is $SYTO_9$/PI. $SYTO_9$ is the "live" cell indicator, whilst PI is representative of "dead" cells. If the dead cell maintains efflux pump activity, PI is removed from cytoplasm, giving a false negative result (Stocks, 2004). Displaced PI from the dead cells that maintain efflux

pump leads to an overestimated number of viable cells and can skew the results. This proves there is no universal test for viability. Testing a parameter with at least two different methodologies supplies other information and therefore complements the results for a reliable conclusion. The main limitations for microscopy in a bioprocess are its lower throughput compared to FC and being time consuming.

2.4 Fermentation modes

Microbial fermentations are preferred when the desired protein is smaller than 30 kDa (Demain and Vaishnav, 2009). Discussed here are three basic modes of operation for microbial fermentations: batch, fed batch and continuous (*Figure 2.6*). A fourth mode of operation, perfusion combines continuous cultivation with a cell retention device that recirculates the cells in the bioreactor. As bacteria have a fast doubling time, there is no need for cell recirculation, so perfusion is limited to cell culture. Lastly, recent perspectives from an industrial viewpoint are summarised.

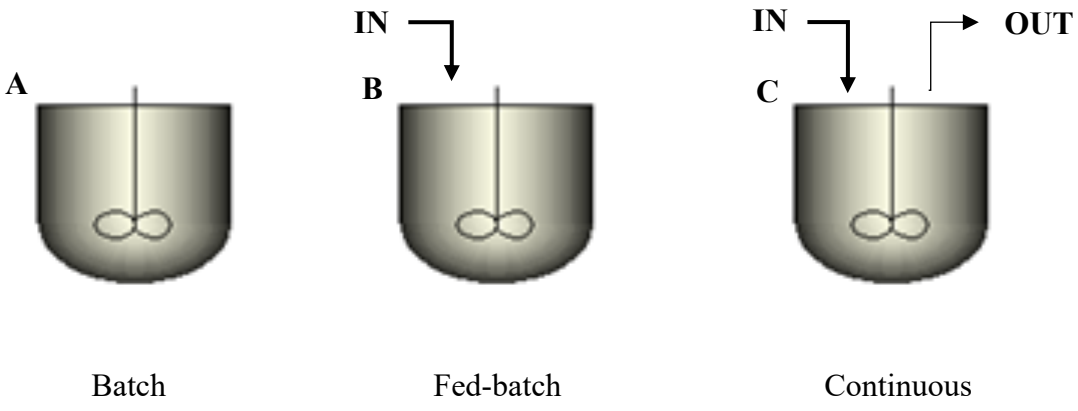

Figure 2.6. A simplified view of the three modes of operation for microbial fermentations: A: Batch. B: Fed-Batch. C: Continuous.

2.4.1 Batch cultivation

Batch is the simplest mode of operation. For years, it dominated the process development and manufacturing of biopharmaceuticals. A batch culture is a closed system, in which nothing is

added or taken away, and consists of an initial limited amount of nutrient medium (*Figure 2.6 A).* From the inoculation point, a batch fermentation follows different growth phases, each characterised by a different growth rate μ.

There are typically four phases described in literature, as follows:

(a) lag phase - characterised by no growth (μ = 0). Cells are non-replicating as they adapt to the new media;
(b) log phase - once they acclimatised to the environment, the cells grow at a maximal rate that is specific for the bacterium and the media. The cell population increases exponentially with time at a constant and maximal growth rate μ_{max};
(c) stationary - growth becomes supressed by either the lack of nutrients or accumulated waste products. The number of cells produced equals the number of cells that die, hence there is no net increase and μ = 0;
(d) death - exponential decrease in the number of living cells.

Overall, the system of a batch cultivation is in a transient state. Only during the exponential phase, the cells grow with constant properties and at a constant growth rate. It must be stressed that the mid-exponential point is representative for balanced growth at maximum growth rate μ_{max}, with no nutrient limitation, which is necessary for physiological studies.

2.4.2 Fed-batch cultivation

Fed-batch fermentations are preferred for both microbial and mammalian culture for the production of biopharmaceuticals. High cell density cultivations achieved under a fed-batch mode are most cost effective for achieving an overexpression of product (e.g. recombinant protein) (Hewitt and Nebe-Von-Caron, 2001, Hewitt *et al.*, 2007). The operation of a microbial fed-batch is also simple, with an *E. coli* fermentation taking 12 - 48 h (Jagschies *et al.*, 2018), hence most marketed biopharmaceuticals are manufactured in a fed-batch reactor.

The distinctive feature of a fed-batch (extensive batch) fermentation is the addition of a feed solution to a batch culture (*Figure 2.6 B).* In particular, top feeding leads to cells growing with excess substrate in the upper part and to cells growing in limited substrate towards the bottom (*Figure 2.7*). The feed solution is a concentrated nutrient (often the carbon source) or multiple nutrients fed continuously or in bolus to the bioreactor. The purpose of adding nutrients is to increase the biomass, with tailoring feeding strategies to bioprocess. Adding

concentrated glucose leads to an ever-increasing glucose limitation and an ever-decreasing specific growth rate. With an ever-increasing glucose limitation, the cells experience different levels of substrate at different time-points. Sampling at 0.15 s interval in large scale reactors identified a relative difference in glucose concentration of 40 mg/L (Larsson *et al.*, 1996). With the increasing level of carbon limitation, the synthesis of by-products are barely, if at all supported (Minihane and Brown, 1986). There is however enough carbon to keep the system functional.

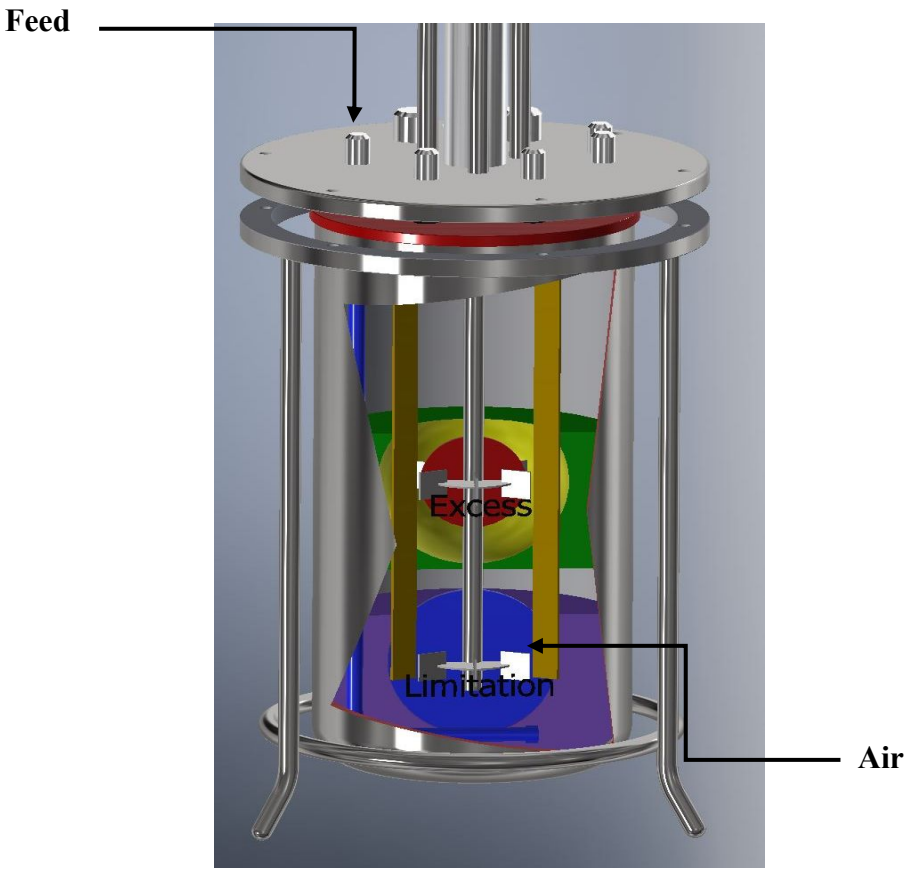

Figure 2.7. Schematic representation of nutrient gradients that occur on a large-scale fermentation, creating zones of nutrient excess and nutrient limitation (created in Autodesk Inventor).

Avoiding overflow metabolism and oxygen limitation is easy on a laboratory scale, but industrial cultivations differ because of the formation of gradients, accentuated by impaired mixing. To this, oxygen limitation occurs mainly in the upper part of the reactor, due to a lower level aeration and the low solubility of oxygen in bioprocess conditions (Käß *et al.*,

2014). This increases the cellular heterogeneities affecting process performance in ways that remain unanswered after extensive research and much controversy.

2.4.3 Continuous cultivation

In continuous cultivation, a flow of media is introduced in the reactor at a constant rate with concomitant removal of the culture broth *(Figure 2.6 C).* While the advantages of continuous fermentation have been widely advocated in the bioprocess industry, the method has not yet taken over the traditional batch and fed-batch bioprocess. Commencing in the early 1920s, but later abandoned primarily due to their complexity, continuous cultivations are an excellent tool for physiological studies of bacteria. The concept is closely linked to the chemostat, where a single nutrient is limiting and used to determine the growth rate (Kindskog, 2018).

The major advantage of a chemostat lies in its ability to provide cells in "balanced growth" that grow with a constant rate μ in a constant environment. The bacterial culture is kept below a certain concentration by diluting it at suitable intervals with fresh medium, so the culture grows exponentially and continuously. The average properties of a continuous culture are constant with the time. A plot of the number of cells or any other cell property per volume against time results in a straight line. The average cell size, RNA per cell, DNA per cell, proteins and nucleoids remains constant and invariant with time (*Figure 2.8*).

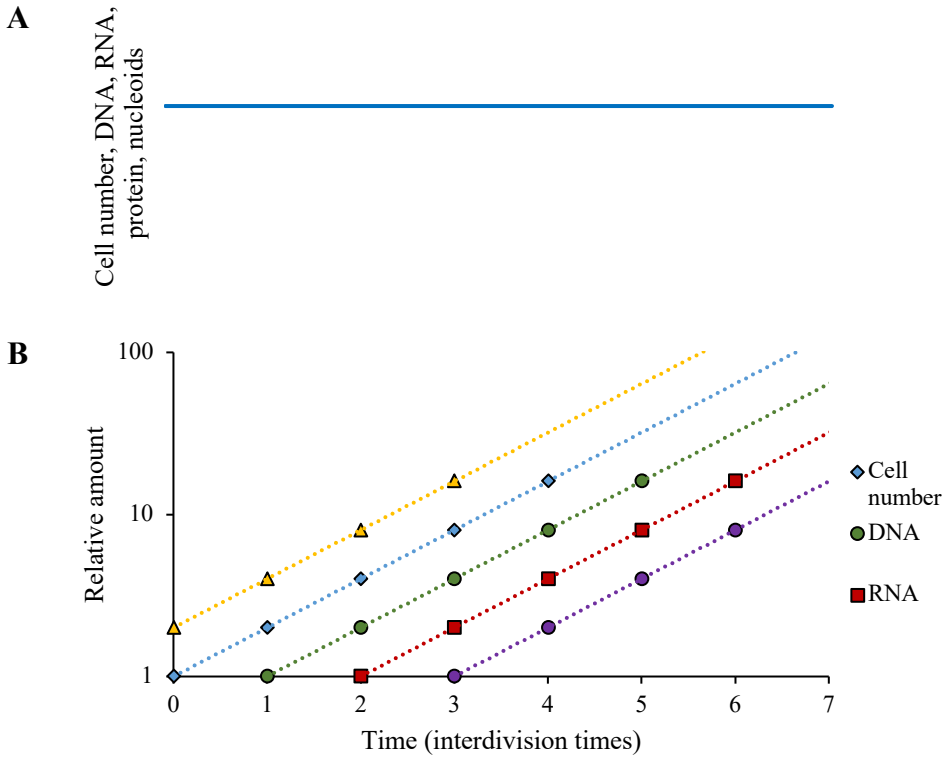

Figure 2.8. Balanced growth of a bacterial culture. The time is interdivision time. A: The determination of cell number, DNA, RNA, protein, nucleoids in balanced growth give straight parallel lines when plotted on semi-logarithm scale. B: The rate of increase of all properties of the cell is the same.

The dilution rate (D) in chemostats dictates the specific growth rate. Based on D, a continuous cultivation may develop in three possible ways:

(a) D > μ_{max} - cells are washed out faster than they can divide, resulting in an incremental decrease in biomass with an increase in residual substrate s_r;

(b) D = μ_{max} - cells grow at maximal growth rate, but any perturbation impacts on the system, making a steady state unattainable;

(c) D < μ_{max} - the rate of the washout is lower than μ_{max} thus there is an increase in biomass initially, which causes a decrease in substrate, which in turn limits the specific growth rate. After some 4 – 5 residence times, the specific growth rate

equalises with the washout rate (D). The biomass and substrate concentration are relatively stable, and the culture is at “steady state”.

Chemostats are of great importance for the study of heterogeneity, owing to a constant growth rate and a single limitation. Few earlier studies reported the physiological changes of bacteria in chemostats (Harder *et al.*, 1977, Harder and Dijkhuizen, 1983), but chemostats have not been used in recent years for physiological studies of bacteria.

In industry, many companies are exploring continuous bioprocessing to reduce cost and increase efficiency (Farid *et al.*, 2014). Many drivers for implementing continuous biomanufacturing exist. The advantages include the following: (a) production using smaller facilities and equipment; (b) potential to achieve a high volumetric productivity, with increased cell viability; (c) better suited for the production of proteins unstable in the culture broth.

At present, continuous biomanufacturing has only limited industrial applications. There are few biopharmaceuticals produced through perfusion in mammalian cells, but at the time of writing**,** there is only one successful example of continuous microbial fermentation. Novo Nordisk adapted a three weeks long continuous fermentations of the yeast *S. cerevisiae* to produce human insulin (Aakesson, 2017). The yeast however exhibits improved secretion capacity, with the product secreted in the media. Thus, the metabolic burden on the yeast cells is minimised.

The current limited applications of continuous bioprocessing are due to increased contamination risks, increased operational complexity and genetic drifts. Mutations are important for industry for two reasons. On the one hand, selection of mutants with desirable characteristics can improve the strain performance, on the other, the processes must be controlled in such a way as to diminish the unwanted formation of mutants (Aiba *et al.*, 1973). Nevertheless, a shift in biopharmaceutical processes is unlikely to happen easily because the industry is highly regulated. Yet the biopharma industry is a complex and constantly evolving environment and it may be that in the future, with further developments, continuous processing may become feasible. Ultimately, it remains a great research tool because of its suitability for physiological studies.

2.4.4 Current approach

Large-scale stainless steel reactors, operated in fed-batch served the industry well for many years. They may continue to be the best option for producing drugs that achieved blockbuster status (Alldread and Robinson, 2015). More recently, disposable or single-use systems are gaining popularity in biomanufacturing. Single use bioreactors (*Figure 2.9*) present several advantages over large stainless steel fermenters. In general, they are cheaper to produce and simpler to operate, with lower energy and water usage, and enable continuous manufacturing. They are suitable for most bioprocesses, although further development is still necessary for pressurised or higher temperature operation (Ding, 2015).

Figure 2.9. HyPerforma single use bioreactors (S.U.B) of 300 L and 30 L, suitable for microbial cultures.

2.5 Heterologous protein production

Many diseases relate to protein absence or malfunction. Most have no cure, but the treatment of symptoms involves the exogenous administration of functional proteins. Obtaining large amounts of human proteins, such as insulin, from native sources faces inherent constraints. The solution to this problem has been to produce human proteins in a range of hosts, which is a staple of the biopharmaceutical industry. Heterologous protein production requires the cloning of human genes into artificial vectors that can replicate easily within cultured cells. Having chosen the host organism, there is a need to engineer synthetic pathways in the chosen cell to introduce the recombinant gene. One way is to rewire the native genomic machinery of the cell, by genomic integration of the heterologous gene. Another way is to introduce the new gene into the cell through a plasmid-based expression system.

Recombinant protein production (RPP) started in 1976 with the founding of Genentech (Russo, 2003). The company successfully produced three recombinant proteins in *E. coli* hosts: somatostatin, insulin and human growth hormone until 1979. The first product licensed (Jagschies *et al.*, 2018) was recombinant human insulin, which began manufacture in 1982 (Frank and Chance, 1983). Since then US FDA and the European Medicines Agency (EMA) approved 186 recombinant proteins in different hosts (Jagschies *et al.*, 2018).

2.5.1 Expression systems

The spectrum of organisms exploited for RPP has expanded from the dominance of *E. coli* to alternative bacteria, animals, plants and insect cells. To yield sufficient quantity of product, the host cell containing the desired protein is cultivated on a large scale. Key determinants for profit margins are the yield of product per host organism and the cost of downstream purification. If the product yield per host and the purification costs are similar, then the choice of host is simple. A prokaryotic system is preferred based on higher growth rates compared to mammalian cells. For less sophisticated drugs that do not require post-translational modifications for drug functionality, bacteria are ideal. These are the initial points considered when choosing the ideal host for RPP (*Table 2.1*).

Host cell	DNA size (Mbp)	Glycosylation	Cost	Reference
E. coli	4.6	No	Low	(Krogh et al., 2018)
Yeast (*Saccharomyces*)	12.1	Capable	Medium	(Welch et al., 2012)
Mammalian (CHO)	2800	Capable, similar to humans	High	(Omasa et al., 2009)

Table 2.1. Comparison of key points in the choice of host cell for RPP in large-scale fermentations.

(a) Prokaryotic expression systems

Bacterial expression systems are well suited for enzyme production and pharmaceuticals without post-translation modification. Bacteria have the advantage of fast growth on simple and inexpensive growth media and the potential for high yields (Chen, 2012). When proteins require a complex mammalian glycosylation or disulphide bonds, however, bacteria are inefficient. In this case, there is usually a preference for eukaryotic cells, although ongoing research and bacterial expression system development are promising.

E. coli dominates amongst microbial systems. It was the first employed by recombinant protein production and it quickly became the gold standard for protein manufacturing. Protein production in *E. coli* seems to be overall cost effective and convenient, driven by the short doubling time of bacteria compared to other hosts. There is a wide knowledge base available, with many strains, expression protocols and vectors suitable for *E. coli* expression. Its extensive use has shown limitations in terms of yield of secreted protein, glycosylation and the formation of inclusion bodies. Despite these limitations, *E. coli* has been used for the secretion of a range of pharmaceuticals that have entered the market in recent years (Kleiner-Grote *et al.*, 2018). Although *E. coli* is one of the most common hosts, it is not always the best choice, and other hosts may be used.

Bacteria from *Pseudomonas* and *Bacillus* species have a high potential to be attractive hosts for biopharmaceuticals. *Pseudomonas* species are of particular interest because of their rapid

growth, and improved secretion and solubility capabilities compared to those of *E. coli* hosts (Krzeslak *et al.*, 2009). In the past, *Vibrio cholera* gained popularity and was engineered to produce the Dukoral vaccine, commercially known as Crucell (Hamorsky *et al.*, 2013). Triacelluvax vaccine, commercially known as Chiron was also produced using three recombinant *Bordetella pertussis* toxins (Monem, 2016).

(b) Eukaryotic expression systems

Yeast and mammalian cells are common industrial hosts for producing a range of RP. The use of yeasts (*Saccharomyces cerevisiae*, *Pichia pastoris, Yarrowia lipolytica)* combines the advantages of unicellular microbes (rapid doubling time and ease of genetic manipulation) with the ability to perform eukaryotic post-translational modifications (Çelik and Çalık, 2012, Vandermies and Fickers, 2019). Hence, yeasts are used for producing proteins that cannot be produced in *E. coli*.

No yeast, however, can provide all the attributes required for recombinant protein expression. The common *S. cerevisiae*, for example, is a GRAS strain (Generally Regarded as Safe) with an increased stress tolerance. Amongst all yeasts, it has the highest glycosylation capacity, which can be both a positive and a negative attribute. In some cases, it may structurally change the desired product through hyperglycosilation, leading to inefficiency. It has however, a limited capacity for secretion compared to that of other yeasts, such as *Pichia pastoris* and *Yarrowia lipolytica*.

Mammalian cells have been used as hosts for RPP for many years. Their main advantage is that they follow a mammalian pattern of expression, supporting proper protein folding and post-translational modifications. The most commonly used mammalian cell line is the Chinese Hamster Ovary (CHO). There are, however, several limitations. The fermentations are expensive, and the yields are lower compared to microbial systems. Nevertheless, mammalian cells are successfully used in large-scale production of most blockbuster drugs, such as monoclonal antibodies and coagulation factors.

2.5.2 Plasmids

E. coli is the preferred bacterial host for the industrial production of simple structured heterologous proteins. To produce such proteins, the DNA sequence encoding the protein is inserted into the host cell by means of a plasmid. A plasmid is an extrachromosomal circular

DNA capable of reproducing independently in a host cell. Plasmids are widely used in genetic engineering, partly due to a few characteristics, such as plasmid stability, ease of manipulation, small size and simple protocols for transferring into hosts (Kumar *et al.*, 1991). Once in the cell, the plasmid carrying the gene of interest is transcribed and translated into the recombinant protein.

Plasmids have the greatest influence on productivity, related to two main factors as follows:

(a) Plasmid copy number

The replication and maintenance of a plasmid in a host cell exerts a burden on its host. A common belief is that the burden is related to the energy and metabolite costs (Karim *et al.*, 2013). For biotechnological applications, it is desirable to know the plasmid copy number, as the gene dosage is crucial for efficient protein production (Jahn *et al.*, 2016). The higher the copy number, the higher the metabolic burden is on the cell. The key to a successful bioprocess is finding an optimum level of gene expression that generates the maximum yield of active protein.

The number in which a gene is present in a cell correlates to the expression level of such gene (Lee *et al.*, 2015). A high copy number plasmid carrying the particular gene results in a large product quantity. If this, however, exerts more stress on the host, the bioprocess efficiency becomes limited, in which case choosing a lower copy number plasmid may be beneficial. While this results in less stress for the host, it takes longer to achieve a high volume of product.

(b) Plasmid stability

Plasmid stability is an essential prerequisite for heterologous protein expression on an industrial scale. Two types of plasmid instability have been described: segregational and structural. Segregational instability relates to the loss of the entire plasmid population from recombinant cells caused by an irregular distribution during cell division. Structural instability relates to the loss or acquisition of DNA sequences on the plasmid. Both types of instability cause plasmid loss, which can dramatically reduce the yield of a recombinant product. Although plasmid loss may occur in any type of fermentation, its detriment would be more problematic in continuous cultivations. Plasmid-free cells would have a growth advantage over the plasmid-bearing cells and would overtake the whole population causing process failure. It has been suggested that continuous bioprocessing leads to plasmid

instability, explaining the priority given to batch and fed-batch at industrial scale (Kumar et *al.*, 1991, Silva *et al.*, 2012).

2.5.3 Regulation of heterologous gene expression

Heterologous genes are either (a) constitutively expressed or (b) induced.

(a) Constitutive expression means that gene expression is "always on". Constitutive expression of heterologous genes in *E. coli* hosts rarely exist. In a constitutive expression system, there is no regulation on the production of heterologous protein, which interferes with normal cell functions. This leads to all sorts of problems from a reduction of cell growth to segregational and structural instability. There is therefore a preference for inducible systems.

(b) Inducible expression means that the gene expression is "switched on" at a specific time, by "induction". The advantage of using inducible over constitutive expression is that it separates the growth and production phase of a bioprocess. The gene expression is normally "switched on" when cells reach a high cell density (HCD), thus beginning the production phase. When inducing gene expression, a factor is varied or a substance, such as isopropyl-β-D-1 thiolgalactopyranoside (IPTG) added. The factor can be a sudden change in the growth temperature for pR promoters (Valdez-Cruz *et al.*, 2010), a depletion of phosphates in the media for phoA promoters (Mikhaleva *et al.*, 2001), or a change in DO and any other nutrient limitation.

Most expression systems in bacteria are derived from the lac promoter of *E. coli*, as it is well characterised at molecular level and well understood. In the majority of cases, IPTG is used, because it is a synthetic analogue of lactose. The inducer binds to the repressor and consequently releases the operator, allowing DNA transcription (Donovan *et al.*, 1996). To take advantage of inducible expression, key parameters need to be determined, such as the induction point and temperature, and the optimal level of inducer.

2.6 *Escherichia coli* expression system

With first production of Hummulin in 1982, *E. coli* evolved into an industrial microorganism (Quianzon and Cheikh, 2012) and subsequently became a robust Good Manufacturing Practices (cGMP) host for heterologous proteins. It is the most frequently used prokaryotic

system for the production of biopharmaceuticals (Altenbuchner and Mattes, 2005, Ferrer-Miralles *et al.*, 2009), and its overall dominance as a cell factory may well continue. It is a proven expression platform for a large range of biopharmaceuticals, with high cell density fermentations (HCD) and well-developed fermentation protocols, few of which are listed below (*Table 2.2*).

Product	Protein size	Indication	Year of approval	Company	Reference
Insulin (Humulin)	5.8 kDa 51 aa	Diabetes	1978	Eli Lilly	(Chance and Frank, 1993)
Infergen (Interferon α2b)	19.4 kDa 166 aa	Cancer, Multiple Mieloma, Hepatitis C	1986	Schering Plough	(Cooper et al., 1987)
Neupogen (Filgrastim)	18.8 kDa 175 aa	Neutropenia associated chemotherapy	1991	Amgen Inc.	(R. O'Keefe, 2005)
Kineret (Anakinra)	17.3 kDa 153 aa	Rheumatoid arthritis	2001	Amgen	(Kaiser et al., 2012)
Preos (Proteotact)	9.4 kDa 84 aa	Osteoporosis	2013	NPS Pharmaceuticals	(Jódar-Gimeno, 2007)

Table 2.2. Examples of biopharmaceuticals produced in *E. coli* hosts.

E. coli success as a host for RP is owing to its rapid growth rate, easier genetic manipulations, and high level of recombinant proteins (Sahdev *et al.*, 2008, Rodriguez *et al.*, 2014). Fermentations with *E. coli* are relatively quick, with the expression of a single protein taking 12-24 h (Jagschies *et al.*, 2018). Complex proteins, such as antibody fragments can take 2-5 days. A few drawbacks exist in *E. coli* expression systems. The existence of LPS (or endotoxins) in the outer cell membrane is a common concern (Koziel *et al.*, 2018).

Endotoxins, which are released at the stage of cell lysis during protein extraction, can cause an acute systemic inflammatory response, with fever, organ failure and even death (Martich *et al.*, 1993). Techniques such as anion-exchange chromatography for endotoxin removal tend to affect the protein quality and quantity (Chen *et al.*, 2009), and increase costs downstream. To improve upon this and bypass the lysis stage, many attempts were made that encouraged protein secretion instead. Furthermore, the protein may be inappropriately folded, and therefore non-functional.

2.6.1 E. coli as a model organism

"Bacterium coli commune" or *Escherichia coli* is named after Theodor Escherich, the paediatrician who first isolated it from the stool of infants in 1885 (Hacker and Blum-Oehler, 2007). It is a common inhabitant of the lower gastrointestinal tract, and therefore it has an optimum growth temperature of 37^0C and is facultative anaerobic. As a facultative anaerobic, it does not require oxygen for growth but grows better in its presence. Additionally, it can switch from aerobic to anaerobic metabolism in certain conditions, such as a concentrated glucose environment, even when the oxygen is plentiful (Hollywood and Doelle, 1976).

Due to its long history and being well known, *E. coli* is a model organism for Gram-negative bacteria. In the lab, by far the most used is *E. coli* K12. A series of mutations have cleared *E. coli* K12 of all virulence determinants, following its isolation from the faeces of a convalescing diphtheria patient in 1922. Thus, K12 and the derivative W3110 strain lack in K and O antigens (Peleg *et al.*, 2005). This means that the strains are non-pathogenic and do not produce LPS.

(a) Growth temperature

E. coli can achieve balanced growth over a range of temperatures, but the temperature influences the cell morphology and function. Reducing the growth temperature from 37^0C down to anything above 8^0C leads to a change of morphology from rods to coccobacilli (Pierce *et al*., 2011). This is in line with lowering temperature reducing the growth rate. These phenomena have previously been observed when Henrici noticed that cell size decreased at lower growth rates compared to mid-exponential phase (Henrici, 1928). When the temperature drops as low as 7^0C, division stops and the cells become long filaments. It is important to stress that for protein production, the product dictates the temperature for the design of experiments, not the host cell.

(b) Cell shape

To achieve robust multiplication, bacteria must perform a variety of tasks. One of these is maintaining their size and shape, whilst reacting to the environment. The shape is important for growth, nutrient uptake and proliferation (Young, 2006). Typically, an *E. coli* cell is described as rod or spherocylinder - a cylinder central area capped at the end by two hemispheres (*Figure 2.10*). The hemisphere measures 0.8 – 1 μm in diameter, with an overall length of 2 – 4 μm (Neidhardt, 1987). These measurements may be more accurate under optimum conditions of growth, such as mid-exponential. This is because cell size is dependent on the rate of growth.

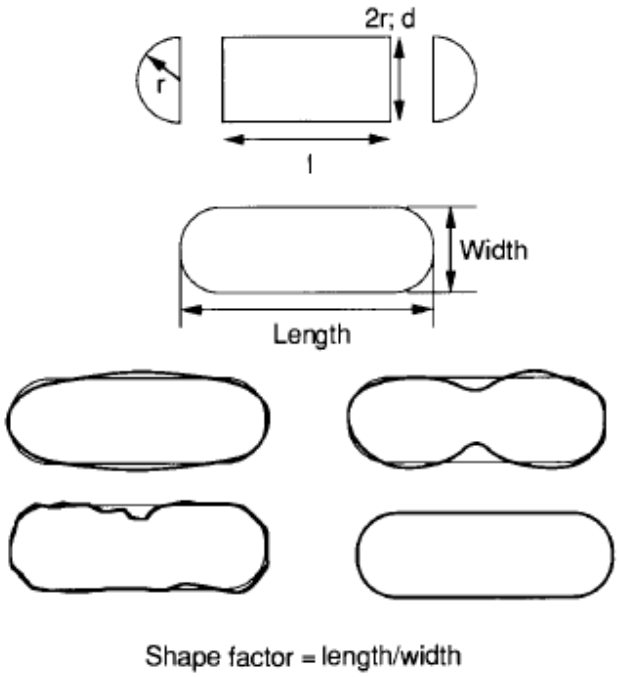

Figure 2.10. Cell shape of *E. coli*. Rods are central cylinders capped at the end by two hemispheres. Examples of actual cell shapes are super-imposed on an ideal cell shape. Total length is the length of the cylinder plus two radii. Irrespective of the actual shape (invaginating, bulging, amorphous), morphology is assessed by the shape factor or aspect ratio (AR) (Cooper, 2006).

In reality, a cell has neither a unique size nor a singular shape. The existence of different cell morphologies has been ignored for decades, since the acceptance of the Cohn-Koch dogma over the consistency of cell forms. There is now sufficient evidence to show that a population of cells are morphologically heterogeneous, with the overall morphology dependant on the

growth conditions. Irrespective of the actual cell shape, changes in cell morphology can be assessed by consistently applying a length/width approach (Cooper, 2006), otherwise known as the aspect ratio (AR).

The interpretation of AR as an indicator of elongation is only true, however, when the cells have the shape of an ellipse. Cells in general have a wide range of morphologies, thus the second most commonly used indicator of shape is the Circularity or form factor. The circularity, defined as $4\pi \bullet \text{Area} / \text{Perimeter}^2$ quantifies membrane irregularities, where a perfect circle has a value of 1, and a line has a value of zero (Russ and Russ, 2017). Russ however identified many ways of being "not like a circle" (*Figure 2.11*).

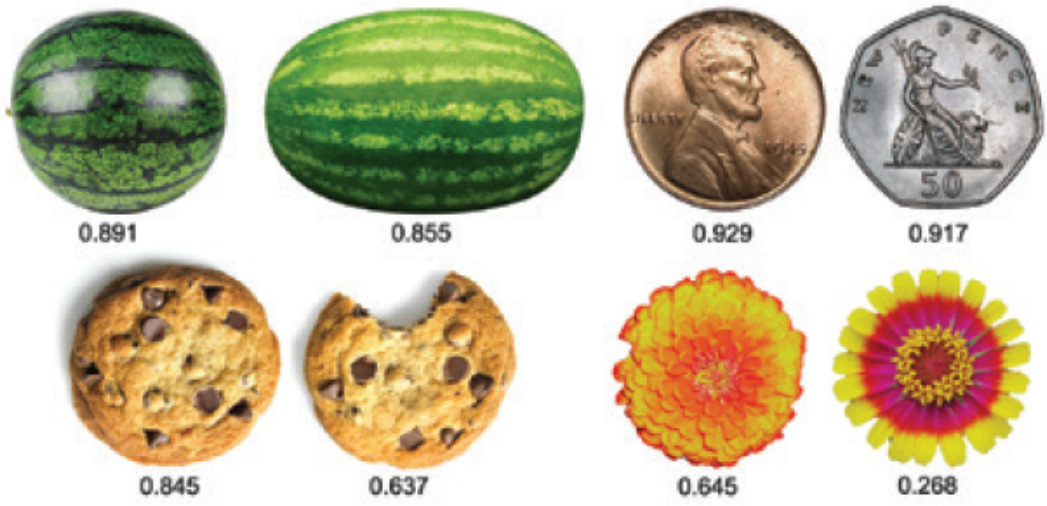

Figure 2.11. Changes in cell shape, each labelled with the measured circularity value (Russ and Russ, 2017).

(c) Asymmetric cell division

In balanced growth, *E. coli* shows exponential growth in volume (an increase in volume over time). The cells increase their length in time, by incorporating new strands of peptidoglycan, with minimal change in cell width (Marr *et al.*, 1966). Once the cell has doubled its length, the formation of septum commences. The septum does not form with any precision at the mid-cell and the daughter cells are not equal. There is now sufficient evidence to show that division is asymmetrical and asynchronous. The division plane is usually located at 0.5 ± 0.013 along the cell length, which implies an uncertainty of 2 - 3% in the location of the

septum (Kerr *et al.*, 2006). In some cases, the division occurs near the pole of the cell, resulting in a highly asymmetric division where one cell does not have a chromosome.

Asymmetric cell division previously explained the variations in cell morphology (Topley *et al.*, 1924). Bacterial pleomorphism has also been included in the writings of Mellon "Bacteria do change their morphologic type and within wide limits; and with this change may go at times important physiological modifications" (Henrici, 1928). The fact that bacteria exhibit morphological changes remained neglected in all investigations for bioprocess industry, where the focus was always on the desired product, not the productive cells. No progress would be made if focus was maintained solely on the product.

2.6.2 Bacterial growth

To achieve a representative biomass, bacterial cells grow and divide, therefore, before delving into fermentations it is desirable to review bacterial growth.

(a) Growth phases

Cells inoculated in a media do not grow all at once, but in a succession of phases, not always identified in the same way. A graph of the number of cells over time shows the classical sigmoid growth curve shape (*Figure 2.12*).

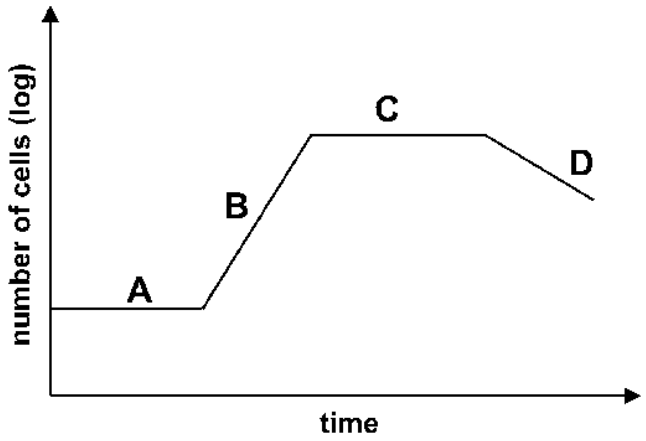

Figure 2.9. Typical four phase pattern of bacterial growth. A: lag phase; B: exponential phase; C: stationary phase; D: death phase.

The four universal growth phases were recognised by Lane-Claypon (Lane-Claypon, 1909). Initially, there is a "latent period" or "lag" in which cells do not increase in number or increase very little. Cells then begin to divide slowly at first, then more rapidly, until reaching

a maximum growth rate (μ_{max}) during mid-exponential of the "exponential" or "logarithmic" phase. Following this, cell division slows down until it stops altogether as cells enter the "stationary" or "resting" phase. The final phase consists of the initiation of cell "death" until a maximum death rate is attained.

Contrastingly, Buchanan described the presence of seven phases (*Figure 2.13*) as follows:

1. lag phase: with no bacterial growth;
2. acceleration phase: growth rate increases;
3. exponential growth: maximum and constant growth rate;
4. decreasing growth: growth rate decreases due to the gradual decrease in substrate concentration and an increased accumulation of toxic metabolites. The substrate is exhausted at the end of this phase;
5. stationary phase: null growth rate because the nutrient is exhausted and there is a high concentration of toxic metabolites;
6. acceleration of the bacterial decay: death rate increases;
7. exponential decay phase: death rate is exponential, caused by endogenous metabolism and cell lysis.

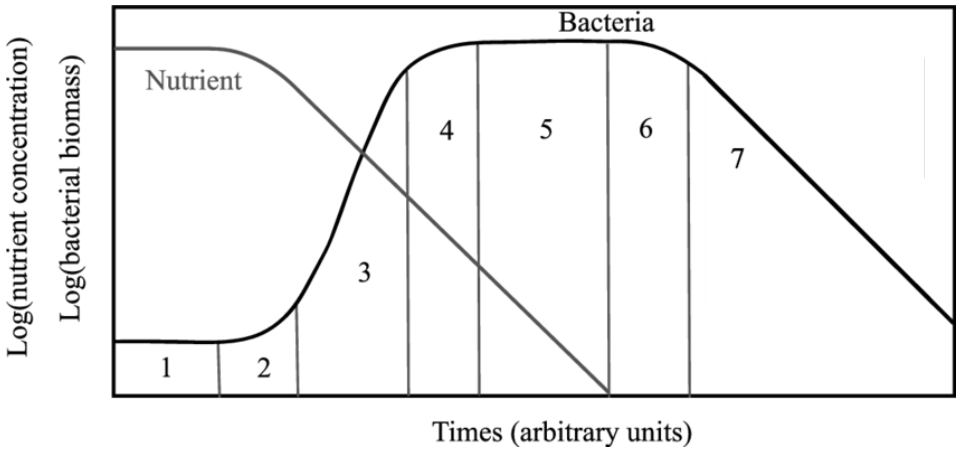

Figure 2.13. Seven phases of bacterial growth defined by Buchanan (1918).

Growth means different things at different levels. At population level, an increase in bacterial density OD_{600} is a common indicator of growth. At single cell level, growth is an increase in the total cell count (TCC) per unit volume. When the average size of the cell becomes constant over time, the increase in OD_{600} correlates with the total cell number. However, from one growth phase to another, the cells change size considerably (Henrici, 1928)

Thus, as Henrici's work pointed out, the cell concentration and bacterial density are not equivalent. When expressing the growth rate as the change of cell density over time, there is an assumption that cells have the same size.

(b) Exponential growth

Considering a unit volume of growing culture containing a number of cells N_0 at time zero, after the first division cycle (where one becomes two), the number of cells is

$$N_1 = N_0 \times 2 \quad (2.1)$$

After n division cycles, the number of cells N is

$$N = N_0 \times 2^n \quad (2.2)$$

For a specific r, replication rate per unit time, at time t, the total number of cells is given by

$$N_t = e^{rt} \times N_0 = 2^{t/Td} \times N_0 \quad (2.3)$$

Where Td is the doubling time,

$$Td = \frac{ln2}{r} \quad (2.4)$$

The cell number doubles every T_d minutes. All properties of the cell increase with the doubling time T_d, such as the cell number, RNA, DNA, protein, nucleoides (*Figure 2.8*). The exponential growth has no limiting factors and is in "balanced growth" (Campbell, 1957).

2.6.3 Balanced growth

Physiological studies of bacteria require controlled conditions with cells in balanced growth, where the growth rate is constant. The cell composition is the primary influence in creating a certain phenotype. It has been known since 1961 that the cell composition is strongly dependent on the growth rate μ (h^{-1}) and media composition (Herbert, 1961).

Balanced growth happens in two conditions, differentiated by the growth rate μ (h^{-1}):

(a) At μ_{max}, in the exponential phase of a batch culture

A batch culture may seem like a poor choice for analysing heterogeneity, because the cells pass through one phase to another (*Figure 2.12*). Dynamic physico-chemical conditions exist within each phase as the biomass, product and substrate concentrations change over time. At mid-exponential time, the cells are in balanced growth. Cells grow with constant properties at a constant rate and achieve a "steady state". There is substrate excess and no inhibition caused by by-products, thus showing the maximum growth rate μ_{max} (h^{-1}). This is representative for "feast", which is the physiological state of cells in an industrial fed-batch reactor near the feeding zone.

(b) At reduced μ, in continuous culture

In a chemostat, cells grow continuously and exponentially, as the biomass is maintained constant with a suitable dilution D. Growth is submaximal with a constant specific growth rate μ_s (h^{-1}) and the biomass is known for a set dilution rate (Lendenmann and Egli, 1995, Egli, 2015, Senn *et al*., 1994). To obtain a stable system with balanced growth, μ_s is maintained lower than μ_{max}, thus limiting (described in Section *2.4.3 Continuous cultivation*). The limitation depends on the composition of the media. If the limitation is on the C source, this is a state of "hunger", which is representative for cells in the lower levels of an industrial reactor. Hungry bacteria may develop scavenging strategies and become more heterogeneous, although the effect of heterogeneity on bioprocess remains unknown.

2.6.4 The occurrence of volatile fatty acids (VFAs)

The accumulation of VFAs is unwanted in a bioprocess due to several negative consequences. At first, the formation of VFAs directs the carbon that is destined for the synthesis of biomass and protein product. Secondly, VFAs inhibit cell growth and affect recombinant product yield (Shimizu *et al*., 1988).

VFAs occur in two conditions. The first is when cells are at a high growth rate in aerobic metabolism. There is no oxygen limitation and the rate of substrate consumption (qS) is at its maximum. This is termed "overflow metabolism". Each cell has an upper limit of substrate utilisation, above which a higher substrate concentration would lead to the occurrence of VFAs. This happens during exponential phase, where the attainment of μ_{max} is independent of

the concentration of nutrient and is limited by the cell itself, not the media components. The second situation is when a local lack of oxygen activates anaerobic metabolism with the subsequent formation of VFAs. This is termed mixed acid fermentation.

The most common VFAs in *E. coli* fermentations at neutral pH are acetate and formate. Many values of IC_{50} concentrations inhibit growth by 50% ranging from 0.5 – 1 g/L (Contiero *et al*., 2000, Roe *et al.*, 2002). As acetate is thought to limit RPP in *E. coli* cells, strategies are sought to reduce acetate formation. These are available at two levels: genetic and bioprocess. At genetic level, genes from the acetate forming pathway are deleted or silenced. However, previous works show that reducing the acetate levels through gene deletion is associated with elevated levels of other VFAs (De Mey *et al*., 2007).

During growth on glucose, the accumulation of acetate may harbour growth, as cells are able to utilise acetate as a carbon source. Nevertheless, acetate cannot be used as a sole carbon and energy source, as the enzyme of glyoxylate bypass is repressed during growth on glucose (Holms and Bennett, 1971). In a mixture of acetate and glucose in batch, glucose is preferred over acetate, whilst in a chemostat where the growth rate is less than ½ μmax, both substrates are used simultaneously (O'Beirne and Hamer, 2000). At a dilution higher than ½ μmax, *E. coli* produce more acetate from acetyl-CoA generating a huge amount of ATP and $NADH_2$ to meet a higher energy demand in order to maintain functionality. This suggests that the inhibitory effect of acetate on growth can be minimised by its consumption, besides preventing overflow metabolism on a lower than maximal μ.

Overall, acetate affects cell physiology, functionality and eventually cell viability, but this is strain dependent, with some more resistant. While acetate is assimilated by the cells, formic acid accumulates in the growth media. Formic acid, usually more toxic than acetic acid is present at smaller quantities, leading to high membrane permeability and the inhibition of DNA synthesis and cell division (Mills *et al*., 2009).

At a bioprocess level, the methods to reduce VFAs consist of the media design, cultivation conditions and feeding control. As far as media composition, a strategy is changing to other carbon sources, such as glycerol or fructose (Holms and Bennett, 1971).

2.6.5 Cytoplasmic expression

High-level cytoplasmic expression may cause the protein to aggregate as inclusion bodies (IBs). The use of a high inducer concentration and expression under strong promoters often

result in high rates of protein translation with misfolded proteins aggregating in inactive IBs. Although IBs mainly occur in the cytoplasm, they may also form in periplasm, if a secretion vector is used. IBs represent a challenge for the recovery of active protein.

Many strategies for preventing the formation of IBs exist. One is decreasing the growth temperature during the production phase to 20^0C. The lowering of temperature decreases the rate of protein synthesis, giving extra time for proper folding. At the same time, a decrease in temperature induces cold shock protein synthesis, allowing chaperones to assist with folding. The cooling process is, however, expensive, while the avoidance of IBs can be accomplished by cheaper means.

Another strategy involves the use of a lower copy number or lower strength promoter (araBAD, rhaBAD). It could also be that the coproduction of chaperones with the RP may facilitate proper folding and a soluble RP. There is no guarantee, however, for proper folding, even when solubility is achieved (Nishihara *et al.*, 2000). The coproduction of chaperones also reduces a cell's resources and therefore decreases yields as host cells are under higher metabolic stress. The fusion of the target gene to the 3 prime-end of a gene highly expressed in *E. coli,* encoding for a soluble product (trxA thioredoxine gene) may reduce the occurrence of IBs and many other strategies exist.

2.6.6 Periplasmic targeting (secretion)

A drawback for recombinant protein expression in *E. coli* is the lack of effective secretion. Secretion of recombinant proteins in the periplasm or culture media is preferred because it leads to increased protein solubility and stability (Kleiner-Grote *et al.*, 2018). Periplasmic targeting is preferred for producing proteins with disulphide bonds in *E. coli* hosts. The downstream processing of RPs secreted in the periplasm is cheaper and more convenient than whole cell lysates. Protein structures containing disulphide bridges, such as antibody fragments are secreted within the periplasm, allowing proper folding to be achieved (Kipriyanov *et al.*, 1997).

2.7 Stress in recombinant protein production (RPP)

The production of a foreign protein in host cells triggers a range of stress responses, that manifest as metabolic load, drain or burden (Glick, 1995, Neubauer *et al.*, 2003). Resources

that could be used for own-cell metabolism and growth are used instead for plasmid maintenance (Wegrzyn and Wegrzyn, 2002), protein folding and degradation of misfolded proteins (van Rensburg *et al*., 2012). RPP coincides with the upregulation of many stress genes and their products (Kyslik *et al.*, 1993, Gombert and Kilikian, 1998, Vostiar *et al.*, 2004, Schaepe *et al.*, 2014, Andersson *et al.*, 1996, Heyland *et al.*, 2011).

Cellular stresses manifest themselves at population level as a lower growth rate in recombinant strains compared to that of the host strain. A recent study shows a preference for fermentation with acetate formation in recombinant strains. This wasteful metabolism occurs when the cell is faced with changing proteomic demands (Basan *et al.*, 2015). At individual cell level, cells react to stress differently, some being more resistant than others. At worst, the overproduction of the protein leads to energetic exhaustion of the host with cell death and subsequent reduction of the RP yield to undetectable levels (Miroux and Walker 1996, Dumon Seignovert *et al.*, 2004).

2.7.1 A definition of "viable" and "dead"

Maintaining high levels viability throughout the bioprocess is critical for achieving a high level of product in high cell density cultivations. Thus, the accurate determination of viability is critical for bioprocess monitoring. Defining "viable" and "dead" is difficult, however, given the lack of consensus.

The traditional approach for defining viability has been the cell's ability to reproduce. Reproductive cells proliferate; dead cells do not. Assessed on agar plates, the counting of colony-forming units (CFU) has become a gold standard in microbial viability assessment (Davey and Hexley, 2011, Oliver, 2010). For a bioprocess, the main disadvantages are the low time efficiency and experimental error. As CFU counting is a retrospective assay, it has no value in bioprocess control and provides little information about population heterogeneity. Between life and death, bacteria have other intermediate statuses, not detected by plate counts. A common status is the *viable but not culturable* (VBNC) state, in which cells are not culturable until they are exposed to a more friendly environment to resuscitate. This state may not actually exist, based on the inability to distinguish between resuscitation or regrowth (Barer and Harwood, 1999).

In a bioprocess, viability is quantified by single cell methods that define the status of the cells based on the assessment of the cell membranes.

2.7.2 Changes in membrane integrity

Assessment of cell membrane integrity is one of the most widely used methods to measure viability. The bacterial membrane has received the most scientific research, as it protects the cell from the environment, allowing nutrient and gas exchange. The membrane must be strong to withstand elongation during division, but fragile enough to break in two when dividing. Membrane integrity is one criterion distinguishing "live" and "dead" cells, identified by how the cell stains with different fluorophores.

PI is the most frequently used marker of cell death. Its popularity in viability assessments stems from its propensity to be excluded from live cells (Zhao *et al.*, 2010) because of its large size. With the advent of fluorescent techniques, the membrane assessment with PI has replaced the traditional trypan blue exclusion test. It is normally assumed that PI^+ cells are "dead" and permanently unculturable, having irreversible damage; "live" cells that do not stain with PI have intact membranes (Sträuber and Müller, 2010, Davey and Hexley, 2011, Davey, 2011).

However, this staining principle has shortcomings. A PI^- cell does not necessarily mean that the cell is viable, nor does the opposite. Short term small breaches of the membrane stained PI^+ may not lead to cell death (Shapiro, 2005). Similarly, not all death is caused by membrane damage, given that Erental identified apoptosis like death (ALD) in bacteria (Erental *et al*., 2014). Induced by DNA damage, the recA-mediated pathway is associated with membrane integrity, thus is PI^- (Erental *et al.*, 2014). There is, however, membrane depolarisation which can be detected by MP sensitive dyes, and a positive TUNNEL assay for DNA fragmentation.

Membrane integrity assays do not detect different stages between "live" and "dead", where cells maintain membrane integrity. Most of the viability tests are end-point assays that show the percentage of "live" versus "dead" (Wlodkowic *et al.*, 2009). In this respect, identifying and monitoring individual cells before they become PI^+ offers greater sensitivity and accuracy (Zhao *et al.*, 2010). This refers to membrane potential assays, described below.

2.7.3 Changes in membrane potential

The cell membrane is important in maintaining cellular homeostasis, by allowing the passage of a variety of anions and cations (H, Na, K and Cl). Different ions move at different rates through the membranes down the concentration gradients (Mason *et al.*, 1993). These characteristics, selective permeability and ionic gradients lead to a small, but measurable difference in the electric potential between the cell interior and exterior. This is called membrane potential (MP) (Mason *et al.*, 1993) and has an important role in cell functioning. The cell interior is more negative than the exterior with approximately 70 mV.
MP has an important role in cell functioning, by controlling ion fluxes across the cell membrane.

Direct measurements of MP are problematic due to the minute size of bacteria. This has been achieved on genetically and pharmacologically enlarged *E. coli* cells (Felle *et al.*, 1980). Usually, MP is measured indirectly using fluorescent dyes that redistribute across the cell membrane (Zaritsky *et al.*, 1981). Given the many functions of the cell membrane, MP assays indicate the status of the cell. In this respect, only living cells maintain MP, thus they are metabolically active cells, capable of generating energy for metabolism and protein synthesis. In contrast, when MP = 0 and ions cross freely through the membrane, the cells are structurally damaged or “dead”. Of note is that MP assays are relevant when referring to cell states between “live” and “dead” and can be used to overcome the shortcomings of the membrane integrity assays.

CHAPTER 3

MATERIALS AND METHODS

Chapter 3 Materials and methods

3.1 Escherichia coli strains

E. coli strains were provided by FujiFilm Diosynth Biotechnologies (Billingham, UK).

The host strain is the non-recombinant *E. coli* W3110 (F^- $lambda^-$ IN (rrnD-rrnE)1 rph^{-1}), referred to as the "host" throughout this work.

The **recombinant strain** is abbreviated *E. coli* CLD1301. This was constructed by including the heterologous gene GFP-A onto the plasmid vector pD441- SR: 240460, a 4679 bp pUC – based plasmid, introduced in the host strain *E. coli* W3110. The plasmid map can be seen in *Appendix D*. The strain offers several advantages to this study. The high copy number plasmid, with 500-700 plasmid copies per cell, allows high expression of recombinant protein (GFP-A) within the cytoplasm. The plasmid carries a T5-isopropyl β-D-1-thiogalactopyranoside (IPTG) inducible promoter, the activity of which is modulated by varying the concentration of IPTG. The plasmid is kanamycin resistant, thus to select for plasmid containing cells, the growth medium was supplemented with 50 μg ml^{-1} kanamycin. Easy quantification of recombinant product is possible because of high-level expression and lower leakiness under LacI repressor.

The product dictates the experimental conditions, not the host cell. To select the most appropriate conditions for the experiments, the important point was identifying the exact nature of the GFP-A from the array of hundreds of GFP emitting in the green spectrum. A pairwise protein sequence alignment of GFP-A was performed using Jalview, and compared against Aequorea victoria-GFP (GFP_AEQVI, UniProtKB – P4221) (*Figure 3.1).*

Pairwise sequence alignment between GFP-A and Aequorea victoria-GFP identified three substitutions: Ser-2 to Arg, Ser-65-Gly and Ser-72-Ala. This confirmed the GFP-A was GFP mut3*, as created by Dr Andersen, which has three mutations compared to wt-GFP, as its name suggests (Andersen *et al.*, 1998). The position 2 mutation S2R is accidental and does not affect functionality (Andersen *et al.*, 1998). The mutations S65G and S72A, located in the chromophore region increase the fluorescent signal with photo-stability caused by increased protein folding at 37°C (Cubitt *et al*., 1995, Delagrave *et al*., 1995). The maturation time of GFP mut3* sits constantly at 45 minutes (Cormack *et al*., 1996).

The S65G and S72A mutations shift the excitation maxima to 488 nm, compared to wt-GFP that has ultraviolet (UV) excitation (Cubitt *et al*., 1995, Delagrave *et al.*, 1995, Cormack *et al*., 1996). The GFP mut3* gene yields green fluorescence that allows single cell detection using a blue 488 nm laser. The mutations in GFP mut3* cause proper folding, without aggregating in IB. Hence GFP mut3* is soluble in cytoplasm, as opposed to wt-GFP which would be mostly present in inclusion bodies when overexpressed at 37°C. This is critical for experimental work, justifying the temperature of 37°C for both growth and induction.

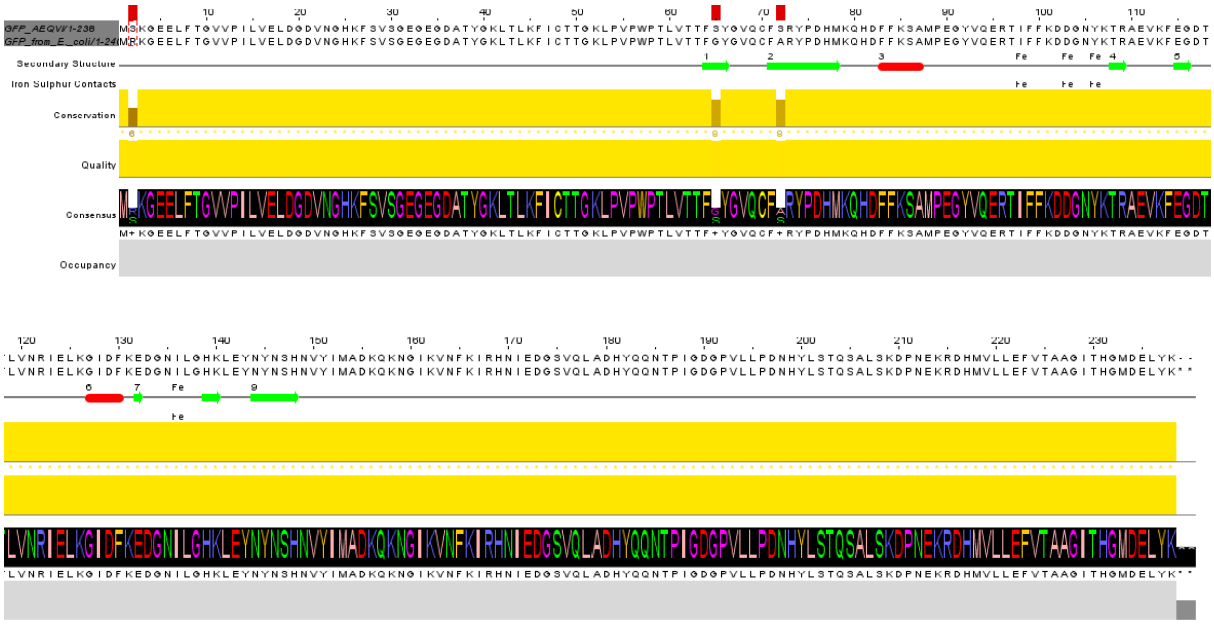

Figure 3.1. Pairwise sequence alignment of GFP-A used against wild type GFP. Jalview created visualisation of the full 238 amino acid sequence (26.9 kDa). Conserved areas are shown in yellow, with three amino acid substitutions shown in ochre.

The temperature of 37^0C is the temperature required for correct folding and maturation of the RP (GFP mut3*). It is also the optimum growth temperature of *E. coli*, but the desired product is the main determinant for experimental design.

The 21-fold increase in fluorescence, compared to wt-GFP could be due to any of the factors: more efficient protein folding at 37°C, increased absorbance at 488 nm, increased protein expression or faster chromophore formation (Andersen *et al*., 1998, Cormack *et al*., 1996). Overall, GFP mut3* allows for efficient monitoring in gene expression studies using single

cell techniques. Following induction, GFP mut3* fluorescence can be detected at early time-points in the cultures of recombinant *E. coli*.

3.2 Cell expansion and seed preparation

Cell expansion and seed preparation were carried out at 37°C, 250 RPM in a MaxQ TM 5000 shaker (Thermo Fischer Scientific, Asheville, NC, US).

A Master Cell Bank (MCB) and a Working Cell Bank (WCB) were prepared for each strain. A single colony was isolated from the agar plate received from FujiFilm Diosynth Biotechnologies (Billingham, UK). A single colony was suspended in lysogeny broth (LB), with added kanamycin 50 µg/ml for the growth of the recombinant strain. After 14 h growth, the culture was mixed with 20% glycerol (w/v) and dispensed in 1 ml aliquots, stored cryogenically at -80°C. WCB was prepared from MCB in a final concentration of 20 % glycerol (w/v), stored at -80°C.

Culture expansion started from WCB in two consecutive steps using batch minimal media with a single carbon source. The carbon source was the same as the one intended for the follow up experiments.

Step A. First seed culture was prepared in a 50 ml conical centrifuge tube (Corning, NY, US) filled with 10 ml batch mineral media. A volume of 10 µl cryopreserved WCB was thawed, vortexed, and further suspended in 10 ml pre-warmed batch media for overnight growth.

When further cultivations used glucose as the sole C source, the cells were washed twice with the corresponding media to remove residual glycerol from WCB. Cultures were centrifuged at 4000 RPM for 5 minutes, using an Eppendorf 5810 Benchtop, and the cell pellet was further re-suspended in 10 ml of corresponding media. No wash steps were necessary when the media used glycerol as the sole carbon source.

Step B. Second seed culture was prepared in a 250 ml Erlenmeyer baffled flask filled with 50 ml batch mineral media. The exponentially growing first seed culture, with a 10 ml volume was used to expand to second seed culture from a starting $OD_{600} \sim 0.05$. The culture was grown and maintained at mid-exponential phase with $OD_{600} \sim 2$, by dilution in pre-warmed media, followed by incubation.

3.3 Growth media and cultivation conditions

A batch and chemostat defined mineral media were used to support clearly C-limited growth up to 4 g l^{-1} for glucose and glycerol respectively. Individual media components were calculated based upon the growth yields, initially described by Raulin, Pasteur's student, and starting from the elemental composition of biomass (Senn *et al.*, 1994, Ihssen and Egli, 2004, Pirt, 1975). Details can be seen in the Appendix A.

3.3.1 Batch mineral media

A 10x stock of batch basal salts was prepared in 800 ml RO water with 128 g $Na_2HPO_4.2H_2O$, 30 g KH_2PO_4 and 17.7 g $(NH_4)_2SO_4$. RO water was added to a final volume of 1 litre, and the 10x basal stock media was autoclaved at 121°C for 15 minutes.

A trace and other minerals stock 100-fold concentrated was prepared with 13 g l^{-1} $MgCl_2.6H_2O$, 8 g l^{-1} $CaCO_3$, 7.7 g l^{-1} $FeCl_3.6H_2O$, 1.1 g l^{-1} $MnCl_2.4H_2O$, 150 mg l^{-1} $CuSO_4.5H_2O$, 130 mg $CoCl_2.6H_2O$, 400 mg l^{-1} ZnO, 120 mg l^{-1} H_3BO_3, 1 g l^{-1} $NaMoO_4.2H_2O$. To these quantities, 79 g l^{-1} $EDTA.Na_4.2H_2O$ was added as chelating agent in equimolar quantities for divalent and trivalent cation. The 100x stock had a pH ~ 3, and was sterilised by autoclaving at 121°C for 20 minutes.

Concentrated stock solutions of carbon sources (w/v) 20% for glucose and glycerol respectively were prepared, autoclaved separately at 121°C for 20 minutes, and added to STR after cooling. The pH of the glucose solution was adjusted to 3 with 1M HCl prior to autoclaving to prevent its degradation and formation of derivatives at high temperatures.

One litre C limited batch medium was made from 100 ml batch basal salts (10x stock), 10 ml trace elements (100x stock), 20 ml biotin (1mg/ml stock), 50 ml thiamine (1mg/ml stock), 20 ml 20% (w/v) carbon source, and 800 ml deionised water. The batch media composition is shown in *Table 3.1*.

Compound	Mass Concentration
$Na_2HPO_4.2H_2O$ [a]	12.8 g l^{-1}
KH_2PO_4 [a]	3 g l^{-1}
$(NH4)_2SO_4$ [a]	1.77 g l^{-1}
$MgCl_2.6H_2O$ [b]	130 mg l^{-1}
$CaCO_3$ [b]	80 mg l^{-1}
$FeCl_3.6H_2O$ [b]	77 mg l^{-1}
$MnCl_2.4H_2O$ [b]	11 mg l^{-1}
$CuSO_4.5H_2O$ [b]	1.5 mg l^{-1}
$CoCl_2.6H_2O$ [b]	1.3 mg l^{-1}
ZnO [b]	4 mg l^{-1}
H_3BO_3 [b]	1.2 mg l^{-1}
$NaMoO_4.2H_2O$ [b]	10 mg l^{-1}
$EDTA.Na_4.2H_2O$ [b]	790 mg l^{-1}
Glucose or Glycerol	4 g l^{-1}
Biotin	20 µg l^{-1}
Thiamine	50 µg l^{-1}
Antifoam Y-30	100 µl l^{-1}

Table 3.1. Composition of the batch mineral media (Ihssen and Egli, 2004).

Kanamycin added 50 mg l^{-1}

[a] Added from 10 x stock solution

[b] Added from 100 x stock solution

Requirements for vitamins and antibiotic

Kanamycin (Sigma-Aldrich) stock was prepared as 10 mg/ml in deionised water and filter sterilised. Kanamycin was added for the growth of *E. coli* CLD1301 in final concentration of 50 µg/ml, to select for plasmids.

Biotin (Sigma-Aldrich) and thiamine (Sigma-Aldrich) were prepared as 1mg/ml stock in deionised water. Biotin does not dissolve in water without raising the pH at 8, so small aliquots of 1M NaOH were added to aid dispersion, prior to sterilisation with a 0.2 µm syringe filter (Millipore, England). The stock solutions were stored at 4^{o}C for no more than two weeks. While there is no intrinsic requirement for vitamins in *E. coli* strains, for a fast growth, they were added to media to the final concentrations of 20 µg l^{-1} and 50 µg l^{-1} for biotin and thiamine respectively.

100 µl Antifoam Y-30 (Sigma Life Sciences, St. Louis, MO), diluted 1/10 in deionised water to aid dispersion was added to the media to prevent foaming in bioreactor fermentations. The final working concentration was 0.01%.

Chemicals were of analytical grade and purchased from Sigma-Aldrich and Alfa-Aesar unless otherwise stated.

3.3.2 Chemostat mineral media

Chemostat media was prepared as 20 L quantity in a 20 L high-density polyethylene (HDPE) carboy. Per litre, the chemostat media contained the following: 2.72 g KH_2PO_4, 2.3 g NH_4Cl, 1.4 g $(NH_4)_2SO_4$, 0.1 ml concentrated H_2SO_4, 10 ml trace elements (100x stock), 20 ml 20% (w/v) C source, 100 µl Antifoam Y-30 dissolved in 965 ml RO water. All components were added before autoclaving at 121°C for 30 minutes; the formation of derivatives from glucose and precipitations from phosphate salts were prevented by lowering the pH to 3.5 through the addition of concentrated H_2SO_4.

Antifoam Y-30 (Sigma Life Sciences, St. Louis, MO) was diluted 1/10 in RO water to aid dispersion. For uniform distribution of media components, a magnetic stir bar was used and autoclaved with the media. During continuous cultivations, the carboy rested on a magnetic stir plate. The carboy was left to cool overnight; the vitamins and antibiotic were added after cooling (as described in *Section 3.3.1 Batch mineral media*).

3.3.3 Induction parameters

Isopropyl β-D-1-thiogalactopyranoside (IPTG) was added to continuous cultivations of *E. coli* CLD1301 containing the plasmid vector pD441- SR to induce the expression of GFP

mut3*. IPTG was added in both the feed carboy and fermenter (in bolus, at switching point) to maintain a constant optimum IPTG concentration during fermentation.

Additionally, IPTG was used in control experiments with *E. coli* W3110 to show the influence of the inducer on the host cell heterogeneity in the absence of a plasmid burden.

IPTG (Sigma-Aldrich) was prepared as 1 and 0.1 M stock solutions in RO water, filter sterilised and stored at 4^0C for up to two weeks or at -20^0C for up to one year.

The **optimum induction temperature** required for correct folding and maturation of GFP mut3* was 37^0C (see Section *Materials and methods 3.1 E. coli strains*).

The **optimum induction time** for protein expression was mid-exponential. Once the cells reached mid-exponential phase (OD_{600} ~ 2), IPTG was added, concomitantly with switching from batch to continuous cultivation.

The **optimum inducer concentration** was determined in batch fermentations using BioLector (see Section *3.4.1 Batch cultivations in Microtiter Plates*).

3.4 Cultivation modes

The gold standard for microbial fermentations in industry is fed-batch, but it is not well suited for the type of work presented here because it does not provide cells in "balanced growth". Batch and continuous operation stirred tank reactors (STR) were used for microbial fermentations for the main scope of this study: the analysis of heterogeneity at different growth rates. The growth rate is constant during both exponential phase of batch and chemostat operation, thus cells are in "balanced growth", an essential requirement for physiological studies of bacteria.

Chemostat operation has two important prerequisites. One is that biomass is limited by a single nutrient, while the others are in excess; the second is obtaining a stable system operated at optimum dilution rate. The answer to these requirements was determined by carrying out multiple microscale fermentations in batch, using microtiter plates (MTP).

Inoculum for fermentations was prepared as described in Section *3.2 Cell expansion and seed preparation*. The seed for MTP fermentations was the first seed culture (Step A); the seed for STR fermentations was the second seed culture (Step B). The initial OD_{600} for all cultivations was ~ 0.05, measured offline with a Jenway 6705 Spectrophotometer.

The inoculum volume was calculated with the following formula:

$$Inoculum_{\ volume} = \frac{desired\ OD_{600}}{actual\ OD_{600}} * Fermentation_{\ volume}$$

where the desired OD_{600} was 0.05; the actual OD_{600} was the measured value of the first and second seed culture, and the fermentation volume was 800 µl and 1500 ml for MTP and STR fermentations, respectively.

3.4.1 Batch cultivations in Microtiter Plates

The media used for MTP fermentations (described in *3.3.1 Batch mineral media*) was batch mineral media. Its composition is well buffered (128g $Na_2HPO_4*2H_2O$ and 30g KH_2PO_4), thus maintaining a pH of about 6.8 (starting value $pH_0 = 7$) during fermentation.

E. coli growth was performed in 48-well FlowerPlates (MTP-48-BOH, m2p-labs GmbH, Baesweiler, Germany), in an automated system (BioLector, m2p-labs GmbH, Baesweiler, Germany). The FlowerPlate is a microtiter plate with an optimised baffled well geometry, the "flower", which is proprietary to BioLector. The novel shape increases the mixing and the gas/liquid mass transfer, and has been validated for performing oxygen unlimited microbial fermentations (Kensy *et al*., 2009). The Flowerplate (*Figure 3.2 C*) was covered with a gas permeable sealing foil with reduced evaporation (F-GPR48-10, m2p-labs GmbH, Baesweiler Germany), and placed in the incubation chamber with 95% controlled humidity. An orbital shaker (LS-X, Kühner AG, Basel, Switzerland) and an X-Y mover (BMG Lab Technologies, Germany) ensured sufficient mixing and dispersion of aeration in each well of the MTP (*Figure 3.2 A*).

Biomass, pH, dissolved oxygen tension (DOT) and fluorescence are measured with non-invasive optical sensors, located on the bottom or underneath of the "flower" plate (*Figure 3.2)*. The sensor spots (optodes) for measuring DOT and pH contain fluorescent dyes that are sensitive to protons and molecular oxygen (*Figure 3.2 B*).

The optodes are continuously washed with cultivation media, and the detectors collect the signal (*Figure 3.2 A).* To allow measurements, the MTP plate has a clear flat polystyrene base. An optical measuring unit (Fluostar, BMG Lab Technologies, Offenburg, Germany) with 620 nm excitation and no emission filter measures biomass as scattered light. An optical Y-fiber bundle

(Prinz Fiber Optics GmbH, Germany) with a 488 nm excitation filter and 520 nm emission measures fluorescence from FP.

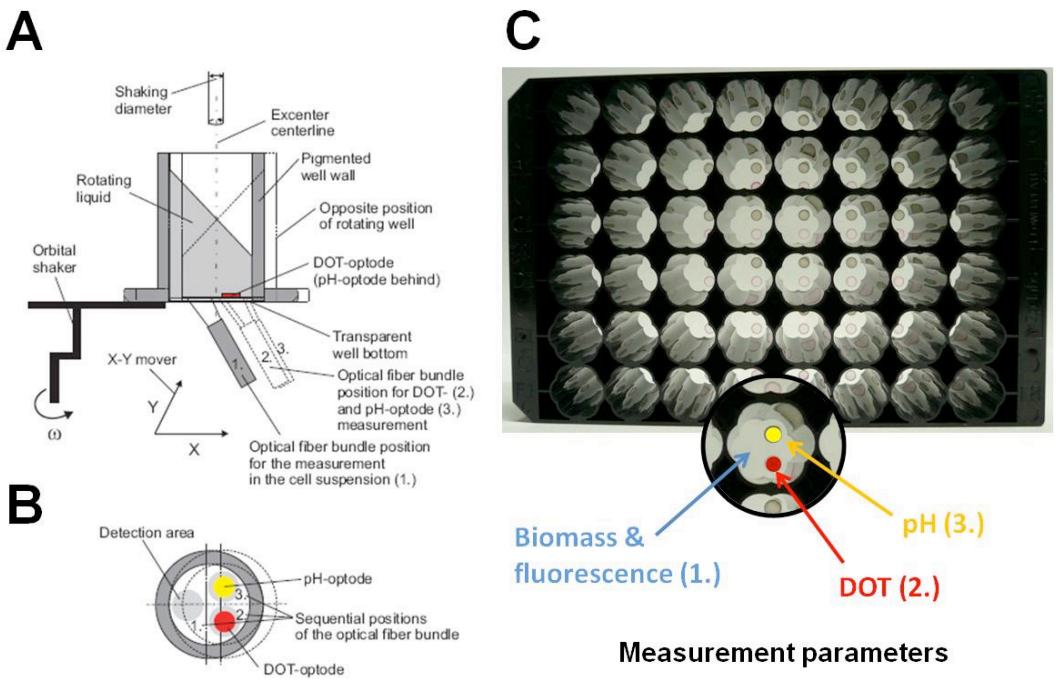

Figure 3.2. Measurement principle of MTP fermentation in the BioLector via back scattering of light from cells and fluorescence emission of molecules. A: Schematic side view of the measurements at different positions under an MTP well with continuous shaking. B: Top view of the MTP well. C: Multiparameter measurement in a FlowerPlate.

The optodes are continuously washed with cultivation media, and the detectors collect the signal (*Figure 3.2 A)*. To allow measurements, the MTP plate has a clear flat polystyrene base. An optical measuring unit (Fluostar, BMG Lab Technologies, Offenburg, Germany) with 620 nm excitation and no emission filter measures biomass as scattered light. An optical Y-fiber bundle (Prinz Fiber Optics GmbH, Germany) with a 488 nm excitation filter and 520 nm emission measures fluorescence from FP.

The wavelengths and gain factors for all optical signals are listed in *Table 3.2*. The gain, representing the sensitivity of the photomultiplier was adapted to the measurements. Gains were maintained constant across experiments and for the analysis of different datasets

.

Optical signal	λ_{ex} (nm)	λ_{em} (nm)	Gain
Biomass (scattered light)	620	-	20
DOT	505	590	60
pH	485	530	45
GFP fluorescence	488	520	50

Table 3.2. Optical signals and applied setup for BioLector online monitoring.

Method:

Triplicate fermentations were performed in 48-well MTP in BioLector (m2p-labs GmbH, Baesweiler, Germany), with three experimental controls and one well with media for sterility control as internal plate standard. The following were maintained constant in all MTP fermentations: initial OD_{600} ~ 0.05, 800 µl filling volume, 1500 1/min shaking frequency, 3 mm shaking diameter and 37°C temperature.

Details of inoculum were given in Section *3.2 Cell expansion and seed preparation*.

On plates without optodes, the cycle time for measurements was 15 minutes. On plates with optodes for additional pH and DOT measurements, the cycle time was 20 minutes. Data from BioLector was expressed in arbitrary units (A.U.) which are sufficient from comparisons across experiments and calculating μ_{max}. For scattered light and fluorescence, the average values of ten initial consecutive data-points were deducted from the total measured value. Recombinant protein expression was induced at mid-exponential point with an optimum amount of IPTG. Control experiments were performed for host and recombinant strain in the absence and presence of IPTG.

Purpose

Microtiter plates (MTP) fermentations in batch were set up on host and recombinant strain for three reasons:

(a) To verify that C is the nutrient that stoichiometrically limits

To verify the limiting range of the C source, host and recombinant *E. coli* fermentations were conducted on batch minimal media with six different C source concentrations (g/L) (1, 2, 3, 4,

7 and 10). The media contained either glucose or glycerol as sole C source (please see Appendix A) and was designed to support C limited growth up to 4 g/L.

Biomass (scattered light) was monitored until stationary phase was attained. When C is the sole growth limiting nutrient, the maximum obtainable biomass (A.U.) in the system is a function of the C source. The final biomass in the system was experimentally determined from the average of five consecutive measurements at stationary phase, and expressed as a function of the concentration of C source. To verify that the glucose or glycerol is the sole C source and that the cells do not metabolise C from other sources (thiamine and biotin), control experiments were performed with all media components, omitting the carbon source.

(b) To determine the growth kinetics of strains, in particular μ_{max}

Following screening in Section *3.4.1 Batch cultivations in Microtiter Plates* (a), a glucose and glycerol concentration was chosen at which the nutrient is in the limiting range. The choice was arbitrary, considering the amount the final biomass desired in the system. BioLector data for both glucose and glycerol were used to determine the kinetics of growth for both host and recombinant strain. The most important parameter μ_{max} was determined during the exponential phase of growth, knowing its dependence on the natural logarithm of the biomass (A.U.).

(c) To screen for the inducer quantity needed for the expression of GFP mut3* protein in *E. coli* CLD1301

Heterologous protein expression in *E. coli* CLD1301 operates on a strong T5 tunable promoter that is isopropyl β-D-1-thiogalactopyranoside (IPTG) inducible. This offers the possibility to vary protein expression to desired levels by varying the amount of IPTG.

Induction profiling with six different concentrations of IPTG (0, 0.05, 0.1, 0.25, 0.5 and 1 mM) was conducted on the recombinant *E. coli* CLD1301. IPTG was added at mid-exponential phase, at OD_{600} of 2. At induction point, measured in cycles by BioLector, the instrument was “stopped”, the gas permeable sealing foil (F-GPR48-10, m2p-labs GmbH, Baesweiler Germany) covering the plate was peeled off backwards. Thereafter, IPTG was added to each tested well, and the plate was re-covered with the sealing foil and returned to

the incubation chamber. Biomass and protein concentration (A.U.) were measured online via scattered light and fluorescence.

The average of ten initial measurements for each biomass and fluorescence were subtracted from the totals. Data was imported into Microsoft Excel for analysis. At low biomass concentrations, in the initial stages of fermentations, few wells presented values smaller than the background; these were not removed from the data set. Specific yield of product to biomass was calculated from measured product concentration (A.U.) to that of the biomass (A.U.).

Furthermore, induction experiments were conducted on the host *E. coli* W3110, to show the effect, if any, of the inducer on the cells that lack the transfected plasmid.

3.4.2 Batch cultivations in STR

Purpose: to achieve mid-exponential steady state for single cell analysis at μ_{max}.

Fermenter Vessel:

The STR is a 3 L glass autoclavable laboratory fermenter (Applikon Biotechnology B.V., Schiedam, The Netherlands) (*Figure 3.3 B*), controlled through an ez-Control tower (*Figure 3.3 A*). A double glass wall allows water recirculation for the maintenance of temperature at the set point. A motorised shaft fitted with two 6-bladed Rushton impellers (*Figure 3.3 B*) produces a unidirectional radial flow for continuous mixing. Three baffles, mounted on the inside of the STR oppose the vortexing effects of unidirectional flow, thus promoting mixing (*Figure 3.3 B*). A condenser, sensors for pH, temperature and dissolved oxygen, various ports (for inoculation, media supplementation, sampling, feed and broth removal) were mounted on the reactor's headplate. A mass flow controller mounted on the ez-Control tower maintains a constant 1 v.v.m air supply.

The BioXpert software monitors online the bioprocess at the population level, by maintaining all critical process parameters (CPPs): pH, temperature, DO. The set points for CPPs were maintained constantly as MTP fermentations (*Figure 3.4)*.

The working volume of each culture was 1.5 L. Volumes of 1.2 L RO-water, 150 ml 10x batch basal salts and 150 µl Antifoam Y-30 were filled in the reactor and autoclaved at 121^0C for 30 minutes (Section *3.3.1 Batch mineral media).* After cooling to room temperature, the following were added via the supplementation port: 15 ml 100x trace elements, 30 ml

(1mg/ml) biotin, 75ml (1mg/ml) thiamine and 30 ml carbon source 20%. The same port was used for adding 50 μg/ml kanamycin for the growth of the recombinant strain.

Inoculum:

The inoculum used for STR fermentations was the second seed culture (Section *3.2 Cell expansion and seed preparation*). This was maintained at mid-exponential phase with OD_{600} ~ 2 by dilution, and injected through the inoculation port into the STR. The starting OD_{600} was 0.05. A volume of media equal to that of the inoculum was withdrawn from STR via the sample port, and used for measuring the initial substrate and pH. The measured pH value was used for calibrating the probe "internally" as sample correction.

Process Parameters:

The following process parameters were applicable to all STR fermentations (*Table 3.3*).

Parameter	Set-point/value
Initial OD_{600}	0.05
Working volume (L)	1.5
Temperature (^{0}C)	37
pH	7
Dissolved oxygen (% air saturation)	50
Airflow	1 v.v.m
Stirrer speed (RPM)	250 – 900

Table 3.3. STR Process parameters

1. Temperature

The temperature was set to 37.0 ± 0.1°C, as measured by a thermometer sensor that fits in a thermo-pocket on the head-plate. The pocket was filled with silicone oil, which conducts heat to enhance measurements. The temperature was maintained at set point by a thermo-circulator that circulates cold and warm water through the double wall (jacket) of the reactor. Growing

bacteria generate a large amount of heat, so a suitable method of cooling is necessary to keep the temperature at optimal level.

2. pH

The pH control was set to 7.0 ± 0.1 using a probe-linked pump on the ez-Control tower. The pH sensor (AppliSens Z001023551, Applikon Biotechnology B.V., Delft, The Netherlands) was first calibrated with pH 4.0 and pH 7.0 buffer standards before the bioreactor was autoclaved. Further, a media sample was withdrawn from the bioreactor, prior to inoculation and the pH was measured offline with a pH bench probe (Mettler-Toledo™, FE20 Five Easy™). The offline pH result was entered into the ez-Control tower for a second calibration using the "sample correction" function. The consumption of carbohydrates lowers the pH, hence a base was used for pH control in most fermentations. When the pH deviates from the set point, two peristaltic pumps are activated to provide alkali (a mix of 1M NaOH/1M KOH) or acid (1M HCl) to the fermentation broth (*Figure 3.3 G*). The pumps operate at a fixed rate of 20 RPM and the tubing used for these additions was the same size for comparable alkali/acid addition.

The base mix (NaOH/KOH) provides equimolar quantities of both Na and K that do not influence the measurements of membrane potential, given that the ions are found on different sides of the cell membrane. HCl was used as an acid pump control, given that the bacteria have no specific requirement for Cl^-.

3. Dissolved oxygen (DO)

Oxygen limitation during cultivations was prevented by setting the dissolved oxygen (DO) level to 50% as measured by a low drift sensor (Applisens Z010023520, Applikon Biotechnology B.V., Delft, The Netherlands). The sensor was inserted in the fermentation broth and autoclaved with the vessel. As the DO measurements are based on the polarographic principle, the probe was polarised at the desired parameters (pH 7 and temperature 37°C) for at least 6 hours before a single point 100% calibration was performed at the maximum stirrer speed, 900 RPM. Following calibration, the stirrer control loop was activated.

4. Stirring & Aeration

Stirring was performed by two 6-bladed Rushton impellers and set to keep the DO at 50% set-point, by increasing the agitation speed from 250 to 900 RPM. The aeration flow rate was 1

v.v.m (vol. vol. min^{-1}) compressed air. The addition of air, the stirring and CO_2 from cell metabolism cause foaming. This was minimised by the addition of Antifoam Y-30.

Remarks on sampling in batch

For monitoring cultivations, *E. coli* cultures were sampled at approximately doubling time intervals from the time of inoculation (time 0) during batch growth.

For the analysis of cellular heterogeneity in conditions of excess nutrients, cells in "balanced growth" at μ_{max} were required. The cells needed to pass through at least four doubling times, thus the "steady state" of the exponential phase was the mid-exponential point. Expressed clearly in time units from inoculation (time 0), mid-exponential sampling was conducted as being representative for balanced unrestricted growth at μ_{max}.

Although the media is C limited, there is no limitation on growth at mid-exponential point. When a limitation occurs, this is visible on the growth curve as an abrupt change in biomass. For example, a limitation occurs in the change from exponential to stationary phase (*Figure 2.13*). At the mid-point of phase 4 (*Figure 2.13*), the substrate level is roughly 10x the substrate saturation constant K_s, assuming Monod kinetics.

3.4.3 Continuous fermentation in STR

Purpose: to achieve chemostat "steady state" for single cell analysis at reduced specific μ. The influence of a reduced growth rate on bioprocess was analysed in terms of reproductive and metabolic ability, membrane integrity and membrane potential.

Media

A carbon limited chemostat media (described in Section *3.3.2 Chemostat mineral media*) was used for continuous fermentations of *E. coli* strains.

Cultivation regime

The cultivation regime comprised of an initial batch phase, followed by a second C-limited chemostat phase. At mid-exponential phase when $OD_{600} \sim 2$, the switching to chemostat was performed by switching ON the inlet and outlet peristaltic pumps.

The feed rate was constant and set to ½ μ_{max}. Maximum growth rate μ_{max} was previously determined in batch. The choice of ½ μ_{max} was supported by a maximum biomass and a

concentration of C source in the “steady state” reactor equivalent to K_s. Fresh media was pumped from a 20L **FEED** carboy (*Figure 3.3 E*) into the STR with an inlet peristaltic pump (Watson Marlow Pumps Group, Rommerskirchen, Germany) (*Figure 3.3 C*). The inlet peristaltic pump was adjusted to support growth at ½ μ_{max}. An outlet pump operating at maximum flow rate (*Figure 3.3 C*) removes concomitantly the culture broth from STR to a **WASTE** carboy (*Figure 3.3 F*). The exit line for continuous removal of the fermentation broth was located at just above 1.5 l working volume of the STR. This is because the effluent media contains a higher volume of gas from metabolism, therefore the exit has to be level-controlled to maintain a constant volume in the system.

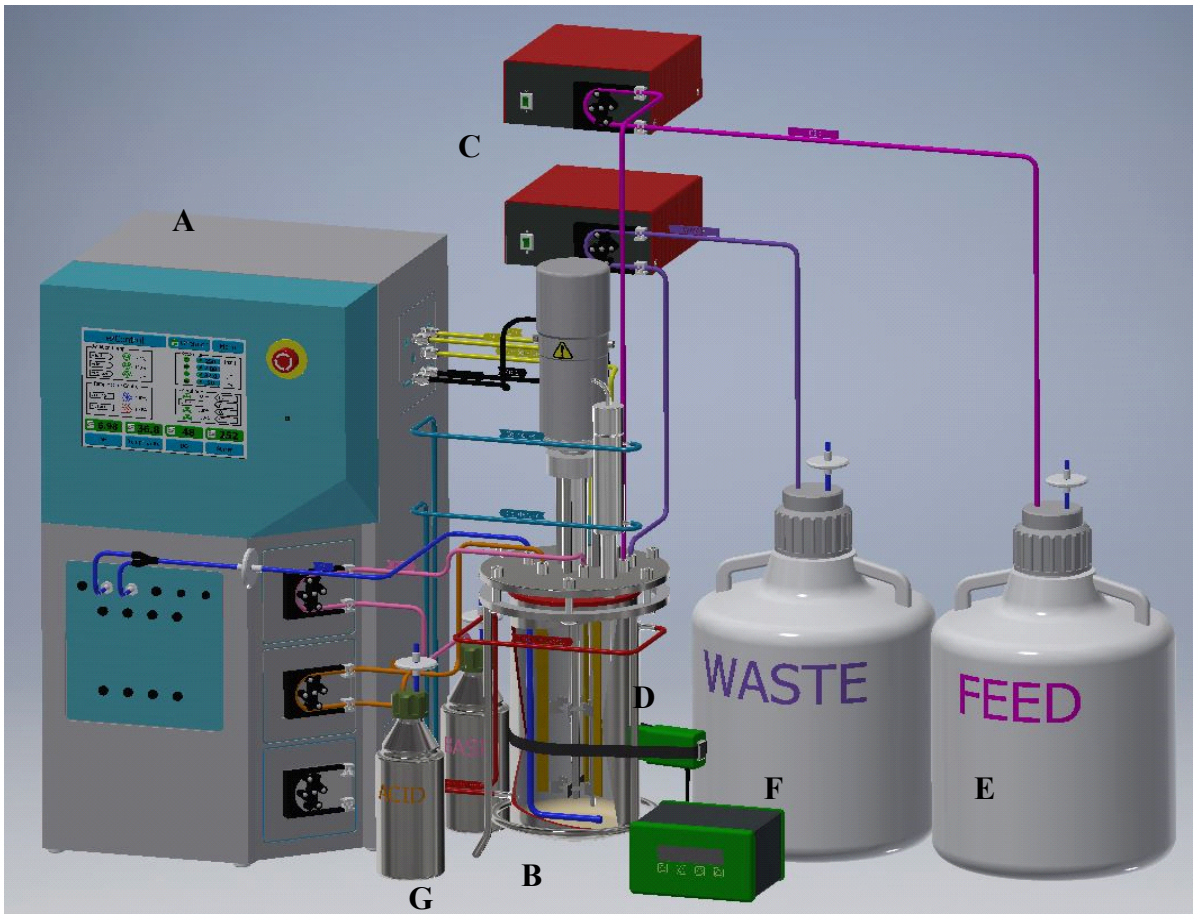

Figure 3.3. Experimental set-up 3D model of continuous fermentations (Autodesk Inventor – see Appendix C). Aerobic cultivations were performed in a 3 L Applikon reactor (B). The inflow gas was compressed air (blue line). BugLab for biomass monitoring was affixed on the outside of fermenter vessel (D). Culture volume was maintained constant by adding media from a 20L FEED carboy (E) whilst pumping out the fermentation broth into a 20L WASTE carboy (F). FEED and WASTE carboys were connected to the reactor via peristaltic pumps (C) with the inlet pump setting the growth rate. Fermentation was controlled through the ez-control tower (A). Temperature, dissolved oxygen and pH were monitored using in-liquid probes. Temperature was maintained by a tempered water loop with instant cooling and heating through the water jacket of fermenter. pH was maintained at setpoint by the addition of acid and base (G) with peristaltic pumps on the ez-control tower. Dissolved oxygen was maintained at set point by a stirrer control loop.

A period of 4 - 5 residence time (R) was allowed for the system to "settle" into steady state. This was confirmed by a constant biomass, a constant DO around set point and a constant metabolic activity, evidenced by a constant alkali addition. When steady state was achieved, samples were collected at approximately doubling time interval for single cell analysis.

Operating parameters such as pH, temperature, DO (*Figure 3.4*) were maintained at the same level as batch fermentations (*Table 3.3*).

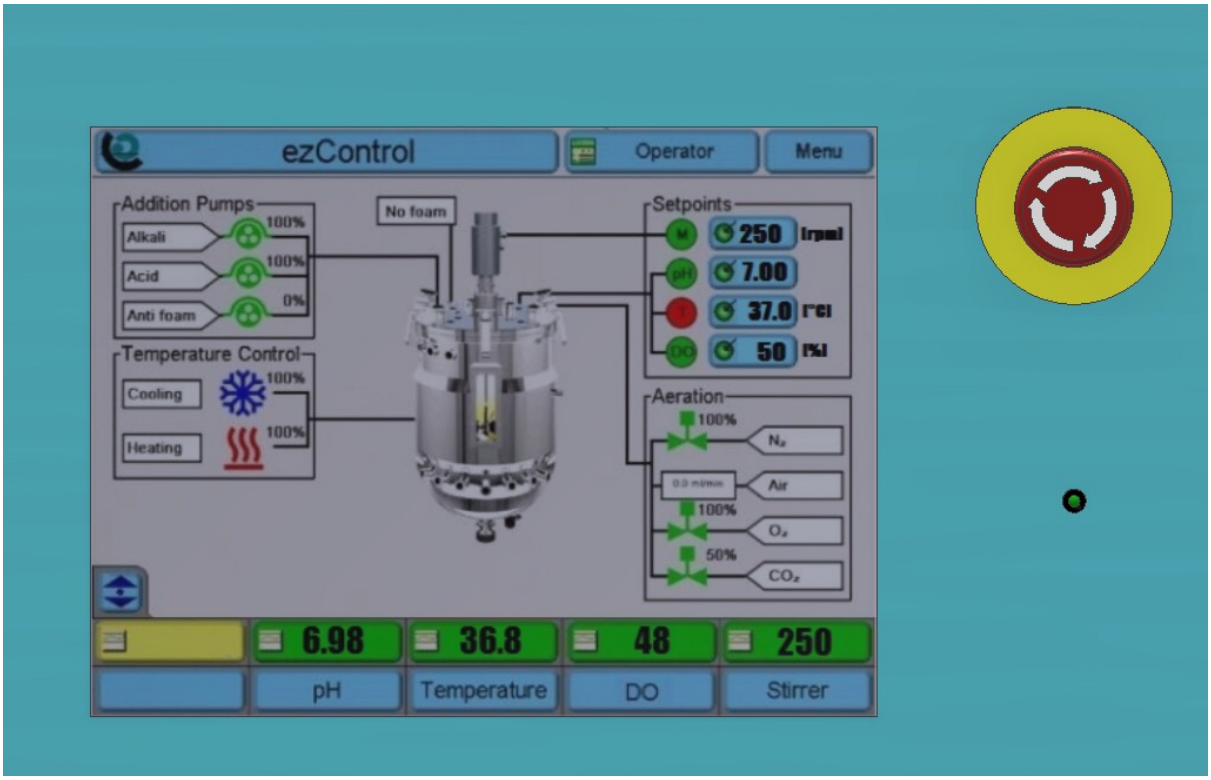

Figure 3.4. Operating parameters (pH, temperature, DO) for *E. coli* fermentations (Autodesk Inventor).

3.5 Process monitoring

Online and offline measurements were carried out for bioprocess monitoring and control.

3.5.1 Critical Process Parameters

Critical Process Parameters (CPPs) such as temperature, stirring speed, pH, dissolved oxygen, alongside media composition were optimised in MTP (data not presented). Two common problems encountered were foaming and media precipitation when changing to continuous

cultivations. These operational challenges were overcome with antifoam and media optimisation.

CPPs were continuously monitored using the Applikon ez-Control (described in Section *3.4.2 Batch cultivations in STR)*. Data was logged online with the BioXpert Software.

3.5.2 Online biomass measurements (BugLab)

Growth was measured with BugLab (BugLab LLC, Concord, CA), a non-invasive biomass sensor, affixed to the outside glass wall of the STR (*Figure 3.5 C*). The near infrared (NIR) BE2100 sensor monitors growth continuously using a combination of lasers (850 nm) and detectors. The laser is directed into the media through the transparent wall of STR. Bacterial cells in suspension within the STR scatter and reflect the light back at the sensor. Photodetectors within the sensor collect the 160-180^0 backscattered light. The measurement principle of BugLab is the same with that of BioLector using MTP, described in Section *3.4.1 Batch cultivations in Microtiter Plates.*

Figure 3.5. BugLab, non-invasive biomass monitor. Measurements through the fermenter wall. A: BE2100 base unit; B: BE2100 optical sensor; C: BE2100 sensor strapped on the glass wall of reactor; D: Virtual Instrument and Data Viewing Software main window.

Biomass is measured inside the reactor non-invasively, with maximum sensitivity at 2 cm from the front of the sensor. In principle, as the concentration of cells increases, the instruments detects a higher signal. The reported measurements are raw "Bug Units", which are generated at the time of manufacture by linearly scaling the measurements against offline OD_{600} at suitable dilutions for a culture of *Saccharomyces cerevisiae*. However, backscattered light is influenced by cell size, hence any measurement made on *E. coli* necessitates a separate calibration.

BugLab measurements were compared across experiments. A baseline calibration was performed just before inoculation to remove the signals originating from the media reflectance. This is similar to "blanking" with sterile media in a spectrophotometer. An individual calibration was obtained for host *E. coli* strain with BugLab measurements as a function of offline OD_{600} and cell dry weight (CDW). The instrument is, however, sensitive to changes in air bubble size, agitation rate and changes in cell morphology. Any slight change in BugLab measurements was compared against offline OD_{600}. The instrument was operated via the Virtual Instrument software.

3.5.3 Optical density

Biomass development in STR was monitored offline as optical density (OD).

OD represents the attenuation of light by the bacterial cells and depends on wavelength (λ).

$$OD(\lambda) = log_{10}\left[\frac{I_0(\lambda)}{I(\lambda)}\right] \qquad (3.1)$$

where $I_0(\lambda)$ is the intensity of the incident light to the sample and $I(\lambda)$ is the intensity transmitted through the sample.

OD of a sample of thickness n is given by the following:

$$OD(\lambda) = (\alpha_\lambda + \tau_\lambda)\, n \qquad (3.2)$$

where α_λ is the absorbance density at wavelength λ and τ_λ is the turbidity at wavelength λ.

Two misconceptions are common in measurements of OD. Neither OD is the turbidity nor the absorbance of a sample, since both components contribute to light attenuation, which is the

actual OD measurement. The absorbance represents the fraction of incident light absorbed by the sample, while the turbidity is a measure of the light attenuation due to light scattering.

OD_{600} was measured using 1.5 ml Kartell semi-micro disposable transparent cuvettes (Fisher) with a Jenway 6705 UV/Visible Scanning Spectrophotometer at a fixed wavelength of 600 nm. A Xenon lamp illuminates the sample, and a detector records the light that passes through. The spectrophotometer measures from - 0.3 to 3 OD_{600} units, with the linear range between 0 - 0.5. For higher measurements, samples were diluted in sterile media and the final OD_{600} was recalculated using the dilution factor.

Sterile media was used for both serial dilutions and for zeroing the spectrophotometer. Cell dilution using sterile media until measurements were within the linear range of the instrument was justified. Firstly, for the measurement to reflect growth, the media for dilution should contain every component of the culture broth except the cells. Secondly, the background colour was maintained. Lastly, by suspending the cells in a media with the same osmolality, osmotic shock and refractive index effects were avoided.

OD_{600} is widely used to quantify growth in biotechnology labs because of its speed, simplicity, low cost, and a long history. While the measurement is instantaneous, there are few considerations. Detection is possible above 10^6/ml cells and prone to errors in early stage of fermentations due to insufficient number of cells. The method is insensitive to changes in cell size or cells agglutinating together, and it remains a bulk measurement at population level. While it does not account for heterogeneity, it nevertheless measures growth.

3.5.4 Total cell counts

Cell growth was measured as total cell counts (TCCs) at single cell level using FC, simultaneously with the assessment of membrane integrity using the cell permeant Thiazole Orange (TO) and the cell impermeant Propidium Iodide, (PI).

Samples were diluted in sterile media up to an $OD_{600} \sim 0.025$, using 4 ml 12 x 55mm round bottom polyethylene FC tubes (Greiner Bio-One, Kremsmunster, Austria). Dilution was necessary to avoid erroneous observations caused by staining artefacts that occur when using the same dye amount for a different cell number. The FC tubes were vortexed for 8 seconds with Vortex Genie2 (Scientific Industries Inc., Bohemia, NY, US) and three subsamples were prepared for each sample.

TO, 42 µM in dimethyl sulfoxide (DMSO) and PI 4.3 mM in water were used for cell staining up to final concentrations of 420 nmol/l and 43 µmol/l for TO and PI, respectively. The dye-cell suspension was vortexed thoroughly and incubated at RT for 5 minutes in the dark. TCC was performed with an Attune Attune Nxt Acoustic Focusing Cytometer (Life Technologies, Carlsbad, CA, USA), equipped with a 488 nm laser. The green and red fluorescence were detected in the BL1 (BP 530/30) and BL2 channel (BP 574/26), respectively. The SSC and FSC detectors were used to gate the population of interest.

The Attune instrument operates a volumetric analysis through a positive displacement syringe and was set to deliver 5 µl from the sample syringe at a flow rate of 25 µl/min. The Attune cytometric software v2.1 (Life Technologies Inc., CA) is able to do TCC of the gated population of interest, excluding the debris. TCC per ml culture was calculated correcting for the dilution factor and the 5 µl sample volume, but all data analysis of flow cytometry files was conducted with Matlab®.

3.5.5 Cell dry weight

The monitoring of cell dry weight (CDW) requires large samples to minimise errors. For a laboratory-scale bioreactor, operating on minimal media with cultures at small densities, CDW was performed as a calibration against other biomass measurements such as OD_{600} and BugLab.

CDW was measured by separating the biomass from the media by membrane filtration with subsequent drying. A 400 ml bacterial culture was grown in a baffled 2 L Erlenmeyer flask in exponential phase at 37^0C, 200 RPM. The final OD_{600} was calculated from the measured OD_{600} in the linear range of the instrument (0 – 0.5), multiplied by the dilution factor. Fully-grown *E. coli* cultures bring about colour changes in the media that affect the OD_{600} measurements. For OD_{600} - CDW calibration, the OD_{600} of the supernatant was deducted from the final OD_{600} value. To measure the OD_{600} of the supernatant, two 2 ml samples from the original exponential culture at OD_{600} of 3.5 were centrifuged to pellet the cells, and the supernatant separated.

The original culture in the exponential phase of growth was diluted in pre-warmed sterile media to six different OD_{600} calibration points of 0.25, 0.5, 1, 1.5, 2 and 2.5. Values above 0.5 were diluted in sterile media until the linear range 0 - 0.5. The cultures were centrifuged, re-suspended in a small amount of PBS and filtered with a pre-weighed Whatman cellulose filter

paper (0.45 µm pore size). The cells and the filter paper were oven dried until a constant weight was achieved. The weight was measured and the CDW calculated, considering the volume used.

A known quantity of sterile media was filtered to measure the precipitate of any salts, and the paper was oven dried until constant weight was achieved and deducted from the total recorded weight. A calibration curve was obtained for each strain tested.

3.5.6 Monitoring volatile fatty acids

Samples were collected to determine the levels of organic acids (acetic, propionic and formic) in the culture media. To stop the bacterial activity, samples were centrifuged within the first two minutes of collection. Further, the supernatant was sterilised with a 25-mm-diameter, 0.22 µm pore size Millex-GS syringe filter (Millex-GS, Millipore Co, Billerica, MA, USA) and frozen immediately to -20°C. The analysis was performed in triplicate on a DIONEX ICS-2100 (DIONEX ICS-2100, Dionex, USA) operated with a Dionex IonPac™ AG11-HC anion protection column (Dionex, USA). Data was analysed by a Chameleon chromatography workstation (Dionex, USA).

3.6 Substrate measurements in the media

Concentrations of substrate in fermentation samples were measured using enzyme-based test kits (Megazyme International, Bray, Ireland), according to manufacturer protocols. A volume of 0.1 ml culture supernatant was mixed with RO-H_2O and a range of buffers to a final volume of 2.1 ml. The concentrations of glucose and glycerol were calculated based on the increase in absorbance measured at 340 nm.

The initial phase of batch starts from 4 g l^{-1} substrate (glucose or glycerol), hence for measurements in the exponential phase of batch, supernatant samples were diluted 1/10 in PBS prior to spectrophotometer measurements. Steady state samples from chemostats were not diluted. Consideration was given to pH adjustment as the buffer pH is 7.6. As the sample size was 0.1 ml, the change in pH was negligible and pH adjustment was deemed unnecessary.

The D-Glucose HK Assay Kit (Megazyme International, Bray, Ireland) is linear within the range of 0.04 - 0.8 g l^{-1} glucose, which corresponds to 4 - 80 µg D-glucose per cuvette when using a 0.1 ml sample mixed in a 2.1 ml total assay volume.

The Glycerol Assay Kit (Megazyme International Ireland, Bray, Ireland) is linear up to 0.35 g l^{-1} glycerol in media, corresponding to 35 µg of glycerol per cuvette when using 0.1 ml supernatant. The minimum quantity detected is 0.008 g l^{-1}, corresponding to 0.8 µg glycerol per cuvette when using 0.1 ml sample in a 2.1 ml total assay volume.

3.7 Monitoring membrane integrity with FC

Membrane integrity was assessed with dual fluorescence flow cytometry with Attune Attune Nxt Acoustic Focusing Cytometer (Life Technologies, Carlsbad, CA, USA. The viability was assessed simultaneously with TCCs, using the dye combination, TO and PI (*Figure 3.6*). Cells were prepared and stained as described in Section *3.5.4 Total cell counts*.

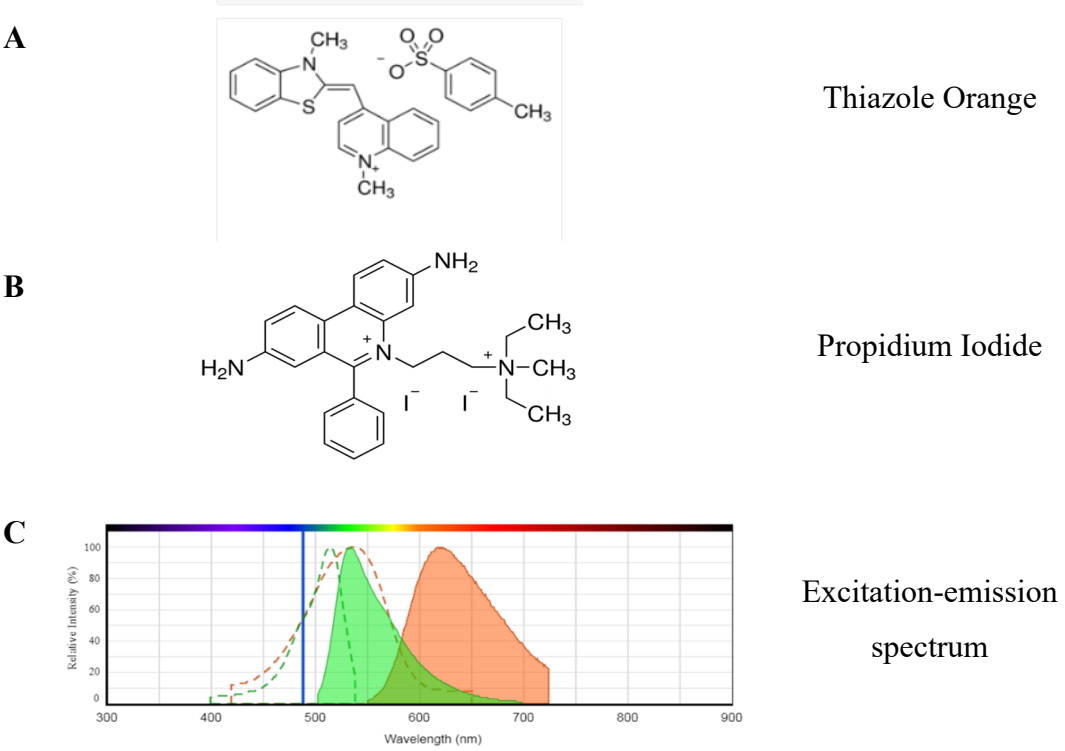

Figure 3.6. Thiazole orange and Propidium Iodide. A: TO chemical structure. B: PI chemical structure. C: TO and PI excitation-emission spectrum. Blue horizontal line represents the 488 nm excitation laser. The absorption is shown in dotted line, while the emission is shown in a solid line for both TO (green) and PI (orange).

TO, 1,3'-dimethyl-4,2'- quinothiacyanine is well known for staining reticulocytes (Lee et al., 1986), and stains both RNA and DNA in bacteria. Its absorption maxima sits at 509 nm with maximum emission at 533 nm (Vanhove *et al.*, 1990, Jouault *et al*., 1994). TO has a single delocalised positive charge from two N-methyl groups (*Figure 3.6 A*). Its lipophilic nature allows the dye to pass freely through the phospholipid bilayer. Although used with FC, TO was not suitable for FM because of rapid photo-bleaching (Shapiro, 2002). The green fluorescence of TO was detected in the BL1 channel (BP 530/30) with a 488 nm excitation laser.

Propidium iodide (PI) is the iodide salt of 3, 8-Diamino-5-diethyl-methyl-aminopropyl-6-phenylphenanthridine. Its side chain is a propyl group with quaternary ammonium at the end opposite of the phenanthridinium ring (*Figure 3.6 B*). Because of a double positive charge, PI is impermeant to the phosholipid bilayer, thus only passing through cells with compromised membranes that are considered "dead". Within "dead" cells, PI binds non-specifically to both DNA and RNA. PI fluorescent signals were detected in the red channel BL2 (BP 574/26).

In combined assay for viability, PI stains the "dead" cells red while TO stains "live" cells green. Both dyes are excited by a 488 nm laser, with the emitted signal separated by compensation (*Figure 3.6 C*).

A positive control for PI^+ or "dead" cells was prepared. *E. coli* cells were grown to 5 x 10^5 cells/ml and the population was separated into two subpopulations. One subpopulation was lysed with nisin treatment. *E. coli* cells with an OD_{600} of 0.25 were incubated with nisin (final concentration, 25 µg/ml) for 1 h, at 37^0C under 250 RPM. This was because the addition of nisin did not lead to immediate cell death, and bacterial membranes were still impermeable to PI after 30 minutes incubation. The lysed cells were harvested and re-suspended in fresh media for antibiotic removal. Lysed and viable cell subpopulations were mixed to obtain different percentages of dead cells: 0, 25, 50, 75 and 100%.

Nisin stock was prepared by dissolving nisin at acidic pH. Nisin (Sigma Aldrich), 1g with 2.5% purity was dissolved in 25 ml 0.02 N HCl and 0.75% NaCl, and then filter sterilised. Killed control bacterial cells were stored in the fridge until used as controls at the beginning, middle and end of the experiment.

Remarks on control

Nisin treated cells were used as control of "death" for experiments that assessed both membrane integrity and membrane potential. The antibiotic has a known efficacy particularly against Gram-positive bacteria (Campion *et al.*, 2017, Garcera *et al.*, 1993), but EDTA used in media as a chelating agent renders *E. coli* cells susceptible to nisin. Nisin causes a rapid dissipation of membrane potential (Helander and Mattila-Sandholm, 2000, Kordel *et al.*, 1989) in addition to creating PI^+ holes in the membrane, detectable with common viability dyes. The *E. coli* cells treated with nisin as described above were PI^+ on FM and FC, and revealed no growth on agar plating.

3.8 Monitoring membrane potential with DIBAC/EB/PI

Changes in MP indicative of bacterial stress were studied by FC using a triple dye combination $DIBAC_{4(3)}$/EB/PI (*Figure 3.7*).

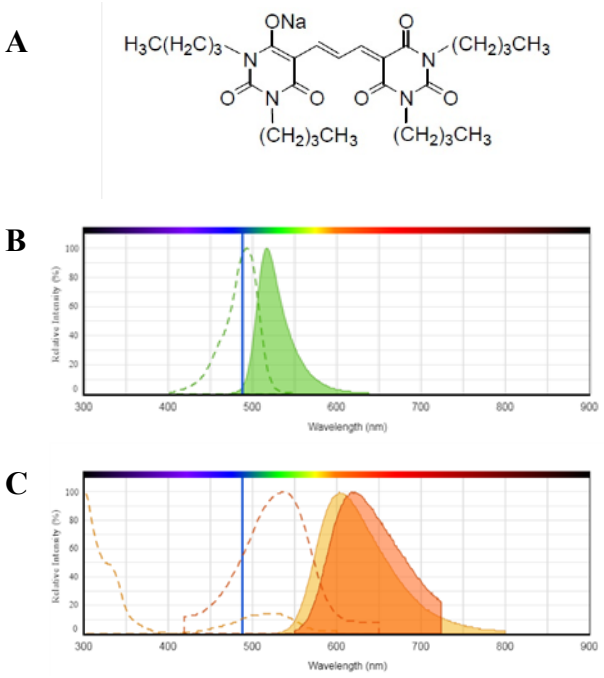

$DIBAC_{4(3)}$

Excitation (dotted line) and emission (solid line) spectrum of $DIBAC_{4(3)}$.

Excitation (dotted line) and emission (solid line) spectra of Ethidium Bromide (light orange) and Propidium Iodide (orange red).

Figure 3.7. $DIBAC_{4(3)}$/EB/PI for membrane potential assessment. A: $DIBAC_{4(3)}$ chemical structure. B: Excitation-emission spectrum of $DIBAC_{4(3)}$. C: Ethidium Bromide and Propidium Iodide Spectra. Blue vertical line is blue 488 nm excitation laser.

$DIBAC_{4(3)}$ (bis-(1, 3-dibarbituric acid)-trimethine oxonol) is an oxonol dye that is negatively charged (anionic), thus excluded from polarised cells that maintain MP. This means well-energised cells have low fluorescence $DIBAC_{4(3)}$ staining. The dye enters the cells with altered MP, thus an increase in $DIBAC_{4(3)}$ fluorescence suggests that the MP gradient no longer exists. Cells that exhibit an increase in $DIBAC_{4(3)}$ fluorescence intensity are considered to have undergone membrane depolarisation, although the dye also stains "permeabilised" cells with MP = 0.

It has been suggested that heat and alcohol killed bacteria exhibit an increase in $DIBAC_{4(3)}$ fluorescence, whilst less drastic treatments, such as nutrient limitation showed no change in $DIBAC_{4(3)}$ fluorescence (Novo *et al.*, 1999). As an increase in $DIBAC_{4(3)}$ fluorescence is more related to membrane integrity than changes in MP, $DIBAC_{4(3)}$ is a useful indicator of membrane permeability that occurs with antibiotic treatment (Diaz *et al.*, 2010).

EB is the bromide salt of 3, 8-diamino-5-ethyl-6-phenylphenanthridine. The N-alkyl group (ethyl group) gives EB a positive charge thus EB is membrane permeant, entering all cell membranes, and binding to both DNA and RNA once inside. EB assesses the efflux pump activity. The dye is retained by cells with inactive efflux pump, thus giving an increase in fluorescence, regardless of membrane status (Kim *et al.*, 2009); the dye is pumped out of cells with functional efflux pumps, thereby decreasing the overall measurable fluorescence (Hewitt and Nebe-Von-Caron, 2001). As EB crosses intact membranes very slowly and is pumped out of the cell, it has widely, but erroneously, been regarded as impermeant and used in dye exclusion tests.

When used simultaneously with PI, the double charge of PI confers a higher binding affinity for double-stranded nucleic acids than EB. Thereby, when cells are permeable to both dyes, PI displaces EB (Nebe-von-Caron *et al.*, 2000). The spectra of EB and PI (described in Section *3.7 Monitoring membrane integrity with FC*) overlaps, meaning they are harder to separate and they require compensation (*Figure* 3.7 *C*).

$DIBAC_{4(3)}$ (FW 516.64) was prepared as 10 mg/ml stock solution in 100% dimethyl sulphoxide (DMSO), stored at -20^{0}C, and 100 µl/ml working solution in RO-water, stored at 4^{0}C. Tween 20 was added to the working solution to a final concentration of 0.5%.

EB (FW 394.3) stock solution 10 mg/ml was prepared in RO-water, stored at -20^{0}C. A working solution at 500 µg/ml was prepared in RO-H_2O, stored at 4^{0}C.

PI (FW 668.4) was prepared in RO-water as 500 μg/ml solution, and stored at 4^0C.

Bacteria growing at exponential phase of growth in STR (in batch and chemostats) were diluted in sterile media to an OD_{600} of ~ 0.025. $DIBAC_{4(3)}$ was added to a final concentration of 10 μg/ml, EB of 10 μg/ml and PI of 5 μg/ml respectively. Stained cells were incubated for 30 minutes at 37^0C, in the dark, before FC analysis.

Under 488 nm laser beam excitation, PI fluorescence was measured above 630 nm, EB fluorescence at 575 nm, and $DIBAC_{4(3)}$ fluorescence at 525 nm. Compensation was used to minimise fluorescence spill-over. The population was gated as active pumping cells that stains with neither of the dyes ($DIBAC_{4(3)}^-$, $EtBr^-$, PI^-), de-energised cells ($DIBAC_{4(3)}^-$, $EtBr^+$, PI^-), depolarised ($DIBAC_{4(3)}^+$, $EtBr^+$, PI^-) and permeabilised cells ($DIBAC_{4(3)}^+$, $EtBr^-$, PI^+).

However, $DIBAC_{4(3)}$ uptake depends on cell size. Active cells that maintain MP will take up less dye than depolarised cells. However, depolarised cells of different volumes contain different amounts of dye, irrespective of their membrane potential, because the concentration of the dye reflects the membrane potential. The flow cytometry measures the amount, not concentration (Shapiro, 2005).

3.9 Monitoring heterologous protein production through flow cytometry

The heterologous protein is GFP mut3*, as described in Section *Materials and Methods 3.1 E. coli strains*. The strength of GFP lies in that the fluorophore forms from moieties from its own polypeptide chain, requiring no co-factors for maturation, other than oxygen and 37^0C temperature (see Section *2.2.1 Green Fluorescent Protein (GFP) – The Green of Biology*). Thereby, the emitted fluorescence intensity is a direct readout of heterologous protein production. The GFP mut3* expression was monitored in combination with PI staining for the assessment of viability, using Attune NxT Acoustic Focusing Flow Cytometer (Life Technologies, CA). PI staining was described previously (Section *3.7 Monitoring membrane integrity with FC).*

Using gating on FSC and SSC, dead cells and debris were eliminated from analysis (*Figure 2.5 A*). GFP was excited by the 488 nm laser and its signal was detected using a 530/30 bandpass filter in the BL1 channel. The red fluorescence of PI was detected using a 574/26 bandpass filter in the BL2 channel.

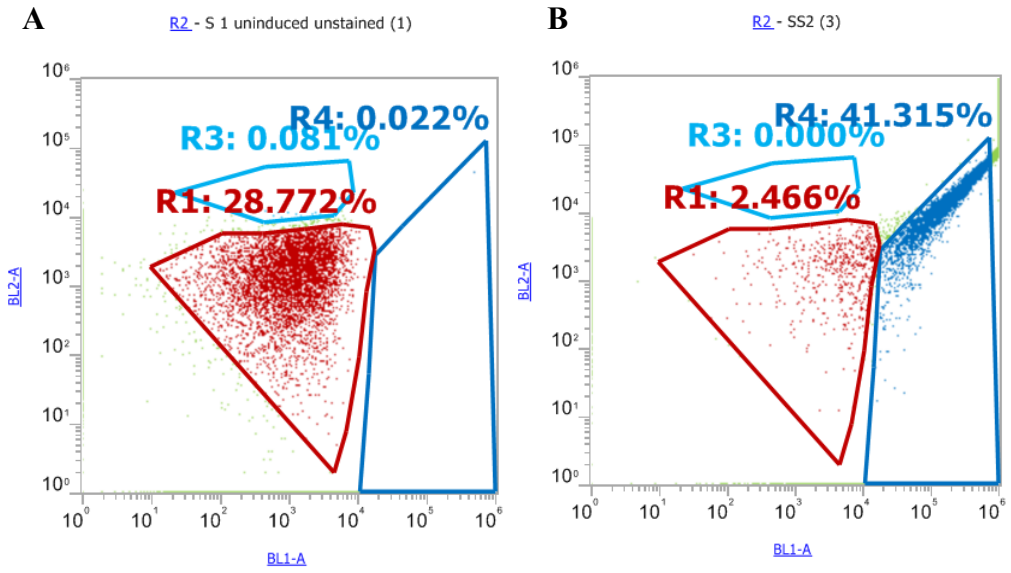

Figure 3.8. Fluorescence data of recombinant *E. coli* CLD1301. A: no inducer (0 mM IPTG); B: 1mM IPTG. BL1 (x-axis) is fluorescence intensity of GFP. BL-2 (y-axis) is the fluorescence intensity of PI. There are three subpopulations: R1 (non-induced cells), R3 (dead cells) and R4 (induced cells). Below 10^4 on BL1 channel are non-induced cells.

GFP fluorescence intensity (BL1, x-axis) was plotted on a log scale against the fluorescence intensity of PI (BL2, y-axis). Signals were amplified with the logarithmic mode so that the background fluorescence of non-induced cells was below 10^4 (*Figure 3.8*). Thereby, a 100-fold increase in fluorescence over background is observed for *E. coli* CLD1301 in the presence of 1 mM IPTG (*Figure 3.8*). The fluorescence of GFP mut3* is known to be very stable, hence it was safely estimated that its half-life was 33 hours (Sanders and Jackson, 2009). Within the following experiments, mature GFP mut3* remained fluorescent in liquid cultures up to three weeks post-harvest (data not shown), thus it was completely stable within the following experiments.

Cells from STR were diluted in PBS to an OD of ~ 0.025 (as described in Section *3.5.4 Total cell counts*). PI 4.3 mM in water was added to each 300 µl of sample for 43 µmol/l final concentration to quantify for dead cells. Samples were briefly vortexed and incubated in the dark at room temperature for 5 minutes prior to analysis.

3.10 Phase and fluorescence microscopy of *E. coli* W3310

Phase and fluorescence microscopy were applied for the study of cell viability ($SYTO_9$/PI), cell morphology and stress ($DISC_{3(5)}$) in *E. coli* W3110.

Viability as a function of membrane integrity of the cell was monitored with BacLight™ (Live/Dead Bacterial Viability Kit, L-7007, Molecular Probes), a dual staining kit containing the green fluorescent $SYTO_9$ and red-fluorescent PI (Kimura *et al*., 2017, Yoon *et al*., 2019). PI (described in Section *3.5.4 Total cell counts*) is suitable for both FC and FM. The dyes show different spectral characteristics (*Figure 3.9*) and abilities to penetrate bacterial cells. $SYTO_9$ stains "live" cells green, and PI stains "dead" cells red.

Samples of 1 ml were collected from STR and centrifuged at 10000×g for 1 minute, to remove the supernatant. The cell pellet was suspended in PBS (1x), and further diluted to OD_{600} of ~ 0.5 in PBS (1x). A "killed" control was obtained by suspending the cell pellet in 70% isopropyl alcohol, incubating in a shaker for 1 hour, followed by centrifugation to remove the alcohol.

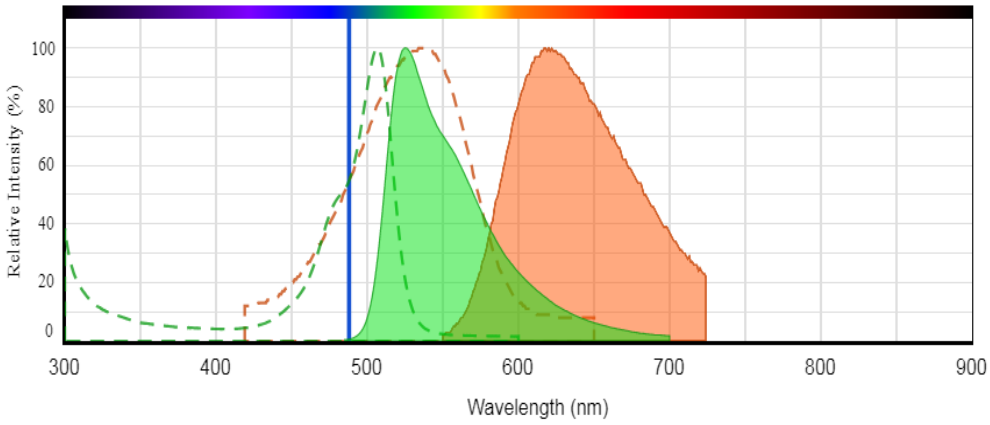

Figure 3.9. Excitation (dotted line) and emission (solid line) spectra of $SYTO_9$ (green) and PI (red). Horizontal blue line represents 488 nm laser. Figure was produced using Life Technologies Fluorescence Spectra Viewer.

The kit contains 3.34 mM $SYTO_9$ and 20 mM PI, both in DMSO. A 1.5 µl volume of an equal proportions of $SYTO_9$ and PI, as provided in the kit, was used to stain 500 µl sample with OD_{600} of ~ 0.5, briefly vortexed and incubated in the dark under shaking for 15 minutes.

A solution of 1.2% electrophoresis grade agarose in RO-water was prepared and maintained at 60°C for up to a week. For slide preparation, 500 µl of molten agarose solution was pipetted onto a Teflon coated Hendley-Essex multispot slide and quickly covered with a regular microscopic slide. The agarose layer was allowed to solidify at RT for 10 minutes. Slides prepared in this manner were used within one hour. The top regular slide was carefully removed and 0.5 µl stained cell suspension was pipetted onto the agarose-coated slide, allowed to air dry and covered with a 18 x 24 mm coverslip. The coverslip addition leads to anoxia, so for microscopy using the MP dye, $DISC_{3(5)}$, the coverslip was added just before imaging.

For MP measurements using $DISC_{3(5)}$, cells suspended in pre-warmed media with OD_{600} of ~ 0.5, were stained with 2 µM $DISC_{3(5)}$ directly in the growth media. Cells were incubated at 37^0C for 5 minutes under 200 RPM shaking, in 2 ml Eppendorf with perforated lids, followed by fluorescence microscopy. A calibration was made to convert the fluorescence of $DISC_{3(5)}$ into absolute MP values, using the Nernst equation to calculate the K_{out} values (mM) corresponding to desired K^+ equilibrium potentials. The intracellular potassium in *E. coli* is about 300 mM (Kuhn and Kellenberger, 1985). The K_{out} values calculated using the Nernst equation were used to prepare reference buffers with different K concentrations. To maintain a 300 mM ionic strength in each buffer, NaCl was added accordingly. K existing in the media (22 mM) was included in calculations, and the cells were imagined in the presence of valinomycin at OD_{600} ~ 0.2 (see Appendix E).

The microscopy was carried out using a Nikon TI-SH-W inverted fluorescence microscope (Nikon GmbH, Dusseldorf, Germany) with motorised stage (Nikon GmbH, Dusseldorf, Germany), with the Nikon Perfect Focus System and a Nikon Plan Apo 100x/1.40 Oil Ph3 objective. For phase contrast imaging, a pE-100 Cool LED illumination unit was used. For fluorescence imaging, a mercury light source was used (Intensilight, Nikon GmbH, Dusseldorf, Germany). The images were acquired with an Andor Zyla 5.5 Mpixel camera (Andor Technology Ltd., Belfast, UK) and saved as standard Nikon nd.2 files, using the NIS Elements imagining software (Nikon, version 4.51).

$SYTO_9$ signal imaging was analysed with a green FITC filter (EX 465-495 nm, DM 505 nm, BA 515-555 nm, Nikon GmbH, Dusseldorf, Germany). A TRITC filter (EX 540/25 nm, DM 565 nm, BA 605/55 nm, Nikon GmbH, Dusseldorf, Germany) was for PI signal imaging. A common CY5 filter (EX 620/60 nm, DM 660 nm, BA 700/75 nm, Nikon GmbH, Dusseldorf, Germany) was used to image the $DISC_{3(5)}$-stained cells.

3.11 Phase and fluorescence microscopy of *E. coli* CLD1301

Phase and fluorescence microscopy were applied for the study of protein production, viability (GFP/PI), cell morphology and stress (GFP/$DISC_{3(5)}$) in induced *E. coli* CLD1301. Non-induced recombinant *E. coli* were analysed for viability ($SYTO_9$/PI), cell morphology and stress ($DISC_{3(5)}$).

Cells were immobilised as described for *E. coli* W3110 (see Section *3.10 Phase and fluorescence microscopy of E. coli W3110*). Non-induced *E. coli* CLD1301 cells were stained with both $SYTO_9$ and PI for viability assessment (see Section *3.10 Phase and fluorescence microscopy of E. coli W3110*). Induced *E. coli* CLD1301 cells were stained only with PI to monitor viability as the expressed GFP mut3* has the same emission spectrum as $SYTO_9$, so they cannot be used simultaneously.

0.5 µl stained cell suspension was pipetted straight onto a slide and covered by an 18x24mm coverslip. Cells were visualised under immersion oil. GFP and $SYTO_9$ use the same green FITC filter (EX 465-495 nm, DM 505 nm, BA 515-555 nm, Nikon GmbH, Dusseldorf, Germany). PI and $DISC_{3(5)}$-stained cells were visualised using TRITC and CY5 filters respectively (see Section *3.10 Phase and fluorescence microscopy of E. coli W3110*). $DISC_{3(5)}$ was used with induced *E. coli* CLD1311 cells to quantify the stress induced by the expression of heterologous protein GFP mut3*, in the virtue of different emission spectra (*Figure 3.10*). Induced *E. coli* CLD1301 cells were analysed for GFP mut3* expression using the FITC filter (EX 465-495 nm, DM 505 nm, BA 515-555 nm, Nikon GmbH, Dusseldorf, Germany), whilst $DISC_{3(5)}$–stained cells were visualised with a CY5 filter (EX 620/60 nm, DM 660 nm, BA 700/75 nm, Nikon GmbH, Dusseldorf, Germany).

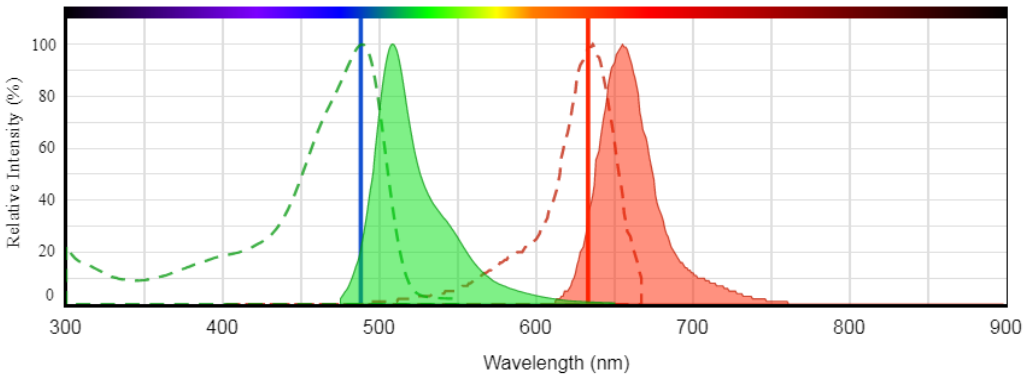

Figure 3.10. Excitation (dotted line) and emission (solid line) spectra of GFP mut3*(green) and $DISC_{3(5)}$ (red). Horizontal blue line represents a 488 nm laser; horizontal red line represents a 633 nm laser.

3.12 Review of fluorophores used in this work

Compound	λ^{ex}_{max} (nm)	λ^{em}_{max} (nm)
GFP mut3*	501	511
$DISC_{3(5)}$	633	669
$SYTO_9$	507	525
Propidium Iodide	534	617
Thiazole Orange	513	532
$DIBAC_{4(3)}$	492	516
Ethidium Bromide	300	603

Table 3.4. Fluorophores used in this study.

3.13 Data acquisition and analysis

FC was performed using an Attune Acoustic Nxt Cytometer® (Applied Biosystems) with Attune Cytometric Software v 3.1 for data acquisition. The instrument is equipped with a 488 nm laser with detectors for: FSC, SSC, and four fluorescence modules BP 530/30 (BL1), BP 574/26 (BL2), BP 695/40 (BL3) and BP 780/60 (BL4). A threshold on SSC was used to eliminate instrument noise. Cell populations were displayed according to their FSC/SSC properties. 5 µl sample volume was selected as a stop for the assessment of viability (TO/PI) and protein production (GFP/PI). 30 µl sample volume was selected as a stop for the assessment of MP, because cells that maintain MP exclude al three dyes in $DIBAC_{3(4)}$/EB/PI. Thus, when counting cells, a "gate" would display the TCCs in 5 or 30 µl respectively at $OD_{600} \sim 0.025$.

Sheath flow rate was 25 µl/min. The data was saved as Flow Cytometry Standard (.fcs) files, which were exported, gated and read at single cell level with Matlab®, and returned as Excel files, with measurements expressed in arbitrary units (A.U.) or percentages (%).

Microscopy data was acquired as Nikon.nd2 files. The files were read using ImageJ v.1.48 (National Institute of Health) in an automatic manner, with a specific workflow run constructed as an ImageJ/Fiji macro. The results were saved as an Excel file, which was analysed for protein production and three shape descriptors: Circularity, Area and AR. Imaging data from mid-exponential phase of growth contains mostly individual bacterial cells, but during continuous cultivations, the cells were agglutinated together. To allow single cell image analysis, the clumps of cells were removed from the data sets by filtering the population on both aspect ratio AR (1 - 6) and cell area (0.5 - 4.5 μm^2). An AR > 6 removes two daughter cells not separated at birth, but it may remove a single filamentous cell where division stopped. The 4.5 μ^2 upper limit for cell area was chosen as a cut-off point for a single cell, considering anything above 4.5 μ^2 as a clump of cells. Data with the outliers removed was saved as an Excel file.

Excel files from both FC and FM were transferred into Minitab® Statistical Software for statistical analysis and data visualisation as boxplots. A significant normal distribution was absent in all analysed data sets, motivating a $\log_{10}$ transformation to be conducted. Following $\log_{10}$ transformation, normality was tested once again. The absence of a significantly normal data distribution led to the use of Mann–Whitney U/Kruskal–Wallis non-parametric tests for testing the significance of the observed differences between groups.

CHAPTER 4

RESULTS

Chapter 4 Cell dynamics in non-recombinant *E. coli* W3110 on glucose.

4.1 Abstract

Predicting individual cell states in an industrial reactor is impossible due to a continuously changing environment, adding to the inherent stochasticity of molecular events. Substrate gradients accentuated by poor mixing are most important for emulating heterogeneity at large scale. Cells grow at a maximal rate μ_{max} in the feeding zone where there is excess nutrient, whilst those at the bottom of the fermenter grow at a slow rate μ, as there is very little nutrient. To understand large-scale heterogeneity in a laboratory-scale STR, cells in balanced growth are required. Cells growing at a constant μ are in balanced growth, a "steady state" in which every cell property increases by the same factor.

This work illustrates the heterogeneity of host *E. coli* W3110 in lab-scale fermentations in STR. To model the heterogeneity of a large-scale fermentation, single cells were observed at two growth rates:

1. The mid-exponential point of a batch culture, where cells grow at $\mu_{max;}$
2. A "steady state" of continuous cultivation, where cells grow at ½ μ_{max}.

The analysis focused on membrane integrity, membrane potential and cell morphology.

4.2 Introduction

E. coli is the main workhorse for expressing non-glycosylated proteins. Its preferred C source is glucose, because it is easily accessible and promotes fast growth (Brückner and Titgemeyer, 2002). It is assumed that cells consume glucose instantaneously, initiating a glycolytic pathway. However, fast growth rates consuming glucose lead to formation of by-products, mainly acetate (Luli and Strohl, 1990). The acetate secretion is a major constraint of high productivity in industrial fermentations as it inhibits growth and decreases biomass, affecting the productivity of recombinant proteins.

The understanding of cellular heterogeneity at large scale is imperative for the development of efficient and cost-effective bioprocesses. Flow cytometry and microscopy were used to determine cell physiology and productivity at single-cell level in host *E. coli* W3110, enabling the determination of a baseline heterogeneity. Two methods of cultivation were utilised to keep cells in "balanced growth" at different growth rates to emulate industrial fermentations.

Firstly, batch fermentations were characterised as they achieve maximal growth rate μ_{max} during the exponential phase. Secondly, a reduced growth rate of ½ μ_{max} was set by the dilution rate D in continuous cultivations. Chemostat fermentations demanded initial experiments in batch to confirm two prerequisites:

a) Identifying the nutrient that stoichiometrically limits growth (discussed in Section *4.3 Determination of the single media limitation on glucose*);

b) Establishing the dilution rate D, which fixes the growth rate (discussed in Section *4.4 Determination of growth rate μ*).

4.3 Determination of the single media limitation on glucose

A single limiting substrate is necessary for chemostat growth. To confirm the growth limiting nutrient is the C source (glucose), triplicate batch cultivations were conducted with host *E. coli* W3110 using BioLector (m2p-labs GmbH, Baesweiler, Germany), as described in Section *3.4.1 Batch cultivations in Microtiter Plates*. The minimal media used to support growth was prepared as described in Section *3.3.1 Batch mineral media*. The expectation is that the growth limiting concentration of glucose, ascertained from biomass yields is 4 g/L.

To verify that glucose was the limiting nutrient, six media of different composition were screened. The glucose concentrations (g/L) were 1, 2, 3, 4, 7 and 10, whilst all other components remained unchanged and in excess (*Figure 4.1*). A well with sterile media was used as plate standard for control of contamination. Biomass (A.U.) was recorded online as 620 nm scattered light, in 15 min cycles. The initial scattered light (A.U.) of six consecutive points was deducted from the measured data to subtract the light scattered by media components, similar to blanking in a spectrophotometer. The inoculum was 20 µl freshly grown *E. coli* W3110 culture in exponential phase of growth with $OD_{600} \sim 2$, which gives an initial $OD_{600} \sim 0.05$ at inoculation (time 0).

The final biomass in stationary phase was averaged between 10-20 h and compared as a function of the glucose concentration (g/L). The final biomass (A.U.) correlated with the concentration of glucose up to 4 g/L (*Figure 4.2*) confirming glucose was the growth-limiting factor. The correlation was not linear at glucose concentrations of 7 and 10 g/L, so a further limitation must be effective in this range (*Figure 4.2*).

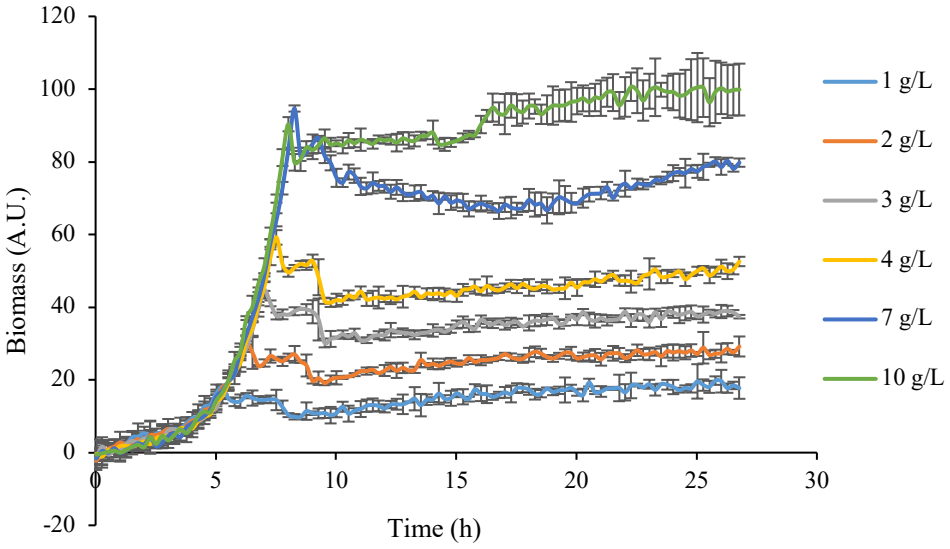

Figure 4.1. Influence of different glucose concentrations on growth of *E. coli* W3110 without IPTG. Online monitoring of biomass (scattered light). Conditions: minimal media with up to 10 g/L of glucose, T = 37^{0}C, V_L = 800 µL, n = 1500, d_0 = 3 mm. Standard error bars represent ± S.D.

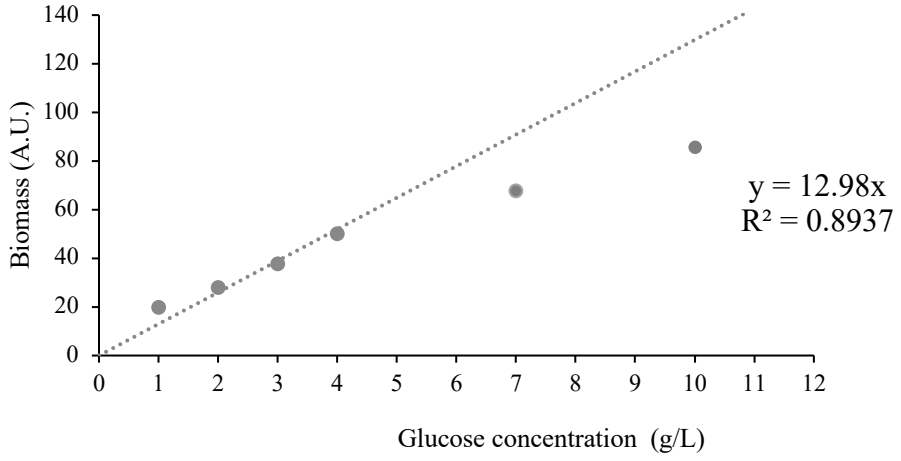

Figure 4.2. Biomass (A.U.) variation (between 10 - 20 h) over glucose concentration (g/L). Each biomass value is the average of triplicate results. A linear relationship indicated that the nutrient was in the limiting range. Conditions: minimal media with glucose concentrations (w/v) including 1, 2, 3, 4, 7 and 10 g/L, while other media components remained unchanged and in excess, T = 37^{0}C, V_L = 800 µL, n = 1500, d_0 = 3 mm.

4.4 Determination of growth rate μ

Determining the growth kinetics of *E. coli* W3110 is required for its application as a cell factory for RPP. The most important parameter for creating cell phenotypes is the specific growth rate μ (h^{-1}). The growth rate of cells near the feeding point of an industrial reactor is μ_{max} (h^{-1}). Contrastingly, near the bottom of the fermenter, the growth is nutrient limited, chosen as ½ μ_{max} (h^{-1}).

The μ_{max} for 4 g/L glucose concentration was calculated using the increment of the natural logarithm of biomass (recorded by BioLector) plotted against time (*Figures 4.3* and *4.4*). At least five points during exponential growth were used. At μ_{max}, there was sufficient nutrient and growth was not inhibited by any by-products.

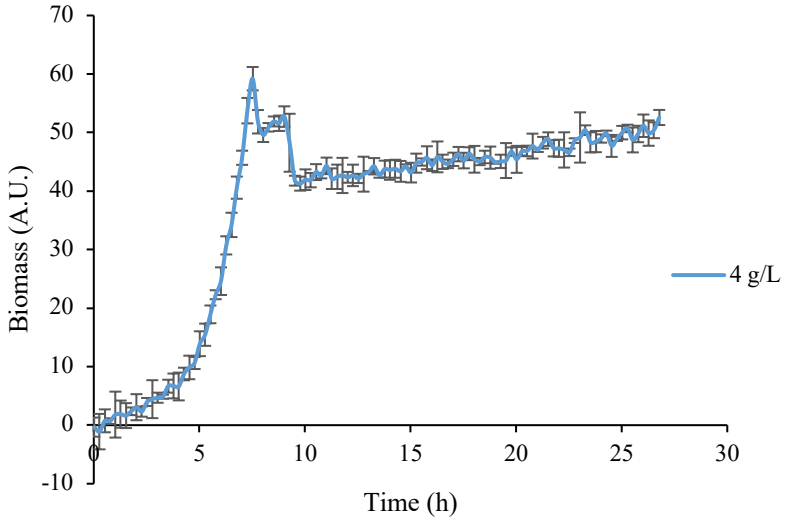

Figure 4.3. Growth of *E. coli* W3110 without IPTG. Biomass (A.U.) as scattered light. Conditions: minimal media 4 g/L glucose, T = 37^{0}C, pH = 7, V_L = 800 μL, n = 1500, d_0 = 3 mm. Standard error bars represent ± S.D.

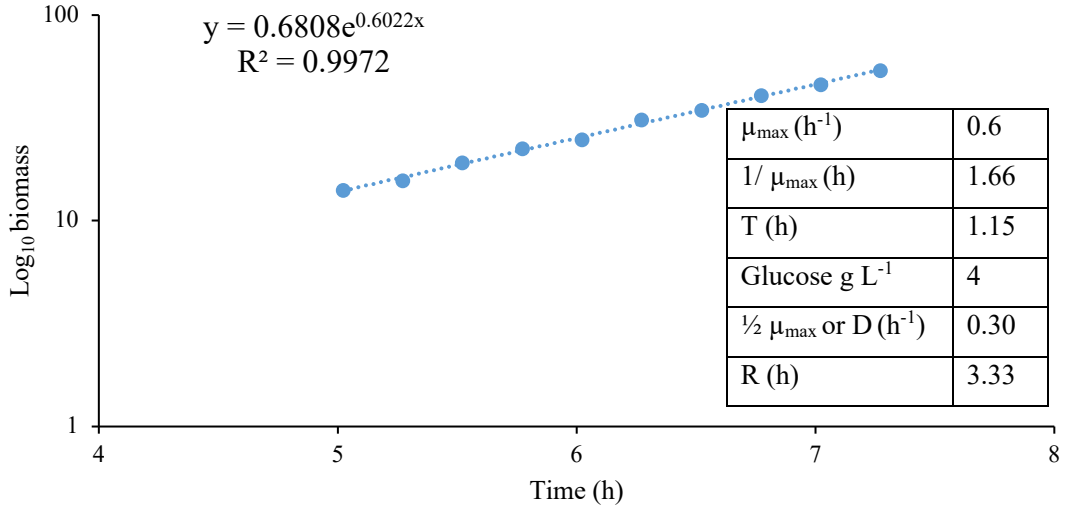

Figure 4.4. Maximum growth rate μ_{max} of *E. coli* W3110. Biomass (A.U.) was recorded as scattered light. Conditions: minimal media 4 g/L glucose, T = 37^{0}C, V_L = 800 µl.

As the plot *(Figure 4.4)* indicates, μ_{max} for *E. coli* W3110 in glucose minimal media is 0.6 h^{-1} with T_d of 1.15 h. The specific µ in chemostat is 1/2 μ_{max}, a rule of thumb to obtain a stable system and avoid washout, thus the corresponding µ for chemostat growth is 0.3 h^{-1} with T_d of 2.3 h. A period of five residence times (R=1/D; *Figure 4.4*), calculated at ~ 15 h was allowed for the system to reach a steady state.

4.5 Cell dry weight determination (CDW)

The biomass, as cell dry weight (CDW) is important in biotechnological processes. The initial concentration of the glucose ($C_6H_{12}O_6$, MW=180 g/mol) in the media was 4 g/L. Glucose was the limiting factor, while other components were in excess (Appendix A). The amount of elemental C in 1 mole of substrate is 72 g, thus the amount of C in a media with 4 g/L glucose is 1.6 g/L. Approximately 50% of carbon (0.8 g) is converted to biomass during metabolism. The elemental C in biomass represents 50% of the CDW, thus the maximum CDW expected at "steady state" in chemostats in fully aerobic cultures is 1.6 g/L, assuming no formation of by-products.

Growth was monitored during the exponential phase as offline OD_{600} (measured by spectrophotometer) and as online Bug Units (with the BugLab sensor). The measurements

were correlated to the weight of the cell pellet, following oven drying at 100°C. A linear correlation exists between OD_{600}, Bug Units and CDW in the exponential phase of growth (*Figure 4.5*). Due to this, OD_{600}, Bug Units and CDW were used interchangeably, although all are population level measurements that do not account for cellular heterogeneity. $OD_{600} \sim 1$ resulted in 0.354 g/L CDW and 1.762 Bug Units (*Figure 4.5*). A major assumption of this calibration is that the cell morphology and average cell size do not change.

The following equations were used to convert the OD_{600} and Bug Units values into CDW for *E. coli* W3110, with or without the recombinant plasmid:

$$1\ g\ CDW/_L = 0.354\ OD_{600} \tag{4.1}$$

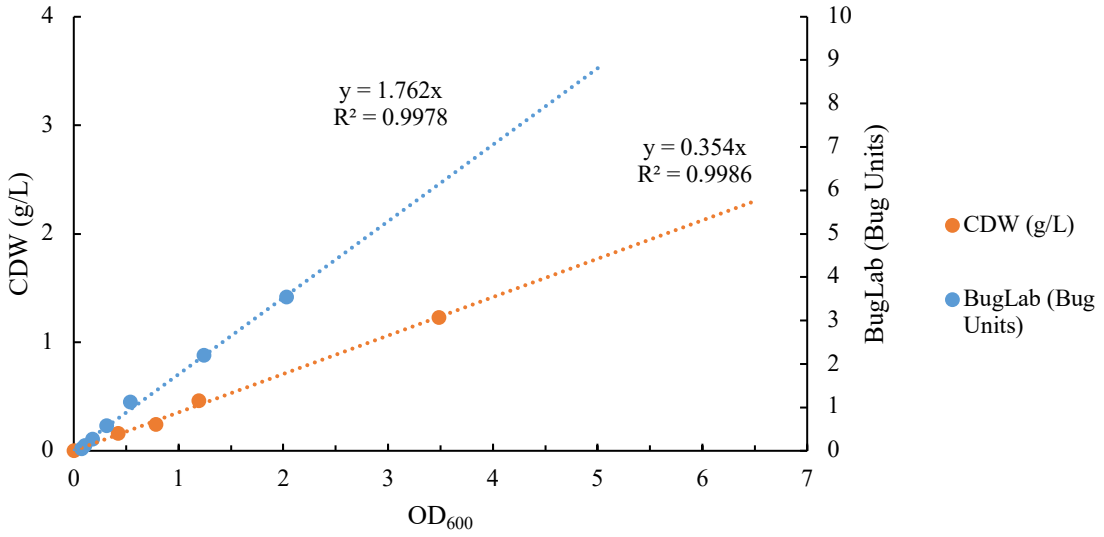

Figure 4.5. Calibration of OD_{600} and Bug Units to CDW. The exponential phase converted into CDW shows a linear regression equation with a high correlation coefficient (R^2).

4.6 Process monitoring at population level

Batch and continuous fermentations were carried out in a 3 L Applikon bench-top reactor (Applikon Biotechnology B.V., Schiedam, Netherlands). The process parameters were summarised in *Table 3.3*. The cultivation comprised of an initial batch phase, followed by a second continuous cultivation phase commencing just past mid-exponential point, when $OD_{600} \sim 2$.

Media for the initial batch phase was prepared as described in Section *3.3.1 Batch mineral media*. Media for the second continuous cultivation phase was described in Section *3.3.2 Chemostat mineral media.* Continuous feeding started just past the mid-exponential point of growth at a constant flow rate (450 ml h^{-1}), and chemostat controls were initiated. The media was aseptically metered using a peristaltic pump (RPM = 30) on the inlet, with concomitant removal of the culture broth using a pump set at maximum on the outlet.

Dilution rate D (h^{-1}) was calculated by monitoring the amount of feed introduced in 24 hours. The nominal flow rate ensured a dilution rate D at 0.3 h^{-1}, with T_d of 2.3 h. Five residence times (~15 h) were allowed to reach "steady state", defined as constant biomass and DO at population level.

As *Figure 4.4* shows, μ_{max} is 0.6 h^{-1} during the exponential phase of batch.
In line with a T_d of 1.15 h, exponential growth sampling occurred every 1 hour.
In line with a T_d of 2.3 h, chemostat growth sampling occurred every 2 hours.
The inoculation in initial batch phase was time = 0. For monitoring of the bioprocess, sampling was as detailed in *Table 4.1.*
Single cell analysis, FC and FM were applied to *E. coli* W3110 cells growing in "balanced growth" at 0.6 h^{-1} (S_4/S_5) and 0.3 h^{-1} (SS1→SS8). Where IPTG was used, a constant 1 mM was maintained in the reactor, by injecting "in bolus" 15 ml 0.1 M IPTG in STR and adding 20 ml 1M IPTG to the 20 L feeding carboy.

Remarks on sampling:

Batch sampling		Chemostat sampling
	Switch from Batch to Continuous at 5.5 h	SS1 (20.5 h)
		SS2 (22.5 h)
S_0 (5 min)		SS3 (24.5 h)
S_1 (1 h)	Allow 5 residence times R ~15 h to reach steady state (SS)	SS4 (26.5 h)
S_2 (2 h)		SS5 (28.5 h
S_3 (3 h)		SS6 (30.5 h)
S_4 (4 h)		SS7 (32.5 h)
S_5 (5 h)		SS8 (34.5 h)

Table 4.1. Sampling during batch and continuous cultivation of *E. coli* W3110 on minimal media with glucose as sole C source (in units of time post inoculation).

Population level monitoring

CPPs (pH, temperature, DO) were controlled at desired set points. To avoid oxygen limitation, a DO of 50% was assured by the automatic increase of the stirrer speed between 250 and 900 RPM. Supporting aerobic metabolism is important as *E. coli* is facultative anaerobic, meaning it switches easily between aerobic and anaerobic pathways. Oxygen levels are even more important for the recombinant strain, as oxygen is the only component needed for the maturation of the heterologous protein, GFP mut3*. The temperature was set to 37^0C, as optimum temperature for the folding and maturation of GFP mut3*.

Bacterial growth was monitored online with the BE2100 Biomass Monitor (BugLab, LLC, Concord, CA), offline as OD_{600} and at-line as TCCs. The supernatant of each sample was analysed for residual glucose and VFAs, with high performance ion chromatography (HPIC).

The inoculum for STR was the second seed culture (see Section *3.2 Cell expansion and seed preparation*), maintained in the exponential phase at OD_{600} ~ 2. As this culture was expanded with the same growth media, there was no observable lag phase in the STR (*Figure 4.6*). The culture followed an exponential phase from the start, with biomass (Bug Units) increasing rapidly, with a reduction of DO as oxygen was increasingly depleted during the exponential

phase (*Figure 4.6*). Soon after the mid-exponential point (5 h), the cultivation was switched to a continuous mode of operation. The biomass (Bug Units) continued to increase post-switching, as the amount of glucose in the STR was not yet limiting.

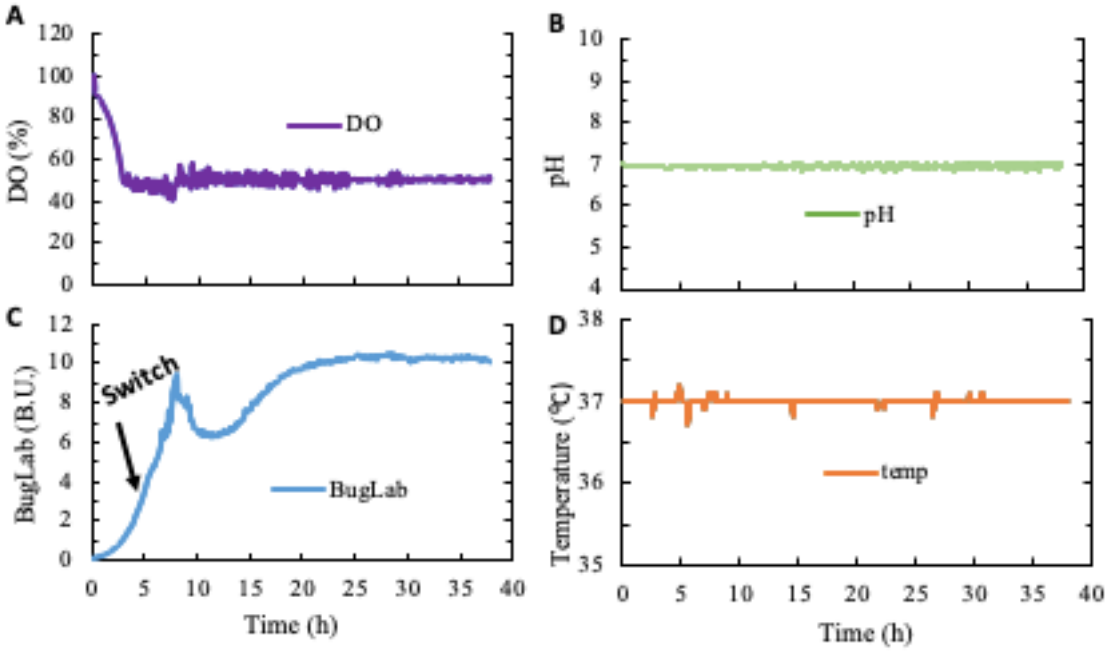

Figure 4.6. Fermentation profile of *E. coli* W3110 on glucose minimal media, no IPTG. This includes changes in dissolved oxygen (A) and biomass (C), whilst pH (B) and temperature (D) are maintained constant at set-points. The cultivation starts at inoculation time = 0, following a batch mode until mid-exponential point is reached at 5.5 h. Thereafter, the culture is switched to continuous mode and 15 h are allowed to reach a "steady state" (arrow indicates the switch).

Monitoring growth

Growth was measured throughout the fermentation as population level OD_{600} and single-cell level TCCs (*Figure 4.7).* The relationship between these two measurements was assessed at growth rates of 0.6 and 0.3 h^{-1}. OD_{600} was a linear function of TCCs during the exponential phase of batch (5 h), up to $OD_{600} \sim 2$ (*Figure 4.8*). An OD_{600} of 1 corresponds to 1.74 $x10^8$ cells/ml. The cell concentration (cells / [ml*OD_{600}]) after 4 doubling times T_d was 1.58 x 10^8.

At $\mu = 0.3\ h^{-1}$, the cell concentration (cells / [ml*OD_{600}]) at "steady state" varied from 1.01 x 10^8 at 22.5 h to 1.38 x 10^8 at 24.5 h (*Figure 4.7 B*). Cells growing at 0.3 h^{-1} (*Figure 4.7* B) were compared against those at 0.6 h^{-1} (*Figure 4.7 A*) based on the assumption they were all the same size. The cell concentration at 22.5 h (for $\mu = 0.3\ h^{-1}$) and 5h (for $\mu = 0.6\ h^{-1}$) varied by a factor of 1.57. This suggests that at different growth rates, cells must be either counted directly or the cell number per OD_{600} must be known. This justifies single cell analysis for bioprocess monitoring and control.

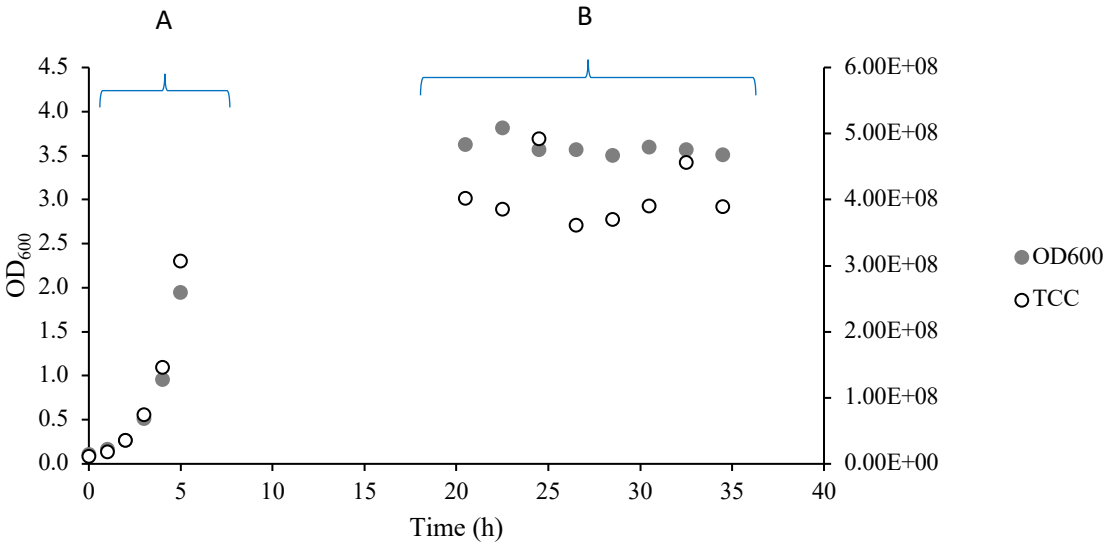

Figure 4.7. Plot of OD_{600} with total cell count (TCCs) for *E. coli* W3110 on glucose minimal media, no IPTG. A) Exponential growth in batch at $\mu = 0.6\ h^{-1}$. B) Growth in continuous culture at $\mu = 0.3\ h^{-1}$. The gap between the two datasets (15 h) is to allow the culture to reach a "steady state".

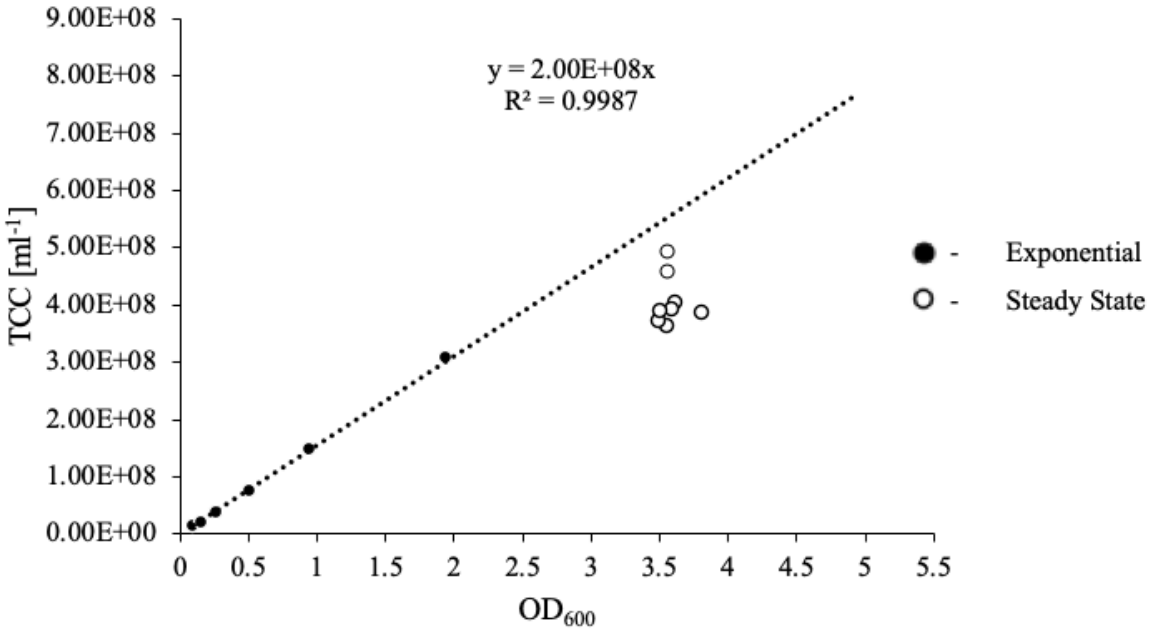

Figure 4.8. Dependence of total cell count (TCCs) over OD_{600} in *E. coli* W3110 on glucose minimal media. Linear relationship observed up to mid-exponential point of growth, when $OD_{600} = 2$.

Monitoring substrate

Glucose concentration was monitored in the absence (*Figure 4.9)* and presence (*Figure 4.10*) of 1 mM IPTG. As the population increased, the glucose depleted from 4 g/L to 2.04 g/L at the mid-exponential point of growth. In glucose-limited chemostats, the residual glucose at "steady state" fluctuated between 0.0013g/L (7.3711µM) and 0.0132 g/L (73.7111 µM), but never fell to zero (*Figure 4.9*).

As the "steady state" glucose level varied by a factor of 10, it can only be a "steady state" when considered over time, where the variability is averaged out. A slight rise in substrate is a consequence of fewer cells, which would in turn increase the growth rate. Similarly, a slight decrease in substrate is associated with a slight increase in biomass, which would lower the growth rate.

IPTG had no influence on substrate depletion.

Biomass measured as OD_{600} increased during batch culture up to 1.82 - 1.89 at mid-exponential point (5 h) (*Figure 4.9* and *4.10*). At steady state, OD_{600} varies between 3.85 - 4.08 for experiments without IPTG (*Figure 4.9*), and 4.10 - 4.17 in the presence of 1mM IPTG (*Figure 4.10*).

However, optical density does not measure the number of cells directly, but correlates the attenuation of light to the cell concentration.

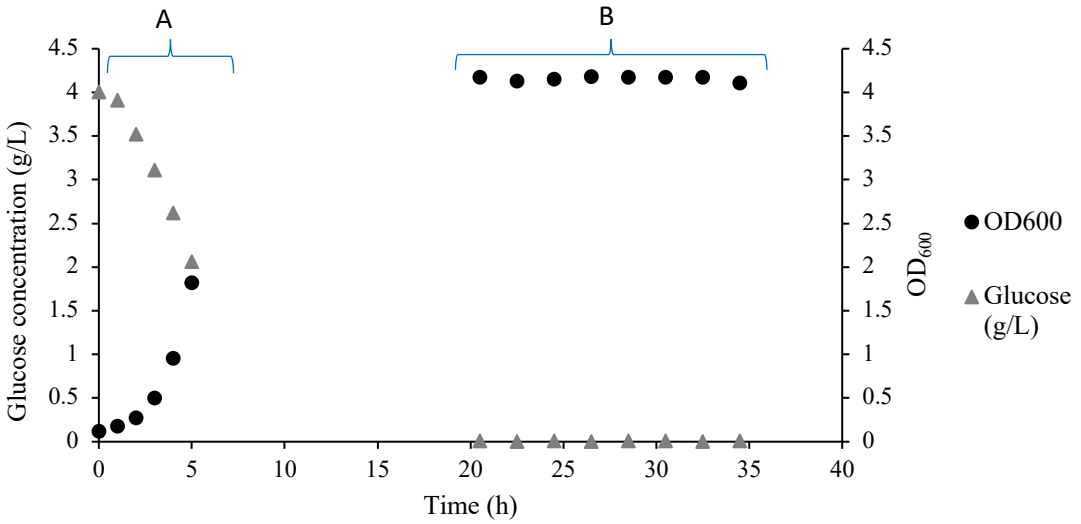

Figure 4.9. Glucose concentration in relation to OD_{600} by *E. coli* W3110 in the absence of IPTG. A: Exponential phase (time 0 - 5 h). B: Continuous cultivation (time 20.5 - 34.5 h).

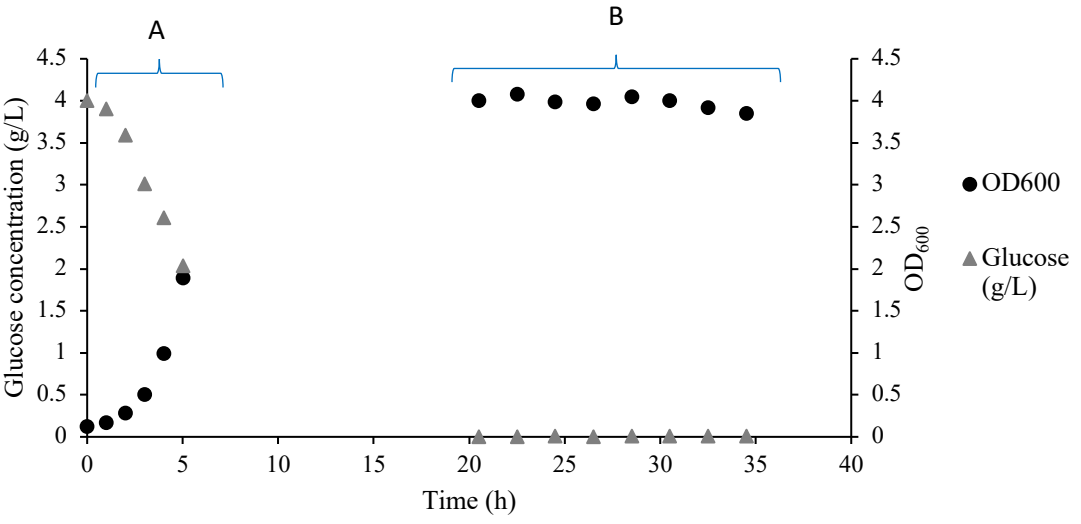

Figure 4.10. Depletion of glucose in relation to OD_{600} development by *E. coli* W3110 in the presence of 1 mM IPTG. A: Exponential phase (time 0 - 5 h). B: Continuous cultivation (time 20.5 - 34.5 h).

Monitoring VFA

Supernatant analysis of *E. coli* W3110 fermentation broth on glucose mineral media showed the presence of both acetate and formate (*Figure 4.11*). The production of VFAs is a major obstacle in the development of a bioprocess because it is a wasteful conversion of valuable carbon that could otherwise be used towards biomass and desired end-products (De Mey *et al*., 2007). The so-called overflow metabolism is growth dependent, producing primarily acetate, although organic acids such as lactate and formate have also been identified (Koh *et al*., 1992, Basan *et al*., 2015).

Results show that during maximal growth on glucose, cells dissimilated both acetate and formate. The acetate formation commenced immediately post-inoculation (time 0), whilst that of formate occurred after 3 T_d (*Figure 4.11*). Both acetate and formate levels increased during growth, reaching 202.36 ppm (2.02×10^{-1} g/L) and 24.73 ppm (2.47×10^{-2} g/L) respectively at mid-exponential point. This is lower than the reported acetate IC_{50} (inhibitory concentration that inhibits growth by 50%) of 0.5 – 1 g/L (Contiero *et al*., 2000, Roe *et al.*, 2002). Additionally, growth at μ_{max} (time 0 – 5 h) exhibits the exponentially growth regime (*Figure 4.11*), and therefore the levels of VFAs reported here are not growth inhibitory.

It is evident, however, that three C sources (glucose, acetate and formate) exist in the media at the mid-exponential point of growth (5 h) (*Figure 4.11*). As glucose was plentiful, shown by growth following an exponential pattern, cells selectively consume glucose as their preferred carbon source. This is known as carbon catabolite repression (Basan *et al*., 2015). Neither acetate nor formate were consumed until the mid-exponential point (5 h), instead they were assimilated in the media, up to the concentrations listed above, that do not inhibit growth. One can see, however, how this might pose a concern in a biotechnological context, if a significant carbon is converted to by-products instead of biomass and target products. Overall, the results indicate that a fast growth is not beneficial for the bioprocess.

At a reduced growth rate in chemostat, acetate and formate levels were diminished, with recorded maxima of 1.89 ppm (1.80×10^{-3} g/L) and 14.38 ppm (1.43×10^{-2} g/L), respectively (*Figure 4.11).* The negligible concentrations of VFAs recorded in chemostat show that cells obtain their energy primarily from aerobic metabolism. This suggests that a reduced growth with a lower glucose level is a viable strategy for minimising the VFAs produced in fermentations. As the available C is directed towards biomass instead of wasteful products,

this shows that a reduced growth is beneficial for the bioprocess and it may further support the use of continuous cultivations for biotechnological applications.

Indeed, chemostat glucose growth also exhibits three carbon sources (carbon, acetate, formate), even if VFAs are negligible. However, as glucose is limiting, any carbon catabolite repression is obsolete (Basan *et al*., 2015). Thus, alternate carbon sources may be co-assimilated when the glucose level is low. Ferenci reported that the cells simultaneously assimilate glucose and acetate, when the residual glucose in chemostats is lower than 5.4 x 10^{-3} g/L (Ferenci, 2008). With residual glucose fluctuating between 1.30 x 10^{-3} g/L to 1.32 x 10^{-2} g/L at "steady state" (*Figure 4.9*), it may be that the substrates are co-assimilated. In this respect, the data does not allow to draw a clear conclusion. Notably, published experimental data often refers to different growth conditions and different strains.

The addition of 1 mM IPTG in control experiments had no influence on the levels of VFAs monitored in continuous *E. coli* W3110 cultivations with glucose as sole carbon source.

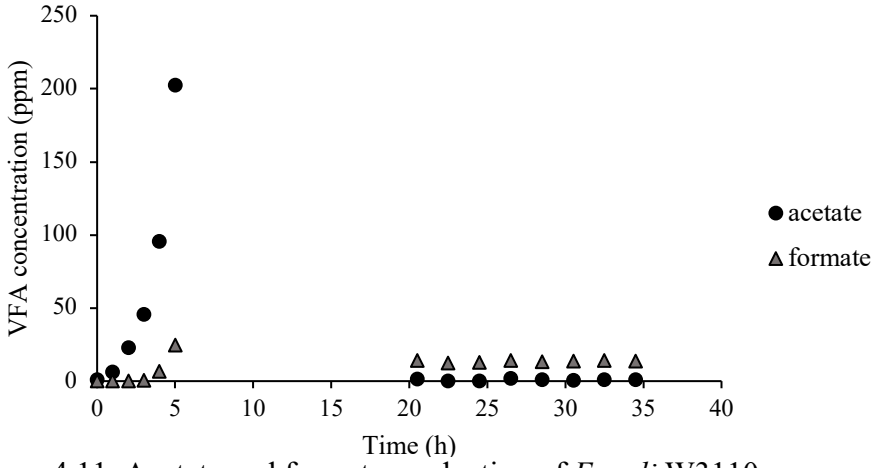

Figure 4.11. Acetate and formate production of *E. coli* W3110 on glucose mineral media without IPTG.

Population level analysis of *E. coli* W3110 with IPTG

To characterise the effect of the inducer (IPTG) on the host *E. coli* W3110, 1 mM was added in continuous cultivations on the glucose mineral media. Cultures were grown aerobically at 37°C, pH of 7, with DO at 50% (*Figure 4.12*).

The starting OD_{600} was 0.05 and a constant 1 mM IPTG was maintained in the STR during the continuous cultivation phase.

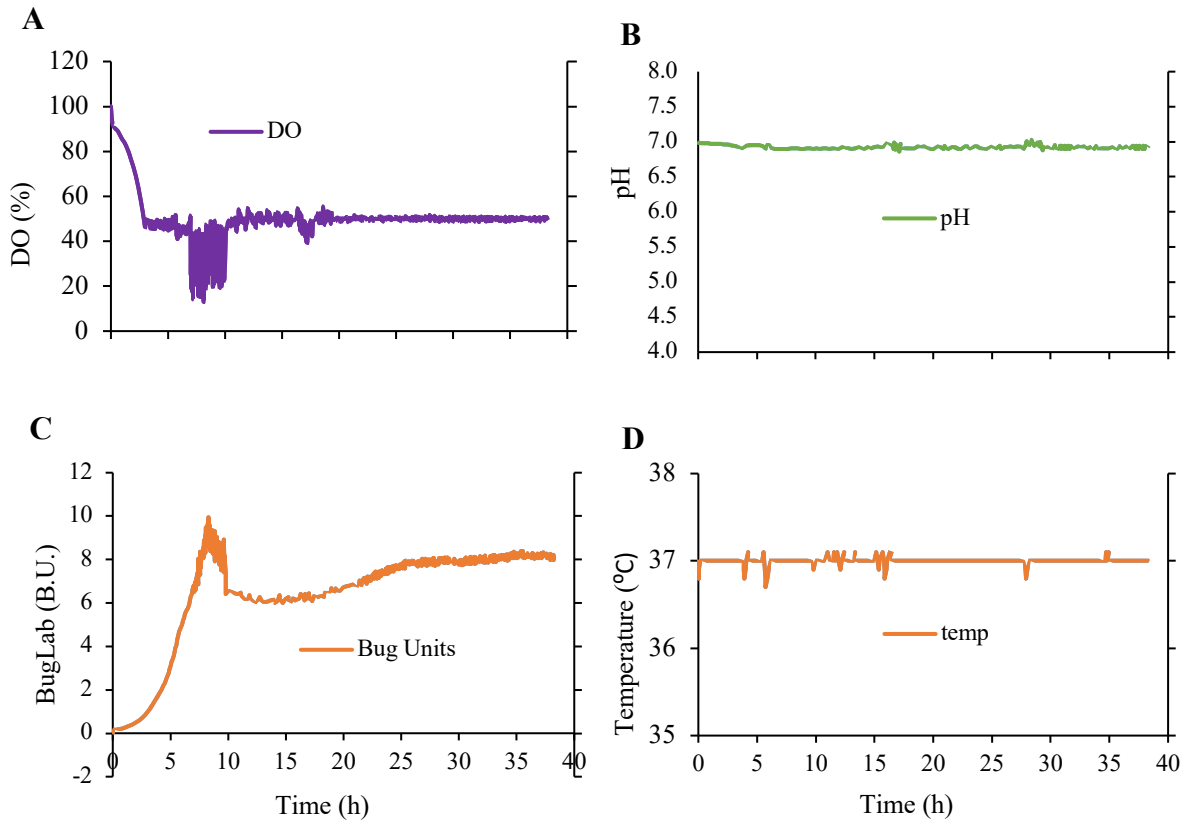

Figure 4.12. Fermentation profile of *E. coli* W3110 on glucose minimal media with 1mM IPTG. This includes changes in dissolved oxygen (A) and BugLab biomass measurement (C). pH (B) and temperature (D) are constantly maintained. Inoculation at 0 h, switched to continuous at 5.5 h, and 15 h allowed for reaching "steady state".

Induced cultures

An additional 1mM IPTG served as an inducer for control experiments. Cells were grown in 0.4% glucose in both the presence and absence of IPTG. The online measurements for biomass with the BugLab sensor are given for host *E. coli* W3110 (*Figure 4.13)*. The difference between the final biomass (arbitrarily chosen past 20 h) in induced and non-induced cultivations was found to be significant (Mann-Whitney, U = 585903, n = 1082, 1082, $p < 0.005$).

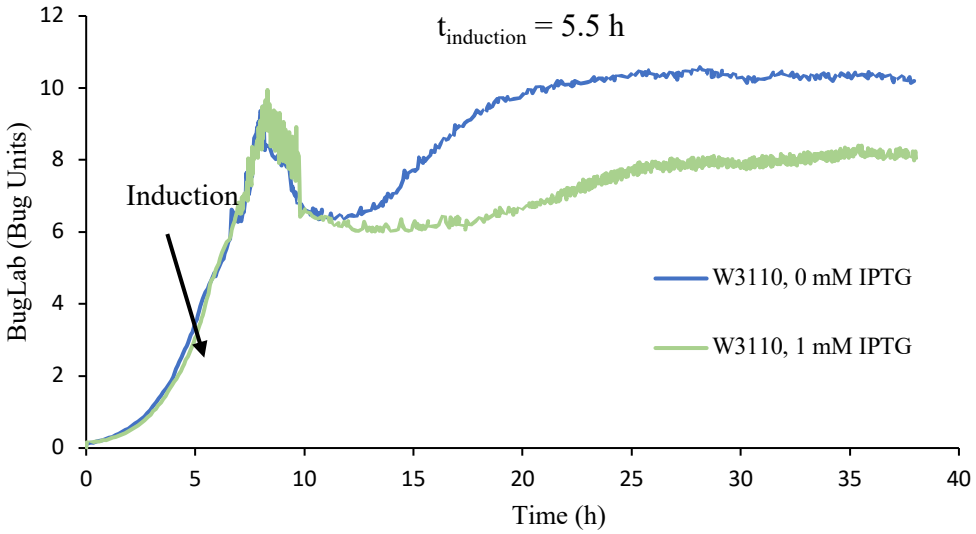

Figure 4.13. Comparison of *E. coli* W3110 biomass (BugLab) as scattered light intensity (B.U.) in non-induced and induced cells. Arrow: time of induction with 1 mM IPTG (mid-exponential at 5.5 h). Conditions: minimal media with 0.4% glucose, T = 37^{0}C, V_L = 800 µL, n = 1500, d_0 = 3mm.

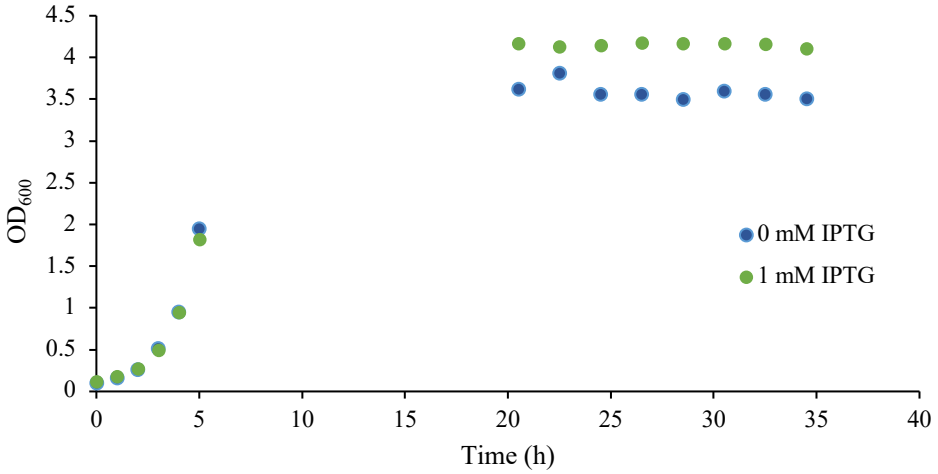

Figure 4.14. Comparison of *E. coli* W3110 biomass (OD_{600}) in non-induced and induced cells. Induction performed with 1 mM IPTG and 15 h are allowed to reach a "steady state".

The median final biomass 10.320 B.U. in media with 0 mM IPTG (X_0) dropped to 7.951 B.U at 1 mM induction (X_1). Thus, the addition of IPTG led to a 22.95% decrease in growth, calculated as "cost" from formula

$$Cost = \frac{X_0 - X_1}{X_0} \; x \; 100 \qquad (4.3)$$

where X_0 and X_1 represent the final biomass on glucose-limited media with 0 and 1 mM IPTG, respectively.

Figure 4.14 shows growth monitored offline as optical density OD_{600}. A lower OD_{600} occurs in non-induced cultures. The difference between the two (*Figure 4.14*) was found to be significant (Kruskal-Wallis, $H = 11.43$, $p < 0.01$).

In the exponential phase of growth, the Buglab sensor data (*Figure 4.13*) was proportional to the optical density (*Figure 4.14*). Contrastingly, at reduced growth rate in "steady state" between 20.5 - 34 h, it was not. *Figure 4.13* shows a higher biomass as scattered light in non–induced cultures, whilst *Figure 4.14* shows a lower biomass as OD_{600} in non-induced cultures. While growth and division are present in continuous culture, shown by an approximately constant biomass (*Figures 4.13* and *4.14*), there is a difference in biomass according to the two measurements. Single-cell analysis was conducted to further determine the contribution of cell numbers and morphological changes to these measurements.

A comparison of the TCC at "steady state" involving both induced and non-induced *E. coli* W3110 (*Figure 4.15*) showed a significant increase of TCC in induced cultures (Kruskal-Wallis, $H = 11.29$, $p < 0.01$). This concurs with the increase in OD_{600} in induced cultures (*Figure 4.14*) and suggests an increased frequency of division in host cells with 1 mM IPTG. It is possible that the addition of IPTG in a glucose-limited environment provides a growth benefit with premature division of cells compared to non-induced cultures. This hypothesis was tested by measuring the aspect ratio (AR) of host cells at "steady state".

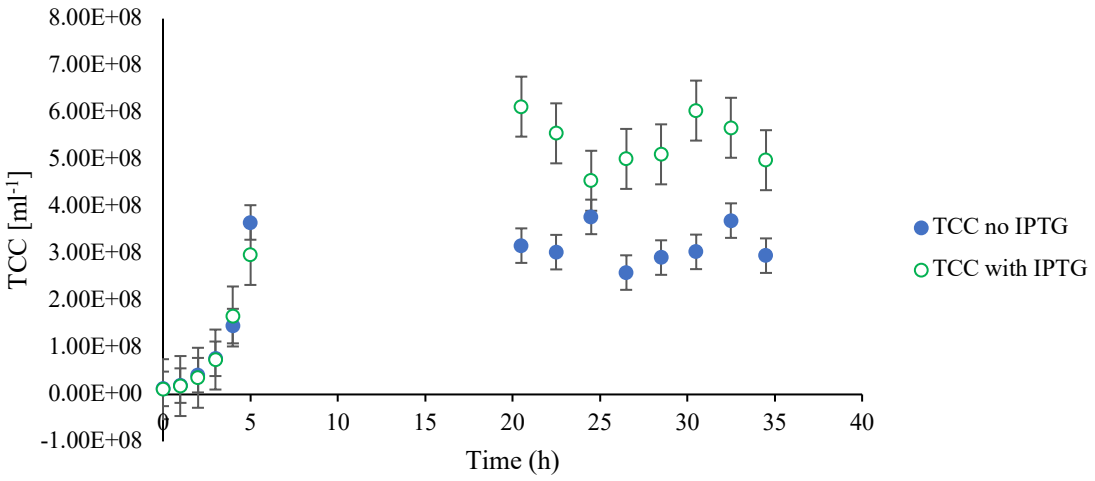

Figure 4.15. Total cell counts (TCC) in three independent experiments. Induction performed with 1 mM IPTG and 15 h are allowed to reach a "steady state". Error bars represent ± S.D.

4.7 Single cell studies of membrane integrity using FC

Cell viability, assessed by membrane integrity was monitored in *E. coli* W3110 growing with glucose as the sole carbon source at two growth rates: μ_{max} and ½ μ_{max}. Samples withdrawn from the bioreactor as described in *Table 4.1* were prepared as detailed in *Section 3.5.4 Total cell counts*. A living bacterial gate (Live) and a dead cell gate (Dead) were set. The detection of TO (green fluorescence) represents viable cells, whilst that of PI (red fluorescence) indicates the dead subpopulation.

For growth at μ_{max} (0.6 h^{-1}), cells in "balanced growth" were obtained around the mid-exponential point of growth, after more than 4 T_d (1.15 h) from initial OD_{600} of 0.05 (see Remarks on sampling, in *Section 4.6 Process monitoring at population level*). Maximal growth has no limitation, thus a maximum viability with healthy cells is expected. The results during the exponential growth phase (0 – 5 h) showed that live (TO^+) cells were over 97% (*Figure 4.16 A*). During chemostat cultivation, while the growth rate is $\mu_{max}/2$, there is a retention of viability (*Figure 4.16 A)*. At "steady state", there is an increase in the percentage of dead cells (staining with PI), ranging from 12 - 16% of cell population (*Figure 4.16 C)*.

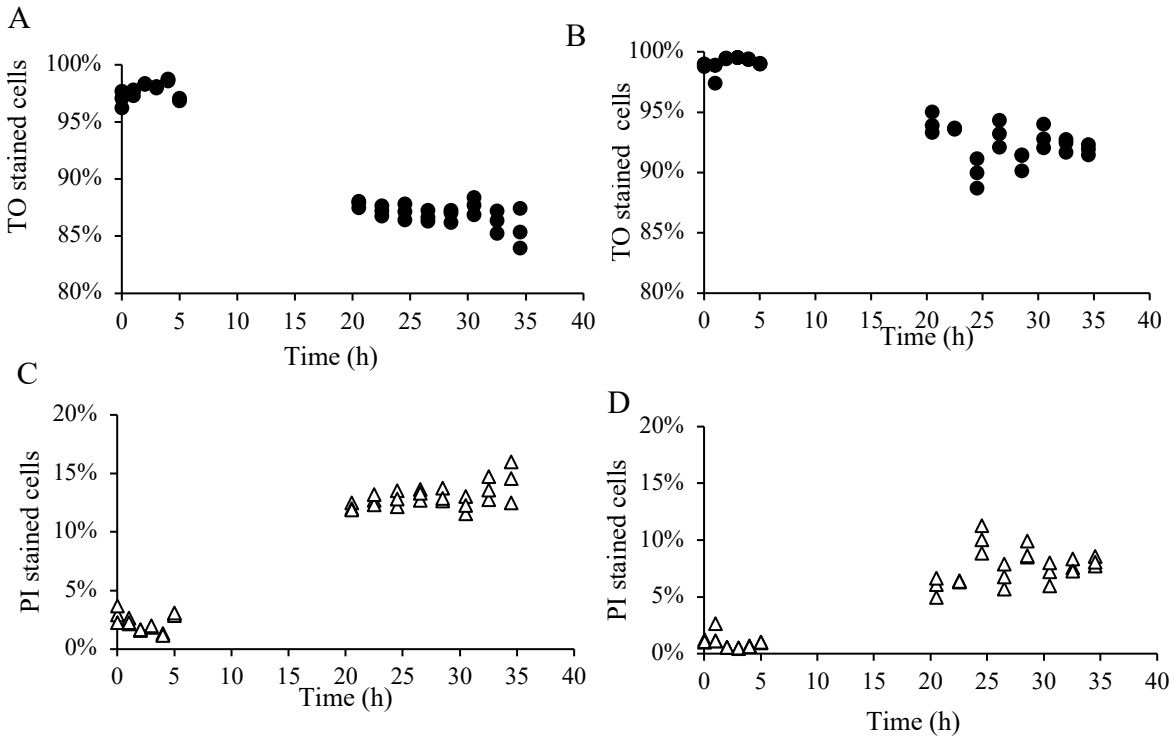

Figure 4.16. Percentage of live (TO^+) cells and dead (PI^+) cells in three *E. coli* W3110 fermentations on glucose. Filled circles represent TO^+ cells, triangles are PI^+ cells. A & C: 0 mM IPTG. B & D: 1 mM IPTG.

4.8 Single cell studies of membrane potential using flow cytometry

MP was analysed using FC and a triple dye combination $DIBAC_{4(3)}$/EB/PI. Cells from the bioreactor were prepared and stained as described in Section *3.8 Monitoring membrane potential with DIBAC/EB/PI*.

Four subpopulations were gated:

a) active ($DIBAC_{4(3)}^-$, $EtBr^-$, PI^-);

b) depolarised ($DIBAC_{4(3)}^+$, $EtBr^+$, PI^-);

c) de-energised ($DIBAC_{4(3)}^-$, $EtBr^+$, PI^-);

d) dead ($DIBAC_{4(3)}^+$, $EtBr^-$, PI^+).

The percentage of each sub-population was evaluated at different growth rates in the presence and absence of 1 mM IPTG.

$DIBAC_{4(3)}$ does not enter active cells that maintain MP. A $DIBAC_{4(3)}$ fluorescence intensity (FI) of 600 A.U. was set as a threshold. Cells exhibiting a higher $DIBAC_{4(3)}$ fluorescence were considered to have undergone membrane depolarisation, where the inside is more positively charged. Most depolarised cells remained impermeable to PI proving PI to be a late indicator of cell death. Upon hyperpolarisation, $DIBAC_{4(3)}$ is excluded from those cells with a decrease in its signal.

At μ_{max} (S5) on glucose media, 83.74% of *E. coli* cells were active, 13.08% were depolarised, 2.30% were dead and 0.87% were de-energised (*Figure 4.17*). Active cells maintained MP and functionality whilst a change in MP towards depolarisation or de-energisation signified a disruption in cell metabolism, with reduced functionality. When MP reduced to 0, the membrane was structurally damaged and positive to PI.

At reduced μ (SS1 - SS8), the percentage of depolarised cells increased in both the absence and presence of IPTG (*Figure 4.17)*. In the absence of IPTG, depolarised cells ranged from 17.16 to 35.14% in SS4 and SS2 (*Figure 4.17 A*). Contrastingly, the mean of depolarised cells was 13.08% at μ_{max} (S5), much lower than at steady state (SS). Large SE values show that although a difference may be present, its significance may be lacking. There was an overlap of SE bars in the S5 and SS4 in the absence of IPTG (*Figure 4.17 A*). No overlap was identified in control experiments using IPTG (*Figure 4.17 B*). In the presence of IPTG, depolarised cells ranged from 33.95 to 47.57 % in SS5 and SS3 (*Figure 4.17 B*).

For both data sets, sub-populations were compared using the chi square test. No significant deviation from the expected levels of depolarised cells existed in either case (with IPTG: Chi Square, $X^2 = 0.970$, D.F. = 7, P = 0.995; without IPTG: Chi Square, $X^2 = 0.998$, D.F. = 7, P = 0.995). Although no deviation from the expected levels was present, the difference in depolarised cells in both conditions was significant, showing IPTG increases cellular depolarisation (Kruskal-Wallis, H = 11.29, $p < 0.01$), IPTG is therefore detrimental to cell functioning.

At reduced μ (SS1 - SS8), the active cells decreased in both the absence and presence of IPTG compared to 83.74% at μ_{max} (S5) (*Figure 4.17*). The active cells were 60.37% to 79.45% in the absence of IPTG and 46.24% to 56.53% in the presence of IPTG. There was no overlap in the SE bars, suggesting that the difference may be significant.

Chi square analysis of the percentages of active cells without IPTG ($X^2 = 1.3070$, D.F. = 7, P = 0.988) and with IPTG ($X^2 = 0.8097$, D.F. = 7, P = 0.997) showed no significant deviation from expected values in either case. Further statistical analysis indicated a significant difference (Kruskal-Wallis, H = 11.29, $p < 0.01$), suggesting that IPTG diminished the cell functioning.

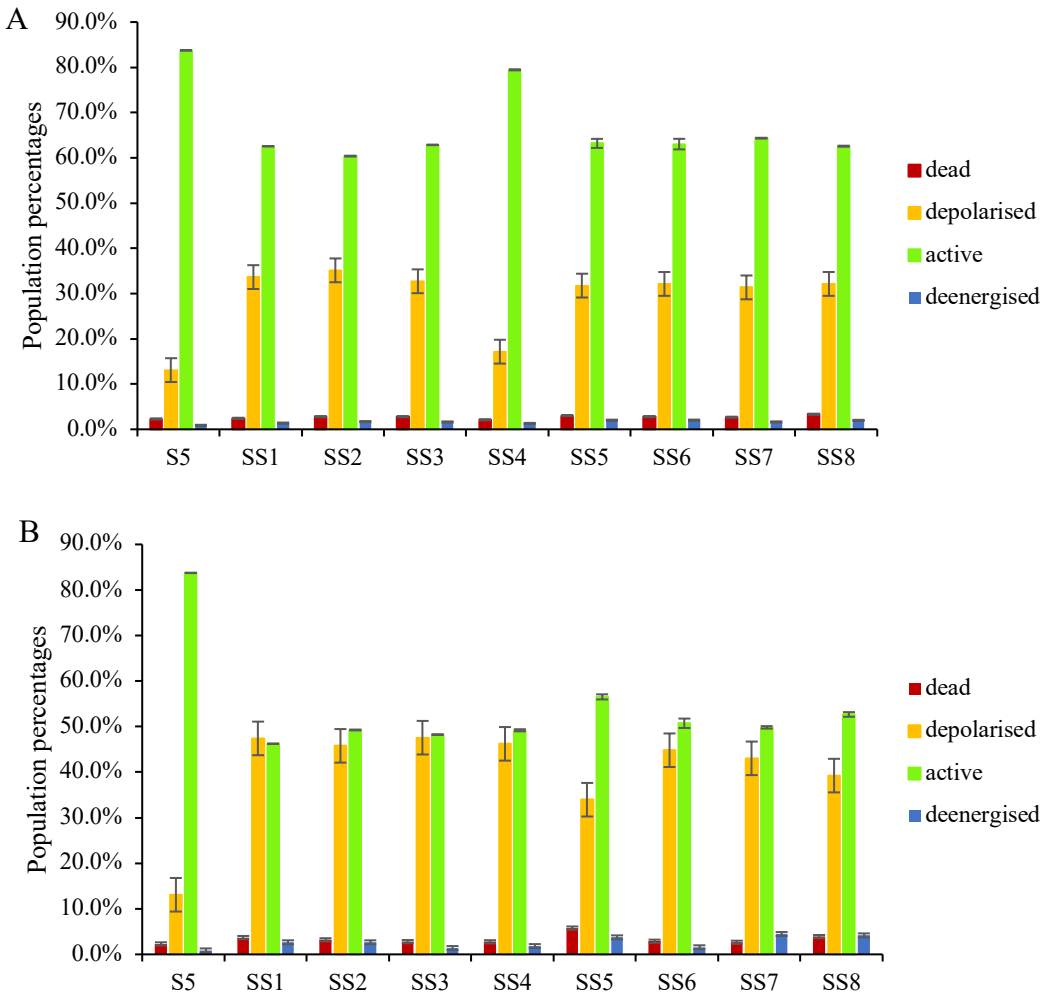

Figure 4.17. Flow cytometry analysis of *E. coli* W3110 cells at different growth rates on glucose minimal media, depicting four subpopulations of cells. A: No induction (0 mM IPTG). B: With 1 mM IPTG. For each graph, S5 is the mid-exponential sample with growth at μ_{max}, while SS1-SS8 are steady state (SS) samples at 2h intervals, with reduced growth at $\mu_{max}/2$. Data presented as mean ± S.E.

4.9 Studies of cell morphology using fluorescence microscopy

Fluorescence microscopy was used to quantify cell morphology, as well as to determine cell viability. Two fluorescent dyes were used $SYTO_9$ and PI, mixed in a fixed ratio within the cell suspension (described in Section *3.10 Phase and fluorescence microscopy of E. coli W3310*). $SYTO_9$ stained "live" cells green, whilst PI stained "dead" cells red. The viability assessment using fluorescence microscopy provided results that correlated with FC showing maximum viability at μ_{max}, with viability retention in chemostats (*Figure 4.16)*, thus FM viability measurements are not included.

Fluorescence images present an intense cell-background contrast, ideal for analysing cell shape. Only cells fluorescing green ("live") were further studied with regard to morphology. Three shape descriptors were measured - area, circularity and aspect ratio (AR). The area is the surface area in μm^2. AR is the ratio between the major and minor cell axes and is a general shape indicator. Circularity is the normalised ratio of area to perimeter, with a circle being 1 and a line 0. Circularity highlights the presence of protrusions or blebs in the membrane. With the aim of measuring what effect the growth rate has on cell morphology, the cell area, circularity and AR were monitored at two different growth rates: during exponential and chemostat growth.

The analysis was performed using ImageJ in an automated manner. To discard incorrectly detected clumps of cells, unseparated mother-daughter cell, overlapping or too small particles detected as cells, the cells were discarded if their contour had:

- An AR < 1 or > 6;
- An area < 0.5 or > 4.5 μm^2.

4.9.1 Cell morphology at maximal growth rate

Following filtering of the above physical parameters, the "live" subpopulation imaged consisted of 99 cells. Actively growing cells at μ_{max} retain the characteristic rod-shape (*Figure 4.18)*, and display the following shape parameters (*Table 4.2*):

	Mean	Minimum	Maximum	Figure
Area (μm^2)	2.06 ± 0.09	0.58	4.47	*4.19 A*
Circularity	0.61 ± 0.01	0.26	0.86	*4.19 B*
Aspect Ratio	2.99 ± 0.11	1.15	5.59	*4.19 C*

Table 4.2. Shape descriptors of *E. coli* W3110 during exponential growth.

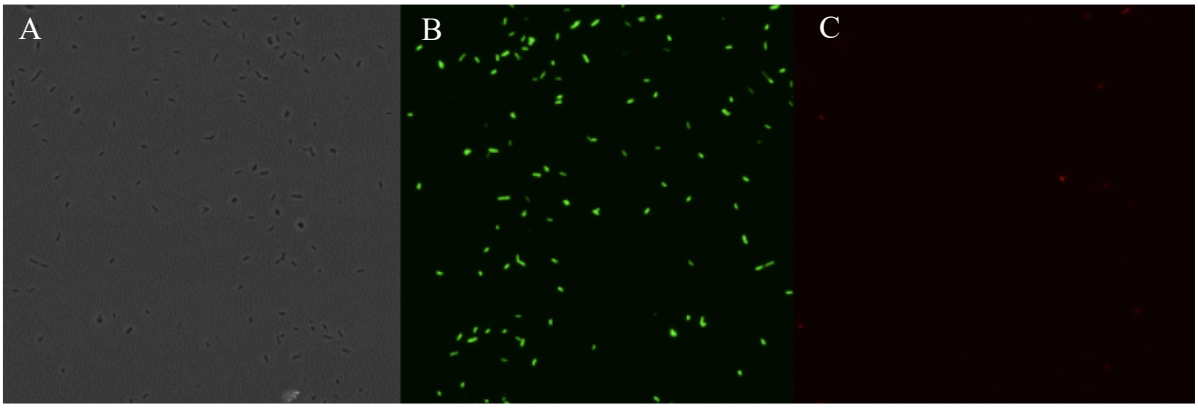

Figure 4.18. Microscopy of $SYTO_9$ (green) and propidium iodide (red) - stained *E. coli* W3110 cells at maximum growth rate with no limitation (mid-exponential point of growth). A: Phase-contrast; B: Viable cells ($SYTO_9^+$); C: Dead cells (PI^+).

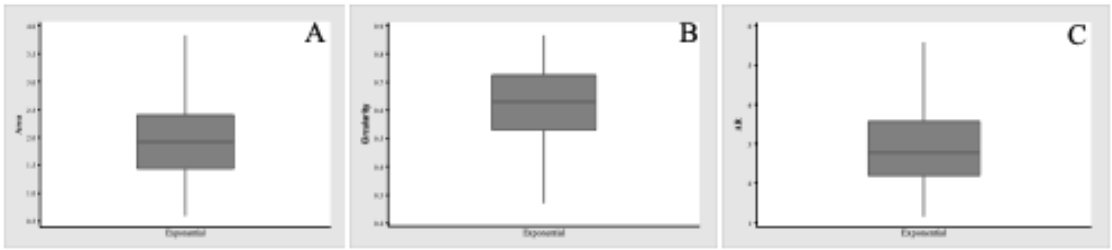

Figure 4.19. Box plots of cell area (A), circularity (B) and aspect ratio (C) at maximum growth rate in 99 "live" *E. coli* W3110 cells. Median indicates values above which 50% of the data are located. Grey box indicates interval into which 50% of the data falls, with top and bottom of the box representing the area Q1 and Q3. Values outside of the 1.5-fold IQR were removed

4.9.2 Cell morphology at submaximal growth rate in the absence of IPTG

a) Cell area

E. coli W3110 cell area distributions were affected by the rate of growth. At μ_{max} during exponential growth, mean cell area was 2.06 μm^2 (*Figure 4.20 A*), whilst during reduced growth in chemostat, cells had a smaller mean area (*Figure 4.20 B).* Hill reported that the cell size increases with growth rate, and a lower growth rate leads to smaller cells (Hill et al., 2013). When the growth rate is ½ μ_{max} during "steady state" chemostat growth, mean cell area ranged from 1.69 to 2.01 μm^2 in SS4 and SS6, respectively, smaller than in the exponential phase. The median cell area during growth at μ_{max} 1.91 μm^2 was also higher than during steady state where it ranged from 1.36 to 1.8 μm^2 in SS4 and SS6, respectively (*Figure 4.20 B*). The results are consistent with a decreased cell size occurring when lowering the growth rate (Hill *et al.*, 2013).

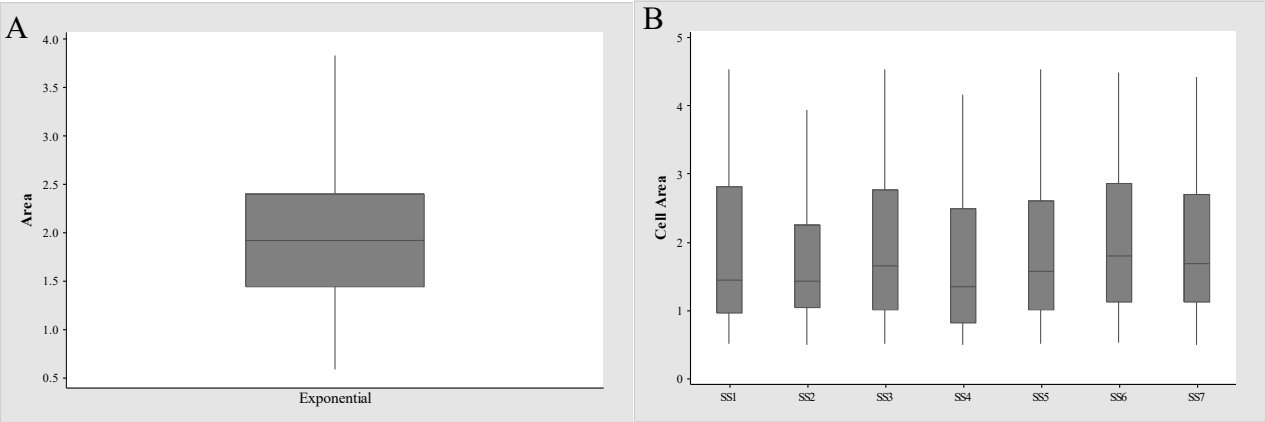

Figure 4.20. Cellular area (μm^2) variability of *E. coli* W3310 during: A: maximal growth rate; B: submaximal growth in continuous culture, with no IPTG. Number of cells per sample was: A. Exponential – 99 cells; B. SS1 – 92; SS2 – 153; SS3 – 166; SS4 – 135; SS5 – 274; SS6 – 292; SS7 – 231 cells. Values outside of the 1.5-fold IQR were removed.

The variability of cell area is smaller at μ_{max} than in chemostats. The smallest coefficient of variance (CV), 43.65 was recorded in the exponential sample, illustrating a more homogeneous data set (*Figure 4.20 A*). In comparison, the chemostat data, where CV ranged from 53.73 – 61.69, showed a more heterogeneous cell area dispersion at lower growth rates. Subsequent testing showed that the differences in the mean cellular area of chemostat samples

were insignificant (Kruskal-Wallis, H = 12.55, p = 0.051). This illustrates that although a high CV is present, a more heterogeneous population is constant at submaximal growth in a glucose-limited chemostat.

A chemostat is based on the assumption that many parameters are at a "steady state" and that it can be maintained indefinitely. Previous experiments, however, questioned the existence of a true "steady state" (Ferenci, 2006). A chemostat maintained indefinitely implies that sampling at different time-points gives constant results. Given the importance of population changes in a chemostat for continuous bioprocessing, a linear regression model was applied to investigate the effect of time on cellular area at "steady state". Although only 30% of the variation in cell area was explained by time at "steady state" ($R^2 = 0.3$), there was a significant linear impact between cellular area and fermentation time ($p < 0.05$).

The regression equation for this model was:

$$Cell\ area = 1.75 + 0.017\ time \qquad (4.4)$$

The mean cellular area increased by 0.017 for every hour of fermentation. However, linear methods assume that all other system properties are constant and that the data is normally distributed. The boxplots of cell areas indicated right-skewed distributions (*Figure 4.20 A* and *B*). Thus, although the model shows a small variation of cell area over time, any linear approach is inadequate to assess cell area if other cell properties are not constant.

b) Circularity

In terms of circularity, there were differences between cells sampled during chemostat and exponential growth (*Figure 4.21*). During growth at μ_{max}, the mean cell circularity was 0.62 (*Figure 4.21 B*), whilst during sub-maximal growth in chemostats, the mean cell circularity ranged from 0.49 to 0.62 at SS4 and SS1, respectively (*Figure 4.21 A*). The trend continued for the median circularity, with exponential cells growing at μ_{max} presenting the highest value of 0.63. During sub-maximal growth at "steady state", the median circularity ranged from 0.49 to 0.60 at SS5 and SS1, respectively (*Figure 4.21 A*).The exponential CV of 21.10 was the lowest of all the samples showing a more homogeneous population. Within "steady state", CV ranged from 22.95 to 33.16, showing varied dispersion from the mean (*Figure 4.21 A*). This illustrates an increase in dispersion or higher heterogeneity in regard to circularity in

glucose-limited chemostats. The boxplots show a left-skewed distribution of circularity during the exponential phase, with a mixture of distributions during “steady state”.

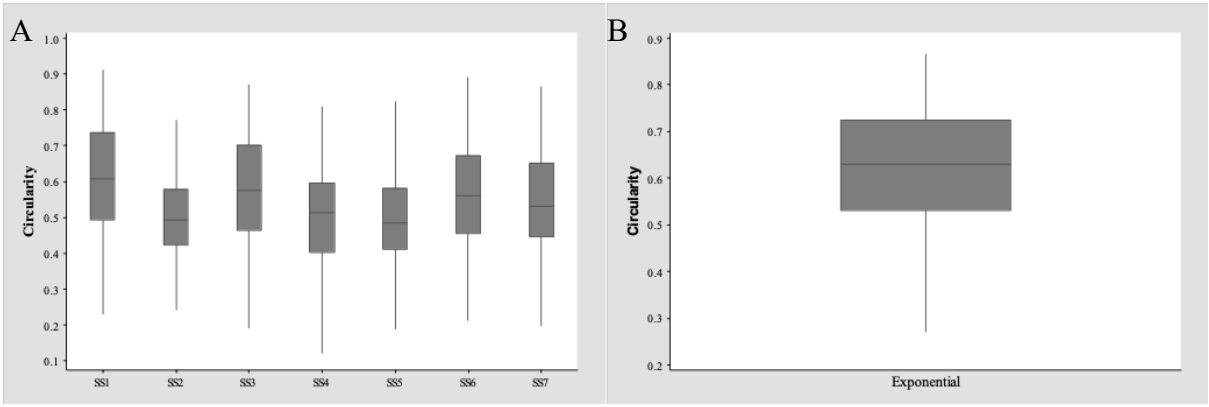

Figure 4.21. Circularity of cells during sub-maximal growth in chemostats (A) and during mid-exponential phase of growth (B). Number of cells per sample was: A. SS1 – 92; SS2 – 153; SS3 – 166; SS4 – 135; SS5 – 274; SS6 – 292; SS7 – 231 cells. B. Exponential – 99 cells. In all data sets, values outside of the 1.5-fold IQR were removed.

To investigate circularity changes during continuous cultivation, a quadratic model was applied. Although only 19% of the variation in circularity was explained by the fermentation time ($R^2 = 0.19$), circularity did vary significantly overall ($p < 0.001$). The regression equation for circularity was:

$$Circularity = 0.64 - 0.029\ time + (0.0016\ time)^2 \qquad (4.5)$$

At the beginning of the “steady state”, cell circularity was 0.64, decreasing slowly with every hour. Although differences in circularity at “steady state” were small, subsequent testing illustrated their statistical significance (Kruskal-Wallis, $H = 74.42$, $p < 0.001$). The 19% variation that the quadratic model accommodates implies other factors affect cell circularity, some of which may be the focus of future studies.

c) Aspect Ratio

Subtle differences in the aspect ratio (AR) were identified at single-cell level, at different growth rates (*Figure 4.22*). Mean AR ranged from 2.76 (SS4) to 3.68 (SS2) at sub-maximal growth in chemostat (*Figure 4.22 A*), whilst at maximum growth rate during the exponential phase, the mean AR was 2.99 (*Figure 4.22 B*). This value was well within the ranges present during chemostat operation. Median values exhibit a similar trend, as the exponential AR median (2.78) was present within the chemostat range of 2.48 - 3.78 (*Figure 4.22)*. There was a large variation of AR values SS1 and SS4, causing large CV values of 42.51 and 42.31 respectively (*Figure 4.22 A*). The differences between the ARs at steady state were significant (Kruskal-Wallis, $H = 66.59$, $p < 0.001$).

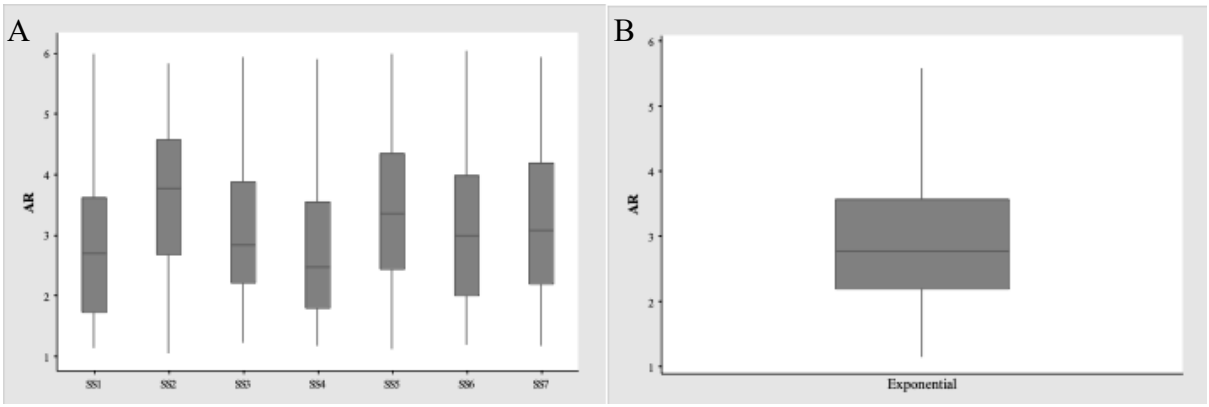

Figure 4.22. Aspect ratio (AR) of *E. coli* W3110 cells at two different growth rates: A) submaximal growth in chemostat no IPTG; B) maximal growth during exponential phase. Number of cells per sample was: A. SS1 – 92; SS2 – 153; SS3 – 166; SS4 – 135; SS5 – 274; SS6 – 292; SS7 – 231 cells. B. Exponential – 99 cells. Values outside of the 1.5-fold IQR were removed.

To investigate the AR changes throughout chemostat growth, a cubic model was applied. Only 30% of the variation in AR was explained by the fermentation time ($R^2 = 0.3$), illustrating that other factors influence the AR, which may be of interest to future studies. Fermentation time and circularity were associated as shown by sequential analysis of the variance ($F = 4.32$, $p < 0.05$). The absence of any significance concerning cubic terms and regression suggests that although an association is present, another model requires applying

(p= 0.22). The regression of both the linear and quadratic models were insignificant (linear: p = 0.766; quadratic: p = 0.927). Maybe the two factors only correlate when interacting, but not individually.

4.9.3 Cell morphology in the presence of IPTG

During initial studies with the recombinant strain *E. coli* CLD1301, it was determined that the optimum concentration of IPTG for induction of GFP mut3* expression was 1 mM (see Section *5.5 Determining the optimum amount of IPTG*). The inducer was added shortly after the mid-exponential point, so for the experiments detailed below, the mid-exponential sample does not contain IPTG. The influence of IPTG on host morphology was quantified at single-cell level under nutrient-limited growth in chemostats, by comparing with cell morphology without IPTG (*4.9.1 Cell morphology at maximal growth rate)*.

a) Cell area

In the presence of IPTG at sub-maximal growth, cell area fluctuates between sampling (*Figure 4.23*). The exponential mean cell area was between the minimum and maximum means during chemostat cultivations (*Figure 4.23, Table 4.3*). The same trend applied to median values:

	Minimum in chemostat	Exponential	Maximum in chemostat
Mean (μm^2)	1.69	1.98	2.45
Median (μm^2)	1.19	1.90	2.48

Table 4.3. Cell area of *E. coli* W3110 during maximal growth (exponential) and steady state growth in chemostat in the presence of IPTG.

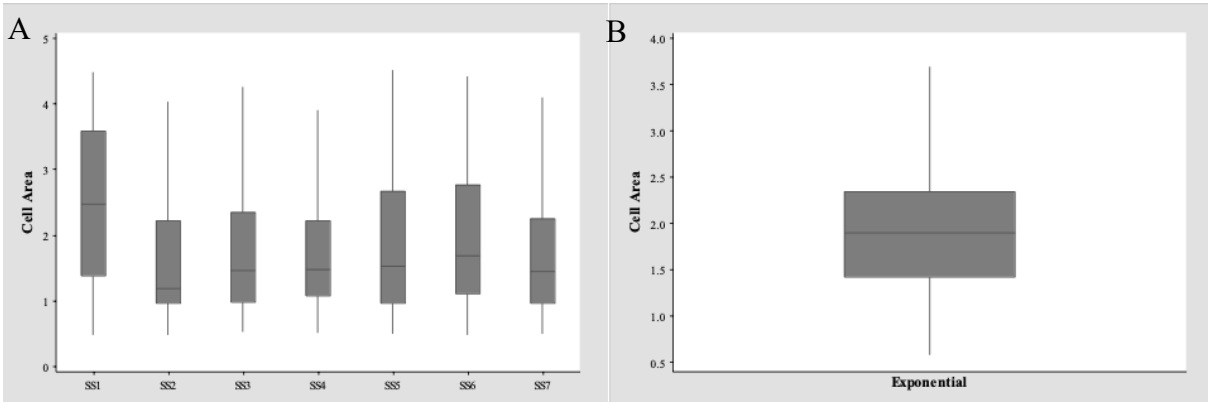

Figure 4.23. Cell area (μm^2) variability of *E. coli* W3310 cells at two growth rates: A: Submaximal growth throughout continuous fermentation with 1mM IPTG; B: Maximal growth at mid-exponential point of growth. Number of cells per sample was: A. SS1 – 102; SS2 – 71; SS3 – 180; SS4 – 293; SS5 – 220; SS6 – 277; SS7 – 288 cells. B. Exponential – 99 cells. Values outside of the 1.5-fold IQR were removed.

The boxplots of cell area indicated right-skewed distributions. The smallest coefficient of variance (CV) was 40.57, recorded in the exponential sample, thus illustrating higher homogeneity (*Figure 4.23 B*). During sub-maximal growth in the chemostat, CV ranged from 48.59 to 62.36, showing a more heterogeneous cell area dispersion when IPTG is present. However, in the absence of IPTG, the CV of cell area ranged from 53.73 to 61.69 (*Figure 4.20 B*). This suggests the heterogeneity is more the result of changing the growth rate rather than IPTG addition. Nevertheless, the differences in the mean cellular area at submaximal growth were significant when IPTG was present (Kruskal-Wallis, $H = 40.05$, $p < 0.001$). The high CV during chemostat cultivations illustrates a more heterogeneous population, but as the cellular area changes significantly throughout "steady state", the attainment of a chemostat becomes unpredictable.

A linear regression model was applied to investigate the cellular area changes over time during chemostat. Although 40% of the variation in cell area was explained by time at "steady state" ($R^2 = 0.4$), there was a significant relationship between the fermentation time and cellular area ($p < 0.01$). The regression equation for cell area at steady state was:

$$Area = 2.045 - 0.0206\ time \qquad (4.6)$$

The model shows the mean cell area decreased by 0.0206 μm^2 with every hour of fermentation when IPTG was present. This small variation suggests that other unexplored influences also affect cell area.

b) Circularity

Major differences in circularity were present when changing the growth rate (*Figure 4.24 B*). Both mean and median circularity were larger during maximal growth, as illustrated in *Table 4.4.*

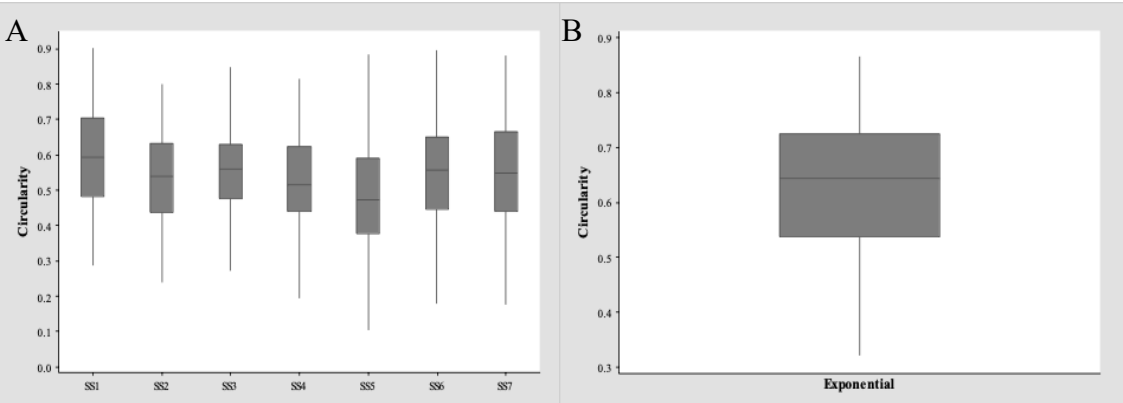

Figure 4.24. Circularity dispersion of *E. coli* W3310 cells at two growth rates: A: submaximal growth; B: maximal growth. Number of cells per sample was: A. SS1 – 102; SS2 – 71; SS3 – 180; SS4 – 293; SS5 – 220; SS6 – 277; SS7 – 288 cells. B. Exponential – 99 cells. Values outside of the 1.5-fold IQR were removed.

Circularity	Exponential	Chemostat minimum	Chemostat maximum	*Figure*
Mean	0.63	0.48	0.60	
Median	0.64	0.47	0.59	
CV	19.91	23.51	34.31	*4.24*

Table 4.4. Cell circularity of *E. coli* W3110 during maximal growth (exponential) and steady state growth in chemostat in the presence of IPTG.

The exponential CV of 19.91 shows a more homogeneous population at μ_{max}. The variance was higher in chemostat, a trend that also exists in the absence of IPTG (*Figure 4.21*). This

suggests that nutrient limitation and IPTG increase heterogeneity in regard to cell morphology.

A quadratic model was applied to analyse the circularity of *E. coli* W3110 cells over time in the presence of IPTG at sub-maximal growth. Although only 19% of the variation in circularity was explained by the fermentation time ($R^2 = 0.19$), circularity did vary significantly overall ($p < 0.001$). The regression equation for circularity was:

$$Circularity = 0.647 - 0.026\ time + (0.0012\ time)^2 \qquad (4.7)$$

At time 0 during chemostat, cell circularity was 0.647, and gradually decreased over time. The small variation that the model accommodates implies other factors may affect circularity, some of which may be the focus of future studies. Differences in circularity at "steady state" (*Figure 4.24 A*) were significant (Kruskal-Wallis, $H = 63.00$, $p < 0.001$). This shows that cell morphology changes within chemostat, originally assumed to be a constant microenvironment.

c) Aspect Ratio

The aspect ratios (AR) of *E. coli* W3110 cells with 1 mM IPTG are shown in *Table 4.5*.

AR	Exponential	Chemostat minimum	Chemostat maximum	*Figure*
Mean	3.03	2.97	3.6	
Median	2.79	2.92	3.51	
CV	24.12	37.92	42.28	*4.25*

Table 4.5. Aspect ratio (AR) of *E. coli* W3110 during maximal growth (exponential) and steady state growth in chemostat in the presence of IPTG.

The mean AR at maximal growth was within the chemostat range (*Figure 4.25)*. The median AR did not follow the trend. The smallest coefficient of variance (CV) was recorded in the exponential sample, illustrating a more homogeneous data set (*Figure 4.25 B*). The large CV values during chemostat growth show a more heterogeneous AR dispersion at lower growth rates in the presence of IPTG (*Figure 4.25 A*).

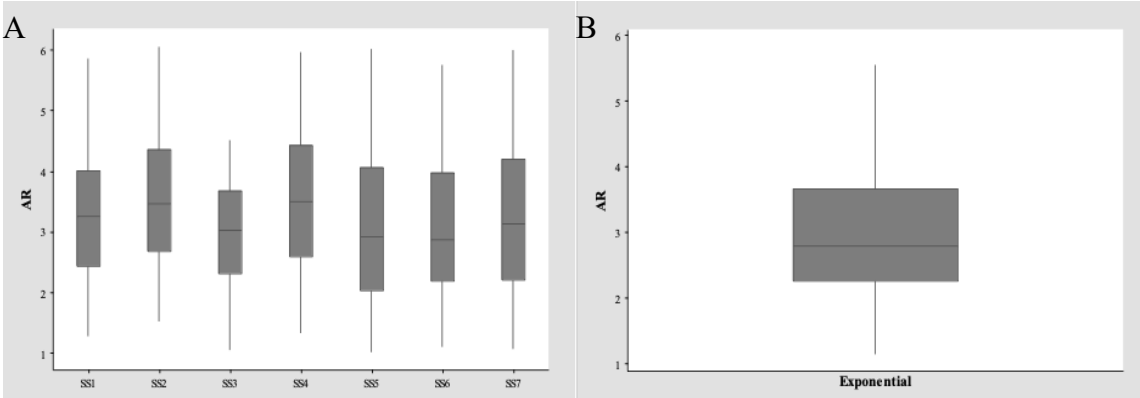

Figure 4.25. Aspect ratio (AR) dispersion of *E. coli* W3310 cells at two growth rates: A: submaximal growth with 1 mM IPTG; B: maximal growth. Number of cells per sample was: A. SS1 – 102; SS2 – 71; SS3 – 180; SS4 – 293; SS5 – 220; SS6 – 277; SS7 – 288 cells. B. Exponential – 99 cells. Values outside of the 1.5-fold IQR were removed.

The differences between AR in chemostat at doubling time intervals were significant (Kruskal-Wallis, $H = 44.28$, $p < 0.001$). The AR variation means that the "steady state" can only exist as such for an instant and therefore not remain in that steady state indefinitely.

Chemostat data was converted into linear, quadratic and cubic models to determine how the AR changes over fermentation time. All regressions were, however deemed insignificant (linear: $p = 0.268$; quadratic: $p = 0.705$; cubic: $p = 0.199$). This illustrates that the time and AR only correlate when interacting with other factors but not independently, therefore other factors affect the AR.

The effect of IPTG on *E. coli* W3110 morphology at sub-maximal growth is shown in *Figure 4.26*. The mean AR in the presence of IPTG is much larger than without IPTG (*Figure 4.26 A*); the difference between the two conditions was deemed statistically significant (Mann-Whitney U, $W = 7863.5$, $p < 0.005$). This trend is consistent when comparing cell area (*Figure 4.26 C*). Cell area in the presence of IPTG is higher than in its absence and the difference was deemed significant (Mann-Whitney U, $W = 7710$, $p < 0.005$). These results show that whilst not influencing the spread of the data, IPTG addition leads to an overall higher AR and cell area, meaning more elongated cells. This presents a problem in a bioprocess as elongated cells may halt division, whilst continuing growth. This implies multiple copies of DNA, but with decreased cell functionality while maintaining a "viable" status and an increase in cellular states. Conversely, the influence of IPTG on circularity of

cells at sub-maximal growth rate (*Figure 4.26 B*) was insignificant (Mann-Whitney U, W = 9187.5, p = 0.578).

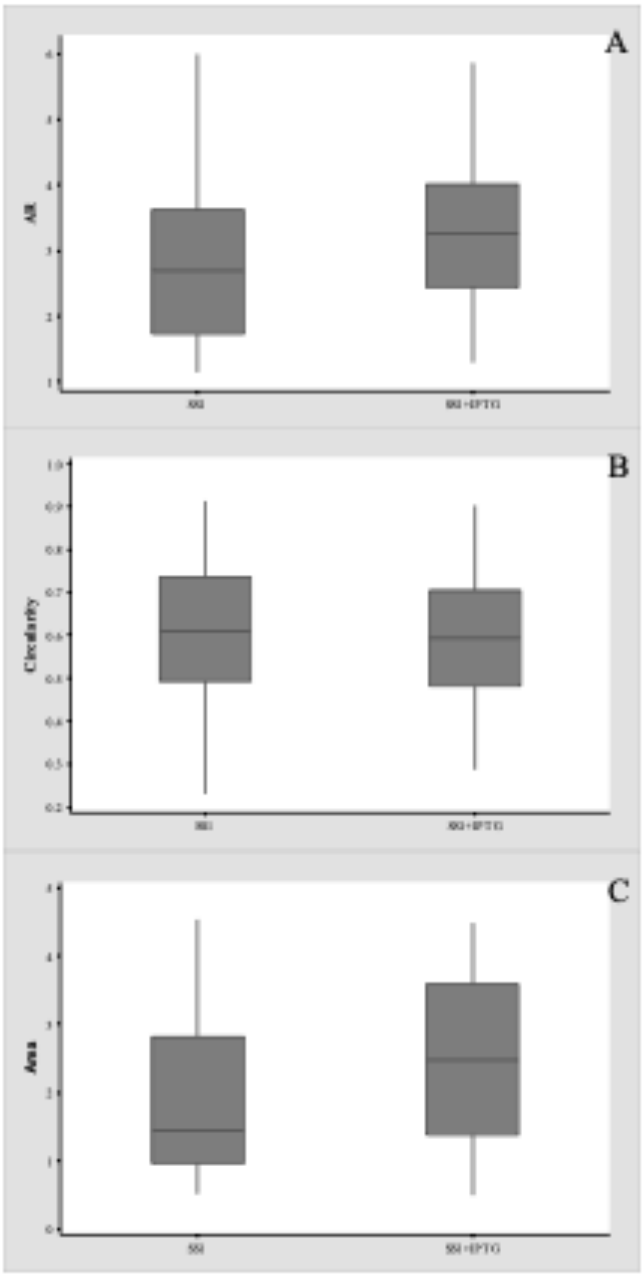

Figure 4.26. Box plot analysis showing the three shape descriptors of *E. coli* W3110 in the absence and presence of 1 mM IPTG at submaximal growth. A: Aspect Ratio; B: Circularity; C: Area. For each individual graph, the boxplot on left indicates measurements made in the absence of IPTG; the boxplot on right indicates measurements made in the presence of IPTG. Number of cells per experiment: SS1 – 92 and SS1+IPTG – 102 cells. Values outside of the 1.5-fold were removed.

4.10 Single cell studies of light scattering (FSC & SSC)

E. coli W3110 scattering signals were extracted from FC data to illustrate population changes at maximal and sub-maximal glucose-limited growth. The light scattered as the cell passes through the laser beam gives rise to two signals: Forward Scatter and Side Scatter. Forward Scatter (FSC) is suggested to be an indicator of cell size, whilst side scatter (SSC) signals granularity (although not applicable to bacterial cells). It has been pointed out that SSC in bacteria is an indicator for cell dry weight (CDW) and total protein content, and that the signals of FSC and SSC become somewhat similar when analysing small bacteria, because of different background interference (Ward et al., 2009).

4.10.1 FSC signal

FSC signals (A.U.) extracted from "live" *E. coli* W3110 cells show the highest mean of 26152 during maximal growth on glucose, while those at submaximal growth range from 14139 to 19252 at SS7 and SS1, respectively *(Figure 4.27).* The median FSC signal (A.U.) at maximal growth rate (19796) was also higher than at sub-maximal growth, ranging from 9712 to 13499 at SS7 and SS1, respectively *(Figure 4.27)*. These trends show an overall bigger cell size at maximum growth (*Figure 4.27*), given that FSC is an indicator of cell size.

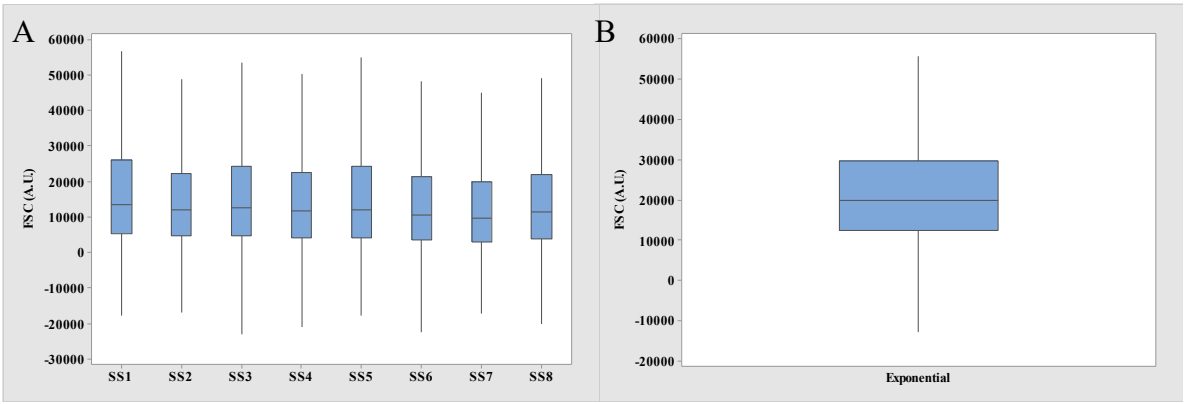

Figure 4.27. Boxplots of forward scatter signal (FSC) of *E. coli* W3110 at the different growth rates in the absence of IPTG. A: submaximal growth; B: maximal growth. Number of cells per sample was: A. SS1 – 22066; SS2 – 20964; SS3 – 26794; SS4 – 16874; SS5 – 20389; SS6 – 21373; SS7 – 24645; SS8 - 20768 cells. B. Exponential – 18025 cells. Values outside of the 1.5-fold IQR were removed.

At sub-maximal growth, the cell size becomes smaller (*Figure 4.27).* These results are in agreement with the studies of cell size by FM (*Figure 4.20*) and support the theory that a lower growth rate leads to smaller cells. However, FSC does not linearly correlate with cell size, as it is also dependant on other factors. The largest standard deviation (SD) of 41329 was recorded at μ_{max} (*Figure 4.27*), illustrating a large spread of data. In comparison, SD at sub-maximal growth ranged between 17360 – 25580, at SS8 and SS4 respectively, suggesting a more homogenous population in regard to cell size (*Figure 4.27*). Contrastingly, FM results of cell area and AR indicate a more homogeneous population at maximal growth, with more cell size heterogeneity at sub-maximal growth (*Figures 4.20* and *4.22).* This shows that the FSC is not an accurate indicator for cell size.

The mean FSC differences at sub-maximal growth are significant (Kruskal-Wallis, H = 11568.88, $p < 0.001$). Differences in AR in chemostats measured by microscopy (*Figure 4.22 A)* were also deemed significant (Kruskal-Wallis, H = 66.59, $p < 0.001$). Combining these with insignificant changes of cell area (*Figure 4.20 B*) at sub-maximal growth (Kruskal-Wallis, H = 12.55, $p = 0.05$), the results suggest that continuous cultivations lead to more stretched cells (elongated with a reduced cell width), and that although the chemostat appears stable at population level, continuous culture leads to a dynamic and ever-changing cell population.

4.10.2 SSC signal

The SSC distributions of *E. coli* W3110 cells are shown as boxplots (*Figure 4.28*).

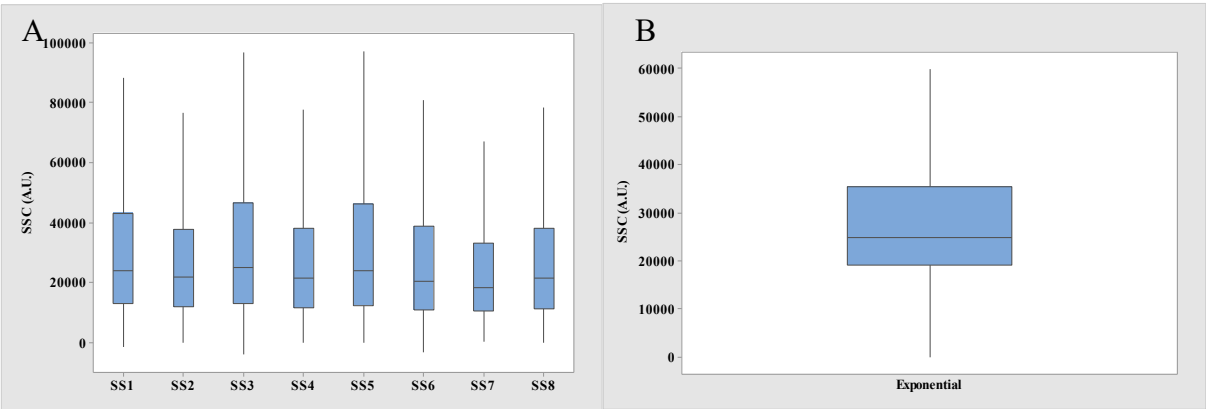

Figure 4.28. Boxplots of side scatter signal (SSC) of *E. coli* W3110 at two different growth rates in the absence of IPTG. A) sub-maximal growth; B) maximal growth. Number of cells per sample was: A. SS1 – 22066; SS2 – 20964; SS3 – 26794; SS4 – 16874; SS5 – 20389; SS6 – 21373; SS7 – 24645; SS8 - 20768 cells. B. Exponential – 18025 cells.

The mean SSC intensity (A.U.) during maximal growth was 34269; a slower growth due to glucose limitation shows values ranging from 25838 to 36660 A.U. at SS7 and SS5, respectively (*Figure 4.28*). These results illustrate a more heterogeneous population in the exponential phase as represented by the high S.D. value of 50683, whilst sub-maximal growth leads to more homogeneous cell populations as S.D .values range from 25002 to 40639 in SS7 and SS3, respectively. Differences between the data sets (SS1-SS8) in chemostat (*Figure 4.28*) were deemed significant (Kruskal-Wallis, $H = 7014.8$, $p < 0.001$).

Scatter measurements with FC were used to investigate the cell phenotype in a population and identify trends. The advantage of light scatter analysis is that FC measures a much larger number of cells than microscopy. Variations of FSC and SSC signals were used to investigate cell population heterogeneity in fermentations of *E. coli* W3110. A shift in SSC signal is expected when changing from maximal (exponential) to sub-maximal growth rate (SS1-SS8). These changes do not correlate with changes in cell size detected through FM (*Figures 4.20* and *4.22)*, which have a more homogeneous population at maximal growth rate with increased cell heterogeneity in chemostat.

4.11 Discussions and conclusions

This study used simultaneous staining protocols with different probes for monitoring heterogeneity in cultivations of *E. coli* W3110 at two different growth rates. FC was used to analyse microbial fermentations by assessing the following: membrane integrity, membrane depolarisation and reproduction capacity.

The results on *E. coli* W3110 host in glucose minimal media have shown a high viability at maximal growth, with retention of viability in glucose-limited chemostats (*Figure 4.16*). This was perhaps expected, given that *E. coli* is a highly versatile, diverse and hardy organism that survives without food for weeks even in colder environments. Growth conditions dictated by GFP mut3* expression in *E. coli* CLD1301 strain (Chapter 5 and Chapter 7) were pH of 7, temperature of 37^0C and DO of 50%, and these are also optimal growth conditions for *E. coli* W3110. Thus, the cell physiology and morphology were assessed along with viability.

Cell physiology was assessed and monitored by FC, using a triple dye combination $DIBAC_{4(3)}$/EB/PI to test for functional states in relation to MP. The fermenter was populated by a range of sub-populations of intact (active), depolarised, de-energised and non-viable (dead) cells, illustrating population heterogeneity. At a maximal growth rate in glucose media

83.74% of *E. coli* cells were active, 13.08% were depolarised, 2.30% and 0.87% were dead and de-energised, respectively (*Figure 4.17*). At sub-maximal growth, an increase in the percentage of depolarised cells was observed in both the absence and presence of IPTG (*Figure 4.17*), indicated by a shift in green fluorescence. A statistically significant difference (Kruskal-Wallis, $H = 11.29$, $p < 0.01$) suggested that the addition of IPTG increased the cell depolarisation. Cell depolarisation does not mean cell death, but a limited function, overcoming the limitation of dual TO/PI viability staining.

An important advantage of chemostat cultivation is that cell density has – in theory – no effect on the physiological state as long as the limitation regime remains the same (Herbert *et al.*, 1956). However, the cell physiology changes significantly within glucose limited chemostats, shown by a number of parameters. To maintain size, cells need to coordinate cell division with growth rate and mass-doubling time. The changes in size were expected in conditions of environmental pressure (glucose limitation) because they are single cells of minute size. Whilst the maintenance of cell size indicates an adaptation mechanism for adjusting to unfavourable events, the cell size changes across chemostats in the absence of IPTG (*Figure 4.20 B*) were insignificant (Kruskal-Wallis, $H = 12.55$, $p = 0.051$). The changes in cell size when IPTG is present (*Figure 4.23*) were, however, deemed significant (Kruskal-Wallis, $H = 40.05$, $p < 0.001$).

At maximal growth rate, the median AR was 2.78, with mean AR of 2.99 (*Figure 4.22 B*). The low CV of 25.10 during maximal growth in the exponential phase (*Figure 4.22 B*) suggests little variation between the cells in the absence of nutrient limitation or environmental pressure. At lower growth rates in the absence of IPTG, the median AR was 2.48 - 3.77 and the mean AR was 2.76 - 3.68 (*Figure 4.22 A*). The large CV range from 42.51 to 42.31 for AR (*Figure 4.22 A*) show a more heterogeneous population in glucose-limited chemostats. Thus, the bigger variation between the cells observed during chemostats illustrates the effect of environmental pressure (glucose limitation) on *E. coli* cells. Growing as single minute entities, cells adapt quickly to the environment and not the other way around.

Furthermore, AR changes significantly with each doubling time at “steady state” without IPTG (Kruskal-Wallis, $H = 66.59$, $p < 0.001$). In the presence of IPTG, mean AR ranges from 2.97 to 3.6, whilst AR median ranges between 2.92 to 3.51 at submaximal growth (*Figure 4.25*). The large CV values of 42.28 (SS1) and 37.92 (SS4) during glucose limitation (*Figure 4.25 A*) show an increase in data distribution away from the mean with population changing AR significantly with doubling time (Kruskal-Wallis, $H = 44.28$, $p < 0.001$). AR for rod-

shaped *E. coli* cells represents the mean cell length divided by the diameter (Zaritsky, 1975), thus, short cells have small ARs, whilst long cells have larger ARs. During transition from maximal growth rate (*Figure 4.22 B*) to limited growth rate (*Figure 4.22 A*), the change in growth rate requires changes in cell size. Dividing before doubling mass reduces the cell size, while dividing after increases cell size.

Although typical rods of various lengths occur during maximal growth in conditions that are favourable for both growth and reproduction *(Figure 4.22 B*), the population is more homogeneous, whilst glucose limitation leads to increased heterogeneity (*Figure 4.22 A*). The problem may be summarised by stating that *E. coli* host cells show wide variations in size (cell area), shape (AR) and functionality (MP) whilst in "balanced growth" in chemostats, which are significant for bioprocess and even more so for continuous bioprocessing. Nevertheless, single cell analysis indicates differences in cell morphology and physiology that are important for recombinant protein production and are not apparent from population level analyses.

CHAPTER 5

RESULTS

Chapter 5 Cell dynamics in recombinant *E. coli* CLD 1301 fermentations on glucose

5.1 Abstract

Recombinant proteins using *E. coli* expression systems are produced at large scale by cultivations in fed-batch reactors. In fed-batch reactors, the cells experience differences in the available substrate, which are more poignant when nutrient is top – fed. Substrate gradients vary widely in large-scale reactors from the concentration of the feed to complete exhaustion. At the top of the fermenter, the cells experience high substrate concentrations (that of the concentrated feed) and exhibit maximum growth rate μ_{max}. Opposite the feeding port, due to relative mixing and biological activity, cells experience nutrient limitation and a reduced growth rate.

To mimic large-scale gradients, fermentations with recombinant *E. coli* CLD1301 were conducted at two growth rates: maximum μ_{max} and reduced growth rate ½ μ_{max}. The sole limitation for the experiments described below is on the substrate: glucose.

5.2 Introduction

Single cell analysis in a bioprocess provides information that is not accessible with bulk measurements on the population level. The heterogeneity of cells in bioreactors used for recombinant protein production has a significant impact on product quality and quantity. Thus, the understanding of heterogeneity is key to bioprocess optimisation. Single cell analysis was applied to cells growing "in balanced growth" at maximal and submaximal growth rates. Single cells were analysed using fluorescence, originating from external probes and an internal recombinant protein (GFP mut3*). The fluorescent probes were used to monitor changes in cells physiological states. The different cell parameters investigated at single cell level were membrane integrity (TO/PI staining), membrane potential ($DIBAC_{4(3)}$/EB/PI staining) and cell morphology. The enhanced GFP mut3* was used as a marker for protein production at single cell level.

5.3 Determination of single media limitation on glucose

Chemostats are important tools for studying cell physiology because they enable control of cell growth rate, in a macroscopically constant environment, where cells are assumed to grow continuously and exponentially at a "steady state". The chemostat is based on a growth-limiting nutrient in the vessel, while all of the others are maintained at a constant excess. The media is therefore suitable for continuous cultivations if the sole limiting nutrient is the C source (glucose).

To evaluate the media suitability, triplicate experiments were performed using BioLector (m2p-labs GmbH, Baesweiler, Germany), as described in Section *3.4.1 Batch cultivations in Microtiter Plates*. The glucose concentrations (w/v) were the same as for the host W3110 strain, including 1, 2, 3, 4, 7 and 10 g/L, whilst the other media components were at a constant excess. The batch minimal media, calculated to produce 1.6 g/L CDW in batch phase has the required buffered capacity to keep the pH value within 7 ± 0.2 (described in Section *3.3.1 Batch mineral media*) and was supplemented with 50 µg/ml kanamycin. One well with sterile media was used as internal standard for control of contamination. Cultivations were performed at 37°C, and growth was monitored as scattered light at 620 nm, recorded online in 15 min cycles. Precultures were prepared as described in Section *3.2 Cell expansion and seed preparation A*, and used to inoculate the BioLector at time 0, with the initial starting OD_{600} was 0.05.

The increase in biomass was monitored for 26.77 h, when the recombinant *E. coli* CLD1301 was in stationary phase (*Figure 5.1*). All cultures exhibited exponential growth, which ended at different time points, depending on when the limitation occurred. The maximum amount of biomass in arbitrary units (A.U.) was obtained in stationary phase, arbitrarily chosen between 22 - 25 h ranged from 20.28 to 81.82 as scattered light. To determine that the limitation was the carbon source, the biomass accumulation was analysed as a function of the glucose concentration. A significant linear relationship was observed between biomass and glucose concentration up to 4 g/L, with R-square (coefficient of determination) value of 0.92 (*Figure 5.2*).

The changes in biomass for glucose concentrations of 7 and 10 g/L were not linear, suggesting another limitation in addition to that of glucose was present within this range (*Figure 5.2*).

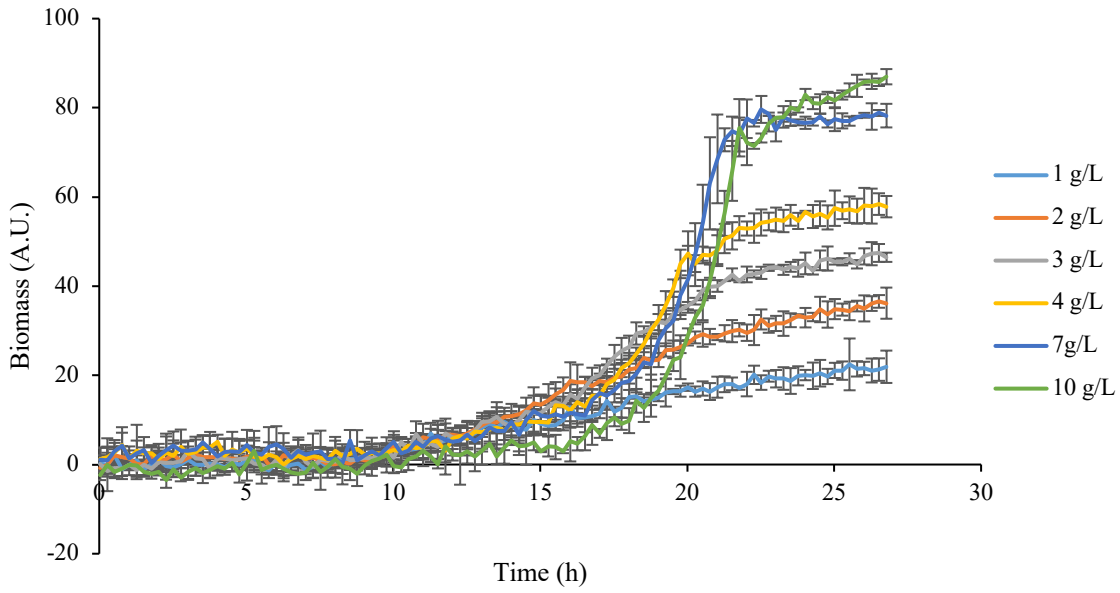

Figure 5.1. Influence of different glucose concentrations on growth of *E. coli* CLD1301 without IPTG. Online monitoring of biomass (scattered light). Conditions: minimal media with up to 10 g/L of glucose, T = 37^{0}C, V_L = 800 µL, n = 1500, d_0 = 3 mm. Standard error bars represent ± S.D.

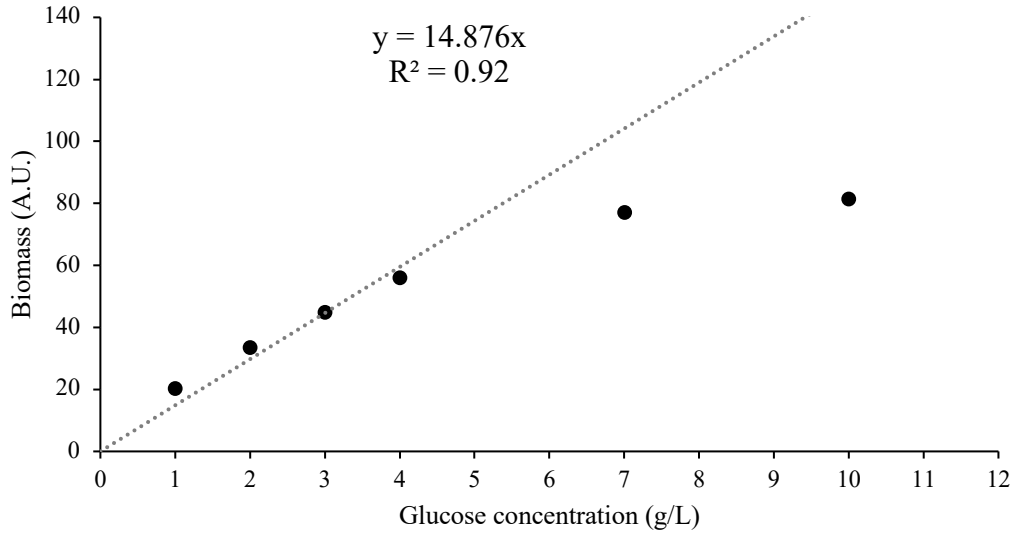

Figure 5.2. Linear relationship between biomass (A.U.) and glucose concentration (g/L) up to 4 g/L, indicating that the nutrient is in the limiting range. Maximum biomass was recorded between 22 - 25 h. Conditions: minimal media including (w/v) 1, 2, 3, 4, 7 and 10 g/L glucose, while other media components remained unchanged and in excess, T = 37^{0}C, V_L = 800 µL, n = 1500, d_0 = 3 mm.

The concentration of 4 g/L glucose was chosen for subsequent chemostat experiments to ensure that the growth was glucose-limited and to allow comparison with the host strain *E. coli* W3110.

5.4 Growth rate and the influence of pDNA on the growth rate

The recombinant strain *E. coli* CLD1301 that produces GFP mut3* was constructed by including the GFP-A gene onto a multicopy plasmid pD441- SR: 240460 in the host *E. coli* W3110. The GFP-A gene is under the control of an IPTG-inducible promoter. The growth characteristics of *E. coli* CLD1301 were determined using BioLector data for the chosen concentration of glucose (4 g/L), with the wild-type host *E. coli* W3110 as control.

It is known that multicopy plasmids in bacteria decrease growth (Flores et al., 2004). The expression of recombinant proteins diverts cell resources from synthesising proteins that are necessary to the cells and causes a reduction in the growth rate (Shachrai et al., 2011). To determine the metabolic burden imposed by the pDNA on the cell, in the absence of protein expression, the final biomass (*Figure 5.3*) and the growth rate (*Figure 5.4)* for recombinant CLD1301 were compared against the host W3110.

The observed inhibitory effects of growth were a delay in the lag phase (*Figure 5.3)* and a decrease in growth rate (*Figure 5.4)* in the recombinant strain compared to the host. The end of lag phase was determined as the time at which the exponential trendline for the logarithmic phase of growth intersected the x-axis (*Figure 5.4).* The lag phase was nearly 9.5 h for the recombinant *E. coli* CLD1301, compared to 0.6 h for the host W3110.

Growth rate was determined using data from the exponential phase. The biomass (A.U.) was plotted in a log-linear graph against corresponding time to determine the growth rate. Maximum growth rate was the slope of the straight line obtained. The growth rates for strains CLD1301 and W3110 growing in minimal media with glucose as the sole carbon source were 0.37 and 0.6 h^{-1}, respectively *(Figure 5.4)*. This showed a reduction in the growth rate of CLD1301 when compared to host W3110. The relative decrease in the growth rate or the cost was 61.39 %, calculated from the following formula:

$$Cost = \frac{\mu_0 - \mu_1}{\mu_0} \; x \; 100 \qquad (5.1)$$

where μ_0 and μ_1 were the growth rates of host W3110 and recombinant CLD1301, respectively, in the absence of induction.

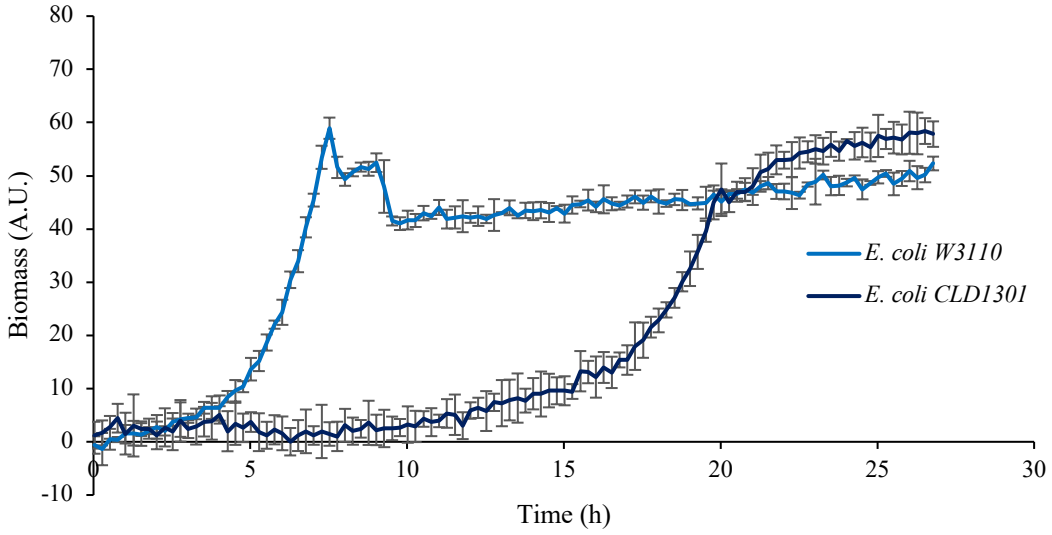

Figure 5.3. Growth (biomass) of non-induced *E. coli* W3110 and *E. coli* CLD1301 cells. Biomass (A.U.) was recorded as scattered light. Conditions: minimal media with 4 g/L glucose as sole carbon source, T = 37^{0}C, V_L = 800 µL, n = 1500, d_0 = 3 mm. Standard error bars represent ± S.D.

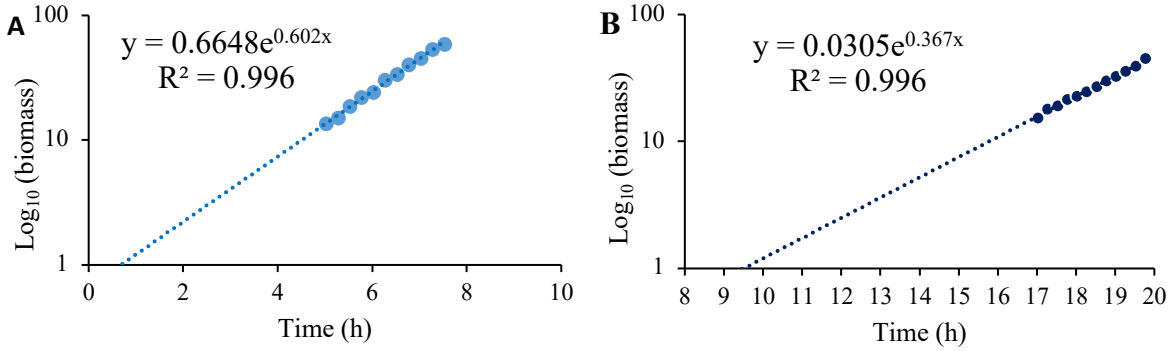

Figure 5.4. Maximum growth rate (μ_{max}) of non-induced cells on glucose as sole C source. A: *E. coli* W3110; B: *E. coli* CLD1301. Biomass (A.U.) was recorded as scattered light. Conditions: minimal media 4 g/L glucose, T = 37^{0}C, V_L = 800 µL.

This metabolic burden stems from the maintenance requirements for the plasmid replication, directing from the cell's energy and resources.

Despite the plasmid burden causing a significant decrease in growth rate (*E. coli* CLD1301: $\mu_0 = 0.367\ h^{-1}$, $R^2 = 0.996$; *E. coli* W3110: $\mu_0 = 0.6\ h^{-1}$, $R^2 = 0.996$) and despite the long lag phase, the final biomass was higher for the recombinant strain compared to the host. The final biomass during stationary phase (22 - 26.77 h) was 48.89 and 56.25 A.U. for *E. coli* W3110 and CLD1301, respectively. The difference in the measured biomass between the host and recombinant strain was significant (Mann-Whitney U, W = 190, n = 19, 19, $p < 0.001$). Nevertheless, the recombinant strain was capable of growth and division under conventional batch fermentation in BioLector, allowing further investigation under continuous mode in STR.

5.5 Determining the optimum amount of IPTG

The recombinant strain *E. coli* CLD1301 contains the heterologous gene GFP-A integrated in the plasmid pD441- SR: 240460. The plasmid has a T5 promoter that allows isopropyl β-D-1-thiogalactopyranoside (IPTG) - inducible high-level expression of the heterologous protein (GFP mut3*). The T5-promoter's activity is modulated by varying the concentration of IPTG.

For optimisation of the IPTG concentration, cultures of *E. coli* CLD1301 were induced at mid-exponential point of growth with varying concentrations (0, 0.05, 0.1, 0.25, 0.5 and 1 mM) of IPTG. The mid-exponential point of growth was the optimum time for induction. If induction was performed earlier, there would not be sufficient biomass in the system to yield recombinant product. If induction was performed later, there would not be enough substrate left for protein production.

Precultures, prepared as described in Section *3.2 Cell expansion and seed preparation A*, were used to inoculate the BioLector with the initial starting OD_{600} was 0.05. Kanamycin 50 µg/ml was added to the growth media (described in Section *3.3.1 Batch mineral media*) as the pD441- SR plasmid contained a kanamycin-resistant gene. The glucose concentration (w/v) was 4 g/L.

As the recombinant product, GFP mut3* (238 aa) is soluble in cytoplasm at 37^0C, this was the temperature for both growth and induction. Product formation (GFP mut3* fluorescence) and

biomass concentration (scattered light) were monitored online for varying amounts of IPTG, and the corresponding signals were given in arbitrary units (A.U.). The time of induction was the mid-exponential point of growth, or time 0 (*Figure 5.5*).As previously reported, the GFP signal is very stable (Andersen *et al.*, 1998). The GFP signal remained relatively constant, in a plateau for at least 18 hours (*Figure 5.5)*. This suggests that the protein is resistant to proteolysis and degradation and is suitable for continuous cultivations.

The maximum GFP fluorescence (A.U.) was obtained approximately ten hours post-induction. The mean signal was 398.77, ranging from 387.89 to 411.83 A.U. with 1 mM IPTG as inducer. The signal (A.U.) under 0.5 mM IPTG ranged from 355.79 to 373.51, with a mean of 364.13 *(Figure 5.5)*. The difference in GFP fluorescence after 10 h post-induction for 1 and 0.5 mM IPTG was significant (Mann-Whitney U, $W = 4732$, $n = 56, 56$, $p < 0.001$). The optimum IPTG concentration that led to the highest amount of product was 1 mM (*Figure 5.5)*. This is in accordance with the published recommendation for the plasmid (https://www.atum.bio/catalog/expression-vectors/bacterial).

Shifting the cell's metabolic resources towards producing recombinant product impedes the cell growth. To see the extent by which a high amount of recombinant product compromises the biomass development, the specific yield (or specific productivity) was determined. Specific yield, representing the amount of product produced per cell per unit time was calculated by dividing the concentration of product to that of biomass. The GFP mut3* fluorescence (A.U.) was a suitable signal for product concentration, and light scatter signals (A.U.) were used for biomass concentration. The signal gain factors (GFP – Gain: 50; biomass – Gain: 20) were maintained across experiments as previously illustrated (*Table 3.2*). The highest specific yield (A.U.) for *E. coli* CLD1301 grown on glucose as sole carbon source was obtained with 1 mM IPTG, proving the optimum concentration of inducer was 1 mM (*Figure 5.6).* This concentration was further transferred to STR experiments.

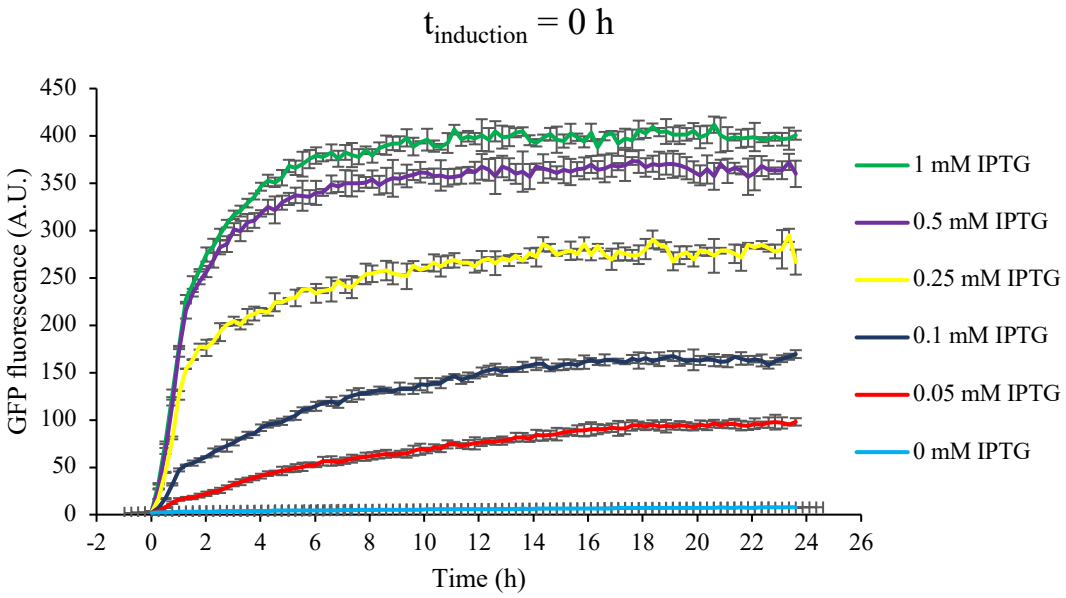

Figure 5.5. Comparison of GFP mut3* fluorescence (A.U.) after induction with varying concentrations of IPTG added at mid-exponential phase of growth. Time 0 represents the time of induction, T = 37^{0}C. Standard error bars represent ± S.D.

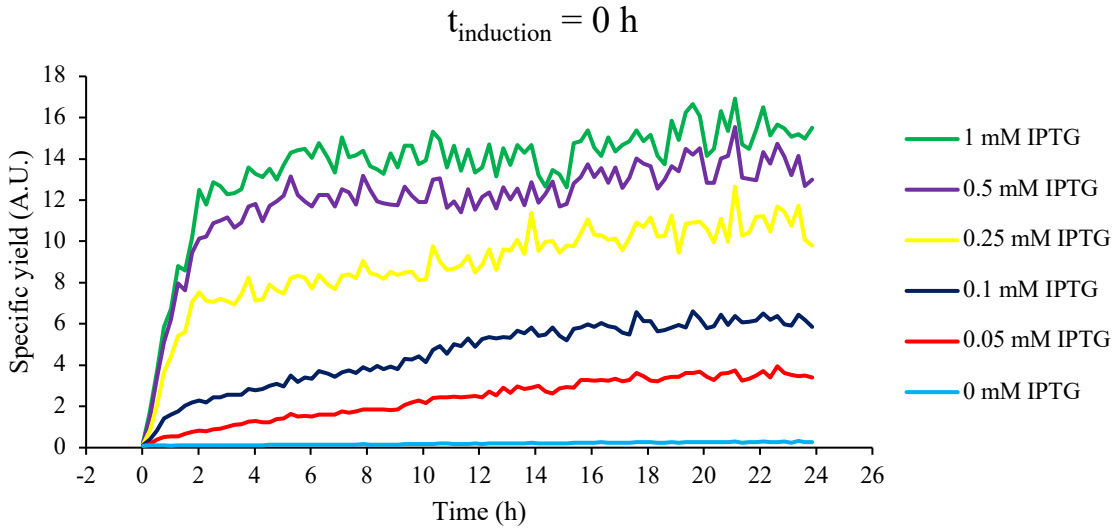

Figure 5.6. Specific product yield (Y_X^P) for *E. coli* CLD1301 on glucose as sole carbon source. Specific product yield calculated as the ratio of protein concentration (GFP fluorescence) to biomass concentration (scattered light intensity). Time 0 represents time of induction. T = 37^{0}C.

5.6 Process monitoring at population level

The recombinant *E. coli* CLD1301 was cultivated with and without induction of GFP to evaluate the influence of recombinant protein synthesis on the growth. Fermentations were carried out in 3 L bench-top fermenters with 1.5 L working volume (Applikon Biotechnology B.V., Schiedam, The Netherlands) from starting OD_{600} ~ 0.05. Oxygen limitation was avoided by maintaining the DO level above 50% saturation by the automated increase of stirrer speed. At mid-exponential point of growth, after sampling for growth at μ_{max}, the chemostat cultivation was started by activating the inlet and outlet peristaltic pumps. The specific growth rate in chemostat was controlled at ½ μ_{max}, and the constant volume was maintained by running the outlet peristaltic pump at maximum speed, while the outlet line was level controlled.

5.6.1 Biomass measurements

The fermentation profiles of *E. coli* CLD1301 on glucose as sole carbon source are depicted in both the absence *(Figure 5.7)* and presence (*Figure 5.8)* of 1 mM IPTG. Batch fermentations in BioLector (*Figure 5.4)* have shown a μ_{max} of 0.37 h^{-1} for the recombinant strain grown on glucose as sole carbon source, thus the chemostat was expected to run at 0.19 h^{-1} (1/2 μ_{max}). A growth rate recovery was observed in STR experiments, with a μ_{max} of 0.67 h^{-1} *(Figure 5.9)*. This could be the result of the cells adapting to the environment by selection of desirable traits and gaining a fitness advantage. Although mutations are known to occur at a reduced growth rate, they were, however, not investigated during this work. As a result of the increased growth rate, chemostat experiments were carried out at a dilution rate (D) of 0.33 h^{-1}. The initial batch phase started from inoculation (time 0) and the cells exhibited exponential growth at μ_{max} of 0.67 h^{-1}. At mid-exponential point (time 5.5 – 5.75 h), when OD ~ 2, the culture was switched to a continuous mode of operation. At transition point, cells switch from unlimited to C-limited growth, controlled by a constant glucose concentration of 4 g/L as the growth-limiting factor. Because of similar growth rates in STR, sampling was maintained as for host *E. coli* W3110 grown on glucose.

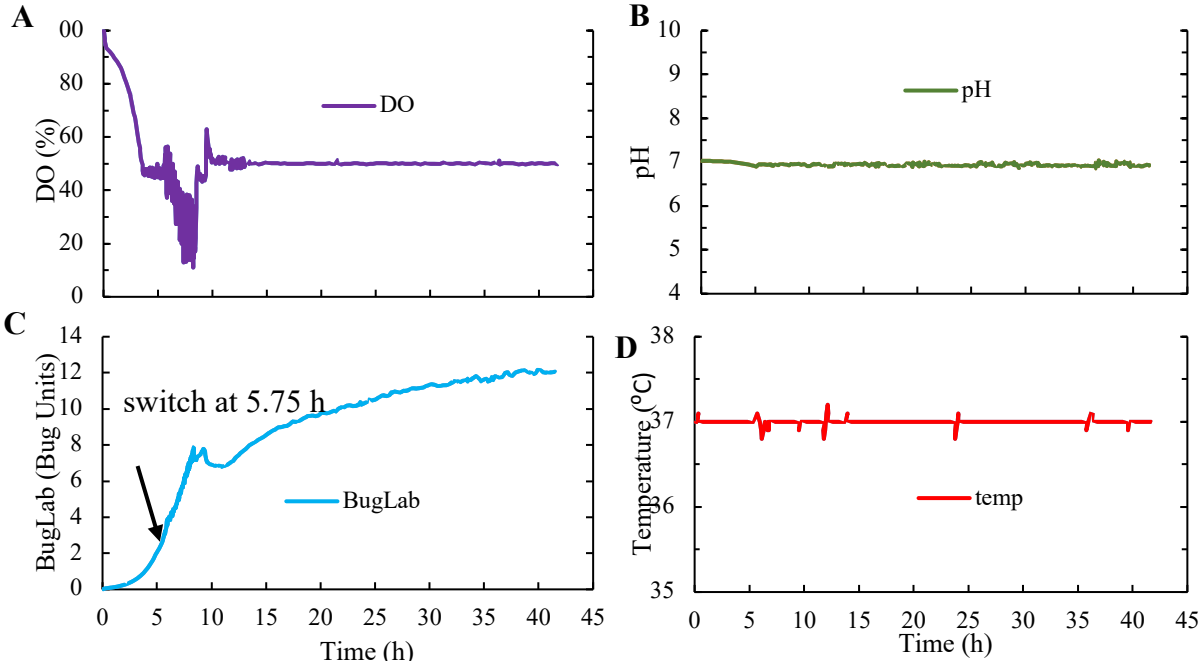

Figure 5.7. Fermentation profile of *E. coli* CLD1301 on glucose as sole carbon source. No IPTG (the arrow indicates the switch). This includes changes in dissolved oxygen (A) and biomass (C), whilst pH (B) and temperature (D) are maintained constant at set-points.

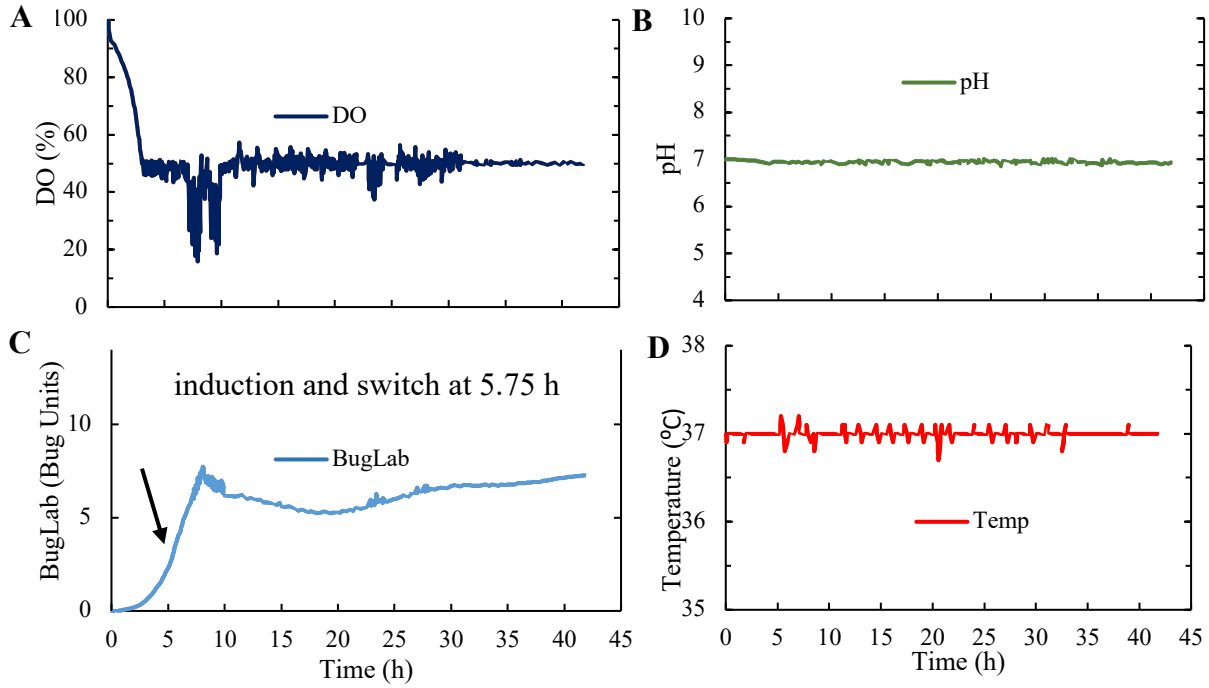

Figure 5.8. Fermentation profile of *E. coli* CLD1301 on glucose as sole carbon source with 1 mM IPTG (the arrow indicates the switch). This includes changes in dissolved oxygen (A) and biomass (C), whilst pH (B) and temperature (D) are maintained constant at set-points.

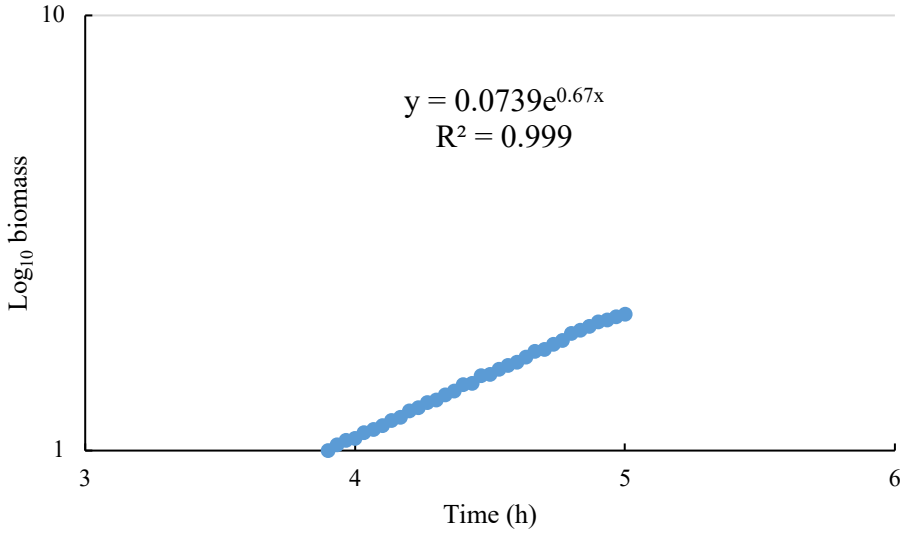

Figure 5.9. Growth rate recovery of *E. coli* CLD1301 on glucose as sole carbon source. Data from *Figure 5.7* obtained with BugLab sensor.

5.6.2 The influence of protein production on growth

The optimised induction parameters (*described in Section 5.5 Determining the optimum amount of IPTG)* were transferred to STR. *E. coli* CLD1301 cells were grown with 4 g/L glucose in both the presence and absence of 1 mM IPTG (*Figure 5.10)*. The final biomass, measured as scattered light, obtained in stationary phase (chosen arbitrarily past 25 h) was compared and the difference was deemed significant (Mann-Whitney U, W = 125250, $p < 0.005$). The median biomass (B.U.) of 11.56 in non-induced cells with 0 mM IPTG (X_0) dropped to 6.76 in *E. coli* CLD1301 induced with 1 mM IPTG (X_1). Thus, the cost of protein production on the growth at submaximal growth in glucose was 41.60%, calculated from formula

$$Cost = \frac{X_0 - X_1}{X_0} \; x \; 100 \qquad (5.2)$$

where X_0 is the final biomass with 0 mM IPTG and $X1$ is the final biomass on glucose with 1 mM IPTG.

While GFP mut3* is a small protein (238 aa), its production limits the resources that the cell could utilise for native protein synthesis. Faced with the large copy number plasmid (500-700 copies per cell), the visible result of producing the recombinant protein is a lower biomass *(Figure 5.10).* A lower biomass is expected given that the protein synthesis uses the same cell machinery and resources for both recombinant and native products. The lower biomass may signal a reduced cell number or increase in cell death, perhaps with added changes in morphology. The system, however, achieves a constant biomass, even if lower, which shows there is still proliferation, suggesting that GFP mut3* is not toxic to the cell.

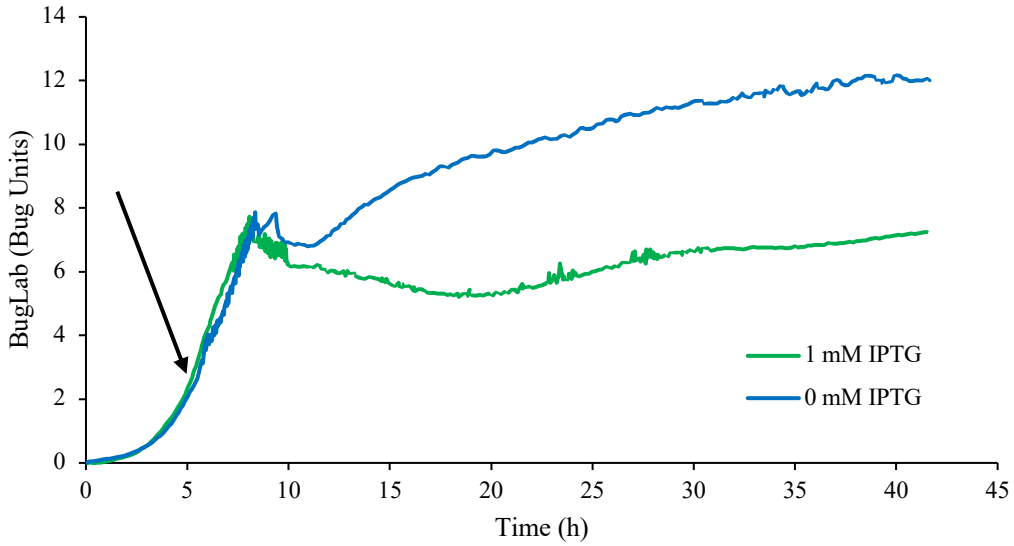

Figure 5.10. Online measurements for *E. coli* CLD1301 biomass (BugLab) as scattered light intensity (B.U.) in non-induced and induced cells. Arrow: time of induction with 1 mM IPTG (mid-exponential at 5.75 h). Conditions: minimal media with 4 g/L glucose.

5.6.3 Monitoring growth at single cell level

The total cell counts (TCCs) were calculated by multiplying the number of events occurring in the region dot plot by 200 (correction for 5 µl analysed volume) and the dilution factor used to lower the sample OD_{600} to 0.025. The average counts across continuous cultivation as measured by FC were 9.19 x 10^8 for non-induced and 4.16 x 10^8 for induced *E. coli* CLD1301, respectively *(Figure 5.11)*. The only difference between the two experiments was the addition of 1 mM IPTG, which induces the recombinant protein expression. This shows that the expression of the heterologous protein (GFP mut3*) causes a drastic decrease in cell

numbers. As the dilution rate is constant across experiments, the decrease in cell number must occur because of a reduced growth rate. The cell number, however, remained at a relatively constant level, showing that cells are still dividing.

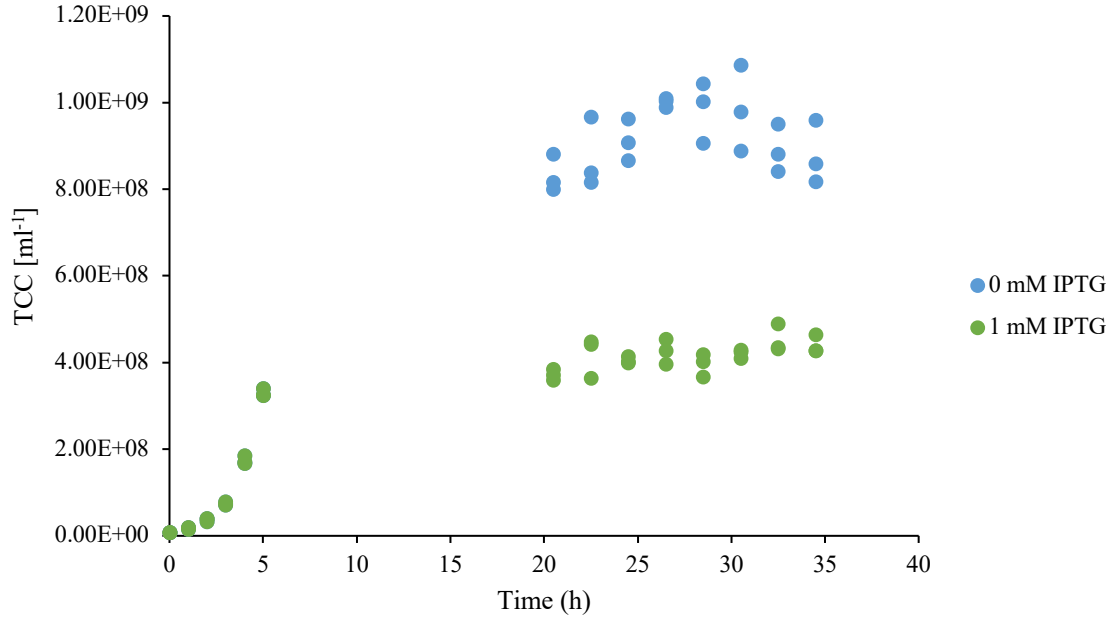

Figure 5.11. Total cell count (TCC) for *E. coli* CLD1301 in three independent experiments on glucose minimal media. The gap between the two datasets (15 h) is to allow the culture to reach a "steady state".

5.6.4 Monitoring substrate

Residual glucose was measured in the supernatant both in the absence and presence of 1 mM IPTG *(Figure 5.12).* As the population increased, glucose depleted from 4 to 2.02 g/L at the mid-exponential point of growth. The residual glucose at "steady state" in chemostat fluctuated from 0.008 g/L to 0.019 g/L and from 0.02 g/L to 0.03 g/L in the absence and presence of IPTG, respectively. All culture supernatant contained residual glucose within the measurement range of the kit.

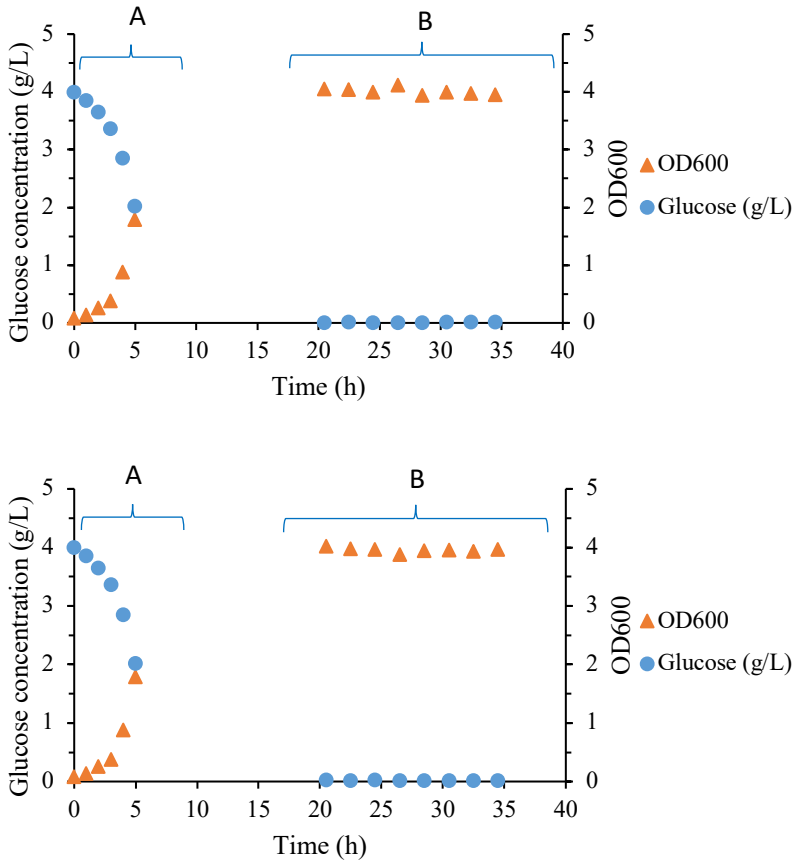

Figure 5.12. Depletion of glucose in relation to OD_{600} development by *E. coli* CLD1301 in the absence (top graph) or presence (bottom graph) of IPTG. A: Exponential phase of growth (time 0 - 5 h) with sampling every hour. B: Continuous cultivation (time 20.5 - 34.5 h) with sampling every two hours.

Biomass measured offline as OD_{600} increased during the batch phase of fermentation up to 5 h post inoculation (OD_{600} = 1.788) (*Figure 5.12)*. At steady state, OD_{600} varied from 3.955 – 4.116 and 3.885 - 4.025 for the non-induced and induced recombinant strain, respectively. This slight variation in OD_{600} does not correlate with the drastic changes in biomass recorded by the BugLab sensor (*Figure 5.10)* or with the decrease in cell number recorded by FC (*Figure 5.11).* As OD_{600} represents a population level measurement correlating the attenuation of light to the cell concentration and there is a decrease in cell number, the slight variation in OD_{600} could be explained only by morphological changes adding to a reduced cell number.

5.6.5 Monitoring VFAs

High performance ion chromatography (HPIC) analysis of *E. coli* CLD1301 supernatant detected the existence of three volatile fatty acids (VFAs) on glucose as sole carbon source: acetate, formate and propionate (*Figure 5.13)*. VFAs are fermentation by-products with negative consequences on recombinant protein production.

At maximum growth rate μ_{max} on glucose as sole carbon source, acetate and formate commenced forming immediately post-inoculation (*Figure 5.13)*. Propionate was not detected. Despite the fully aerobic conditions *(Figure 5.8)*, the production of VFAs occurred because the cells surpassed the threshold growth rate of glucose consumption. Both acetate and formate levels increased with growth, reaching 129.51 ppm (1.30×10^{-1} g/L) and 19.72 ppm (1.97×10^{-2} g/L) at 5 h post-inoculation. The rate at which the acetate formed was exponential, shown by acetate levels following the growth curve (*Figure 5.13*). Three carbon sources were present in the media (glucose, acetate and formate) at maximum growth rate. As glucose was plentiful, shown by the exponential growth curve, *E. coli* cells consumed their preferred carbon source, glucose. At 5.5 h post-inoculation, the system was switched to continuous cultivation, therefore the levels of VFAs never accumulated in quantities that would inhibit growth. At a high growth rate on glucose as sole carbon source, there is, however, acetate, at a level corresponding to the rate of growth. As carbon is converted to VFAs instead of biomass and recombinant protein, a fast growth rate on glucose is not beneficial for improving recombinant protein production.

At ½ μ_{max}, during chemostat growth, traces of formate and propionate were identified. The acetate was either not detected or was negligible with a maximum of 0.85 ppm (8×10^{-4} g/L). The formate varied from 16.34 ppm (1.63×10^{-2} g/L) to 21.09 ppm (2.11×10^{-2} g/L), whilst propionate varied from 3.85 ppm (3.85×10^{-3} g/L) to 9.78 ppm (9.78×10^{-3} g/L). This shows that a lower growth rate reduces the amount of VFAs and allows an efficient conversion of carbon towards biomass and recombinant protein. The growth rate limitation, however, has to be on carbon specifically. The most popular minimal media (Sambrook, 2001) has the main limitation on nitrogen (see Appendix A). Regardless of the growth rate, a chemostat using the common defined media would invariably lead to the formation of acetate because it is the nitrogen that limits growth, which in turns places carbon in excess.

IPTG had no effect on the levels of VFAs detected in supernatant.

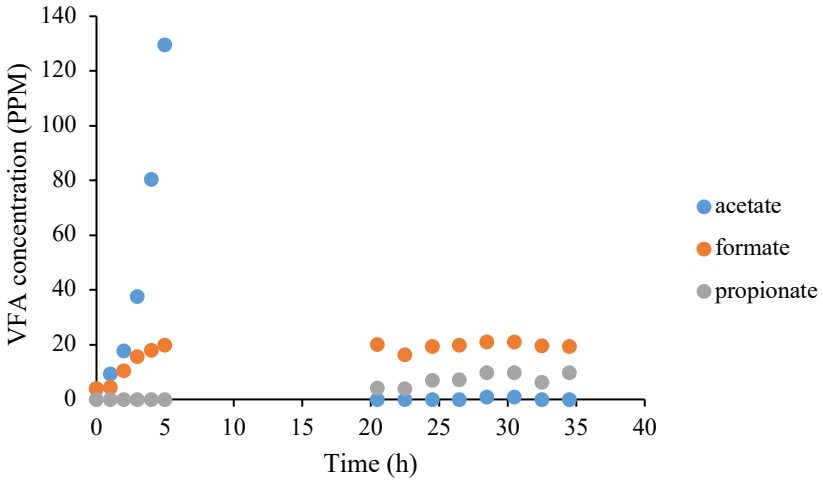

Figure 5.13. VFAs production of *E. coli* CLD1301 on glucose mineral media without IPTG. The gap between the two datasets (15 h) is to allow the culture to reach a "steady state".

5.7 Single cell studies of membrane integrity using FC

The amount of recombinant product correlates closely with the metabolism of the viable biomass. To determine the cell viability, membrane integrity was analysed using TO and PI with flow cytometry (FC). Viable cells show green fluorescence, whilst dead cells show red, comparable to cells treated with 70% ethanol used as a "dead" control.

The membrane integrity was determined for cells harvested from both unlimited (mid-exponential) and glucose-limited (chemostat) cultivations. The results were expressed in percentages of cells that stain with either dye plotted as green over red fluorescence. The viability of *E. coli* CLD1301 was about 97% immediately following inoculation, at time point 0 (*Figure 5.14)*. During the maximal growth rate, the frequency of TO-stained cells increased to around 99%. Only 1% of cells were PI positive at 5 h post-inoculation, before switching to a continuous mode of operation.

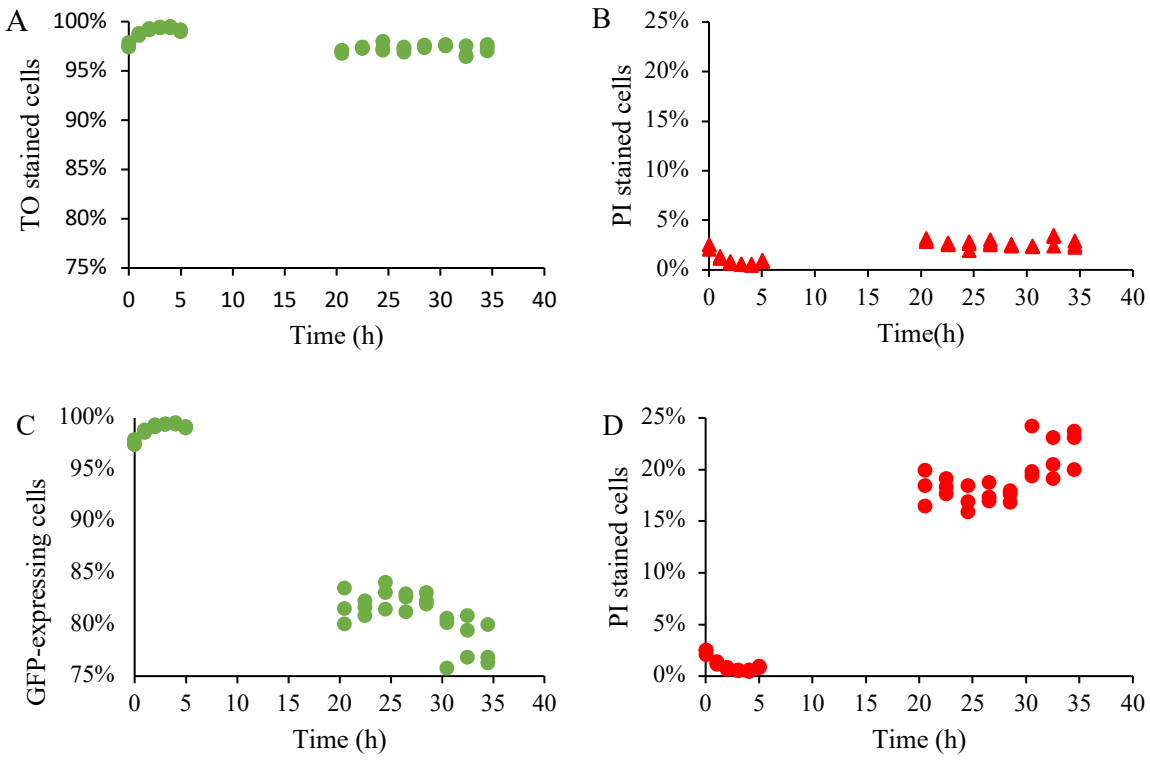

Figure 5.14. Percentage of live (TO^+) cells and dead (PI^+) cells in three independent fermentations of *E. coli* CLD1301 on glucose. Green circles represent TO^+ cells, red circles are PI^+ cells. A, B) 0 mM IPTG. C, D) 1 mM IPTG.

At submaximal growth rate on glucose, in the absence of IPTG, the share of PI positive cells fluctuated around a mean of 2.70%. Conversely, the share of TO positive cells fluctuated around a mean of 97.30% in non-induced recombinant *E. coli* CLD1301 (*Figure 5.14)*.

In the presence of IPTG, the recombinant strain produced the protein GFP mut3*. The frequency of viable cells once recombinant protein production began, decreased to an average of 81% across steady states. Conversely, only 19% of cells could be assigned to the "dead" gate based on alcohol-killed cells. Overall, there was a significant increase in the fraction of the "dead" subpopulation in the induced compared to non-induced *E. coli* CLD1301 cells.

5.8 Single cell studies of membrane potential using FC

The physiological heterogeneity of *E. coli* CLD1301 cells was analysed quantitatively by flow cytometry using the dye combination $DIBAC_{4(3)}$/EB/PI. Samples from STR were diluted

in DBS to achieve an OD_{600} of 0.025 prior to staining (described in Section *3.8 Monitoring membrane potential with DIBAC/EB/PI*). The percentage of each sub-population was evaluated at different growth rates in the absence of 1 mM IPTG. The experiments were not performed in the presence of IPTG because when inducing the culture, the fluorescence of the recombinant protein GFP mut3* overlaps that of $DIBAC_{4(3)}$.

Four subpopulations were identified based on the differential uptake of the fluorophores:

a) active cells ($DIBAC_{4(3)}^-$, $EtBr^-$, PI^-) did not take up any of the dyes;

b) depolarised cells ($DIBAC_{4(3)}^+$, $EtBr^+$, PI^-) are $DIBAC_{4(3)}$ and EtBr double-stained cells;

c) deenergised cells ($DIBAC_{4(3)}^-$, $EtBr^+$, PI^-) are EtBr-stained cells;

d) dead cells ($DIBAC_{4(3)}^+$, $EtBr^-$, PI^+) are $DIBAC_{4(3)}$ and PI double-stained cells.

The percentage of active cells ($DIBAC_{4(3)}^-$, $EtBr^-$, PI^-) in *E. coli* CLD1301 population dropped from 87.17% at maximal growth rate to an average of 57.02% at submaximal growth rate in chemostats (*Figure 5.15)*. The difference in the shares of active cells across glucose-limited growth in chemostat (SS1-SS8) was not significant (Kruskal-Wallis, $H = 8$, $p = 0.433$). This correlated with no significant deviation from the expected ratio of active cells (Chi Square, $X^2 = 0.477$, $P = 1.0$).

The share of depolarised cells ($DIBAC_{4(3)}^+$, $EtBr^+$, PI^-) increased from 8.05% to an average of 33.15% in samples taken from maximal and submaximal growth on glucose, respectively (*Figure 5.15)*. No statistical difference was present between the proportion of depolarised cells in all steady states (Kruskal-Wallis, $H = 8$, $p = 0.433$). This is backed up by no significant deviation away from expected values of depolarised cells (Chi Square, $X^2 = 1.02713$, $P = 0.994$).

At submaximal growth in glucose-limited chemostats, the mean of active and depolarised cells across all steady states (SS1-SS8) was 57.02% and 33.15% respectively - a significant difference (Mann-Whitney U, $W = 100$, $p < 0.005$).

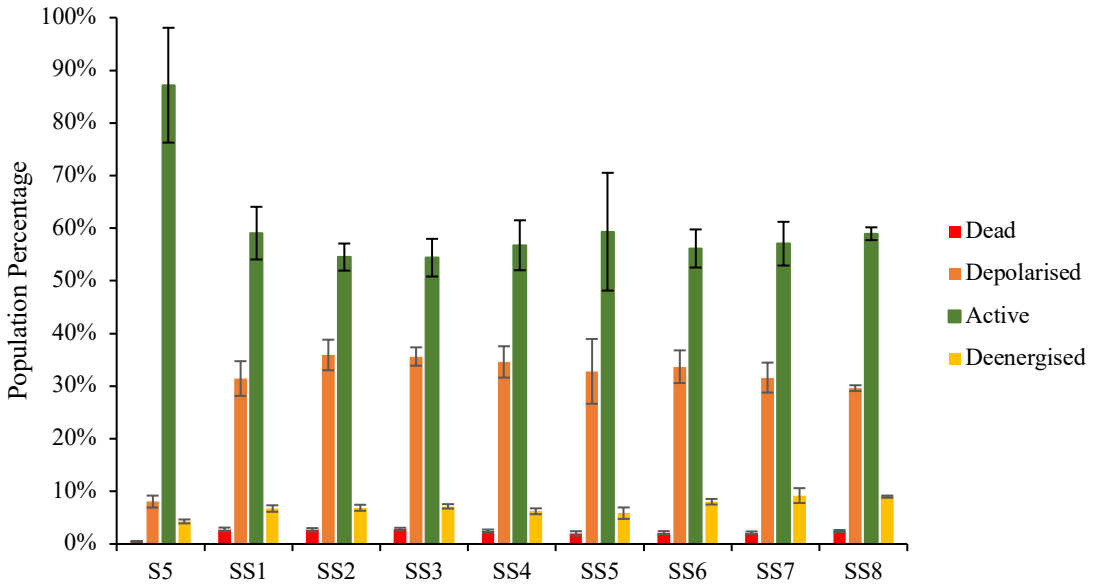

Figure 5.15. Flow cytometry analysis of *E. coli* CLD1301 cells at different growth rates on glucose as sole carbon source. No induction (0 mM IPTG). S5 represents the mid-exponential sample, while SS1-SS8 are steady state (SS) samples at 2 h intervals, with reduced growth at $\mu_{max}/2$. Data presented as mean ± S.E. depicts four subpopulations of cells: active, depolarised, dead and deenergised.

5.9 Studies of cell morphology using fluorescence microscopy

Induced recombinant cells were stained with PI. For comparison, non-induced cells were stained with SYTO$_9$/PI. The staining was described in Section *3.10 Phase and fluorescence microscopy of E. coli W3310*. Only the "live" cell population fluorescing green was analysed. The analysis was performed in an automated manner, by running a macro written for ImageJ, which is available in Additional File (Appendix F). Cell size was determined from fluorescent images as "cell area", and cell shape was analysed as "aspect ratio" (AR) and circularity (or form factor).

5.9.1 Cell morphology at maximum growth rate

At maximum growth rate, *E. coli* CLD1301 cells presented the following as illustrated in *Table 5.1.*

	Mean	Median	±S.D.	CV	*Figure*
Cell area (μm^2)	2.03	1.78	1.08	53.29	*5.16 A*
AR	3.23	3.06	1.27	39.45	*5.16 B*
Circularity	0.56	0.55	0.15	26.66	*5.16 C*

Table 5.1. Shape descriptors of *E. coli* CLD1301 during exponential growth.

5.9.2 Cell morphology in the absence of IPTG

a) Cell area

The distributions of cell size cell were influenced by the growth rate. Maximum growth rate showed a mean cell area of 2.03, with a median of 1.78 μm^2 (*Figure 5.16 A)*. At reduced growth in glucose-limited chemostats, cell area heterogeneity was observed with cells of different sizes populating the fermenter. The mean cell area ranged from 1.58 to 2.61 μm^2 in SS4 and SS1, respectively. Contrary to previous reports that lowering the growth rate decreased cell size (Hill et al., 2013), a highly heterogeneous environment was observed for *E. coli* CLD1301 when reducing the growth rate by a factor of 2. The differences in the mean cellular area at submaximal growth were significant (Kruskal-Wallis, $H = 105.57$, $p < 0.001$). This shows that the chemostat does not exists in a "steady state", if cells cannot maintain size.

b) Aspect ratio

The mean aspect ratio (AR) at maximal growth rate was 3.23, with median 3.06 (S.D. 1.27, CV 39.45) (*Figure 5.16 B).* In chemostat, the mean AR ranged from 1.95 and 3.81 at SS1 and SS8, respectively - a range which includes the exponential mean (*Figure 5.16 E*).

The trend was consistent when comparing the median AR. The exponential value of 3.0610 is present within the chemostat range from 1.702 and 3.871 at SS1 and SS8, respectively. The CV as a measure of heterogeneity varied at submaximal growth on glucose as sole carbon source from 29.80 (SS8) to 44.31 (SS1), a range which includes the exponential CV.

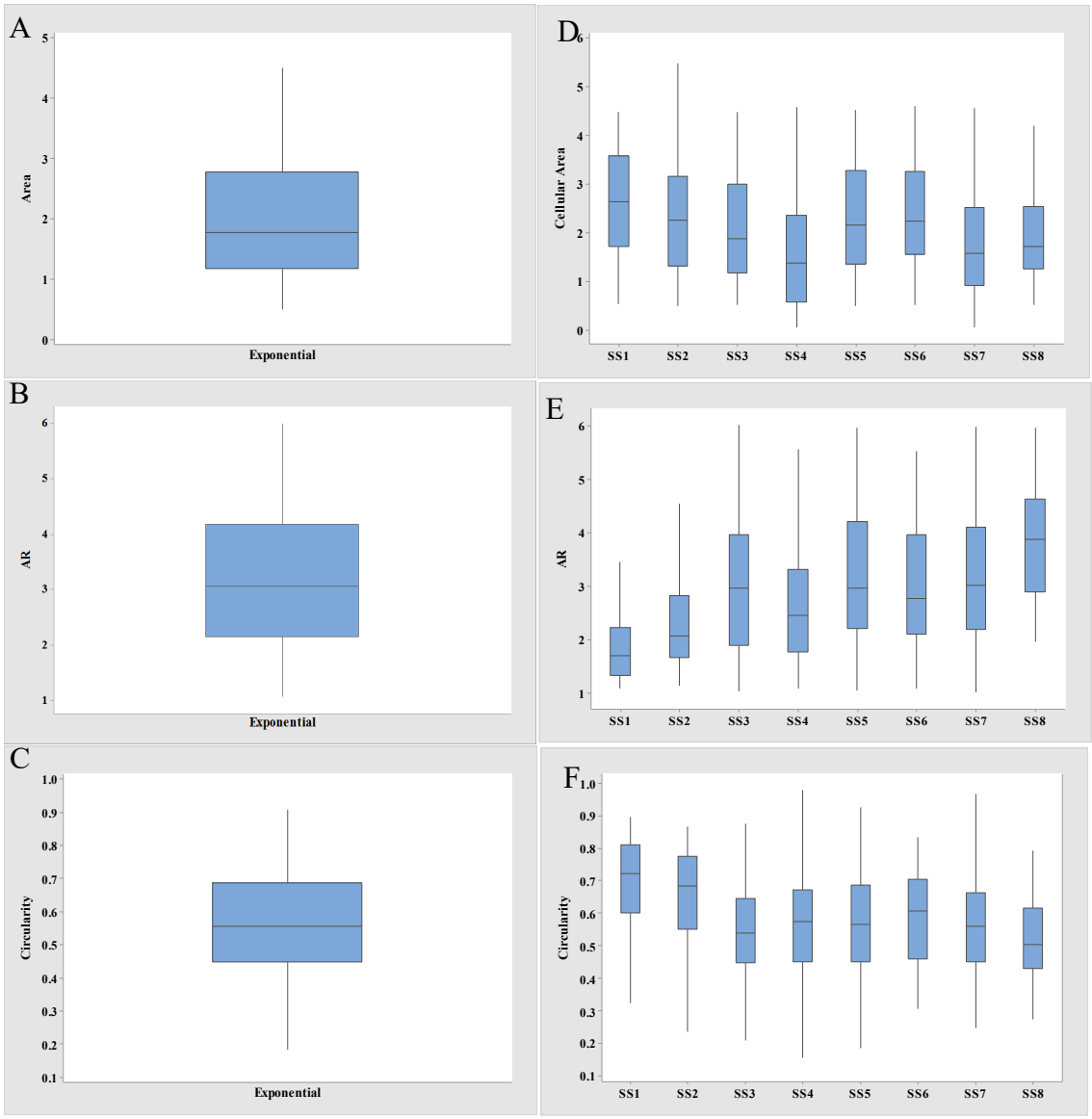

Figure 5.16. Box plots of morphological descriptors of *E coli* CLD1301 at maximum growth rate (A, B, C) and submaximal growth rates (D, E, F). Horizontal line marks the median, box marks the 25th and 75th percentile, whiskers mark the 5th and 95th percentile. Number of cells per sample was: A: SS1 – 95; SS2 – 232; SS3 – 191; SS4 – 113; SS5 – 168; SS6 – 87; SS7 – 667; SS8 – 409 cells. B: Exponential – 716 cells. Values outside of the 1.5-fold IQR were removed.

c) Circularity

During maximal growth on glucose, the mean cell circularity was 0.56, with a median of 0.55 (S.D. 0.15, CV 26.66) (*Figure 5.16 C).* At submaximal glucose-limited growth, the mean cell

circularity ranged from 0.53 and 0.70 at SS8 and SS1, respectively, a range that includes the exponential (*Figure 5.16 F)*. Statistical testing, however, showed that the circularity varied significantly between groups at "steady state" on glucose-limited growth (Kruskal-Wallis, $H = 124.11$, $p < 0.001$).

This indicates that the cells do not maintain their shape, also observed on microscopy images. A proportion of cells do not grow in straight lines, while some lost the ability to maintain cell width. Filaments were observed in both "live" and "dead" cell subpopulations. The cell inability to maintain a robust shape could be related to a deficiency in synthesising peptidoglycan in the cell wall, which may be of a genetic nature. What it is clear is when placed under significant internal stress of replicating a 500-700 copies non-native plasmid, while suffering the external stress induced by carbon limitation, the cells do not maintain shape. This happens in the absence of protein expression, as the cells are not yet induced.

5.9.3 Cell morphology in the presence of IPTG

a) Cell area

Cell area fluctuates in the presence of IPTG at sub-maximal growth (*Figure 5.17 A*). The mean cell area during chemostat cultivations ranged from 1.79 to 2.07 μm^2 at SS1 and SS8, respectively. The exponential mean of 2.03 μm^2, representing cells in the absence of inducer (*Figure 5.16 A*) is included within the chemostat range (*Figure 5.17 A*). A similar trend was observed for the median, ranging from 1.09 (SS2) to 2.21 μm^2 (SS5) at submaximal growth rate (*Figure 5.17 A*), and including the exponential 1.78 μm^2.

The exponential CV of 53.29 (*Figure 5.16 A*) is also included in the range observed during submaximal growth from 44.85 at SS5 to 75.84 at SS2 (*Figure 5.17 A*). Differences in cell area at submaximal growth on glucose for cells expressing the recombinant product were deemed significant (Kruskal-Wallis, $H = 25.26$, $p < 0.01$). This means that the cells are unable to maintain size in chemostats when faced with an added carbon-limitation on the top of metabolic burden caused by recombinant product.

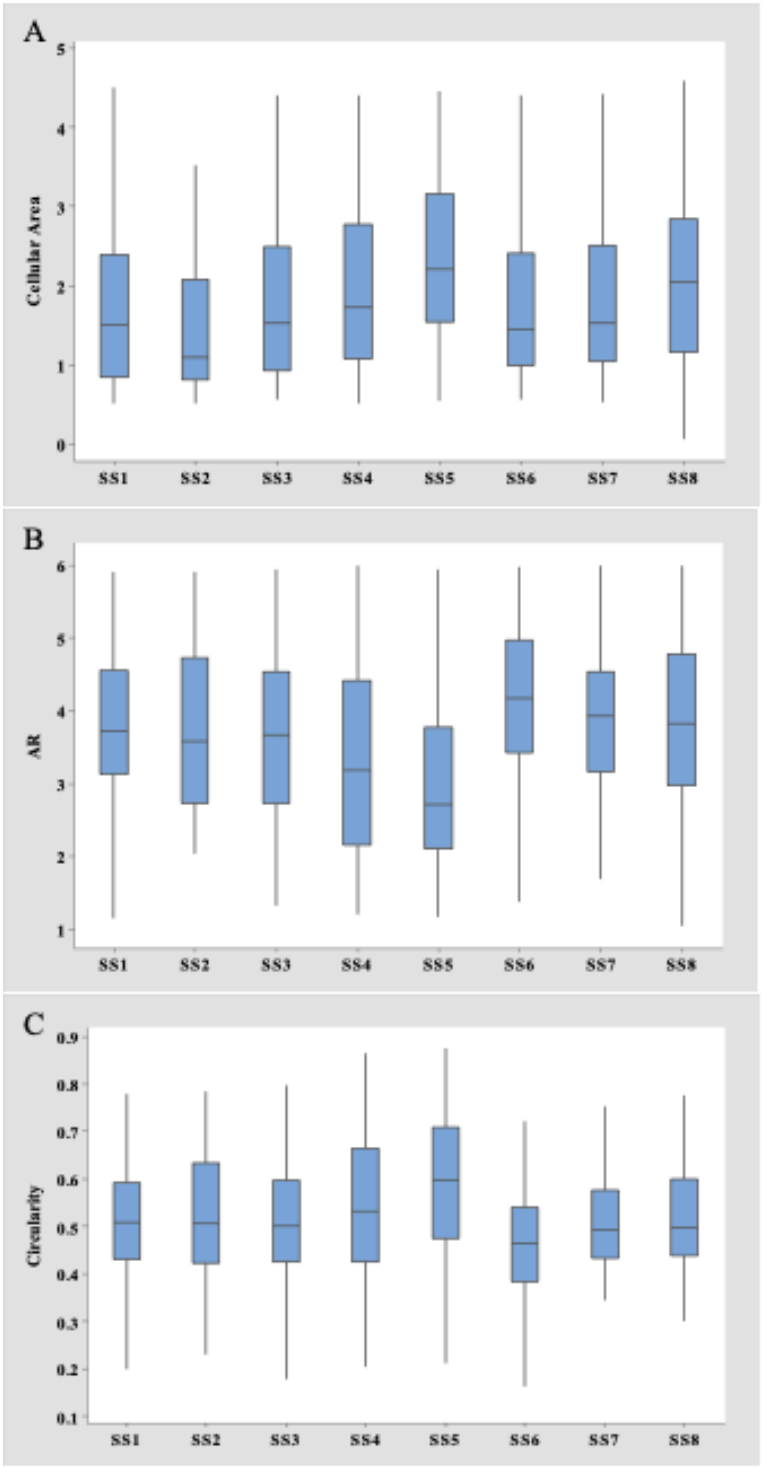

Figure 5.17. Shape descriptors in *E. coli* CLD1301 on submaximal growth rate on glucose with IPTG. Number of cells per sample was: SS1 – 143; SS2 – 58; SS3 – 129; SS4 – 156; SS5 – 87; SS6 – 111; SS7 – 55; SS8 – 83 cells.

b) Aspect ratio

The mean AR of *E. coli* CLD1301 ranged at submaximal glucose-limited growth from 2.96 to 4.12 in SS5 and SS6 respectively (*Figure 5.17 B).* This refers to the AR of cells producing the recombinant product. At maximal growth, the mean AR was 3.23 (*Figure 5.16 B*), a value within the chemostat range. A similar trend was observed for the median exponential AR of 3.06, a value that is contained within the chemostat range from 2.72 (SS5) to 4.18 (SS6). The differences between AR of cells in chemostat were significant (Kruskal-Wallis, $H = 62.74$, $p < 0.001$). This shows that the system is not in "balanced growth" when producing high quantities of recombinant product. If balanced growth existed, and the cells elongate before division to the maximum AR as chosen as threshold filter (6), then after division, all cells would range in AR between 3-6. Therefore, the distributions of AR in chemostats are largely heterogeneous and AR varies with the fermentation time.

c) Circularity

Differences in the circularity of *E. coli* CLD1301 producing the recombinant protein are shown in *Figure 5.17*. Circularity is an indicator of the cell's ability to maintain shape. During sub-maximal growth in a glucose-limited chemostat, mean cell circularity ranged from 0.461 to 0.5938 at SS6 and SS5, respectively. A maximum circularity of 1 observed in SS8 suggests the shape of a line, such as a filamentous cell. Values tending towards zero suggest round cells and were observed in all samples at submaximal growth on glucose. The differences in cell circularity at submaximal growth on glucose were deemed significant (Kruskal-Wallis, $H = 62.74$, $p < 0.001$). This shows that cells are unable to maintain their shape at submaximal growth rate, when faced with the additional burden of producing recombinant proteins.

5.9.4 The influence of IPTG on cell morphology at submaximal growth rate

IPTG induced the expression of the target protein GFP mut3* in recombinant strain *E. coli* CLD1301. Cells were imaged in the absence and presence of 1 mM IPTG. SS4 was arbitrarily chosen across two different experiments to determine the effect of IPTG addition. Morphology descriptors (area, AR and circularity) were compared between non-induced and induced cells, following extraction with ImageJ (*Table 5.2* and *Figure 5.18)*.

Variable	Mean	SE Mean	SD	CV	Median
SS4 Area (μm^2)	1.58	0.11	1.18	75.19	1.38
+SS4 Area (μm^2)	1.98	0.086	1.08	54.33	1.72
SS4 Circularity	0.57	0.016	0.17	30.01	0.58
+SS4 Circularity	0.54	0.012	0.15	27.99	0.53
SS4 AR	2.66	0.11	1.11	41.83	2.46
+SS4 AR	3.31	0.11	1.31	39.65	3.19

Table 5.2. Shape descriptors for *E. coli* CLD1301 at submaximal growth rate in the absence and presence (+) of IPTG. Number of cells per sample was: SS4 – 113; +SS4 – 156 cells.

The boxplot of the cell area distribution (*Figure 5.18 A*) clearly illustrates the significant increase in mean values (from 1.58 to 1.98 μm^2), and in median values (from 1.38 to 1.72 μm^2) in induced compared to non-induced cells. There is also a significant increase in cell AR from 2.66 to 3.31 for the mean values and 2.46 to 3.19 for the median values in induced recombinant cells compared to cells in the absence of inducer (*Figure 5.18)*. These observations are consistent with previous reports that the overproduction of recombinant protein results in an increased stress response with cell filamentation that leads to cessation of growth. A greater spreading with larger CV values was observed at submaximal growth in the absence of IPTG compared to cells in its presence for all morphological descriptors (*Table 5.2*).

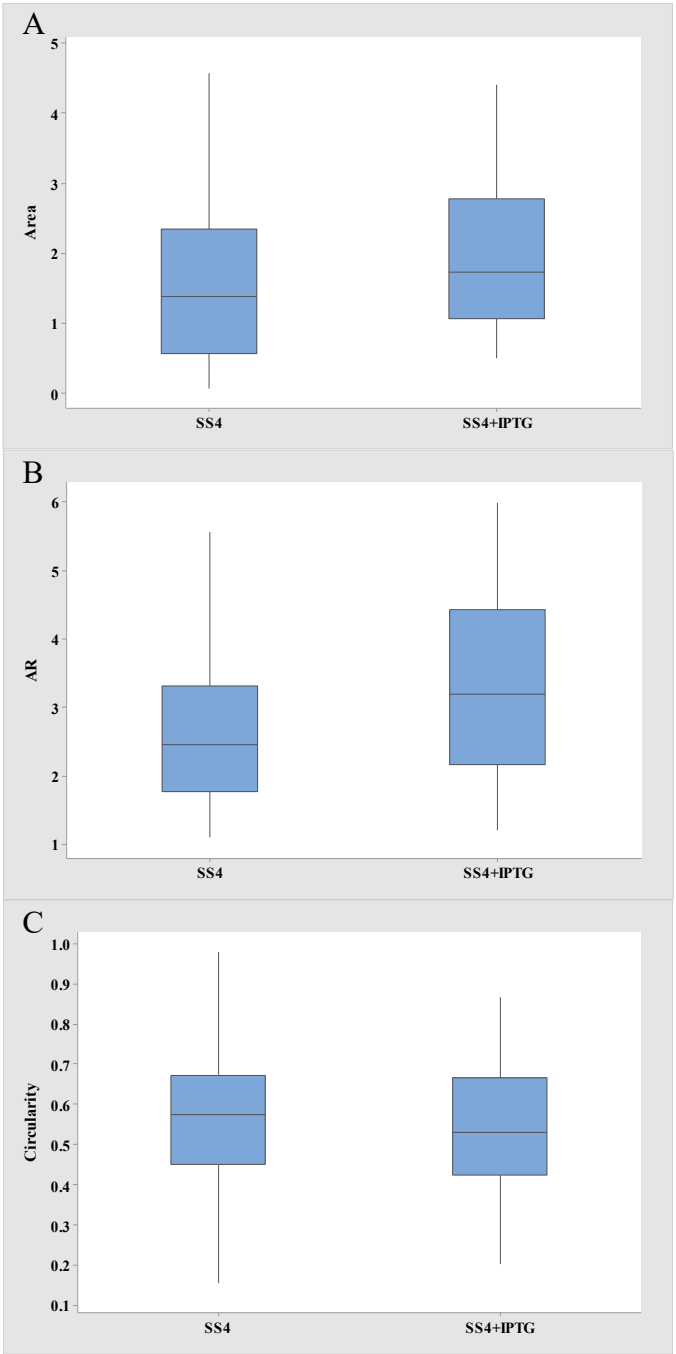

Figure 5.18. Box plots of morphological descriptors of *E coli* CLD1301 showing the influence of IPTG on cell morphology at submaximal growth rate on glucose. Horizontal line represents the median, the box marks the 25th and 75th percentile, whiskers mark the 5th and 95th percentile. Number of cells per sample was: SS4 – 113; +SS4 – 156 cells. Values outside of the 1.5-fold IQR were removed.

The effect of IPTG on the *E. coli* CLD1301 was deemed significant for both cell area (Mann-Whitney U, W = 13298.5, $p < 0.01$) and aspect ratio (Mann-Whitney U, W = 12781, $p < 0.001$. The addition of IPTG however, had no significant effect on circularity (Mann-Whitney U, W = 16120, $p = 0.170$).

5.10 Single cell studies of protein production

The recombinant *E. coli* CLD1301 carries the plasmid vector pD441- SR: 240460 containing the GFP-A gene. To measure GFP mut3* protein expression at single cell level, the GFP signal was measured by fluorescence microscopy (FM) and flow cytometry (FC). The measurements of fluorescence from induced protein expression were compared against background fluorescence. The latter occurs in the absence of induction, resulting from cell auto-fluorescence and leakiness (recombinant protein expression in the absence of inducer).

5.10.1 Protein production evaluated with flow cytometry

The heterogeneity in protein production was measured as GFP fluorescence using the BL1 channel. Samples from STR, containing 12.5 μg/ml kanamycin were diluted in DBS buffer to a final $OD_{600} \sim 0.25$, before FC analysis. The threshold of signal intensity was set to 10000 A.U., with values above the threshold considered positive for protein expression, resulting from both leakiness and IPTG-induced. A "GFP gate" was set that separated cells with green fluorescence above the threshold.

The fluorescent signal of *E. coli* CLD 1301 cells was heterogeneous for both basal and IPTG-induced fluorescence (*Figure 5.19*). To illustrate the difference in heterogeneity, the basal fluorescence of un-induced unstained cells was compared with the IPTG-induced fluorescence (*Figure 5.19).* A total cell number of 46302 were analysed for the IPTG-induced cell fluorescence (in SS8) and 1775 for the basal fluorescence (S5). Both samples had been diluted to a final $OD_{600} \sim 0.25$, but a different cell number occurred as most of the non-induced cells fell in a different gate, the "un-induced" one. The cells assigned to the "induced" gate (46302 and 1775, respectively) exhibited the green fluorescence of GFP mut3*, whether they are IPTG-induced or not.

The IPTG-induced culture (SS8 - 46302 cells) displayed a mean green fluorescence of 544920 A.U., with S.D. of 276019 and CV of 50.65. The non-induced unstained exponentially

growing culture (S5 - 1775 cells) displayed a mean of 66199 A.U., with S.D. 143738 and CV of 217.13 (*Figure 5.19*). As the mean fluorescence varied greatly between the samples SS8 and S5, SD was used as a measure of data spread. The lower S.D. spread shows that the basal level fluorescence was more homogeneous. Although the GFP expression (A.U.) in non-induced cells varies widely from 10022 to 997841, the cell number remained low, and the higher levels of expression represent leakiness from population outliers (*Figure 5.19*). As the cell number expressing leaky proteins are low, and the level of induced GFP signal was much higher than the background, the background fluorescence was considered negligible (*Figure 5.19*). The lower signal for background fluorescence compared to the GFP signal, may be explained by the tight LacI control that reduces basal expression to allow easier quantification of recombinant product.

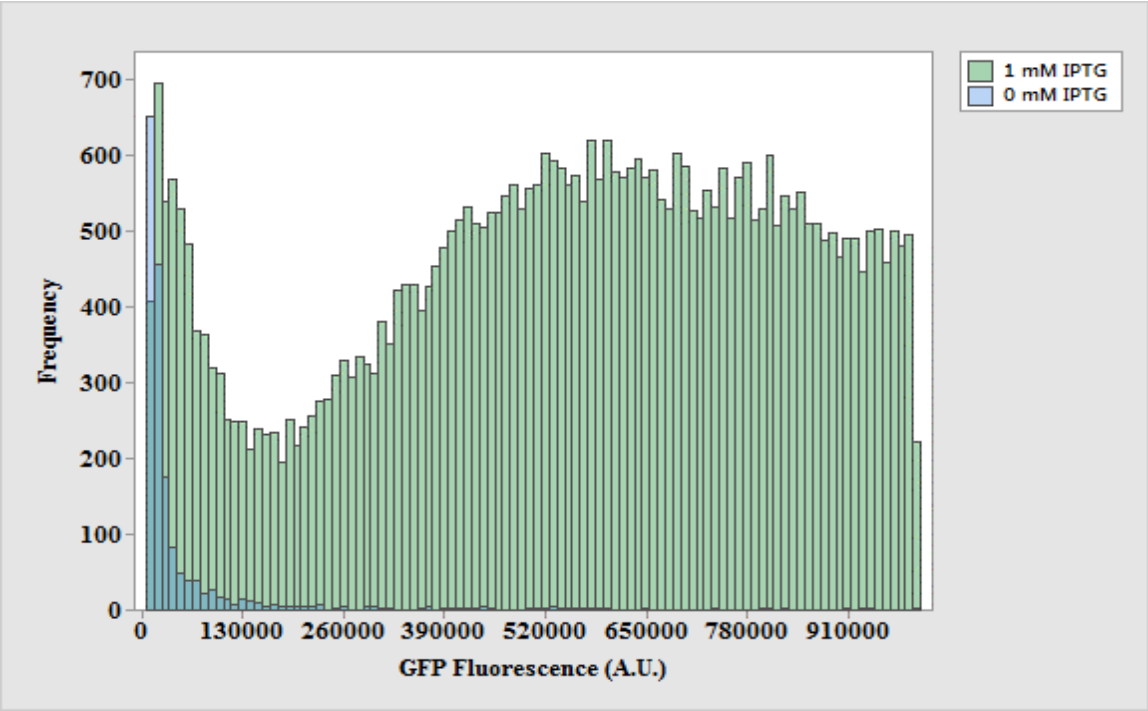

Figure 5.19. Flow cytometry analysis of GFP signal in the presence (1 mM) and absence (0 mM) of IPTG. Histogram shows the frequency (number of cells) and the fluorescence intensity of *E. coli* CLD1301, containing the GFP mut3* gene on an IPTG-inducible plasmid. Data with 1 mM IPTG, shown in green represents SS8 (46302 cells), data with 0 mM IPTG, shown in blue represents the non-induced unstained S5 (1775 cells).

The IPTG-induced fluorescent signal remained relatively constant, displaying neither a rise nor decline during continuous cultivation over 14 h. The *E. coli* CLD1301 grown on glucose as the sole carbon source yielded the fluorescence values (A.U.) shown in *Table 5.3* with 95% confidence intervals (*Table 5.4*). This shows that the recombinant protein GFP mut3* was produced in continuous cultivations of *E. coli* cells.

Variable	N	Mean	S.D.	Min	Q1	Median	Q3	Max
SS1	40319	545192	268335	10014	353065	561446	763414	999868
SS2	34317	538236	279642	10014	337007	563276	766933	999977
SS3	39104	558829	266852	10014	369873	580595	775597	999972
SS4	35200	562139	273656	10010	369240	593432	788908	999985
SS5	47285	553466	278271	10002	355152	585002	782352	999980
SS6	27077	547616	273678	10057	353804	568124	772952	999996
SS7	52968	549774	277183	10001	353925	577295	776837	999979
SS8	46302	544920	276019	10020	347217	568821	772554	999976

Table 5.3. Fluorescent protein signal of GFP mut3* in *E. coli* CLD1301 cells at steady state (SS1-SS8) while growing on glucose as sole carbon source.

Variable	CV	95% Confidence Interval for mean		95% Confidence Interval for median		95% Confidence Interval for S.D.	
SS1	49.22	542573	547811	557721	564982	266496	270200
SS2	51.96	535277	541195	558491	567300	277565	281750
SS3	47.75	556184	561474	576820	584532	264995	268736
SS4	48.68	559280	564998	589149	597855	271649	275692
SS5	50.28	550958	555974	580820	588231	276508	280056
SS6	49.98	544356	550876	563076	572587	271392	276003
SS7	50.42	547413	552134	574089	580907	275524	278863
SS8	50.65	542406	547434	564760	572881	274253	277809

Table 5.4. Confidence intervals (CI) for GFP mut3* fluorescence in *E. coli* CLD1301 cells at steady state (SS1 - SS8) while growing on glucose as sole carbon source.

Boxplots show that the GFP signal was maintained in continuous cultivation over 14 h. There is cell-to-cell heterogeneity in the fluorescence signal, illustrated by data spread, but the total protein content across the steady state remained relatively stable, with neither increase nor decrease of protein production (*Figure 5.20*).

The percentage of producing cells from the assessment of viability also remained relatively constant (*Figure 5.14).*This suggests that despite the cell-to-cell heterogeneity in protein production, the total yield remained constant (*Figure 5.20*). Higher levels of protein production are desirable in a bioprocess, particularly a fed-batch one, yet not so much in continuous cultivations, where a high producing phenotype would perish.

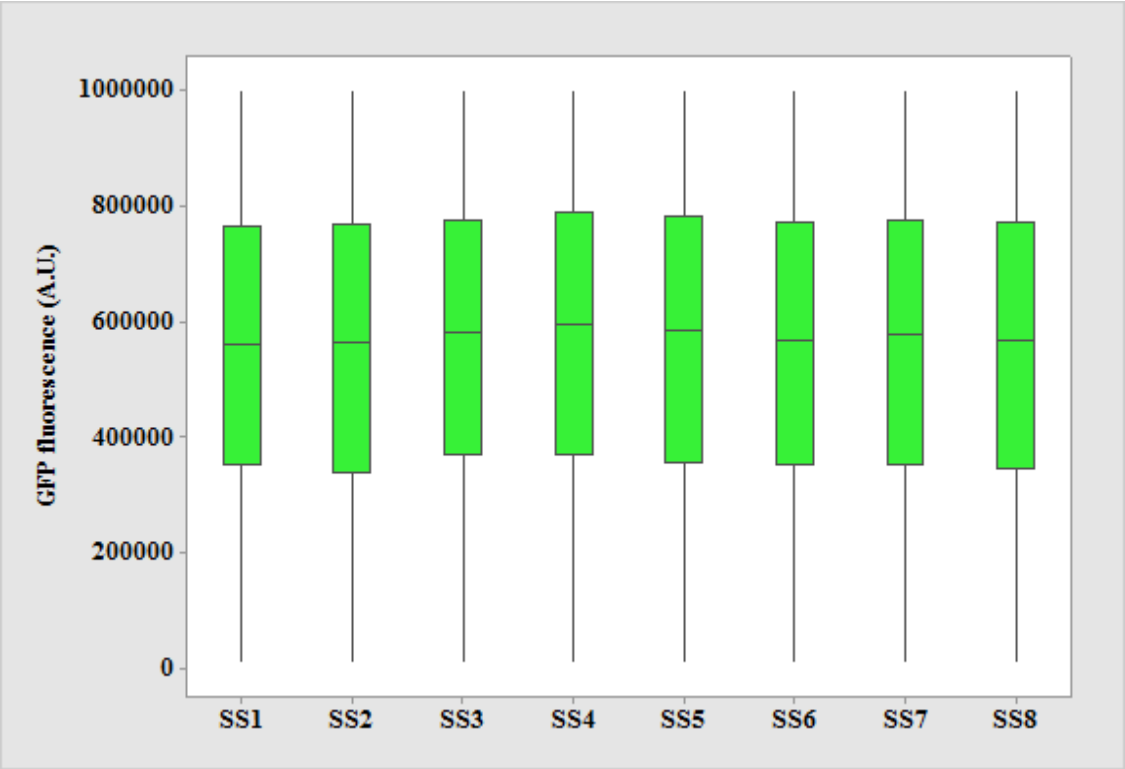

Figure 5.20. GFP mut3* fluorescence (A.U.) at steady state (SS1-SS8) after induction with IPTG added at mid-exponential point of growth. Number of cells per sample was: SS1 – 40319; SS2 – 34317; SS3 – 39104; SS4 – 35200; SS5 – 47285; SS6 – 27077; SS7 – 52968; SS8 – 46302 cells.

5.10.2 Protein production evaluation with fluorescence microscopy

Fluorescence microscopy was conducted as described in Section *3.11 Phase and fluorescence microscopy of E. coli CLD1301*. The automated analysis script was written in ImageJ 1 macro language (available in Appendix F). The ImageJ macro displayed the output as mean fluorescence intensity. Camera exposure time was selected to minimise cell autofluorescence. Particles smaller than 0.5 μm^2 were excluded from the analysis to eliminate artefacts. No upper threshold was imposed so as not to eliminate the cells with clear changes in morphology that actively produce the recombinant product.

The protein production detected by FM varied amongst steady states (*Figure 5.21*). There was a significant difference between fluorescence across steady states (Mann-Whitney U, W = 482.60, $p < 0.001$). Given the constraints of low cell numbers in analysis (66 cells in SS2, and 318 in SS4), studies of gene expression with microscopy proved unsatisfactory, particularly when FC was readily available and able to provide a robust response from a much larger cell population.

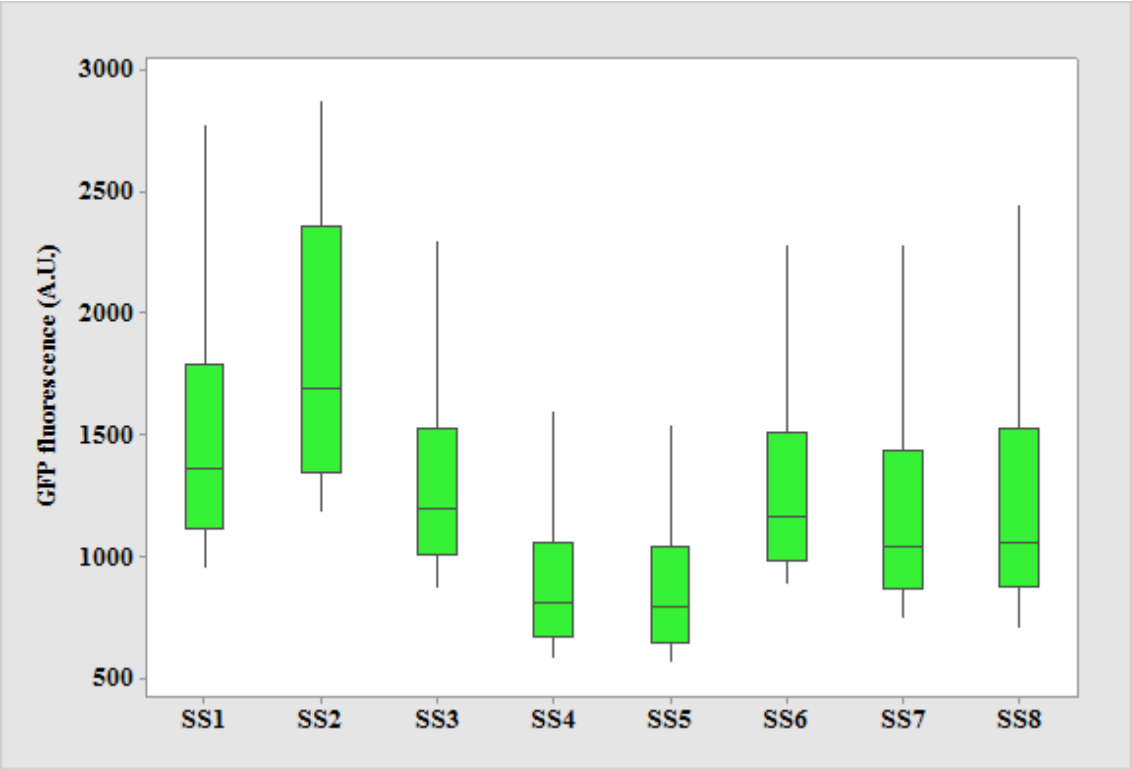

Figure 5.21. GFP mut3* fluorescence (A.U.) at steady state (SS1-SS8) after induction with 1 mM IPTG maintained constant in the reactor. Number of cells per sample was: SS1 – 158; SS2 – 62; SS3 – 81; SS4 – 318; SS5 – 98; SS6 – 259; SS7 – 132; SS8 – 97 cells.

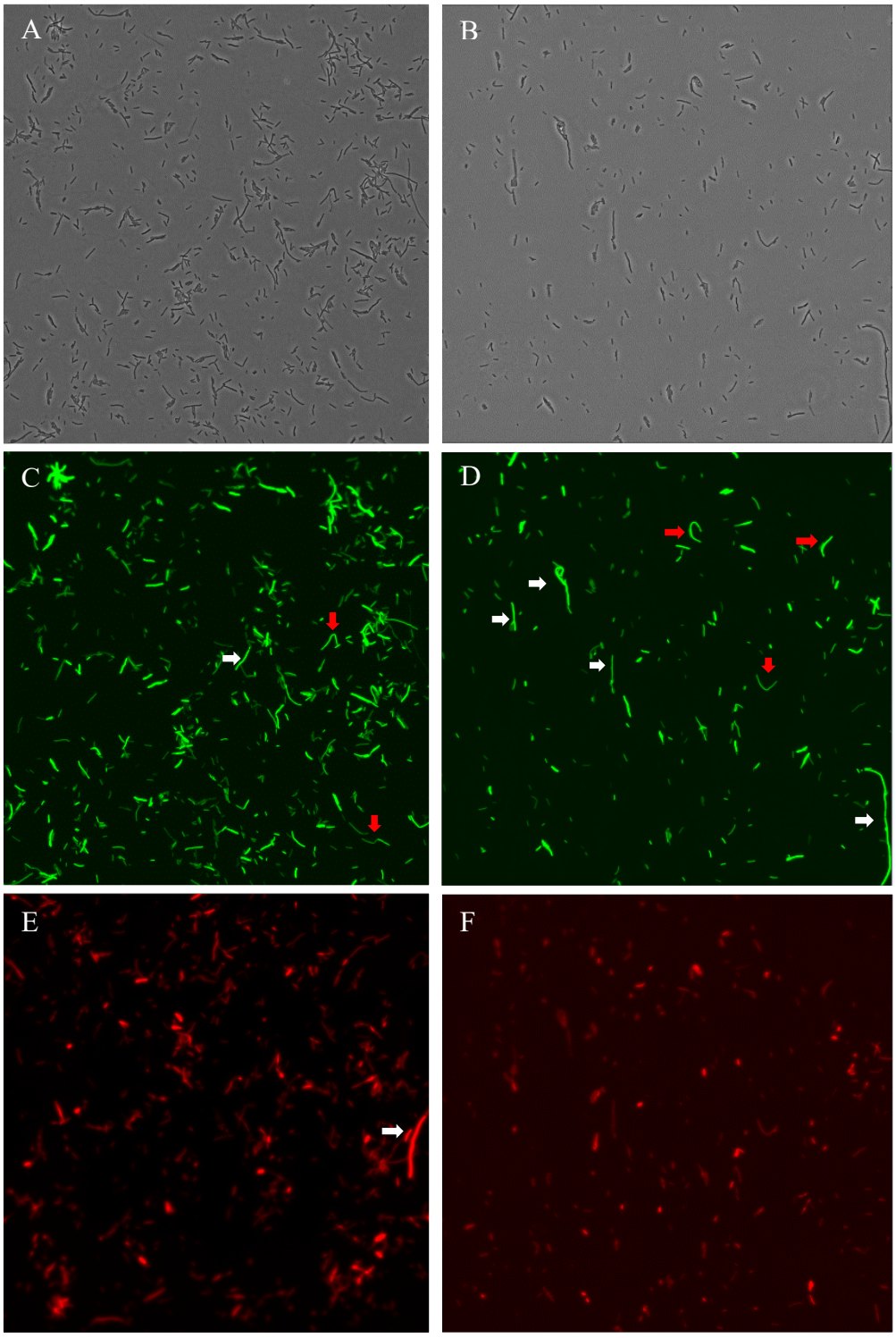

Figure 5.22. Phase contrast and fluorescent images of *E. coli* CLD1301 induced with 1 mM IPTG and stained with propidium iodide (PI). A, C, E represents the SS1 sample, and B, D, F represents the SS2 sample. White arrows indicate filamentous cells, red arrows indicate deviation from central axis (twisted cell morphologies).

Figure 5.22 shows the phase and fluorescence microscopy of SS1 (images A, C, E) and SS2 (images B, D, F) for the induced *E. coli* CLD1301 on glucose as sole carbon source. All cells exhibit either IPTG-induced green fluorescence or red fluorescence. The green fluorescence represents the titre of recombinant product, while the red fluorescence shows the "dead" cells. The white arrows show filamentous cells – cells that continue with DNA replication, but stop dividing. The filamentous cell that exhibit green fluorescence (*Figure 5.22 C* and *D*) are metabolically active, producing recombinant protein. The filamentous cell in *Figure 5.22 E* displays red fluorescence of PI, therefore is considered "dead".

5.11 Discussion and conclusions

This chapter presented fermentations *E. coli* CLD1301 grown on glucose as the sole carbon source. To mimic the glucose gradients existing in large-scale fed-batch reactors, recombinant *E. coli* cells subject to a glucose upshift and downshift were studied with single cell resolution. The mid-exponential point of growth was used for unlimited glucose growth, and chemostat cultivations were used for glucose-limited growth.

The main findings for the recombinant strain on glucose as sole carbon source were:

Growth: The recombinant strain *E. coli* CLD1301 showed altered growth in BioLector, with an increase in lag phase from 0.6 h recorded in the host W3110 to 9.5 h in the recombinant strain (*Figure 5.3*). The recombinant cells also grew slower than the host cells. The observed growth rate was 0.367 and 0.602 h^{-1} for recombinant and host strain respectively (*Figure 5.4*). This clearly showed a relative decrease in the growth rate of 61.39% caused by the maintenance and replication of the plasmid, in the absence of IPTG-induced expression.

The further addition of an optimum 1 mM IPTG to induce recombinant protein expression led to an additional biomass reduction of 41.60%. This was the cost of recombinant protein expression on the biomass development. Because of this, the biomass development and protein expression are separated in industrial bioprocesses, with high cell density cultivations proceeding product expression. The reduction in biomass was most likely the result of a competition for resources for both native and recombinant protein synthesis using the same pathways. The results obtained here suggest that the reduction in biomass was triggered by a decrease in total cell count (TCC) in induced cultures compared to non-induced ones (*Figure 5.11)*. A reduction in the total cell count by a factor of 2 was observed whilst maintaining the

same external dilution rate. This showed that the addition of IPTG with subsequent protein expression lowered the rate of cell growth.

Studies of viability with TO/PI showed a 99% viability during maximal growth on glucose with only 0.1% of cells gated as "dead". The share of "live" cells decreased during submaximal growth on glucose to an average of 97.30% across the steady state, in the absence of IPTG. The fraction of "live" cells decreased further with the IPTG addition to 81%. This showed that the burden induced by protein expression led to an increase in the share of "dead" cells (*Figure 5.14*), alongside a TCC reduced by half (*Figure 5.11)*.

The energetic state of *E. coli* CLD1301 was studied with $DIBAC_{4(3)}$/EB/PI in the absence of inducer *(Figure 5.15*). The recombinant cells showed an average of 87.17% active cells during maximal growth on glucose. The share of active cells decreased with the lowering of the growth rate, to an average of 57.02%. Conversely, the lowering of the growth rate increased the number of depolarised cells. These resulted in a decrease in cell functionality in conditions of nutrient downshift, which resembles an industrial fed-batch fermenter where cells experience nutrient limitation.

Protein expression was monitored at individual cell level by monitoring the production of GFP mut3*. *E. coli* CLD1301, containing the GFP-A gene expressed the recombinant protein, GFP mut3* at a stable and near-constant level, which was determined by flow cytometry (*Figure 5.20*). Contrary to reports showing GFP was not detrimental to its host, it was found that the protein production reduced both the TCC (*Figure 5.11*) and online biomass as scattered light (*Figure 5.10*). It does not however provide a growth arrest, since there is still proliferation in the system, as evidenced by a low, but relatively constant biomass (*Figure 5.10*). This shows that it is not toxic to the cell.

Protein expression monitored by fluorescence microscopy had an important drawback. The insufficient cell numbers detected with microscopy were further reduced by the automated analysis. While it provided an objective and quantitative measurement of gene expression, the data was insufficient to draw any robust conclusions. The existence of GFP, however, helped the cell detection and imaging, allowing the observation of details that would be invisible with FC.

The fluorescent signal remaining relatively constant over the course of the continuous cultivation, suggested the potential for continuous bioprocessing. Furthermore, the biomass keeping at a relatively low 6.75 Bug Units (*Figure 5.8*) suggests there is still division, a

prerequisite for continuous cultivation of bacteria. Fluorescence microscopy, despite its inability to provide a reliable signal for protein production, detected few warning morphological changes for continuous bioprocessing. The continuous induction with IPTG, led to a decrease in the CV of the cell area, circularity and AR (*Table 5.2*). Many cell morphologies were observed, and most disconcerting of all was the filamentous growth (*Figure 5.22*). It is most likely that the filamentous cells were eliminated from the quantitative analysis of morphology, during the application of single cell filters. It is, however, highly probable that filamentous growth resulted from an imbalance in synthesising the proteins necessary for division when faced with a huge burden of producing proteins non-native to the cell. There is still growth in filamentous cells, but no cell division. The filaments are metabolically active before becoming PI-positive, and this suggests there is still protein production (*Figure 5.22 C* and *D*). While this does not represent any caveat in an industrial fed-batch bioprocess, it would be ineffectual in continuous bioprocessing where cells must divide continuously and exponentially. For this reason, periplasmic targeting or genetic approaches should be investigated if continuous bioprocessing is the end-goal.

These results have provided evidence of the changes that occur in an industrial scale reactor used to produce recombinant proteins. FC is extremely valuable for bioprocess monitoring in quantifying protein expression and heterogeneity within a bacterial culture, but is not sensitive enough to morphological changes of small bacterial cells.

CHAPTER 6

RESULTS

Chapter 6 Cell dynamics in non-recombinant *E. coli* W3110 fermentation on glycerol

6.1 Abstract

There is sufficient evidence in literature to show two zones of heterogeneity are created in a microbial fed-batch reactor, primarily due to gradients of substrate. Next to the feeding port, there is a zone of maximal growth with an excess of nutrients. At the bottom of the fermenter, there is a nutrient limiting zone with limited growth. To probe and monitor the heterogeneity in cultivations of *E. coli* W3110, single cell measurements were made by implementing simultaneous staining with different fluorescent probes.

This chapter refers to experiments and analysis made on the host *E. coli* W3110 strain grown on glycerol minimal media. Population heterogeneity is determined in conditions of maximal growth at μ_{max} and submaximal growth, which is glycerol-limited by a factor of 2. The analysis focused on viability in regard to membrane integrity, cell functionality in relation to membrane potential (MP) and cell morphology. The measurements were used to compare the effect of utilising glycerol instead of glucose as a carbon source for microbial fermentations.

6.2 Introduction

Protein expression in *E. coli* is the most common way of producing recombinant proteins in industrial and laboratory fermentations. Glycerol has become an abundant carbon source due to its generation as a by-product in biodiesel production. As more emphasis and demand is put onto renewable fuels, more glycerol is created. With every 10 lbs of biodiesel produced, a lb of crude glycerol is generated (Yang *et al*., 2012). Biodiesel production is expensive and a major goal is reducing costs. With the possibility of using glycerol as a substrate for high value products, microbial biotechnology adds value to the productive chain in the biodiesel industry.

Glycerol has been tested as a carbon source for *E. coli* fermentations and is the second choice for bacterial fermentations. Luo reported that growth on glycerol leads to less inhibitory products, such as acetate and an increase in the yield of recombinant protein (Luo *et al.*, 2006). The accumulation of acetate is unwanted in the bioprocess because it inhibits growth at concentrations as low as 0.5 g/L (Nakano *et al.*, 1997, Koh *et al.*, 1992). Reduced acetate

occurs because of a reduced growth rate on glycerol compared to glucose, where levels of acetate are far below those shown to inhibit growth and product formation (Guebel *et al.*, 2009).

To probe large-scale cell heterogeneity and determine its significance in bioprocess, batch and continuous cultivations were carried out in STR. Mid-log point of batch growth provided cells in "balanced growth" at maximal growth rate μ_{max}, whilst chemostats provided cells in "balanced growth" at submaximal growth rate that is glycerol limited. Meaningful chemostat cultivations required experiments in batch to confirm two prerequisites. The first was identifying the nutrient that limits growth (discussed in *Section 6.3 Determination of the single media limitation on glycerol*) and the second is establishing the dilution rate D, which sets the growth rate in chemostat cultivations (detailed in *Section*

6.4 Determination of growth rate*).*

6.3 Determination of the single media limitation on glycerol

To determine that the nutrient that limits growth solely is the C source (glycerol), triplicate experiments in batch were conducted on the host *E. coli* W3110 strain by applying BioLector (m2p-labs GmbH, Baesweiler, Germany), as described in *Section 3.4.1 Batch cultivations in Microtiter Plates*. To support growth, batch mineral media was used (see *Section 3.3.1 Batch mineral media)* with different concentrations of glycerol, while the other components were maintained at a constant excess. Based on media composition in terms of biomass yields, the expectation is that the growth limiting concentration of glycerol is 4 g/L, the same as for glucose (Chapter 4).

The concentrations (w/v) of glycerol used were 1, 2, 3, 4, 7 and 10 g/L (*Figure 6.1*). A well containing sterile media was included as standard for contamination control. Growth was monitored as biomass (A.U.), recorded as 620 nm scattered light at 15 minute interval. The initial average of six consecutive points was subtracted from the total light scatter measurements to account for light scattered by media components. BioLector cultivations were inoculated with 20 µl culture in mid-log phase of growth with an OD_{600} ~ 2, giving an initial OD_{600} ~ 0.05 at time-point 0 (*Figure 6.1*).

.

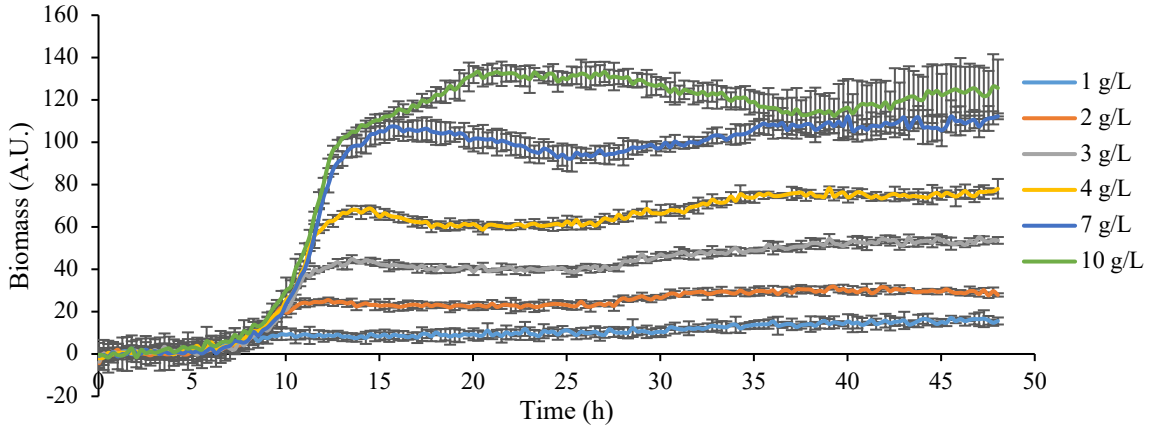

Figure 6.1. Influence of different glycerol concentrations on growth of *E. coli* W3110 without IPTG. Online monitoring of biomass (scattered light). Conditions: minimal media with up to 10g/L of glycerol, T = 37^{0}C, V_L = 800 µL, n = 1500, d_0 = 3 mm. Standard error bars represent ± S.D.

The growth curves of *E. coli* W3110 in minimal media with glycerol as sole C source, as monitored by BioLector are shown (*Figure 6.1)*. After an initial lag phase, cells begin exponential growth until glycerol is exhausted and the stationary phase begins at different time points depending on when the glycerol limitation occurs. Cultivations were stopped at 48.03 h, when the cultures were in the stationary phase, with no further growth expected.

To establish the range for which glycerol is the sole limiting nutrient, the maximum biomass, measured between 20 - 30 h, was plotted as a function of the glycerol concentration (g/L). Maximum biomass ranged from 12.61 – 134.34 A.U. within the specified time and is linearly dependent on the concentration of glycerol up to 7 g/L (*Figure 6.2).* This confirmed that glycerol concentration of 4 g/L used for subsequent chemostats experiments is the sole limiting nutrient.

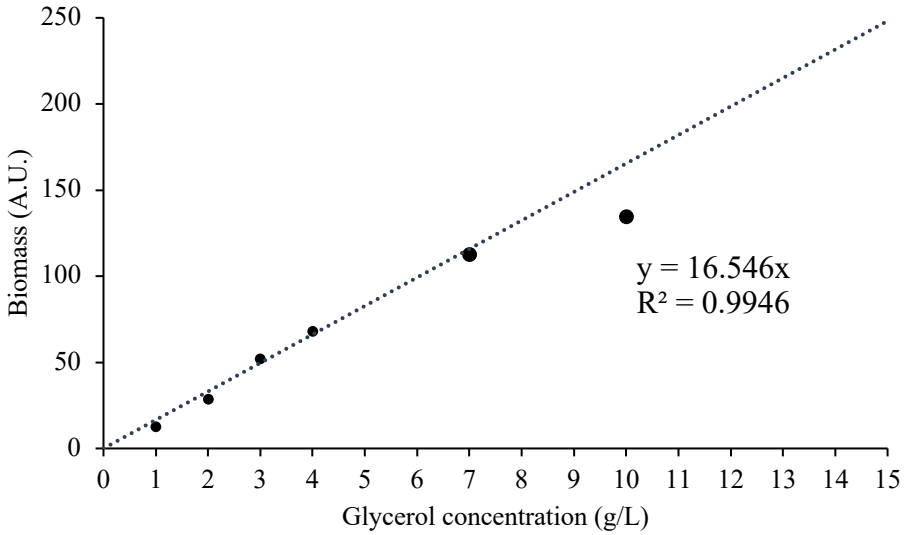

Figure 6.2. Maximum *E. coli* W3110 biomass (A.U.) during 20 – 30 h of batch growth. The abscissa is the glycerol concentration (g/L). A linear relationship indicates that the nutrient is in the limiting range. Cells were grown in minimal media containing different concentrations (w/v) of glycerol: 1, 2, 3, 4, 7 and 10 g/L glycerol. The rest of the media components were in excess and maintained constant. Conditions: T = 37^{0}C, V_L = 800 µL, n = 1500, d_0 = 3 mm.

6.4 Determination of growth rate

To establish the growth rate for chemostat operation, the maximum growth rate μ_{max} was first determined in batch for the chosen concentration of 4 g/L glycerol (*Figures 6.3* and *6.4*). Growth during exponential batch is inherent to cell metabolism, with no external limitation.

Using at least 5 time-points from the exponential portion of the growth curve, chosen between 8 - 11 h (*Figure 6.1)*, the corresponding biomass at each time was plotted as log against time. The slope of the straight line is the maximum specific growth rate μ_{max}. The net growth rate for glycerol was 0.50 h^{-1}, with a doubling time T_d of 1.37 h (*Figure 6.4)*. The T_d is longer than 1.15 h on glucose (*Figure 4.4)*, thus *E. coli* growth with glycerol is slower than with glucose. The chemostat was operated at a fixed dilution rate, D, which was ½ μ_{max} to promote reaching a "steady state" and to allow comparison with glucose growth. Thus, D was set to 0.25 h^{-1}, ensuring a T_d of 2.74 h during sub-maximal growth in chemostat. Five residence times R, calculated at 20 hours were allowed for the culture to reach "steady state" at D of 0.25 h^{-1}

(R=1/D, *Figure 6.4)*.

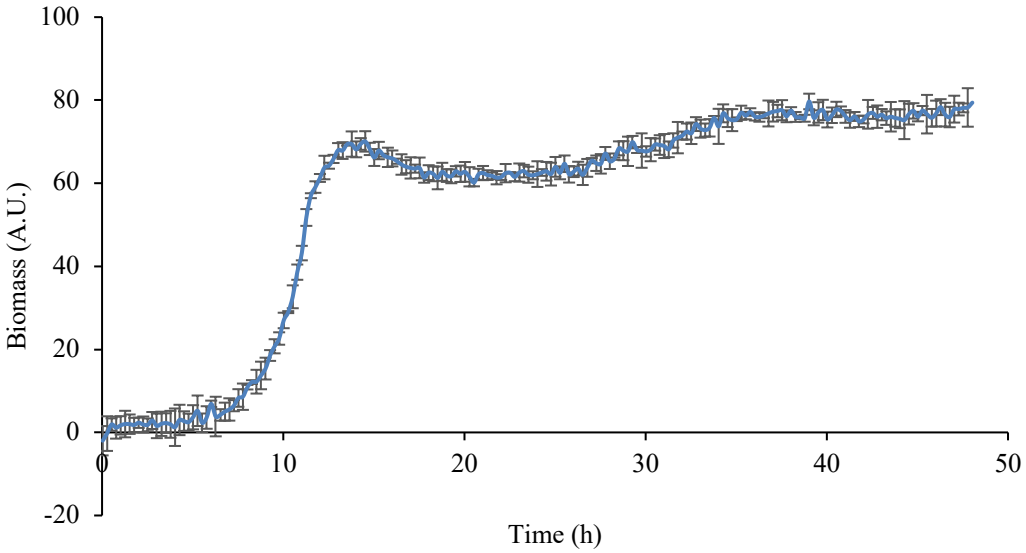

Figure 6.3. Growth of *E. coli* W3110 without IPTG. Biomass (A.U.) as scattered light. Conditions: minimal media 4 g/L glycerol, T = 37^{0}C, V_L = 800 µL, n = 1500, d_0 = 3 mm. Standard error bars represent ± S.D.

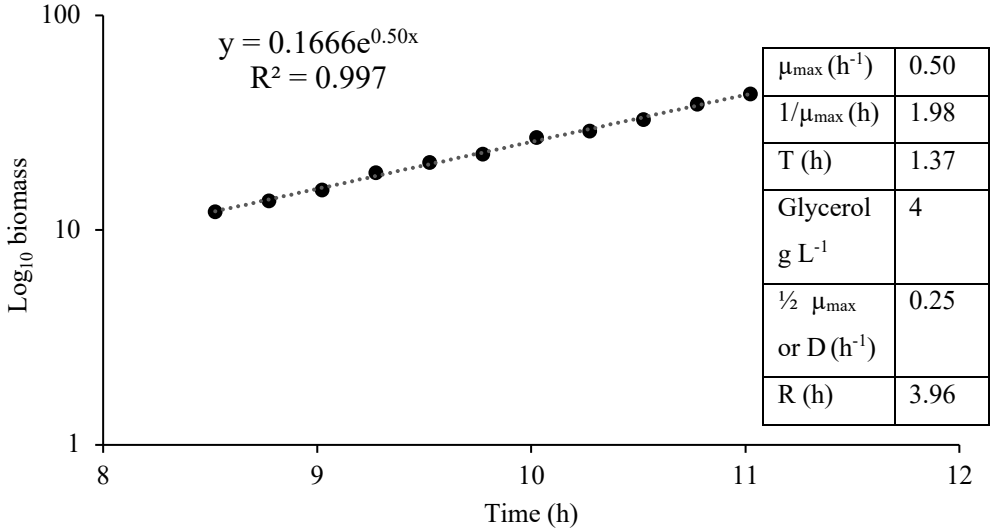

Figure 6.4. Maximum growth rate μ_{max} of *E. coli* W3110 without IPTG. Biomass (A.U.) as scattered light. Conditions: minimal media 4 g/L glycerol, T = 37^{0}C, V_L = 800 µL. Data points chosen from eleven time-points from exponential phase.

6.5 Cell dry weight determination

Optical density to cell dry weight (CDW) correlation for *E. coli* W3110 of 0.354 g/L cell dry weight per unit OD_{600} was measured previously (*Figure 4.5).*

The correlation was described by the equation y = 0.354 x with the R^2 value of 0.997 (where y = CDW (g/L), and x = OD_{600}).

6.6 Process monitoring at population level

Controlled fermentations of *E. coli* W3110 with glycerol minimal media were carried out in triplicate under aerobic conditions, with 1 v.v.m. airflow at 50% DO on loop, pH controlled at 7 and temperature at 37^0C. Dissolved oxygen was controlled at a 50% set point by the automatic modulation of the stirrer speed between 250 and 900 RPM. The pH was automatically maintained by the addition of 1M NaOH/KOH and 1M KCl via peristaltic pumps. Process parameters were previously listed (*Table 3.3*).

The STR was a 3 L bioreactor with 1.5 L working volume (Applikon Biotechnology B.V., Schiedam, The Netherlands). The bioreactor was inoculated with the second seed culture (described in Step B, *Section 3.2 Cell expansion and seed preparation*), maintained at mid-exponential growth. The initial OD_{600} in the bioreactor was ~ 0.05 at inoculation (time 0). Growth proceeded unrestricted in batch with μ_{max} of 0.50 h^{-1} during the exponential phase. The switching to glycerol-limited chemostat was performed past the mid-exponential point of growth, when OD_{600} ~ 2. A continuous feed supply with glycerol-limited media was started at a constant flow (378 ml h^{-1}). This ensured a specific growth of 0.25 h^{-1} during continuous cultivation. The 1.5 L working volume was maintained by a peristaltic pump set at 21 RPM on the inlet and a peristaltic pump set at maximum RPM on the outlet.

A defined mineral media was used with 4 g/L glycerol (w/v) as sole carbon source.

Remarks on sampling

The doubling time was 1.37 h during exponential batch and 2.73 h during chemostat growth (*Figure 6.4)*. Sampling was therefore conducted every 2 h for the batch phase, and every 3 h for the chemostat phase of growth. During batch growth, samples were obtained through the sampling port of the STR; during chemostat cultivation, samples were taken from the exit line. Sampling was conducted as detailed in *Table 6.1*. Single cell analysis was applied to

cells growing in "balanced growth" at μ_{max} of 0.50 h^{-1} (S4) and at 0.25 h^{-1} for glycerol-limited growth (SS1 - SS8). When IPTG was used, 1 mM optimal concentration was maintained in the STR.

Batch sampling		Chemostat sampling
	Switch from Batch to Continuous at 8 h	SS1 (28 h)
		SS2 (31 h)
S_0 (5 min)		SS3 (34 h)
S_1 (2 h)	Allow 5 residence times R ~ 20 h to reach steady state (SS)	SS4 (37 h)
S_2 (4 h)		SS5 (41 h)
S_3 (6 h)		SS6 (44 h)
S_4 (8 h)		SS7 (47 h)
		SS8 (50 h)

Table 6.1. Sampling during batch and continuous cultivation of *E. coli* W3110 on glycerol minimal media (in units of time post-inoculation)

6.6.1 Measurements of biomass

The target starting OD_{600} was ~ 0.05. The fermentation profiles of *E. coli* W3110 on glycerol minimal media are shown in both the absence (*Figure 6.5)* and presence (*Figure 6.6)* of 1 mM IPTG. The batch phase started from inoculation (time 0) and the cells exhibited exponential growth at a maximum growth rate of 0.50 h^{-1}. At mid-exponential point (time 7.5 h), when OD ~ 2, the culture was switched to continuous growth with a dilution rate (D) of 0.25 h^{-1} (1/2 μ_{max}). Steady state was monitored between 28-50 h.

Single cell analysis was carried out at different points during fermentations, depending on the growth rate. Sampling for maximal growth rate was carried out at mid-exponential point of growth (7.5 h), and for sub-maximal growth during chemostats at 7-8 subsequent times at least one division apart.

Biomass was measured online as light reflected with the BugLab sensor. OD_{600}, TCCs and single cell analysis were analysed immediately following sampling. Dry biomass was calculated by a calibration curve. Samples for HPIC were sterile filtered and stored at -20^{0}C until analysis. Samples for residual glucose were maintained at 4^{0}C until analysis.

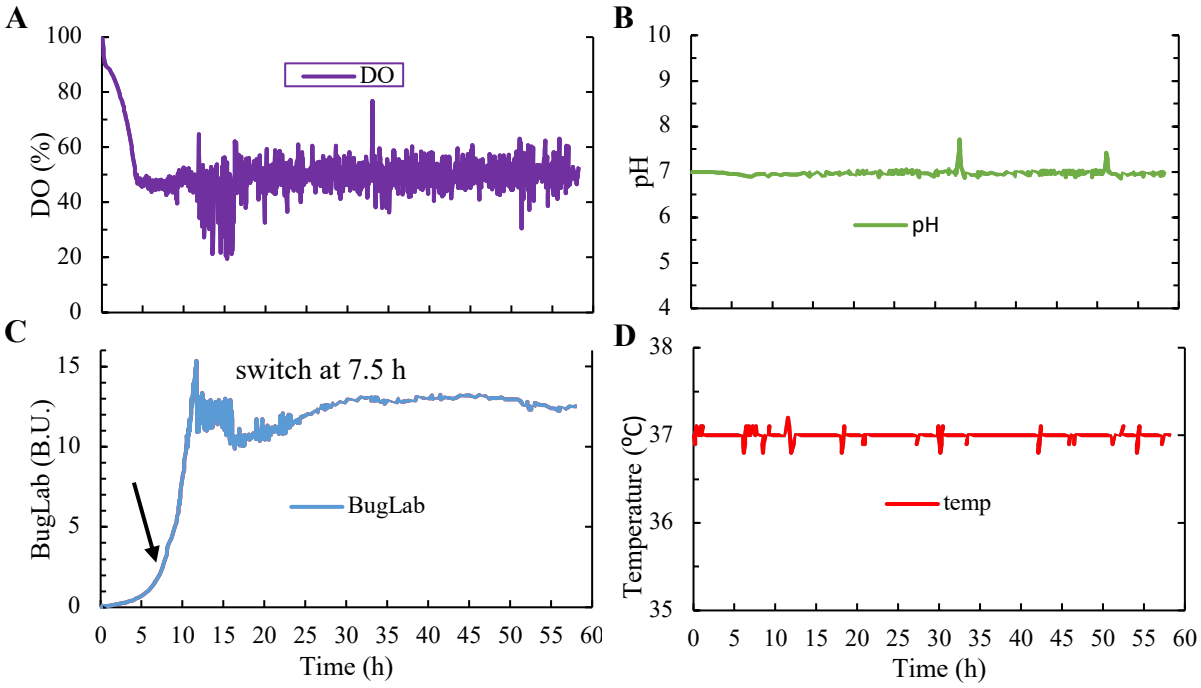

Figure 6.5. Continuously monitored dissolved oxygen (A) and biomass (C) in an *E. coli* W31110 fermentation on glycerol minimal media in the absence of IPTG (the arrow indicates the switch). pH (B) and temperature (D) are maintained constant at set-points.

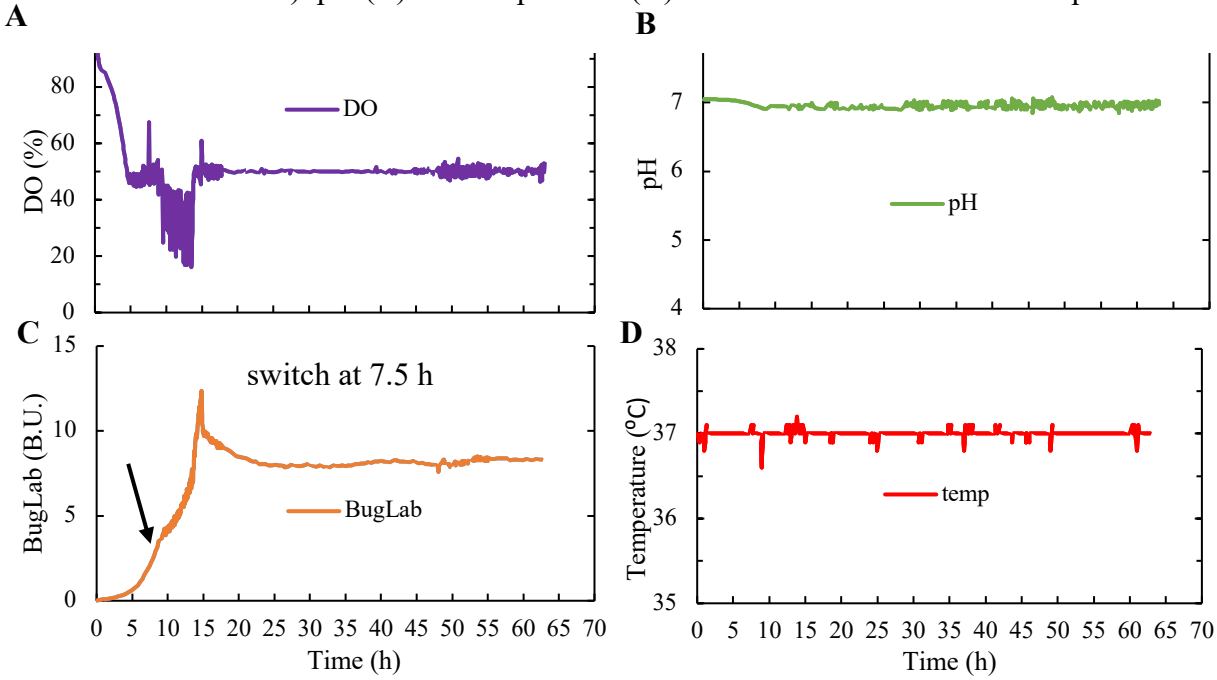

Figure 6.6. Dissolved oxygen (A) and biomass (C) changes during *E. coli* W3110 growth on glycerol minimal media with 1mM IPTG (the arrow indicates the addition of IPTG). pH (B) and temperature (D) are maintained constant at set-points.

The BugLab sensor signals during *E. coli* W3110 fermentations with glycerol as sole carbon source are shown in the absence (*Figure 6.5*) and presence (*Figure 6.6*) of 1 mM IPTG. Contrary to a long lag phase observed in BioLector batch cultivations (*Figure 6.3)*, no lag phase was observed in fermentations in STR (*Figures 6.5* and *6.6).* The cultures entered exponential phase directly, showing that the cells were actively growing from inoculation (time 0). The switch to continuous was performed at mid-exponential point of growth (indicated by arrows in *Figures 6.5* and *6.6)*. The BugLab sensor was used to determine whether the biomass signal remained stable over continuous culture, thus signalling the attainment of "steady state". Following switching to continuous at 7.5 h, the biomass continued to increase, as glycerol was not yet limiting the system. At mid-exponential growth, there was 2.09 g/L glycerol in the fermentation broth (*Figures 6.9)*.

The biomass control during steady state was also monitored offline as OD_{600}, determined by spectrophotometry (*Figure 6.7*).The OD_{600} values remained relatively stable throughout steady state, between 4.23 and 4.83 (*Figure 6.7).* Given that OD_{600} is a population level measurement, this was correlated with single-cell level total cell counts (TCCs) analysed by flow cytometry. The relationship between OD_{600} and TCCs was assessed at two different growth rates: 0.50 h^{-1} and 0.25 h^{-1} respectively. OD_{600} was a linear function of TCCs during maximal growth up to $OD_{600} \sim 1.08$ (*Figure 6.7*). An OD_{600} of 1 at maximal growth rate corresponds to 2 $x10^8$ cells/ml (*Figure 6.7).* The cell concentration (cells / [ml*OD_{600}]) after 4 doubling times T_d is 2.1 x 10^8, an increase from the 1.58 x 10^8 observed on glucose growth (*Figure 4.8*). This suggests that an increase in growth rate decreases the specific cell concentration per OD_{600}. The need for single cell analysis in a bioprocess becomes apparent, given that cells grow at different growth rates in a bioprocess.

At submaximal growth, however, the cell concentration (cells / [ml*OD_{600}]) at "steady state" varied between 1.31 x 10^8 at SS4 (37 h) and 1.62 x 10^8 at SS8 (50 h). This calculation was based on the assumption that all cells had the same size, and did not consider changes in morphology. At different growth rates, cells must be counted directly or the TCC per OD_{600} must be known. However, the OD_{600} values and the BugLab sensor signal remained relatively stable at submaximal growth on glycerol, indicating that there was growth and division in chemostat, which is a paramount consideration for continuous bioprocessing. Furthermore, it indicated that biomass was controlled at a constant level during chemostat and signalled the "steady state".

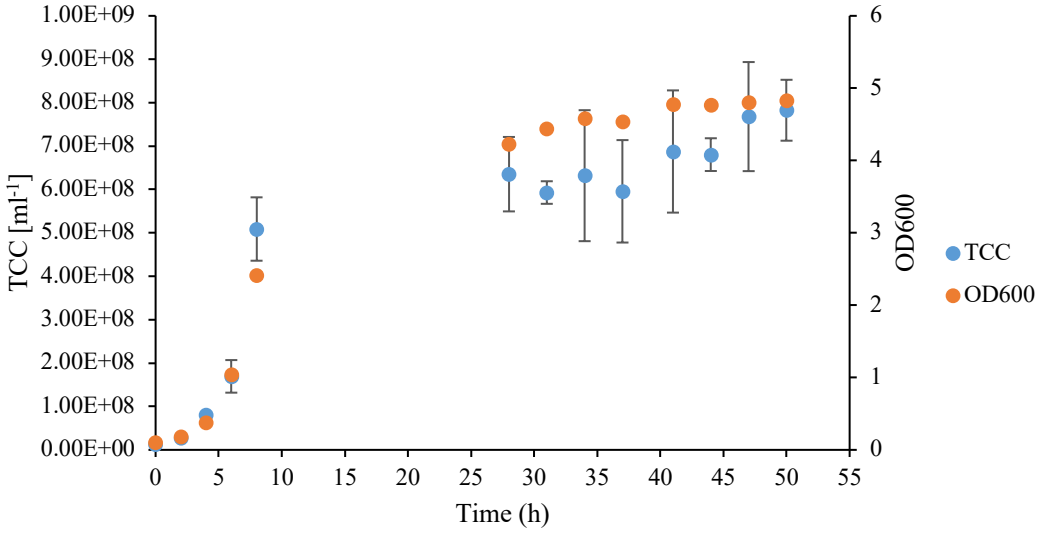

Figure 6.5. Plot of OD_{600} with total cell count (TCCs) for *E. coli* W3110 on glycerol minimal media, no IPTG. The gap between the two datasets (20 h) is to allow the culture to reach a "steady state".

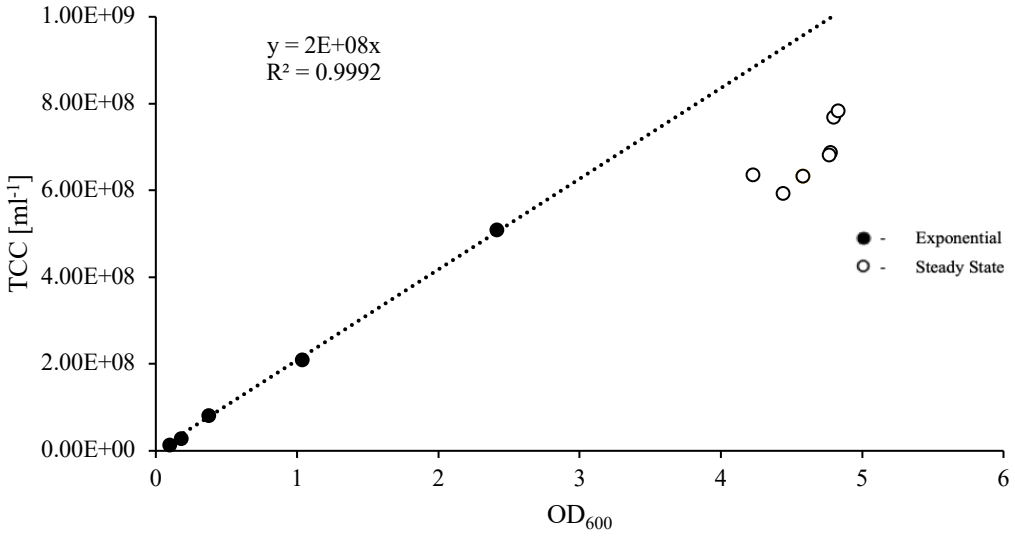

Figure 6.6. Dependence of total cell count (TCCs) over OD_{600} in *E. coli* W3110 on glycerol minimal media. Linear relationship observed up to $OD_{600} = 2.4$.

6.6.2 Monitoring substrate

The concentrations of glycerol during *E. coli* fermentations were determined as described previously (Section *3.6 Substrate measurements in the media).* The results are illustrated in *Figures 6.9* and *6.10.*

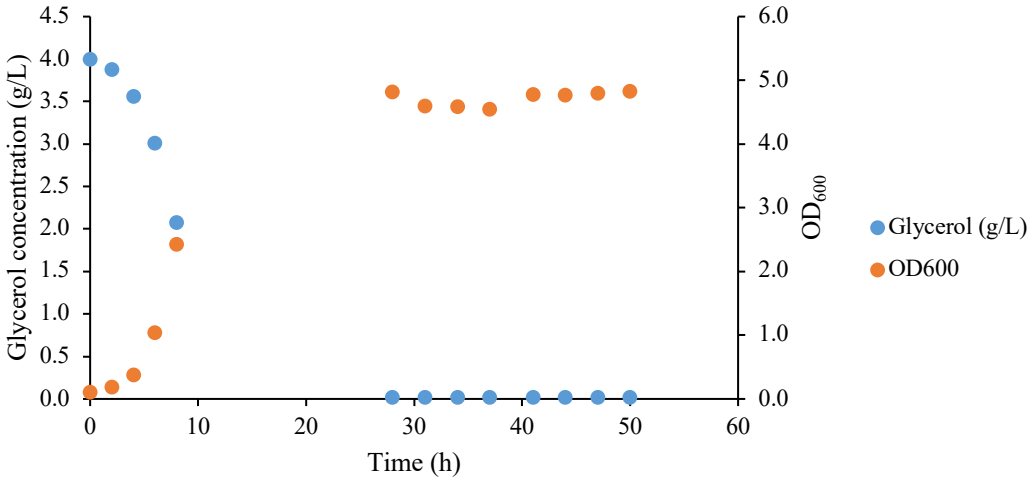

Figure 6.9. Glycerol consumption pattern and biomass production in strain *E. coli* W3110 with no IPTG. The gap between the two datasets (20 h) is to allow the culture to reach a "steady state".

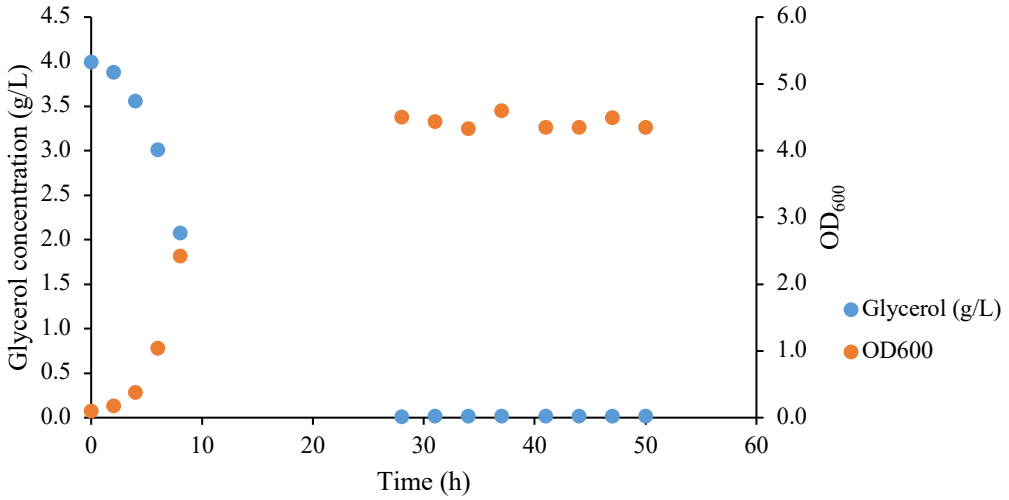

Figure 6.10. Glycerol consumption pattern and biomass development in *E. coli* W3110 with 1 mM IPTG. The gap between the two datasets (20 h) is to allow the culture to reach a "steady state".

The initial concentration of 4 g/L glycerol was consumed by *E. coli* slower than glucose, with a concomitant increase in biomass. Minor quantities of residual glycerol were detected in samples taken from the chemostat (28 - 50h). The glycerol-limited conditions in chemostats were sufficient to promote growth, monitored both offline (*Figures 6.9* and *6.10*) and online *(Figures 6.5* and *6.6*). A higher biomass was observed on glycerol than glucose, both as OD_{600} (*Figures 6.10* and *4.10*) and the BugLab sensor signal *(Figures 6.5* and *4.6).* This is most likely due to *E. coli* cells more efficiently converting the carbon from glycerol into biomass than from glucose.

6.6.3 Monitoring VFAs

Concentrations of VFAs were analysed by HPIC from the supernatant fraction. Aerobic fermentation of *E. coli* W3110 on glycerol minimal media identified traces of fermentation by-products, including acetate, formate and propionate (*Figure 6.11*).

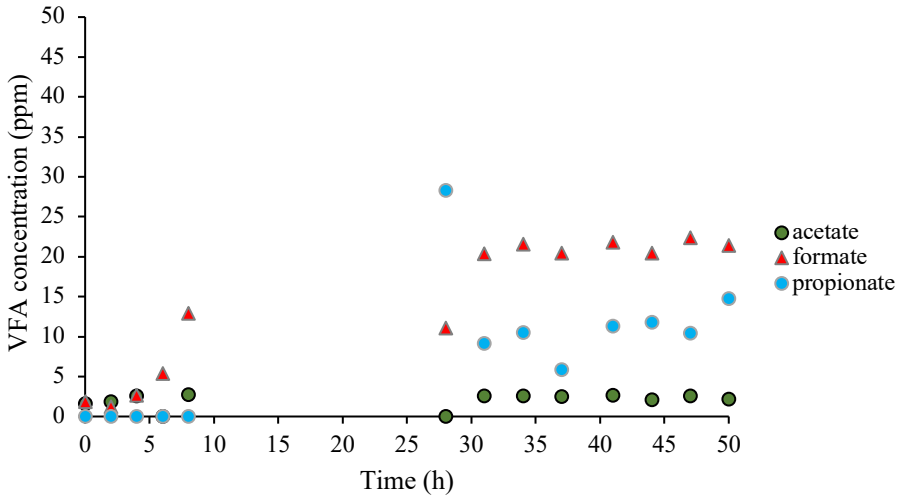

Figure 6.11. Fermentation by-products produced in *E. coli* W3110 on glycerol minimal media without IPTG. The gap between the two datasets (20 h) is to allow the culture to reach a "steady state".

At maximum growth rate on glycerol as sole carbon source, trace amounts of acetate were identified, with a maximum of 2.68 ppm (2.68×10^{-3} g/L) at mid-exponential point of growth (7.5-8 h). The maximum growth rate μ_{max} on glycerol was 0.50 h^{-1} (*Figure 6.4)*. Contrastingly, with glucose as sole carbon source with μ_{max} of 0.6 h^{-1}, the level of acetate was

202.36 ppm (0.292 g/L) at mid-exponential point of growth (*Figure 4.11*). The low levels of acetate could be explained in two ways. Either acetate was produced in trace amounts or was produced in higher amounts and consumed immediately.

Thus, four C sources were present within the media at mid-exponential point of growth with glycerol as sole carbon source: glycerol, acetate, formate, propionate. There is no catabolite repression, given that glycerol is not the preferred carbon source of *E. coli*. As the cells exhibit exponential growth, neither does the glycerol limitation exist or the VFAs levels inhibit growth. The levels of formate increased slowly during growth at μ_{max}, up to 12.86 ppm at mid-exponential point of growth (7.5 - 8h). This was still lower than 24.73 ppm obtained at mid-exponential on glucose as sole carbon source (*Figure 4.11*).

At reduced growth rate on glycerol, traces of acetate and formate were detected. Acetate varied between 2.11 and 2.60 ppm, and formate between 11.06 and 22.36 ppm, respectively. However, during chemostat growth, acetate may be used as a carbon source, as conditions are nutrient-limited. The low levels of VFAs detected suggest that the overflow metabolism is not prominent on glycerol as a sole carbon source. A significant amount of carbon is directed towards biomass, instead of wasteful products. Thus, growth on glycerol is beneficial for microbial fermentations used for heterologous protein production.

It is worth noting that the addition of 1 mM IPTG showed no influence on the measured levels of VFAs.

6.6.4 Influence of induction on growth of E. coli W3110

The optimised induction parameters (*described in Section 7.5 Determining the optimum amount of IPTG) w*ere transferred to STR. Cells were grown with 4 g/L glycerol in both the presence and absence of 1 mM IPTG. The online signals for biomass as scattered light are given in *Figure 6.12*. The final biomass obtained in stationary phase, chosen arbitrarily past 25 h was compared and the difference was deemed significant (Mann-Whitney U, W = 998, $p < 0.005$). The median final biomass 12.89 B.U. in media with 0 mM IPTG (X_0) dropped to 8.08 B.U at 1 mM induction (X_1). Thus, the cost of induction on the growth of the host strain at submaximal growth in glycerol was 37.31%, calculated from the formula

$$Cost = \frac{X_0 - X_1}{X_0} \, x \, 100 \qquad (6.1)$$

where X_0 is the final biomass on glycerol with 0 mM IPTG and X is the final biomass on glycerol with 1 mM IPTG.

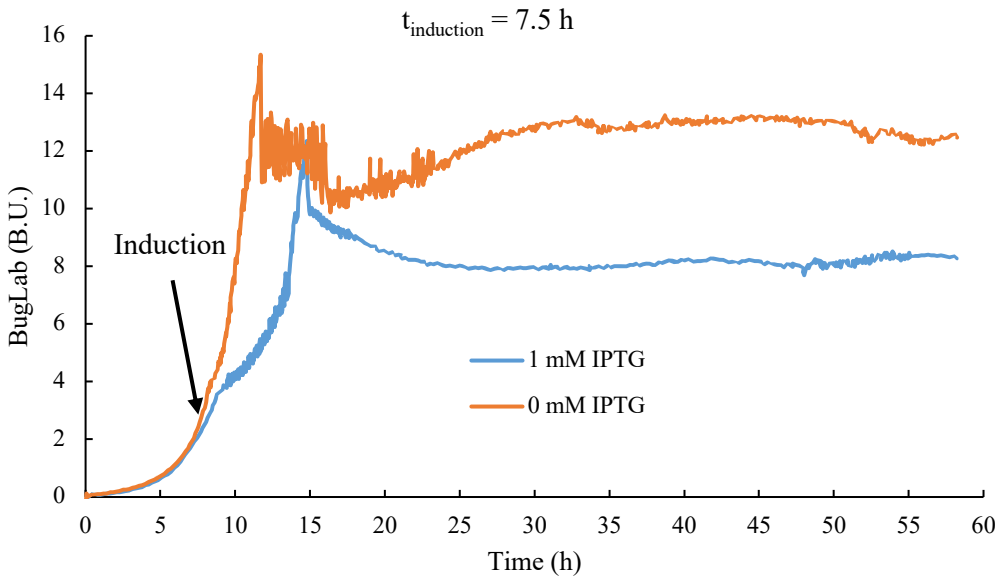

Figure 6.12. Online measurements for *E. coli* W3110 biomass (BugLab) as scattered light intensity (B.U.) in non-induced and induced cells. Arrow: time of induction with 1 mM IPTG (mid-exponential at 7.5 h). Conditions: minimal media with 4 g/L glycerol.

6.7 Single cell studies of membrane integrity using flow cytometry

Despite the evidence of growth with BugLab signal and OD_{600}, neither the measurements of scattered light or light attenuation can distinguish between the living and dead cells. However, in a bioprocess, and even more so in a continuous bioprocess, the amount of obtained product is associated with metabolism and reproduction. Hence, *E. coli* W3110 cell viability was analysed by using the combination dye TO/PI with flow cytometry. PI stains dead cells with red fluorescence and TO stains live cells with green fluorescence. Region analysis of dot plots (BL1-A vs BL2-A) was carried out on the "live" and "dead" gates at unrestricted maximum growth rate and submaximal growth rate. The results are shown as percentages of live/dead sub-populations (*Figure 6.13*). During the exponential growth phase at μ_{max}, the percentage of cells with green and red fluorescence was 94.90% and 5.10%, respectively.

In the absence of IPTG, the amount of cells in the "live" gate that are TO^+ decreased from the exponential phase to averages of 90.40% at SS1, 91.20% at SS2, 92.94% at SS3, 93.24% at SS4, 93.14% at SS5, 93.48% at SS6, 92.25% at SS7, and 92.87% at SS8. Conversely, the amount of cells in the "dead" gate increased from 5.10% at mid-exponential to 9.60% at SS1, 8.80% at SS2, 7.06 % at SS3, 6.76% at SS4, 6.86% at SS5, 6.52% at SS6, 7.75% at SS7, and 7.13% at SS8.

In the presence of IPTG, the fraction of cells that stain with TO were 90.06% at SS1, 89.87% at SS2, 91.60% at SS3, 89.58% at SS4, 88.29% at SS5, 89.74% at SS6, 89.36% at SS7, and 91.20% at SS8. The fraction of TO^+ cells *E. coli* was significantly different from the fraction of TO^+ cells treated with IPTG (one-way ANOVA, $f = 21.48$, $p < 0.001$). As the other parameters were identical in both experiments, the decrease in TO^+ cells must therefore be the result of the IPTG addition.

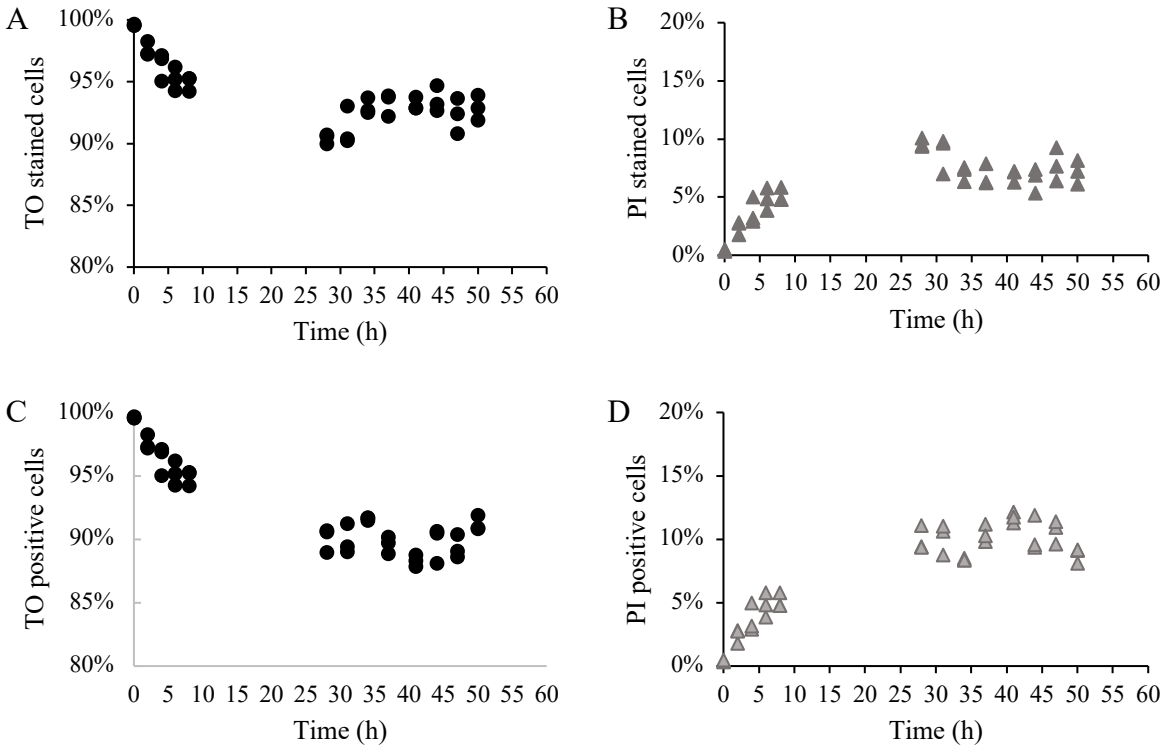

Figure 6.13. Percentage of live (TO^+) cells and dead (PI^+) cells in three *E. coli* W3110 fermentations on glycerol. Filled circles represent TO^+ cells, triangles are PI^+ cells. A, B) 0 mM IPTG. C, D) 1 mM IPTG.

6.8 Single cell studies of membrane potential using FC

Cell viability and energetic status was further assessed with $DIBAC_{4(3)}$/EB/PI staining using FC. The samples were analysed immediately following staining and the percentages of each sub-population were evaluated at different growth rates in the presence or absence of 1 mM IPTG (*Figure 6.14*). Four subpopulations were gated:

a) active ($DIBAC_{4(3)}^{-}$, $EtBr^{-}$, PI^{-});

b) depolarised ($DIBAC_{4(3)}^{+}$, $EtBr^{+}$, PI^{-});

c) deenergised ($DIBAC_{4(3)}^{-}$, $EtBr^{+}$, PI^{-});

d) dead ($DIBAC_{4(3)}^{+}$, $EtBr^{-}$, PI^{+}).

$DIBAC_{4(3)}$ is excluded from cells that maintain MP, which are "active" or with intact membranes. It enters depolarised cells, binding to intracellular proteins and displaying increased fluorescence. Thus, a higher $DIBAC_{4(3)}$ signal reflects membrane depolarisation, while a lower $DIBAC_{4(3)}$ fluorescence indicates de-energised cells. Both depolarisation and de-energisation are cell states with reduced functionality. Dead cells are cells that are PI^{+}, with permeabilised cell membranes, whereas the other sub-populations are PI^{-}.

At maximal growth on glycerol as sole C source (S4), 70.8% of *E. coli* cells were active, 22.85% depolarised, 6.03% dead and 1.02% were de-energised (*Figure 6.14*). At maximal growth rate on glucose 83.74% of cells were active, 13.08% depolarised, 2.30% dead and 0.87% de-energised (*Figure 4.17).* As all parameters were identical between both experiments, and there was no carbon limitation, this suggests that glycerol as a carbon source increases the membrane depolarisation and membrane permeability.

.

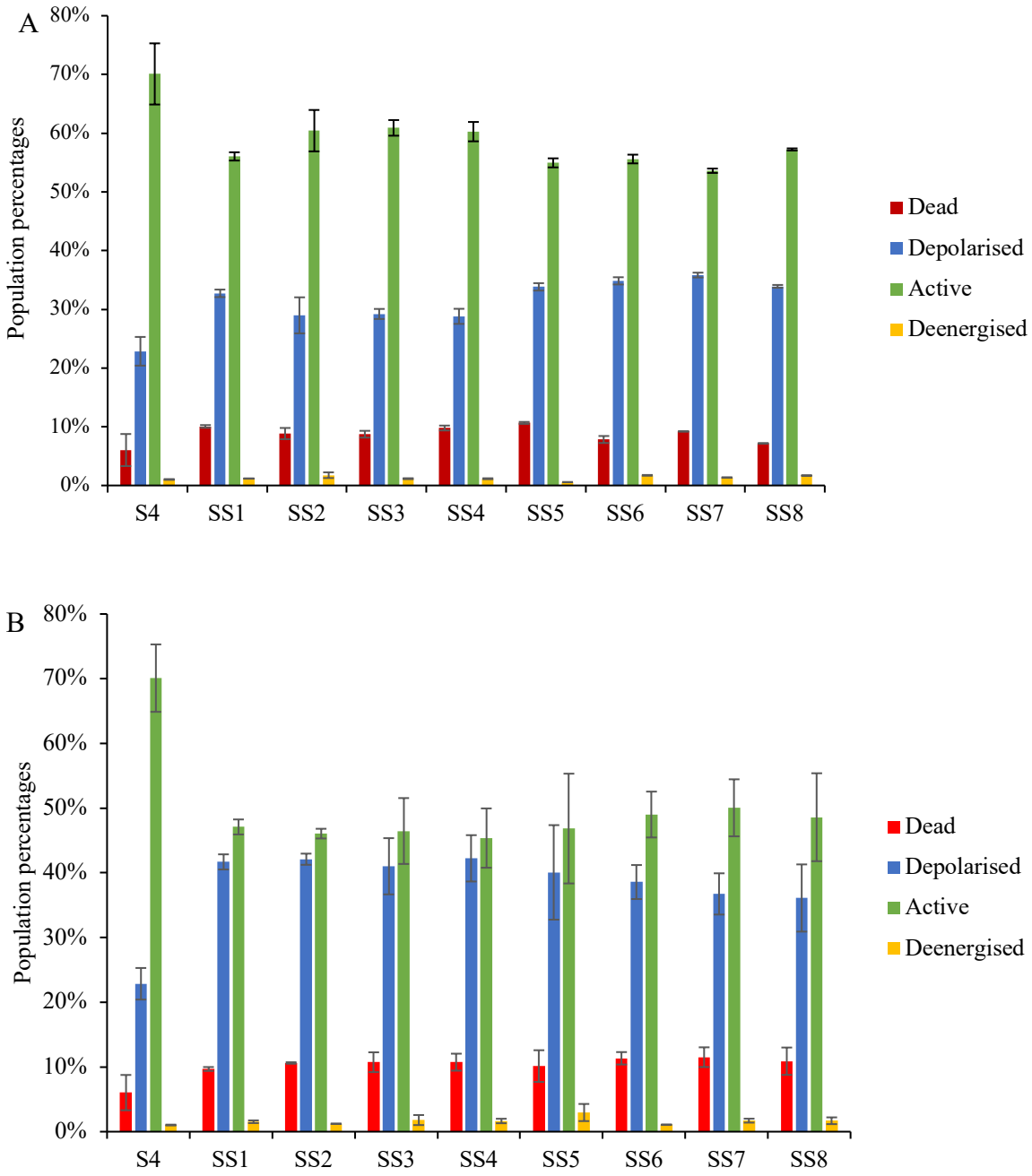

Figure 6.14. Flow cytometry analysis of *E. coli* W3110 cells at different growth rates on glycerol minimal media. For each graph, S4 is the mid-exponential sample, while SS1-SS8 are steady state (SS) samples at 3h intervals, with reduced growth at $\mu_{max}/2$. Data presented as mean ± S.E. depicts four subpopulations of cells: active, depolarised, dead and deenergised. A: 0 mM IPTG. B: 1mM IPTG.

At submaximal growth in chemostat (SS1 - SS8), the percentage of depolarised cells increased in both the absence and presence of IPTG (*Figure 6.14*). In the absence of IPTG, depolarised cells ranged from 28.80 to 35.83% in SS4 and SS7 respectively (*Figure 6.14*). Conversely, the mean of depolarised cells was 22.85% at maximal growth (S4). In the presence of IPTG, depolarised cells ranged from 36.10 to 42.24% in SS8 and SS4, respectively.

To test for the influence of IPTG on depolarised cell subpopulation grown on glycerol-limited media, the means of depolarised cells at "steady state" were compared in the absence and presence of IPTG. In the absence of IPTG, the mean percentage of depolarised cells at submaximal growth (SS1 - SS8) was 32.19%; in the presence of IPTG, the mean percentage was 39.81% (*Figure 6.14*). The difference between the mean percentages of depolarised cells was deemed significant (one-way ANOVA, $f = 28.15$, $p < 0.001$). This suggests the addition of IPTG increases membrane depolarisation, although explaining only 32.97% of variation within the data set, thus suggesting that the effect may be indirect.

At reduced μ (SS1 - SS8), the percentage of active cells fluctuated from 53.60 to 60.90% in the absence of IPTG, and 45.37 to 50.04% in the presence of IPTG, respectively. Conversely, the percentage of active cells at maximal growth (S4) was 70.8% (*Figure 6.14*). To test for the influence of IPTG on cell functionality during submaximal growth on glycerol, the "active cell subpopulations" were compared across "steady states". In the absence of IPTG at steady state, the mean of "active" cells was 57.38%, while in its presence was 47.43%. The fraction of "active" cells was significantly different in the presence of IPTG (one-way ANOVA, $f = 37.61$, $p < 0.001$). This predicts that 40.66% of variation can be explained by the addition of IPTG. Although IPTG decreases cell functionality, its effect on "active" cells may be indirect, thus other parameters may require further investigation.

Comparisons were made between the "active" *E. coli* W3110 cell populations at steady state on glucose and glycerol-limited media to see the influence of a changing C source. At submaximal growth in the absence of IPTG, a higher proportion of active cells were present when glucose (64.79%) was used as a carbon source, rather than glycerol (57.38%). The difference was deemed significant following statistical analysis (one-way ANOVA, $f = 28.93$, $p < 0.001$), suggesting that growth on glycerol lowers the proportion of active cells.

6.9 Studies of cell morphology using fluorescence microscopy

Fluorescence microscopy was used to characterise the heterogeneity of *E. coli* cells undergoing aerobic fermentation grown on glycerol as the sole carbon source. Morphology metrics were calculated from fluorescent images following staining with $SYTO_9$/PI in the absence and presence of IPTG.

6.9.1 Cell morphology in the absence of IPTG

a) Cell area

The results of cell area changes are shown in *Figure 6.15.* The highest cellular area was observed at maximal growth rate, during the exponential phase of growth, with a mean of 1.66 μm^2 (*Figure 6.15 B*). At submaximal growth, differences in means of cell area were prominent within samples, ranging from 0.85 to 1.53 μm^2 in SS3 and SS4, respectively. Cell area indicates the cell size, thus overall larger cells were present at maximal growth on glycerol as a sole carbon source. Although glycerol is not the preferred C source of *E. coli*, this may be expected due to the presence of readily available food sources with no growth limitation.

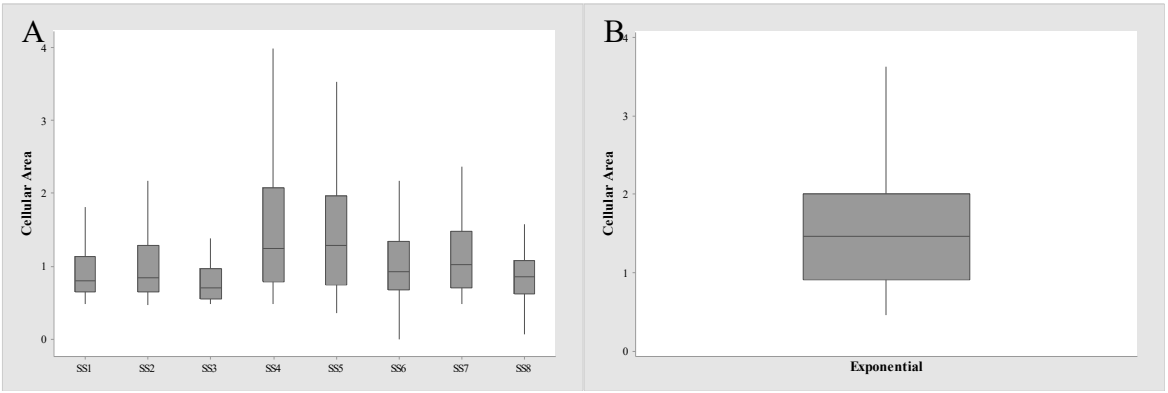

Figure 6.15. Cell area distributions of "live" *E. coli* W3110 grown on glycerol as the sole carbon source at: A) submaximal growth rate in chemostats (SS1: 173; SS2: 205; SS3: 248; SS4: 135; SS5: 272; SS6: 198; SS7: 211; SS8: 187 cells. B) maximal growth rate (148 cells). Each boxplot shows the median (black horizontal line), indicating values above which 50% of the cells are located. Grey boxes indicate the interval into which 50% of the data falls, with top and bottom of the box representing the area where 25% of values are located above and below.

Cell size heterogeneity, illustrated by CV and SD values, shows the largest SD of 0.97 during maximal growth (*Figure 6.15 B*). Submaximal growth in chemostat presents a range of SD

values, ranging from 0.45 to 0.96 in SS3 and SS4, respectively (*Figure 6.15 A*). However, the CV of 58.38 during exponential phase is not the largest out of the samples. The highest CV is 64.63 in SS8, whilst the lowest CV is 52.84 in SS7, a range that accommodates the exponential CV.

Although a high CV shows an increased heterogeneity, no conclusive trends could be established, as not all CV values at submaximal growth are larger than CV obtained during exponential growth. The difference between cell area at submaximal growth was, however deemed significant (Kruskal-Wallis, $H = 40.62$, $p < 0.001$). This showed that cell size during chemostats varies with sampling, thus the fermentation time influences the cell area distribution of *E. coli* W3110 cells grown on glycerol in the absence of IPTG.

b) Circularity

The circularity is a dimensionless indicator of cell shape that quantifies the irregularities of the cell membranes. The changes in cell circularity at maximal and submaximal growth rate (where no IPTG was present) shows many similarities (*Figure 6.16)*. The lowest mean circularity was 0.52, present at maximal growth, during the exponential phase (*Figure 6.16 B*). During submaximal growth in chemostat, the cell circularity means varied from 0.52 to 0.59 in SS4 and SS5, respectively (*Figure 6.16 A*). Only a 0.009 difference was present between the exponential and the chemostat (SS4) circularity, which may be entirely due to chance. A similar trend is present when comparing median circularity. The exponential (0.53) is only 0.002 outside the lowest of the values obtained during submaximal growth. The median circularity in chemostat growth ranges from 0.53 to 0.61 in SS4 and SS5 respectively.

The CV during submaximal growth on chemostat was 28.82, a value that sits within the chemostat CV range of 20.37 to 32.13. Subsequent statistical testing on the changes in circularity during submaximal growth on glycerol showed no significant difference (Kruskal-Wallis, $H = 11.99$, $p = 0.101$). Conversely, a significant difference was present during submaximal growth on glucose as sole carbon source, with circularity decreasing every hour (Kruskal-Wallis, $H = 74.42$, $p < 0.001$) (*Figure 4.21*).

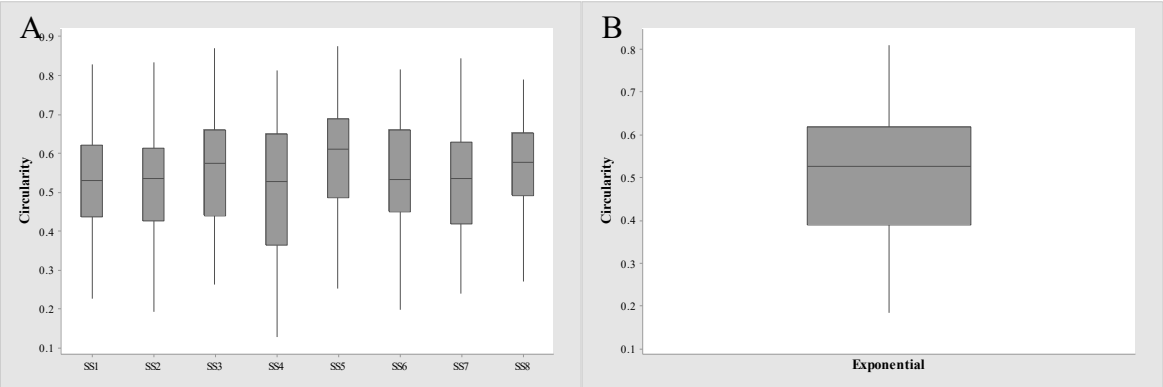

Figure 6.16. Circularity distributions of "live" *E. coli* W3110 cells with glycerol as the sole carbon source at: A) submaximal growth rate: SS1: 173; SS2: 205; SS3: 248; SS4: 135; SS5: 272; SS6: 198; SS7: 211; SS8: 187 cells. B) maximal growth rate (148 cells). The median of each boxplot (black horizontal line) indicates values above which 50% of the cells are located. A grey box indicates the interval into which 50% of the data falls, with top and bottom of the box representing the area where 25% of values are located above and 25% below.

c) Aspect Ratio

Aspect ratio indicates the elongation of an ellipse fitted to the cell shape, reported by length divided by breadth. *Figure 6.17* shows the distributions of the measured aspect ratio (AR) of *E. coli* W3110 cells grown with glycerol as sole carbon source.

During maximal growth, *E. coli* W3110 presents a mean AR of 3.16, a median AR of 2.99, ranging from 1.16 to 6, with Q1 at 2.14 and Q3 at 3.93 (*Figure 6.17 B*). During submaximal growth in glycerol-limited chemostats, the mean ARs range from 2.33 to 3.24 in SS5 and SS3, respectively, a range which accommodates the exponential mean of 3.16.

A similar trend is prominent when comparing the SD of unrestricted maximal growth to that of glycerol-limited growth. The exponential SD of 1.17 is present with the range of SD during chemostat growth, ranging from 0.86 to 1.35 in SS7 and SS3, respectively. The SD represents the data spread away from the mean, thus showing that the AR heterogeneity of the exponential phase overlaps with the values obtained during chemostat growth. The same trend was maintained across CV values. The CV during chemostat ranged from 34.17 to 42.80 in SS7 and SS4, respectively. The exponential CV was 36.90, a value which is present within the range observed in chemostats. Subsequent statistical analysis showed that the difference

between AR during submaximal growth on glycerol was deemed significant (Kruskal-Wallis, $H = 29.51$, $p < 0.001$).

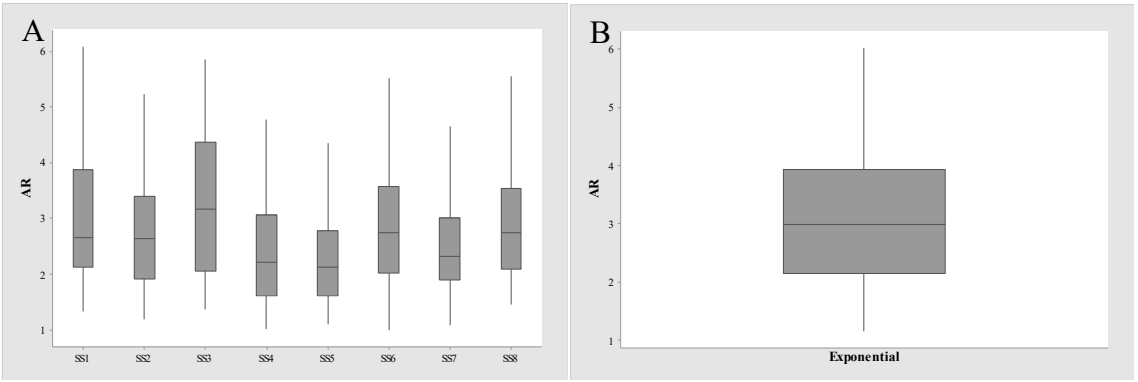

Figure 6.17. Distributions of aspect ratio (AR) during growth of *E. coli* W3110 on glycerol as the sole carbon source. Only the "live" subpopulation was analysed at: A) submaximal growth rate; SS1: 173; SS2: 205; SS3: 248; SS4: 135; SS5: 272; SS6: 198; SS7: 211; SS8: 187 cells. B) maximal growth rate (148 cells). The median (black horizontal line) indicates values above which 50% of the data is located. The grey box represents the interval into which 50% of the data falls, with top and bottom of the box representing that 25% of values are located above and 25% below.

6.9.*2 Cell morphology in the presence of IPTG*

To determine the effect of IPTG on host cell morphology, control experiments were conducted in the presence of 1mM IPTG. This was determined as the optimum inducer quantity for the induction of recombinant protein in the plasmid containing cells (*Figure 7.5).*

a) Cell area in the presence of IPTG

The highest cell area was observed during maximal growth, with a mean of 2.14 (*Figure 6.18 A*). This shows larger cells are present, which may be expected as conditions are not nutrient-deficient. The mid-exponential sample (*Figure 6.18 A*), however does not contain IPTG, as induction was carried out post-sampling for maximal growth rate. Conversely, the mean of cell area during submaximal growth with IPTG ranged from 1.58 to 2 in SS6 and SS8, respectively (*Figure 6.18 B*). In the absence of IPTG, the mean cell area during submaximal growth was ranging from 0.85 to 1.53 at SS3 and SS4, respectively (*Figure 6.15*).

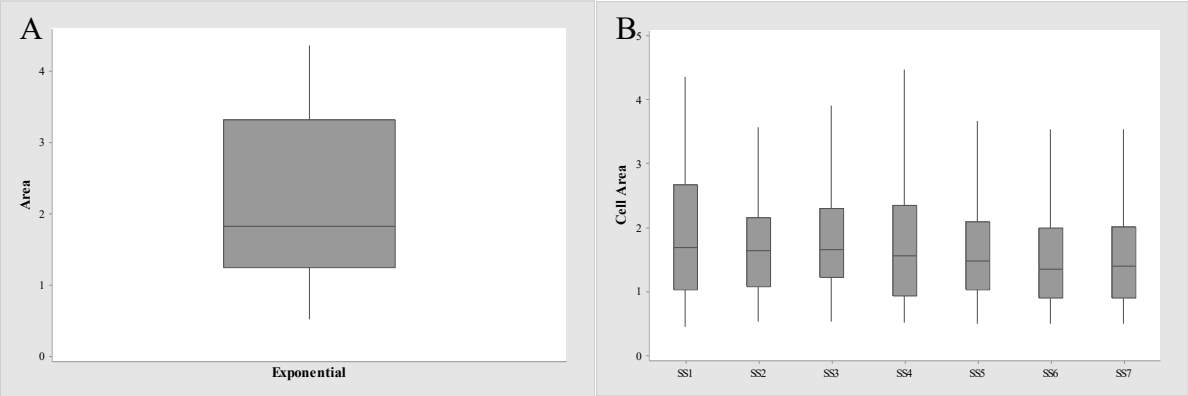

Figure 6.18. Boxplots of cell area of "live" *E. coli* W3110 grown on glycerol as the sole carbon source at: A) maximal growth rate (148 cells); B) submaximal growth rate with 1 mM IPTG: SS1: 182; SS2: 193; SS3: 210; SS4: 176; SS5: 151 SS6: 204; SS7: 276 cells. Each boxplot shows the median (black horizontal line), indicating values above which 50% of the cells are located. Grey boxes indicate the interval into which 50% of the data falls, with top and bottom of the box representing the area where 25% of values are located above and 25% below.

Although the SD during exponential phase was the largest of all samples (1.09), the exponential CV (50.98) is not the highest, as the mean is higher. At submaximal growth in glycerol-limited chemostats, the SD values range from 0.82 to 1.06 in SS2 and SS1, respectively. The highest CV is 58.56 in SS7, and the lowest is 46.96 in SS2, a range accommodating the exponential CV. A higher CV would signal an increased heterogeneity in cell size, but as the exponential CV (50.98) sits in the range obtained during chemostat growth, no conclusive trend can be established. The difference in heterogeneity of cell area during submaximal growth on glycerol-limited chemostats in the presence of 1mM IPTG were deemed significant (Kruskal-Wallis, $H = 40.62$, $p < 0.005$). This shows a difference in heterogeneity between samples, which may be influenced by the fermentation time, but nevertheless signals a deviation from "balanced growth".

b) Circularity in the presence of IPTG

Figure 6.19 shows the circularity distributions of the "live" sub-population of *E. coli* W3110 cells on glycerol as sole C source. Maximal growth rate achieved the highest mean circularity of 0.55. Submaximal growth in glycerol-limited chemostats with IPTG exhibits a range of means of circularity, from 0.50 to 0.53 in SS5 and SS3, respectively. The results (*Figures 6.19 A* and *B*) are not directly comparable, as two factors differ: the addition of IPTG and the growth rate.

The median exponential circularity was 0.54, whilst the median circularity at submaximal growth on glycerol with 1 mM IPTG ranged from 0.49 – 0.53 in SS5 and SS3, respectively. The exponential SD was 0.14, whilst the chemostat SD values ranged from 0.10 to 0.12 in SS5 and SS4, respectively. Statistical testing showed that the differences in circularity at submaximal growth rate in glycerol-limited chemostats with an added inducer are significant (Kruskal-Wallis, $H = 13.81$, $p < 0.05$). This suggests a change in circularity at "steady state" in the presence of IPTG, a contrast from the previous finding concerning circularity in the absence of IPTG (Kruskal-Wallis, $H = 11.99$, $p = 0.101$). Circularity signals irregularities in the cell membrane, thus the addition of IPTG causes significant deviations of cell form between sampling in an assumed "balanced growth".

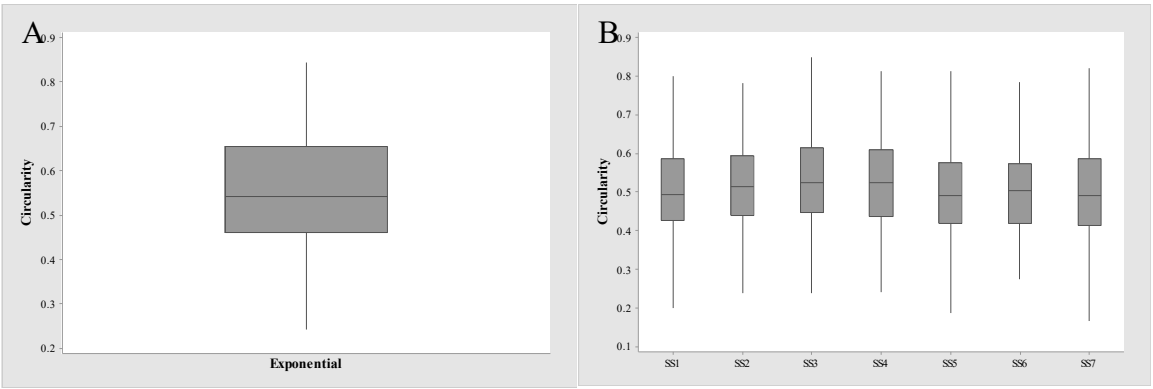

Figure 6.19. Distributions of circularity during growth of *E. coli* W3110 on glycerol as sole carbon source at: A) maximal growth no IPTG (148 cells); B) submaximal growth rate with 1 mM IPTG: SS1: 182; SS2: 193; SS3: 210; SS4: 176; SS5: 151 SS6: 204; SS7: 276 cells. The median of each boxplot (black horizontal line) indicates values above which 50% of the cells are located. A grey box indicates the interval into which 50% of the data falls, with top and bottom of the box representing the area where 25% of values are located above and 25% below.

c) Aspect Ratio in the presence of IPTG

Aspect ratio (AR) indicates the elongation or stretching of a shape, calculated as "length divided by breadth". The AR distributions of *E. coli* W3110 with glycerol as sole carbon source, in the presence of IPTG are shown in *Figure 6.20.* Maximal growth showed a mean AR of 3.25, with SD of 1.13, and CV of 36.90.

Submaximal growth in the presence of IPTG exhibited several AR distributions: the mean ranged from 3.56 to 3.98 in SS1 and SS6, respectively; the SD ranged from 1.04 in SS5 to 1.22 in SS8, whilst CV ranged from 26.67 to 33.11 in SS5 and SS1, respectively. The differences between mean AR at submaximal growth on glycerol were deemed significant (Kruskal-Wallis, $H = 19.76$, $p < 0.005$). This indicates the AR distributions are not independent of time, suggesting that the cells deviate from "balanced growth" when IPTG is present.

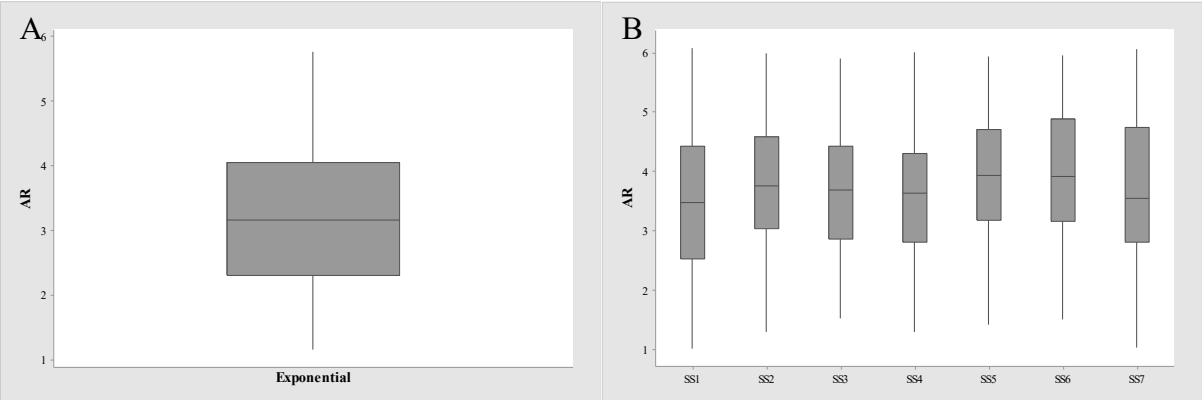

Figure 6.20. Aspect ratio (AR) distributions of *E. coli* W3110 on glycerol as the sole carbon source. A:) maximal growth rate, no IPTG (148 cells); B) submaximal growth rate with 1 mM IPTG (SS1: 182; SS2: 193; SS3: 210; SS4: 176; SS5: 151 SS6: 204; SS7: 276 cells). Horizontal line within the box marks the median, boundaries of the box plot indicate the 25th and 75th percentile of the distribution, whiskers mark the 5th and 95th percentile of the distribution. Values outside of the 1.5-fold IQR were removed.

In the absence of IPTG, the CV during glycerol-limited growth ranged from 34.17 to 42.80 in SS7 and SS4, respectively (*Figure 6.17 A*). In the presence of IPTG, the CV ranged from 26.67 to 33.11 in SS5 and SS1, respectively (*Figure 6.20 B*).

The influence of the inducer on cell size and shape at submaximal growth on glycerol (SS1) is shown in the absence or presence of 1 mM IPTG (*Figure 6.21).* A higher median AR of 3.48 and cell area of 1.69 were present in the presence of IPTG rather than in its absence, where values were 2.66 and 0.80, respectively. The differences between AR (as shape indicator) and area (as size indicator) were deemed significant following subsequent statistical testing (AR: Mann-Whitney U, W = 5275.0, $p < 0.001$; Area: Mann-Whitney U, W = 4228.0, $p < 0.0001$). Given that all other parameters were maintained constant, larger elongated cells with an overall bigger size exist in the presence of IPTG.

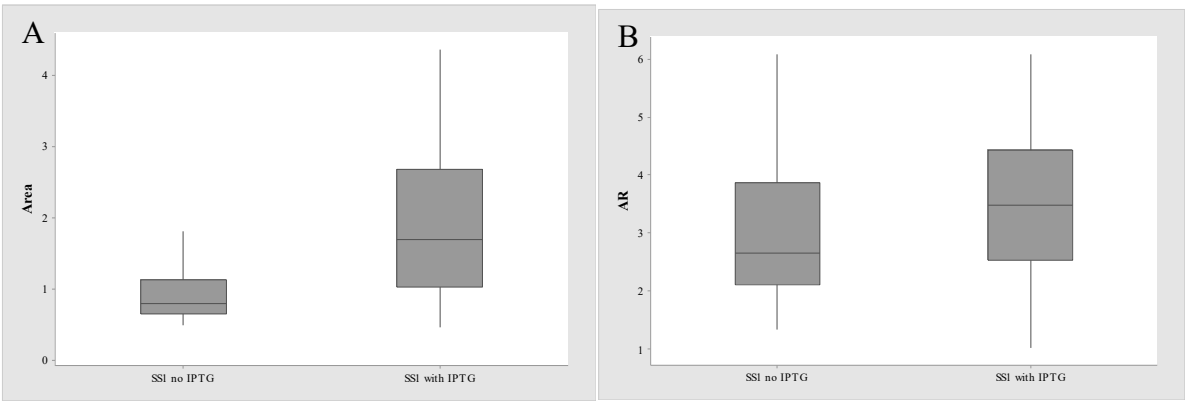

Figure 6.21. Shape descriptors of "live" *E. coli* W3110 at submaximal growth rate on glycerol as sole carbon source in the presence (176 cells) or absence with 1mM IPTG (135 cells). A): cell area; B: aspect ratio (AR). The median (black horizontal line) indicates values above which 50% of the data is located. The grey box represents the interval into which 50% of the data falls, with top and bottom of the box representing the area where 25% of values are located above and 25% below. Values outside of the 1.5-fold IQR were removed.

6.10 Single cell studies of light scattering (FSC & SSC)

FSC signals were extracted from "live" *E. coli* W3110 cell sub-population. The mean FSC (A.U.) during maximal growth on glycerol as sole carbon source was 16335 (*Figure 6.22*). At steady state, the means fluctuated from 18886 to 23005 A.U. at SS2 and SS7, respectively (*Figure 6.22*). The lowest SD as an indication of data spread was 17641 recorded during exponential phase, whilst during chemostats, SD ranges from 19094 to 36688 in SS2 and SS6 respectively. If FSC indicates cell size, the higher values during chemostats are not in agreement with microscopy results, where larger cells were observed at maximal growth on glycerol. This may be due to the higher background of FSC signals when analysing small bacterial cells.

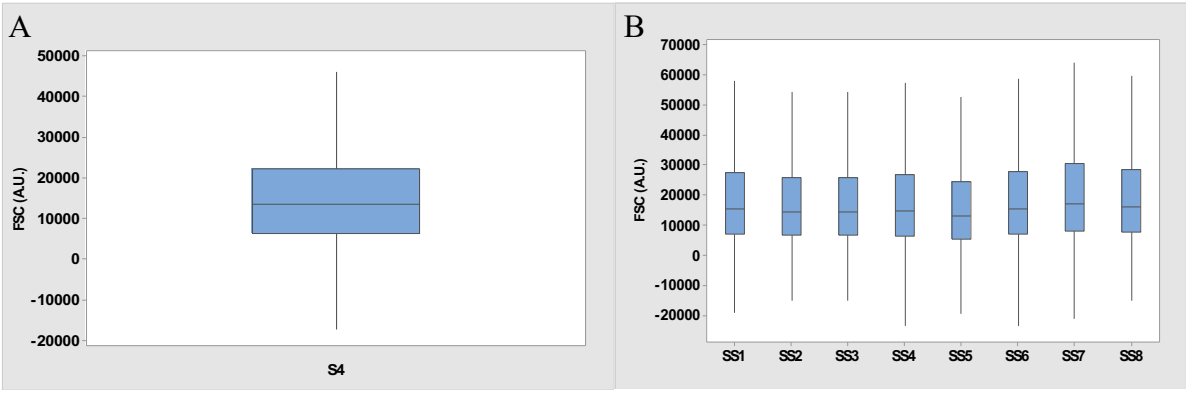

Figure 6.22. Boxplots of forward scatter signal (FSC) of *E. coli* W3110 at two different growth rates in the absence of IPTG, with glycerol as sole carbon source. A: FSC values of cells during the exponential phase. B: FSC values of cells from steady state samples. The median (black horizontal line) indicates values above which 50% of the data is located. The grey box represents the interval into which 50% of the data falls, with top and bottom of the box representing the area where 25% of values are located above and 25% below. Values outside of the 1.5-fold IQR were removed.

The lowest mean SSC signal of 25251 A.U. was observed during maximal growth with glycerol as sole carbon source (*Figure 6.23*). The means of SSC increased during submaximal

growth on glycerol from 34160 to 37901 at SS6 and SS7, respectively (*Figure 6.23*). A trend of increasing side scatter signals was identified during submaximal growth on glycerol, with increased heterogeneity in SSC signals. The SD during maximal growth was 23784, whilst the SD during chemostat cultivations ranged from 30484 to 47677 A.U. at SS2 and SS6, respectively. This suggests an increase in cell size during submaximal growth on glycerol in the absence of IPTG.

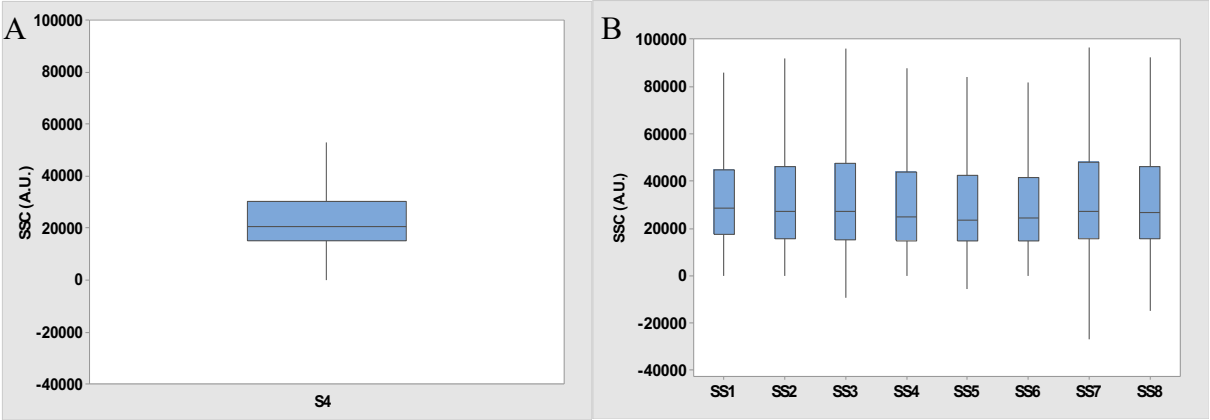

Figure 6.23. Boxplots of forward scatter signal (SSC) of *E. coli* W3110 at exponential (A: S4) and steady state (B: SSC1 - 8) growth rates in the absence of IPTG, with glycerol as sole carbon source.

6.11 Discussion and conclusions

This chapter presented the cellular dynamics in *E. coli* W3110 population grown on glycerol as sole carbon source. To mimic the substrate gradients experienced by cells in microbial fermentations used to produce recombinant proteins, two growth rates were investigated: μ_{max} and ½ μ_{max} as glycerol-limited growth.

The main findings for glycerol growth were:

Growth: *E. coli* W3110 showed altered growth, as monitored by BioLector with an extended lag phase compared to glucose. The cells grew slower on glycerol than glucose. The net growth rate for glycerol was 0.50 h^{-1}, with a doubling time of 1.37 h (*Figure 6.4*). The doubling time was longer than 1.16 h on glucose (*Figure 4.4*). A higher biomass was measured as both OD_{600} and BugLab signal for glycerol growth compared to glucose, in the

absence of IPTG. The addition of IPTG carries a cost on the growth of host strain at submaximal growth in glycerol calculated at 37.31%.

Total cell counts (cells/ml) were described by the equation TCC [ml^{-1}] = 2 x 10^8 OD_{600}. This holds true for maximal growth rate of *E. coli* W3100 for both substrates: glycerol and glucose. Neither TCCs nor population level measurements can quantify the "viable" from the "dead" cells, which justified single cell fluorescent-based viability assessments.

Studies of viability showed that during unrestricted growth at μ_{max} on glycerol, cells with green and red fluorescence were 94.90% and 5.10%, respectively (*Figure 6.13*). Conversely, the percentage of cells with green fluorescence (TO^+) was higher than 97% (*Figure 4.16 A*) during growth on glucose, the preferred carbon source of *E. coli.* The fraction of "live" cells decreased during submaximal growth to values ranging from 90.40% to 93.48% at SS1 and SS6, respectively in the absence of IPTG. The fraction of "live" cells decreased further with the addition of IPTG (one-way ANOVA, $f = 21.48$, $p < 0.001$), showing that IPTG addition increases cell death.

Cell energetic state was studied with $DIBAC_{4(3)}$/EB/PI. At maximal growth on glycerol as sole C source (S4), 70.8% of *E. coli* cells were active, 22.85% depolarised, 6.03% dead and 1.02% de-energised (*Figure 6.14*). Conversely, unrestricted growth with glucose as sole carbon source showed a higher share of active cells, with less depolarised cells and dead cells. On their preferential carbon source, 83.74% of cells were active, 13.08% depolarised, 2.30% dead and 0.87% de-energised (*Figure 4.17*). As the only difference was the carbon source, this showed glycerol increases the membrane depolarisation and permeability, leading to an increase in cell death and a decrease in cell function.

Morphology assessment showed overall larger cells were present at maximal growth on glycerol as sole carbon source compared to submaximal growth without IPTG. The addition of IPTG led to larger elongated cells than those in its absence (*Figure 6.20*). The differences between AR (as shape indicator) and area (as size indicator) in the presence and absence of IPTG were significant (AR: Mann-Whitney U, $W = 5275.0$, $p < 0.001$; Area: Mann-Whitney U, $W = 4228.0$, $p < 0.0001$).

Furthermore, *E. coli* W3110 cells consumed glycerol slower than glucose, resulting in negligible amounts of VFAs. This shows a better conversion of glycerol into biomass compared to glucose, demonstrating the potential benefit of utilising glycerol as carbon source in microbial fermentations for high value products. As data indicated that growth and division

were present in chemostat cultivations on glycerol, this justified carrying out the experiments with the recombinant plasmid transfected into the host *E. coli* W3110 cells.

CHAPTER 7

RESULTS

Chapter 7 Cell dynamics in recombinant *E. coli* CLD 1301 fermentations on glycerol

7.1 Abstract

Recombinant protein production in industry frequently uses glycerol in fed-batch cultivations. Substrate gradients vary widely in large-scale fed-batch cultivations. Cells frequently experience the concentrated feed at the top of the fed-batch fermenter and nutrient limitation bordering on complete exhaustion at the bottom. While cells at the bottom of the fermenter grow at a reduced rate μ, those at the top are at a maximum $\mu_{max.}$

To simulate substrate gradients that exist on an industrial scale, the growth of recombinant strain *E. coli* CLD1301 was evaluated at two different growth rates. An enhanced GFP mut3* was used as a model recombinant protein, as it was optimised for easy detection with both fluorescence microscopy and flow cytometry. The GFP-A gene coding for the protein was enclosed in plasmid pD441- SR: 240460, which is IPTG-inducible.

Single cells were measured during batch phase with excess glycerol and during glycerol-limited continuous cultivations. Populations were characterised with respect to their morphologic parameters, membrane integrity, membrane potential and total cell counts, all with single cell resolution. The measurements were compared with the host *E. coli* W3110 to show the influence of the plasmid maintenance (for non-induced cultures) and protein production (for induced cultures). Protein production was compared with fermentations carried out on glucose (discussed in Chapter 5), considering the population heterogeneity.

7.2 Introduction

Reports suggest that poor performance of bioprocesses arises from cell-to-cell heterogeneity, which is thought to arise from suboptimal reactor conditions such as limited nutrients and aeration. It has been suggested that heterogeneity in large-scale microbial fermentations improves the productivity of recombinant proteins (Fragoso-Jimenez *et al.*, 2019). The actual mechanism by which cellular heterogeneity influences the bioprocess remains unknown. The understanding of heterogeneity is however, key to process optimisation and requires single cell analysis.

To experimentally simulate a large-scale industrial bioprocess at laboratory scale, fermentations of a recombinant *E. coli* harbouring an enhanced GFP mut3* were carried out in both excess and limited nutrient. Cells were measured at single cell level with respect to morphological and physiological characteristics. The enhanced GFP mut3* was used as a reporter for protein production at single cell level.

7.3 Determination of single media limitation on glycerol

Chemostats allow the investigation of cell responses to a change in a single factor, typically the growth rate. The chemostat is based on a single growth-limiting factor, while the other components were maintained in a constant state of excess. For the growth to be representative for large-scale fermentations using glycerol, the growth-limiting factor in the media should be carbon. To assess the suitability of the media for chemostat cultivations, the glycerol concentration (w/v) was varied between 1 and 10 g/L, whilst the other components were maintained at a constant excess. The media (described in Section *3.3.1 Batch mineral media*) was buffered to maintain the pH at approximately 6.8 (starting $pH_0 = 7$).

Cultures grown as described in Step A, Section *3.2 Cell expansion and seed preparation* were used to inoculate 800 µl media plus kanamycin in 48 MTP FlowerPlates (MTP-48-BOH, m2p-labs GmbH, Baesweiler, Germany). The experiments were performed in triplicate with one well with sterile media used as an internal standard for sterility control. The plates were sealed with a gas permeable foil (F-GPR48-10, m2p-labs GmbH, Baesweiler Germany), and placed in the incubation chamber (BioLector, m2p-labs GmbH, Baesweiler, Germany) under shaking at 37^0C. The initial OD_{600} was 0.05 at time 0. Growth and fluorescence, expressed in arbitrary units (A.U.), were measured online every 15 minutes. Background values for both biomass and fluorescence (A.U.) were subtracted from the first five measurements following inoculation.

Figure 7.1 shows the growth curves of *E. coli* CLD1301 on minimal media with glycerol as the sole carbon source. After a long lag phase of approximately 23 h, the culture began the exponential phase characterised by maximum growth rate μ_{max}. Growth then stopped abruptly and the culture entered the stationary phase ($\mu = 0$), illustrated by a plateau in the growth curve (*Figure 7.1*). Stationary phase occurred at different time points dependant on when the glycerol limitation occurred. The arrows in *Figure 7.1* show the entrance to stationary phase for two glycerol concentrations (4 and 7 g/L). The lower the carbon concentration, the sooner

growth stopped and the lower the final biomass (A.U.). During the stationary phase, growth ceases because the limiting substrate (assumed carbon/glycerol) is depleted (residual substrate = 0).

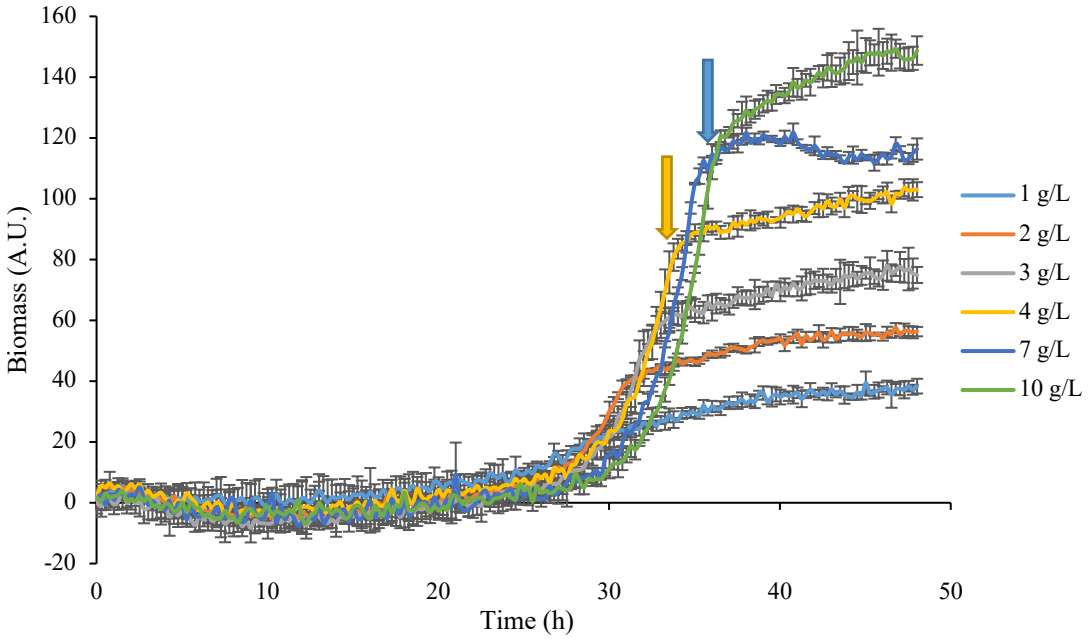

Figure 7.1. Biomass (A.U.) as scattered light for *E. coli* CLD1301 on glycerol as sole carbon source, in the absence of inducer. Conditions: minimal media with up to 10 g/L glycerol, T = 37^{0}C, V_L = 800 µL, n = 1500, d_0 = 3 mm. The arrows show the entrance to stationary phase. Standard error bars represent ± S.D.

Cultivations were stopped at 48.03 h, when the culture was in stationary phase. To determine that the limiting substrate is glycerol and thus the other nutrients are both non-limiting and in excess, the maximum biomass during 37 - 47 h was plotted against the glycerol concentration (*Figure 7.1*). The limiting nutrient carbon's mass is subject to conservation of mass, so during the stationary phase (residual carbon = 0), all the initial carbon from media will only be found in biomass carbon, assuming no by-products. Thus, the biomass rises linearly with the carbon source if the carbon source is limiting. A significant linear relationship was noted when plotting the final amount of biomass as a function of glycerol concentration up to 4 g/L, with R square value of 0.9625 (*Figure 7.2*).

The changes in biomass for 7 and 10 g/L do not follow the linear regime, showing that glycerol becomes a non-limiting substrate. Given the initial calculations used for media

composition, the limiting factor for media with glycerol concentrations (w/v) of 7 and 10 g/L may well be nitrogen, as sole or secondary limitation (Appendix A). However, the above experiments confirmed that at 4 g/L glycerol the media is glycerol limited, and the other nutrients are in excess and not limiting.

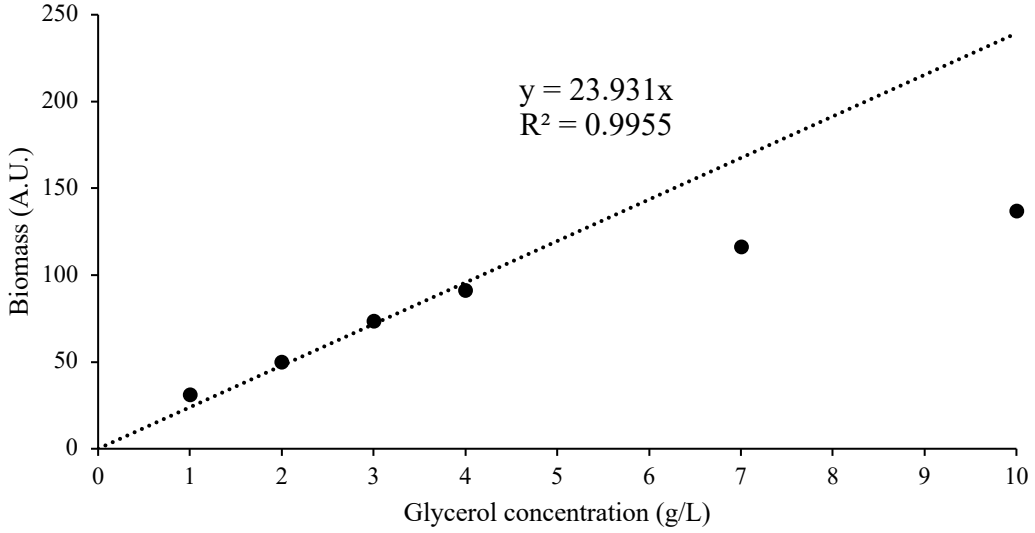

Figure 7.2. Maximum biomass (A.U.) of *E. coli* CLD1301 during 37 - 47 h of batch growth. The linear relationship between biomass (A.U.) and glycerol concentration (g/L) up to 4 g/L indicates that the nutrient is in the limiting range. Conditions: minimal media including (w/v) 1, 2, 3, 4, 7 and 10 g/L glycerol, while other media components remained constant and in excess, T = 37^{o}C, V_L = 800 µL, n = 1500, d_0 = 3 mm.

7.4 Growth rate and the influence of pDNA on the growth rate

The growth characteristics of the recombinant strain *E. coli* CLD1301 were determined using BioLector. To determine the metabolic burden imposed by the pDNA, in the absence of protein expression, the host *E. coli* W3110 was used as the control. The final biomass (*Figure 7.3*) and the growth rates (*Figure 7.4*) were compared between the two strains, in the absence of induction.

Cells were grown under fully aerobic conditions in batch media (described in Section *3.3.1 Batch mineral media*) with 4 g/L glycerol as sole C source. The media had the required buffered capacity to keep the pH value within 7 ± 0.2, and was supplemented with kanamycin

for the growth of the recombinant strain. The starting OD_{600} was 0.05 for both conditions, from a culture grown in a corresponding media ± kanamycin (described at Step A, Section *3.2 Cell expansion and seed preparation)*.

A significant difference was observed in the growth pattern and biomass (scattered light) (*Figure 7.3),* and the growth rate (*Figure 7.4*). The biggest noticeable difference was in the growth pattern, with different lag phases. The end of the lag phase was determined as the time at which the exponential trendline for the exponential phase intersected the time (x-axis). The lag phase was 3.6 h for the host strain, but nearly 23 h for the un-induced recombinant *E. coli* CLD1301, on glycerol growth as sole carbon source.

To determine the growth rate, a trendline was applied to at least five points during the exponential phase. The slope of the linear regression of the semi-log time plot of biomass (A.U.) represents the maximum growth rate. The growth rates were determined to be 0.50 h^{-1} for *E. coli* W3110 and 0.39 h^{-1} for *E. coli* CLD1301. Thus the cost, or the relative decrease in growth rate was determined to be 21.90%, calculated from formula

$$Cost = \frac{\mu_0 - \mu_1}{\mu_0} \; x \; 100 \qquad (7.1)$$

where μ_0 and μ_1 are the growth rates of the host and the recombinant strain respectively, both in the absence of inducer (0 mM IPTG).

Despite a drop in the growth rate caused by the pDNA, the final biomass was higher for the recombinant strain CLD1301 than the host strain W3110. The final biomass was 96.92 A.U. for the un-induced recombinant strain and 78.81 for the host W3110, respectively. The difference in the final biomass (from the stationary phase) was deemed significant (Mann-Whitney, U = 3197, n = 46, 46, $p < 0.001$). This showed that despite a long lag phase and a lower growth rate, the recombinant strain was capable of good growth under batch fermentations in BioLector.

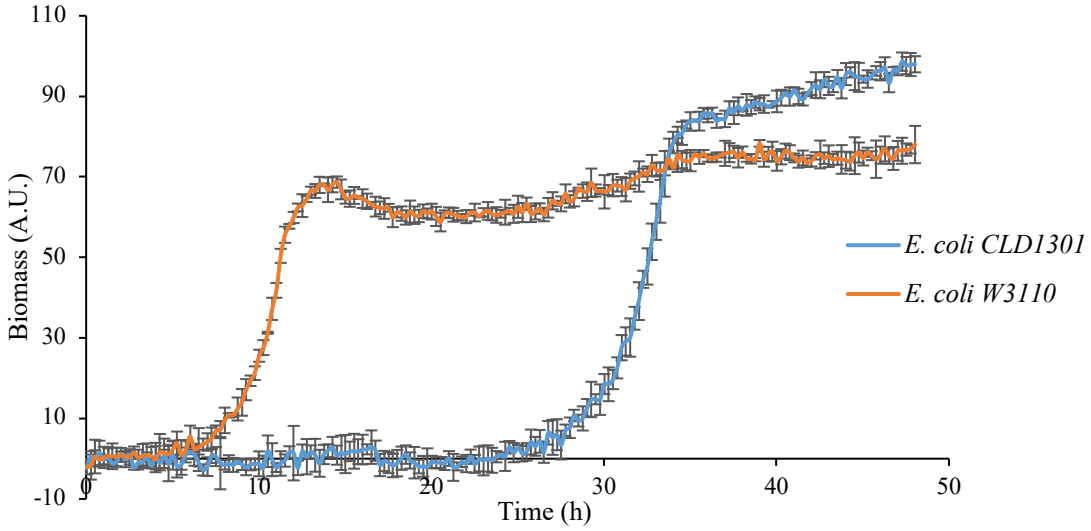

Figure 7.3. Comparison of *E. coli* W3110 and *E. coli* CLD1301 biomass (A.U.) as scattered light with no induction. Conditions: minimal media with 4 g/L glycerol as sole carbon source, T = 37^{0}C, V_L = 800 µL, n = 1500, d_0 = 3 mm. Standard error bars represent ± S.D.

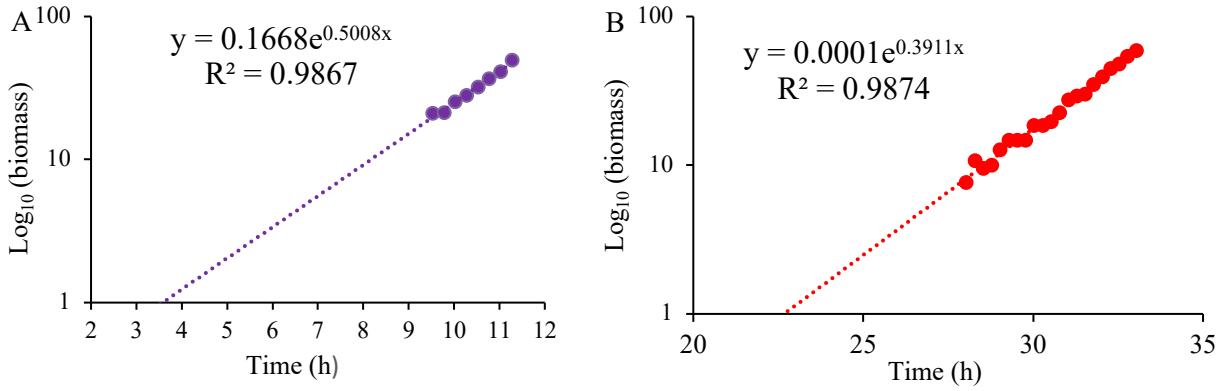

Figure 7.4. Maximum growth rate μ_{max} on glycerol as sole C source, no IPTG. A: *E. coli* W3110; B: *E. coli* CLD 1301. Biomass (A.U.) was recorded as scattered light. Conditions: minimal media 4 g/L glycerol, T = 37^{0}C, V_L = 800. A minimum 5 points of exponential phase of growth were chosen.

7.5 Determining the optimum amount of IPTG

An optimal inducer concentration is essential for the expression of recombinant protein. The inducer for the recombinant protein was IPTG. To determine the optimum amount of inducer, cultures of *E. coli* CLD1301 were induced at mid-exponential point of growth with varying concentrations of IPTG. Many protocols use a range of IPTG concentrations between 0.1 – 1 mM in *E coli* fermentations. Two concentrated stock solutions were prepared to allow the final IPTG concentrations (0.05 – 1 mM) in the MTP well. As dictated by the recombinant product, the temperature for both growth and induction was 37ºC.

Experiments were performed in triplicate using BioLector (m2p-labs GmbH, Baesweiler, Germany), as described in Section *3.4.1 Batch cultivations in Microtiter Plates*. The growth media used for cultivations was described previously (in Section *3.3.1 Batch mineral media*). The carbon source consisted of 4 g/L glycerol (w/v). The media was supplemented with kanamycin prior to cultivation, to achieve a final concentration of 50 µg/ml. This was necessary because the pD441- SR plasmid enclosed in the recombinant strain contained a kanamycin-resistant gene.

A 20 µl of a mid-exponentially growing *E. coli* CLD1301 culture (prepared as described in Step A, Section *3.2 Cell expansion and seed preparation)* was used to inoculate the BioLector with the initial OD_{600} of 0.05. The culture was allowed to follow a batch growth until the mid-exponential point of growth before induction. A mid-exponential induction is optimal because there is sufficient biomass in the system and sufficient residual carbon for the heterologous product. Neither an early nor late induction would be effective since there would not sufficient biomass in the system (in early inductions) and not enough resources for the heterologous product (in late inductions).

Biomass (scattered light) and product formation (GFP mut3* fluorescence) were measured in 15 min cycles and expressed as arbitrary units (A.U.).

The induction profile of *E. coli* CLD1301 in a 48 well FlowerPlate is shown in *Figure 7.5*. Time 0 represents the time of induction.

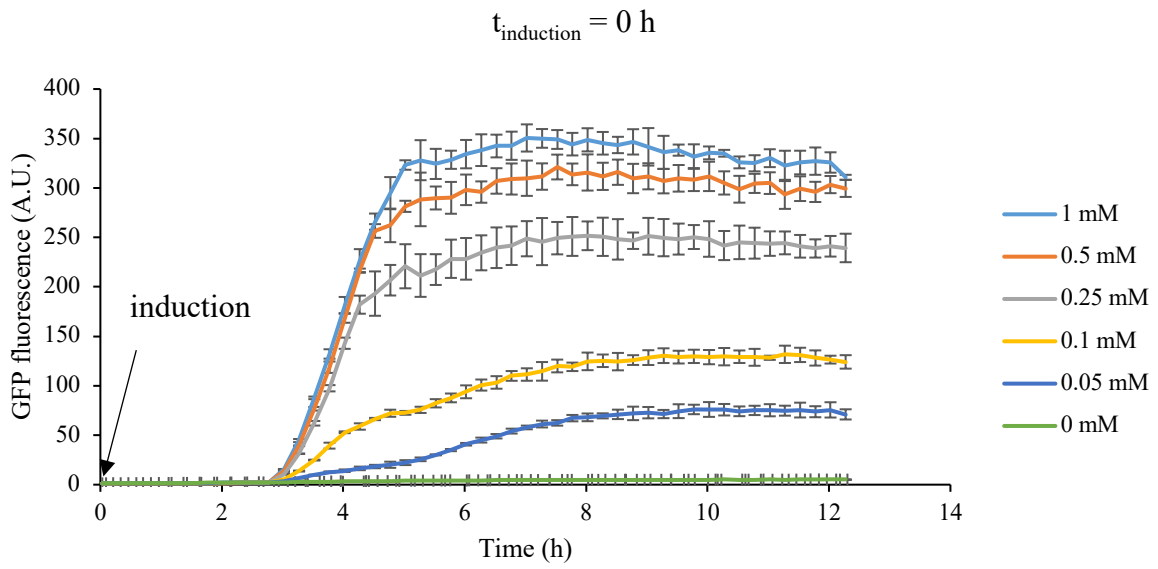

Figure 7.5. Comparison of GFP mut3* fluorescence (A.U.) after induction with varying concentrations of IPTG added at mid-exponential point of growth. Time 0 represents the time of induction, T = 37^{o}C. Standard error bars represent ± S.D. Conditions: minimal media 4 g/L glycerol, T = 37^{o}C, V_L = 800 µl.

The maximal achieved level of GFP mut3* is shown as a function of the inducer concentration. The maximum GFP mut3* fluorescence (A.U.) was obtained approximately six hours post-induction. When protein expression was induced with 1 mM IPTG, the mean GFP mut3* signal was 336.37, ranging from 310.75 to 350.54 A.U. When protein expression was induced with 0.5 mM IPTG, the fluorescent signal (A.U.) ranged from 293.54 to 321.17, with a mean of 306.64 *(Figure 7.5*). The difference in GFP fluorescence between 6 - 12.27 h for 1 and 0.5 mM IPTG was significant (Mann-Whitney U, W = 1019, n = 56, 56, P < 0.001). Therefore, the optimum IPTG concentration that led to the highest amount of product was 1 mM (*Figure 7.5*). Moreover, in the absence of IPTG (green line in *Figure 7.5*), the non-IPTG induced expression (A.U.) had a mean of 4.88 ± 0.04. This originated from both cell autofluorescence and leakiness, but following further investigations (with FM and FC) was considered negligible for single cell analysis.

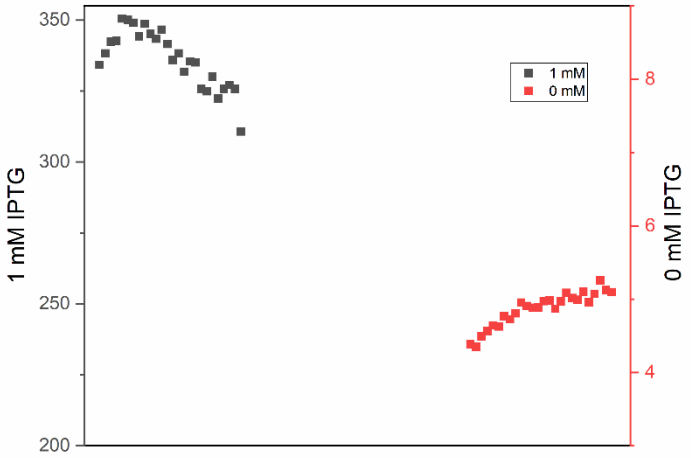

Figure 7.6. Maximum fluorescence signal (in black) and maximum background fluorescence (in red). The signal was recorded over 6.02 - 12.27 h in batch growth of *E. coli* CLD1301 – data from Figure 7.5.

The fluorescent signal of 1 mM IPTG-induced cultures was compared against the non-IPTG induced cultures (*Figure 7.6)*. This was important because the background fluorescence (in the absence of inducer) could interfere with the spectrum of GFP mut3* and therefore with single cell analysis. The measured fluorescence (A.U.) showed that the GFP mut3* signal was high enough against the low background, so the background signal was ignored. At the same time, the mean value of 4.88 A.U. (*Figures 7.5* and *7.6)* was caused by the cell autofluorescence instead of leakiness, because the fluorescence followed the growth curve (data not shown).

The decrease in the signal measured by BioLector across 6.02 - 12.27 h (*Figures 7.5* and *7.6* – black dots) is not caused by the instability of the protein, but by the culture reaching the stationary phase of growth. The exponential phase lasted around 8.5 h, with ~ 4.25 h both to reach mid-exponential and from mid-exponential to stationary phase. The increase in background fluorescence (red dots - *Figure 7.6*) is most probably the result of increased cell stress as there is no nutrient in the stationary phase.

Recombinant protein expression uses the host cell resources and has been shown to reduce the biomass (Wu *et al.*, 2016). To see how severe a high amount of recombinant product

compromises the biomass development, the specific productivity was calculated by dividing the concentration of protein product (GFP mut3* fluorescence) by the biomass (scattered light). The signal gains (GFP – Gain: 50; biomass – Gain: 20) were maintained as previously illustrated (*Table 3.2*).

Figure 7.7 shows the specific productivity of *E. coli* CLD1301 cells for 0.05 – 1 mM IPTG, monitored for 12.27 h post-induction, with an un-induced control. The fluorescence intensity per cell started to increase at 2.77 h and continued during the exponential phase, becoming constant during the stationary phase (*Figure 7.7*). Induction with 1 mM IPTG showed the highest specific productivity (with a mean of 4.27 A.U.) which sustained over the course of the batch fermentation *(Figure 7.7*). A significant difference exists between 1 and 0.5 mM IPTG (Mann-Whitney U, W = 1027, P < 0.0001), proving that 1 mM was the optimum concentration of inducer. This is consistent with the plasmid recommendation (https://www.atum.bio/catalog/expression-vectors/bacterial) and was subsequently used in the STR experiments.

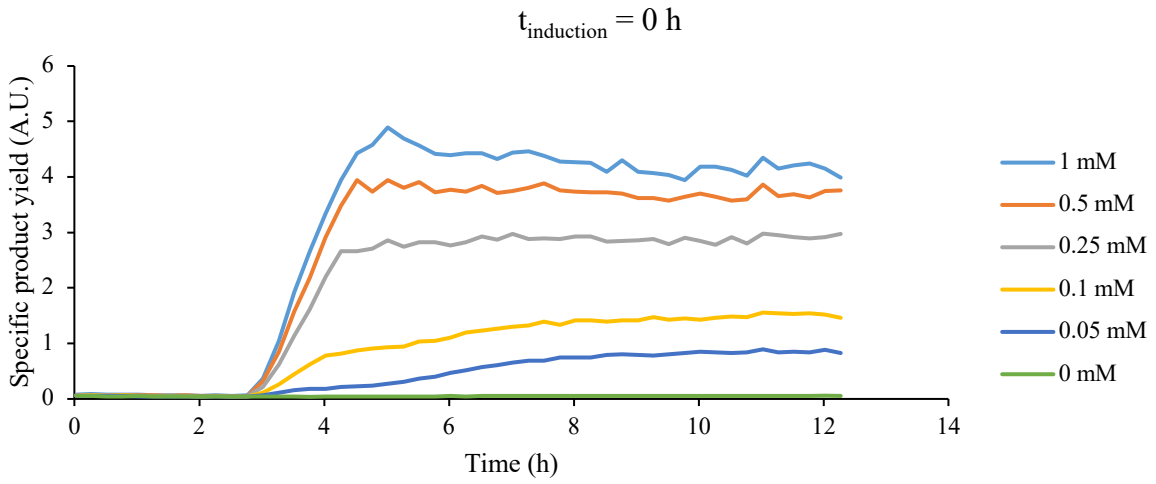

Figure 7.7. Specific product yield (Y_X^P) for *E. coli* CLD1301 on glycerol as sole carbon source. Specific product yield calculated as the ratio of protein (GFP fluorescence) to biomass concentration (scattered light intensity). Time 0 represents time of induction. T = 37^{0}C.

7.6 Process monitoring at population level

Since *E. coli* CLD1301 was capable of growth rates and biomass development comparable to the host strain in batch fermentations with BioLector, the next step was to assess the growth characteristics and protein production under industrial conditions. To mimic the industrial gradients existing at large scale, continuous cultivations were carried out at a ½ μ_{max} dilution rate. Fermentations were performed with and without induction of GFP mut3*expression to evaluate the influence of recombinant protein synthesis on the growth.

7.6.1 Measurements of biomass

The fermentation profiles of *E. coli* CLD1301 on glycerol as sole carbon source are depicted in both the absence (*Figure 7.8)* and presence of 1 mM IPTG (*Figure 7.9*). BugLab was used for the online measurements of the biomass.

The chemostat was first grown in "batch" from the inoculation (time 0), when OD_{600} was ~ 0.05 (*Figures 7.8* and *7.9*). The cells grew rapidly at a maximum growth rate of 0.39 h^{-1} with T_d of 1.77 h during the initial batch phase. At mid-exponential point (time 8 - 9 h), when OD ~ 2, the culture was switched to continuous growth with a dilution rate (D) of 0.20 h^{-1} (1/2 μ_{max}). At this point, the BugLab signal displayed on overshoot –the biomass rose above the steady state levels as too much of the limiting substrate was present. The doubling time in chemostat was 3.54 h. Residence time was 5.11 h and 25 h were allowed for the culture to reach steady state, which was monitored between 33.5 - 54.5 h. Steady state was defined by a relatively constant OD_{600}.

The BugLab sensor displayed a linear response during the exponential phase of growth. The sensor signal varied, however during glycerol-limited growth in chemostat, when the spectrophotometer showed the biomass remained relatively constant, but the BugLab did not (*Figures 7.8* and *7.9).* This could be due to oversensitivity to changes in cell morphology, a low biomass, or a high agitation rate. Contrasting with growth on glucose, no growth rate recovery was observed in STR compared to BioLector growth (*Figures 7.8* and *5.9*). In line with a T_d of 1.77 h and 3.54 h during exponential and chemostat growth respectively, sampling was conducted every 2 h during batch and every 3 h during chemostat growth, as previously detailed in *Table 4.1*, with the only difference that 25 h were allowed for the system to reach steady state growth.

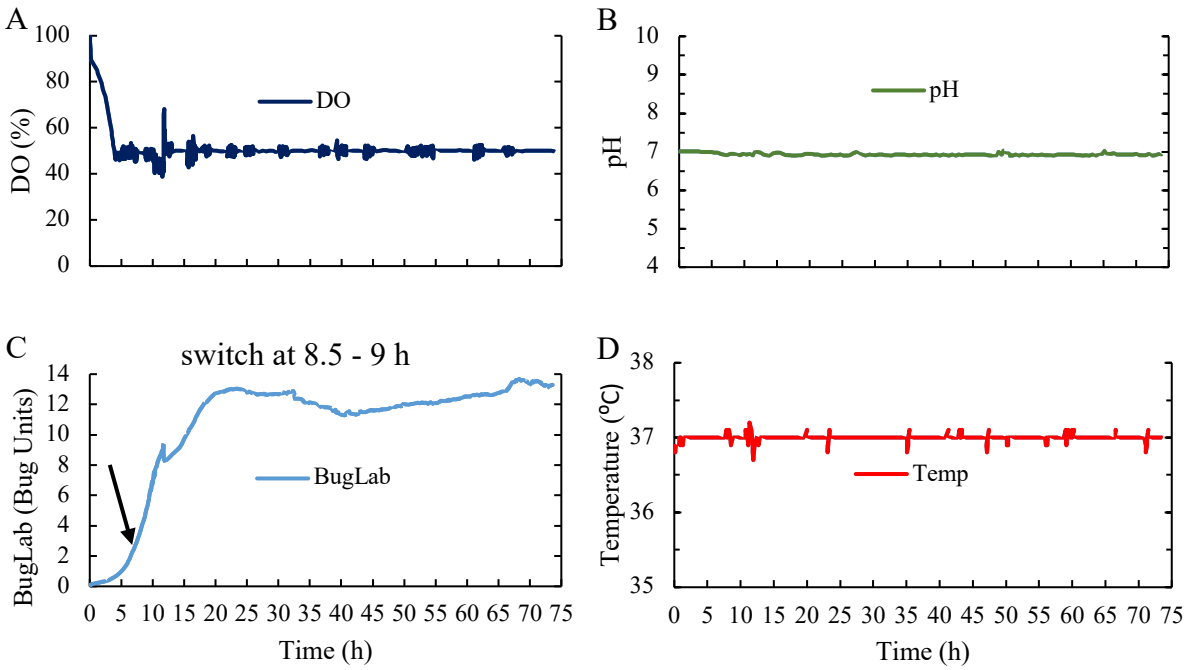

Figure 7.8. Changes in dissolved oxygen (A) and biomass (B) in an *E. coli* CLD1301 fermentation on glycerol minimal media in the absence of IPTG (the arrow indicates the switch). pH (B) and temperature (D) were kept constant.

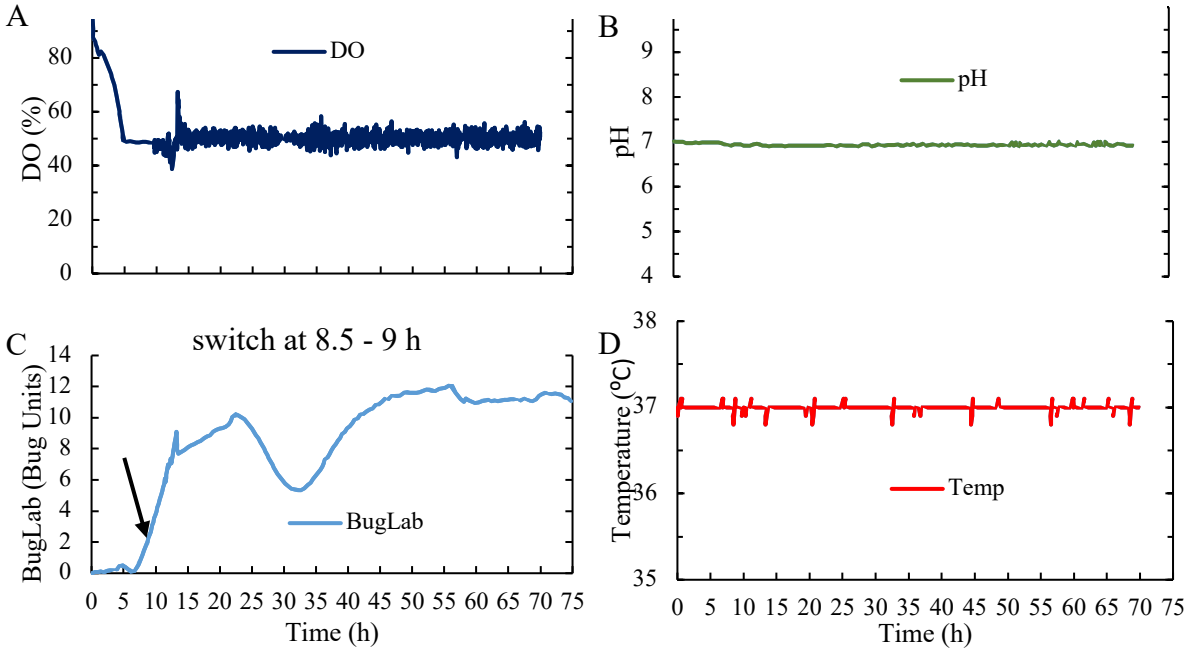

Figure 7.9. Changes in dissolved oxygen (A) and biomass (B) in an *E. coli* CLD1301 fermentation on glycerol minimal media in the presence of IPTG (the arrow indicates the switch). pH (B) and temperature (D) were kept constant.

Single *E. coli* CLD1301 cells were analysed growing in "balanced growth" at 0.39 h^{-1} (S_4) and 0.20 h^{-1} (SS1 - SS8). Where IPTG was used, the 1 mM optimal concentration was maintained in the reactor.

At single cell level, biomass was determined as the absolute cell concentration using Attune Nxt Acoustic Focusing Cytometer (Life Technologies, Carlsbad, CA, USA) – see Appendix B for instrument specifications. The Attune measures the cell numbers directly by controlling the flow of the sample through its interrogation point. The sample volume was 5 µl, thus the total cell count (TCC) was calculated by multiplying the number of events by 200 (correction for volume) and by the dilution factor (used to lower the OD_{600} of the sample to 0.025). The TCC for *E. coli* CLD1301 in the presence and absence of 1 mM IPTG are given in *Figure 7.10*.

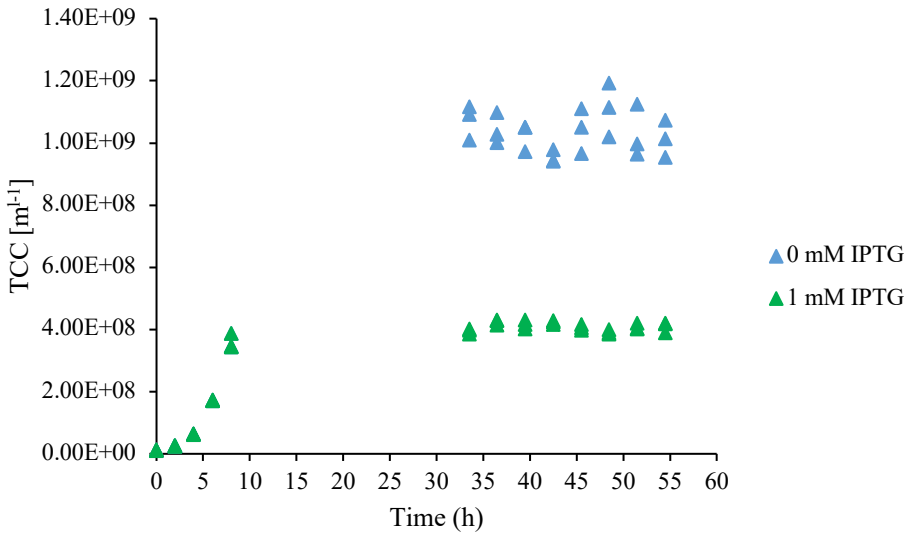

Figure 7.10. Total cell counts (TCCs) for *E. coli* CLD1301 on glycerol minimal media in the absence or presence of inducer (1mM IPTG). A minimum of 25 h was allowed to reach the steady state, as illustrated by the gap.

The mean TCC values across the steady state were 1.03 x 10^9 with no IPTG and 4.08 x 10^8 for induced *E. coli* CLD1301. The difference in cell numbers was significant (one-way ANOVA, $f = 1970.27$, $p < 0.0001$). This shows a drastic decrease in cell numbers by the addition of IPTG which induces protein expression.

The average TCC on glucose growth was 4.16 x 10^8 (*Figure 5.11*), which is similar to the 4.08 x 10^8 on glycerol (*Figure 7.10*). The decrease in cell number on both glucose and glycerol caused by induction occurs as a consequence of the imposed metabolic load. Instead of carrying out its own metabolic and division tasks, the cell is forced to utilise a huge part of its resources (in the form of ATP or aa) to express the foreign DNA as protein in the cell. The bigger the plasmid size and copy number, the bigger the metabolic load. Whilst the plasmid encoding the GFP –A gene is small, it is the high copy number of 500 - 700 that reduces the cell resources for both plasmid maintenance and expression into foreign RNA and protein. The efficient high yield production in HCD cultivations at large scale creates a high metabolic load, but this is not a problem since growth (and division) is separated by the production stage in fed-batch cultivations. A drop in the cell number could occur as a result of plasmid instability, where the plasmid is lost from the recombinant cell, although this is not common in high copy number plasmids. By losing the plasmid and the in-built resistance provided by kanamycin, the cell can no longer thrive in a media containing kanamycin and will die.

Whilst this shows some of the consequences of high expression at large industrial fed-batch scale, a transition to continuous bioprocessing could only occur if the metabolic burden is reduced to a level that no longer constrains cell's division. Despite the advantages of a high volumetric productivity, a successful continuous bioprocess can only happen if cells are able to divide continuously and exponentially in high numbers. The reduction in cell numbers in continuous cultivations may mean a 1 - 2 days fed-batch is preferable.

7.6.2 Measuring substrate

Residual glycerol was measured in the supernatant both in the absence (*Figure 7.11 A*) and presence (*Figure 7.11 B*) of 1 mM IPTG. The concentration of glycerol decreased in time during maximal growth at 0.39 h^{-1} from 4 to 2.08 g/L at the mid-exponential point of growth. The residual glycerol was at a relatively "steady state" in chemostat, ranging between 3.3 x 10^{-3} g/L (36.03 µM) to 5. 96 x 10^{-3} g/L (64. 78 µM) and from 9.95 x 10^{-3} g/L (108.10 µM) to 1.26 x 10^{-2} g/L (136.92 µM) in the absence and presence of IPTG, respectively. Residual glycerol was, however present in all sample supernatant within the measurement range of the glycerol assay kit (Megazyme International Ireland, Bray, Ireland).

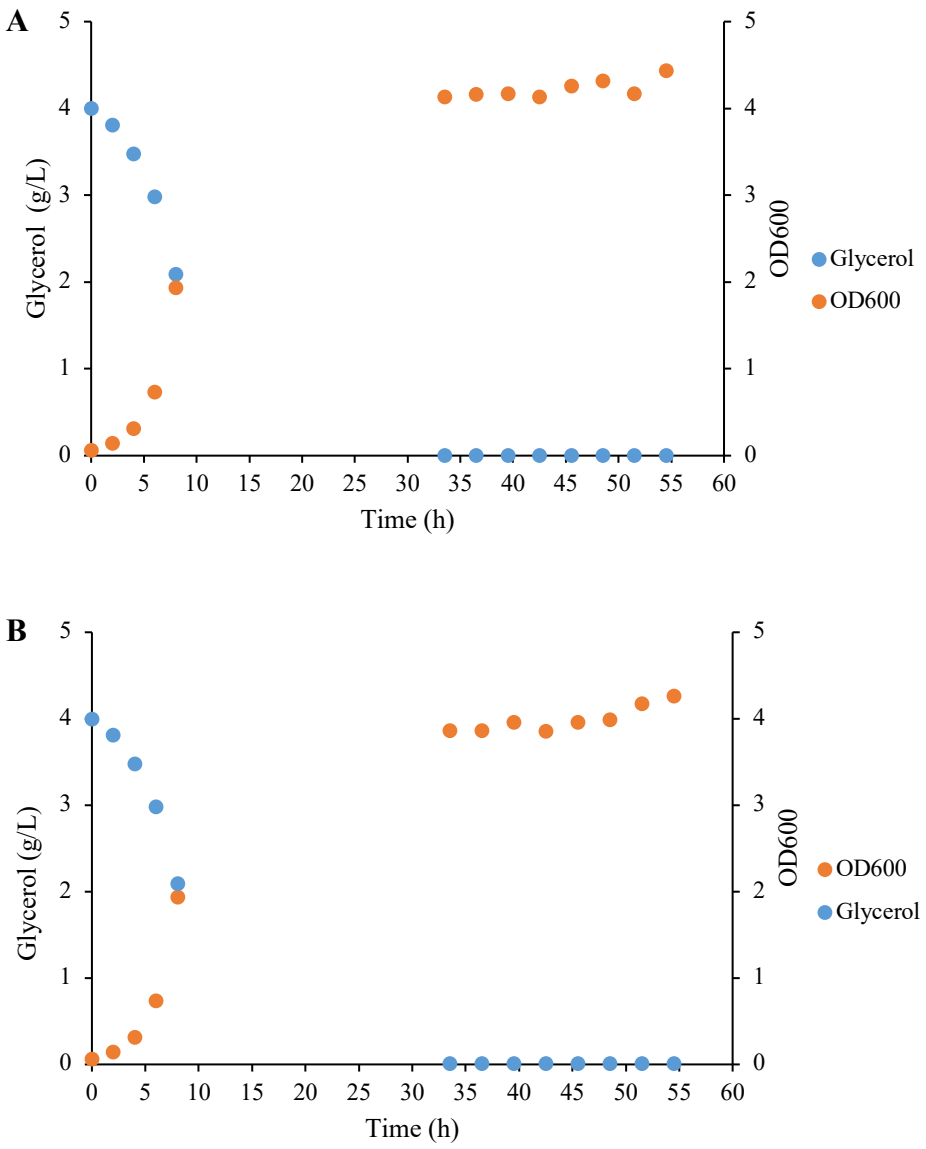

Figure 7.11. Glycerol consumption pattern and biomass production in strain *E. coli* CLD1301 in the absence (A) and presence (B) of 1mM IPTG.

7.6.3 Monitoring VFAs

Strain *E. coli* CLD1301 was found to produce no acetate when glycerol was used as a carbon source (*Figure 7.12*). Formic acid was the primary VFA, with the level of formate increasing during the batch phase up to 6.78 ppm (6.78 x 10^{-3} g/L) at 8 h post inoculation. Thus, at maximal growth rate on glycerol, two carbon sources were found in the media (glycerol and formate). At the maximum growth rate of 0.39 h^{-1}, there was no glycerol limitation and the concentration of formate did not inhibit growth.

Formic acid was also present within the chemostat, fluctuating from 7.65 to 10.49 ppm across the "steady state" at submaximal growth. These levels are lower than those detected during the growth of the host strain W3110 (*Figure 6.11*) and as no propionic or acetic acid were formed, this shows a better conversion of carbon. As more carbon is directed towards biomass instead of by-products, this shows glycerol is a beneficial substrate in *E. coli* fermentations.

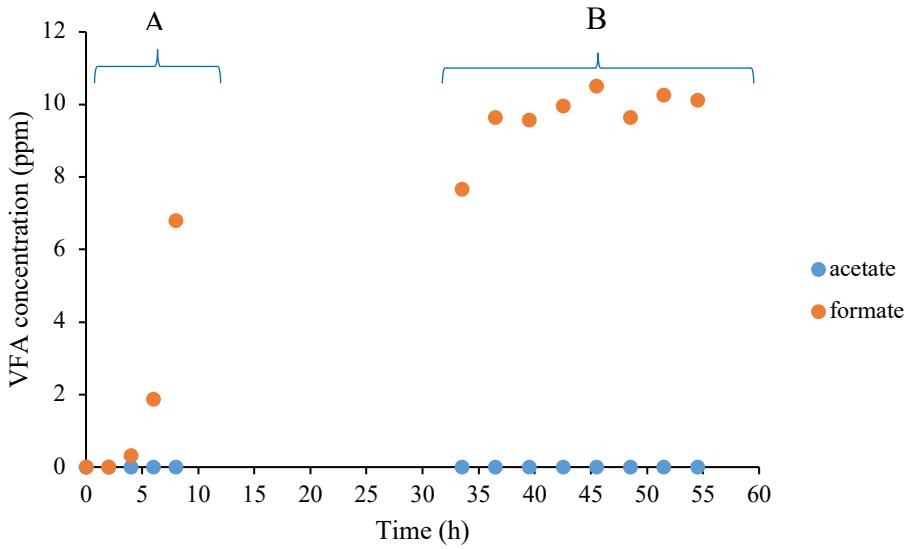

Figure 7.12. VFA concentration over the time course of *E. coli* CLD1301 fermentation using glycerol 4 g/L. A: Batch fermentation; B: Continuous fermentation. A minimum of 25 h were allowed to reach steady state.

7.7 Single cell studies of membrane integrity using FC

The metabolic burden caused by the plasmid disrupts the cell metabolism and may cause cell death. Cell death in a bioprocess is linked to a decrease in product yield. To assess whether the GFP mut3*expression affects the host viability, membrane integrity was evaluated in the absence and presence inducer, using FC. Non-induced cells were stained with TO and the membrane impermeable PI. Induced cells were stained with PI only, as described in *Section 3.5.4 Total cell counts*. Cells carrying the GFP-A-pD441- SR: 240460 were induced at mid-exponential point by the addition of 1 mM IPTG.

The proportion of live and dead cells was determined using FC for each time point at maximal and submaximal growth (*Figure 7.13*). During maximum growth at μ_{max}, without inducer, the

proportion of cells with green fluorescence and red fluorescence at 8 h post inoculation was 85.77% and 14.54%, respectively *(Figure 7.13 A* and *B*). There is no nutrient limitation during exponential growth, but there is the internal stress of plasmid maintenance. TO^+ cells did not reduce significantly when lowering the growth rate, presenting a mean of 84.77% on glycerol-limited growth. Conversely, PI^+ cells were 15.23% on glycerol-limited growth.

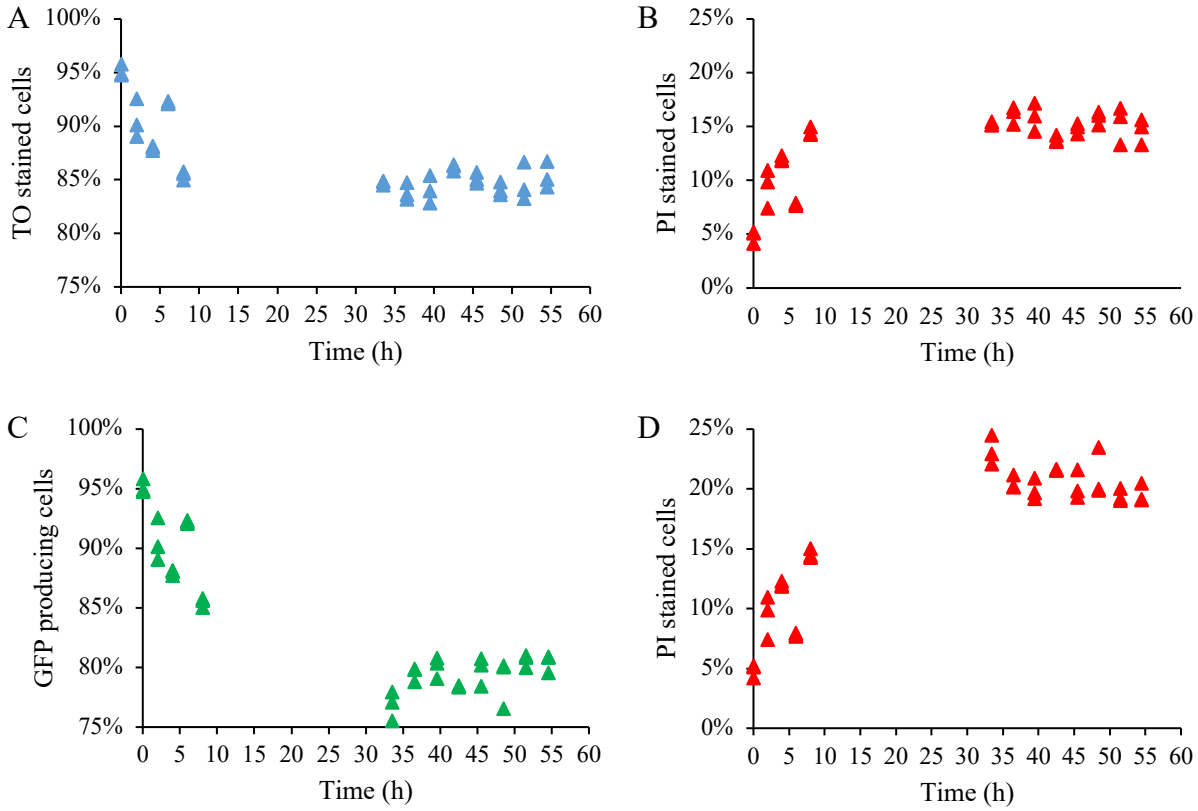

Figure 7.13. Percentages of live (TO^+ and GFP producing) cells and dead (PI^+) cells in three *E. coli* CLD1301 fermentations on glycerol. Blue triangles represent TO^+ cells, green triangles represent GFP-producing cells, red triangles are PI^+ cells. A, B) 0 mM IPTG. C, D) 1 mM IPTG.

In the presence of IPTG, GFP producing cells during submaximal growth on glycerol were 79.35% (*Figure 7.13 C* and *D*). This confirmed that the recombinant protein was being produced in glycerol-limited cultures. However, the reduction in viability from 84.77% to 79.35% caused by induction was significant (one-way ANOVA, $f = 6306.29$, $p < 0.001$). This could be the combined result of heterologous protein expression, carbon starved cells and the

increase in membrane permeability caused by the accumulation of formate in the media. Conversely, there was a significant increase in the PI^+ cells following induction, to a mean of 20.62% (one-way ANOVA, $f = 6306.29$, $p < 0.001$).

7.8 Single cell studies of membrane potential using FC

In industrial bioprocessing, bacteria require energy not only for recombinant protein synthesis, but also for own maintenance and metabolism. The energetic capacity of the cells was estimated from the changes in membrane potential, using the triple dye combination $DIBAC_{4(3)}$/EB/PI with FC. Four distinct subpopulations were visible:

a) active ($DIBAC_{4(3)}^-$, $EtBr^-$, PI^-);

b) depolarised ($DIBAC_{4(3)}^+$, $EtBr^+$, PI^-);

c) de-energised ($DIBAC_{4(3)}^-$, $EtBr^+$, PI^-);

d) dead ($DIBAC_{4(3)}^+$, $EtBr^-$, PI^+).

The percentage of each was measured in both nutrient excess and limitation to mimic the industrial conditions. All measurements were, however, made in the absence of inducer as its addition would induce the expression of GFP mut3*, whose green fluorescence overlaps that of $DIBAC_{4(3)}$. Freshly harvested cells from STR were prepared and stained as described in Section *3.8 Monitoring membrane potential with DIBAC/EB/PI*.

PI labels cells that have lost their membrane integrity and is a common indicator of cell death by virtue of being a large molecule excluded by intact cell membranes. At maximum growth rate on glycerol as sole carbon source and no IPTG, 20.49% ± 0.13 of cells were PI^+ (S4). During glycerol limited continuous cultivation, the PI^+ cells ranged from 14.20 ± 0.36 and 22.73% ± 1.91 of the total population at SS5 and SS1 respectively (*Figure 7.14*).

Only a small number of cells were de-energised, which was not influenced by carbon limitation. The active subpopulation, ($DIBAC_{4(3)}^-$, $EtBr^-$, PI^-)-stained decreased in line with the growth rate. The active subpopulation accounted for 31.32% ± 2.55 at maximal growth rate (S4). Lowering the growth rate reduced the active subpopulation to 9.01% ± 0.43 and 30.99% ± 7.2 at SS1 and SS2, respectively.

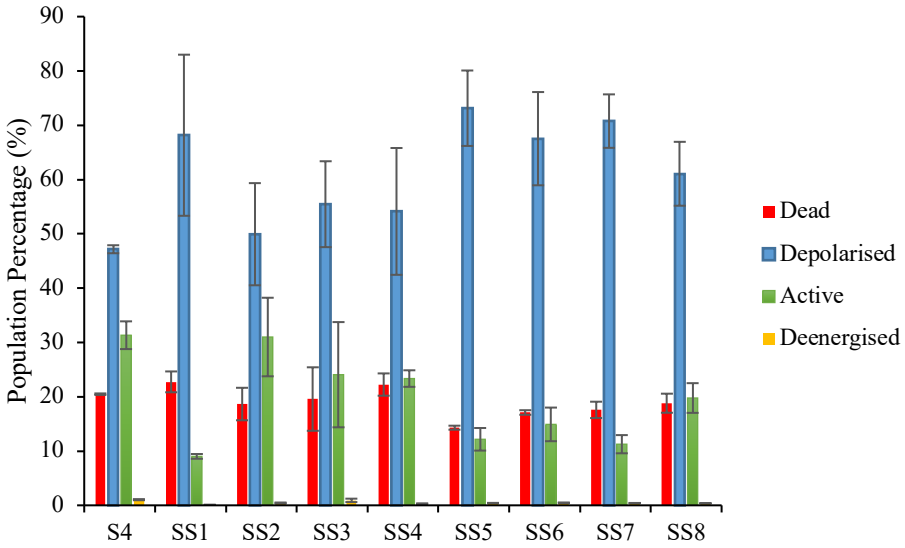

Figure 7.14. Flow cytometry analysis of *E. coli* CLD1301 cells at different growth rates on glycerol as sole carbon source, with no added inducer (0 mM IPTG). S4 is the mid-exponential sample (8 h post-inoculation) representing unrestricted balanced growth. SS1 - SS8 are steady state samples at sub-maximal growth rate ($\mu_{max}/2$). Data presented as mean ± S.E. Four subpopulations exist: active, depolarised, dead and deenergised.

The share of depolarised cells increased from 47.16% ± 0.73 at maximal growth rate (S4) to 49.93% ± 9.40 and 73.13% ± 6.94 at SS2 and SS5, respectively. This shows that reducing the growth rate and thereby applying a carbon limitation increases cell depolarisation, while reducing the number of active cells. As membrane potential is an indicator of cell energy, it shows a decline in cell functionality in an increasing number of cells.

To test for the plasmid burden on cells grown on glycerol as sole C source, the number of depolarised cells and active subpopulations were compared with both recombinant and host strains during unrestricted growth on glycerol (S4). As there is no carbon limitation or induction during the exponential phase, the difference represents the effect of plasmid maintenance on the cell. The overall mean of depolarised *E. coli* CLD1301 cells was 3109.7, almost three times that of 1102, exhibited by the host W3110 strain. The difference between the number of depolarised cells (in a 30 µl sample diluted to $OD_{600} = 0.025$) was deemed significant (one-way ANOVA, $f = 159.34$, $p < 0.001$). This shows that 94.49% of the difference in the depolarised cells is explained by the plasmid burden, which increases cell depolarisation three-fold during maximal growth rate on glycerol, simply due to the energy requirements for plasmid maintenance.

The means of active cell subpopulations during maximal growth on glycerol were 3397 for host W3110 and 2066 for recombinant CLD1301. The difference, in the absence of both induction or nutrient limitation is due to the energy requirements for plasmid maintenance when the substrate is glycerol. A significant difference was present between the active cell subpopulations in host and recombinant strains (one-way ANOVA, $f = 22.11$, $p < 0.01$). Only 65.53% of the difference in the number of active cells is can be explained by the different conditions, which is the maintenance of a recombinant plasmid. While the metabolic load caused by plasmid maintenance reduces cell functionality, only a small percentage can be explained, so other parameters must interact to reduce the "active" cells.

7.9 Studies of cell morphology using fluorescence microscopy

Cell morphology (shape) is biologically important and there are many advantages of staying small. A higher surface to volume ratio provides a higher rate of nutrient diffusion, so shape is important for growth and nutrient uptake. Shape is also important for proliferation, with cells accelerating or postponing division in response to their environment, resulting in small or larger cells respectively.

To quantify shape maintenance, three parameters were investigated under glycerol excess and limitation, challenged with plasmid maintenance (for non-induced cells) and protein expression (for induced cells):

a) area (μm^2);

b) circularity;

c) aspect ratio (AR).

The analysis was automated by running the ImageJ Macro in Appendix F. Recombinant *E. coli* CLD1301 cells were prepared for microscopy as previously described (*3.10 Phase and fluorescence microscopy of E. coli W3310*) on a 1.2% agarose pad. Florescence microscopy was performed with the $SYTO_9$/PI staining for the non-induced and PI for the induced cells.

7.9.1 Cell morphology at maximum growth rate

A large proportion of cells were removed from the image of *E. coli* CLD1301 through automatic filtering by area and aspect ratio. The area (as a measure of cell spreading), cell circularity (as a measure of irregularities or blebbings in the membrane) and AR (as a measure

of elongation) were quantified for 137 *E. coli* CLD1301 cells growing at maximum growth rate with non-limiting glycerol (*Figure 7.15, Table 7.1*).

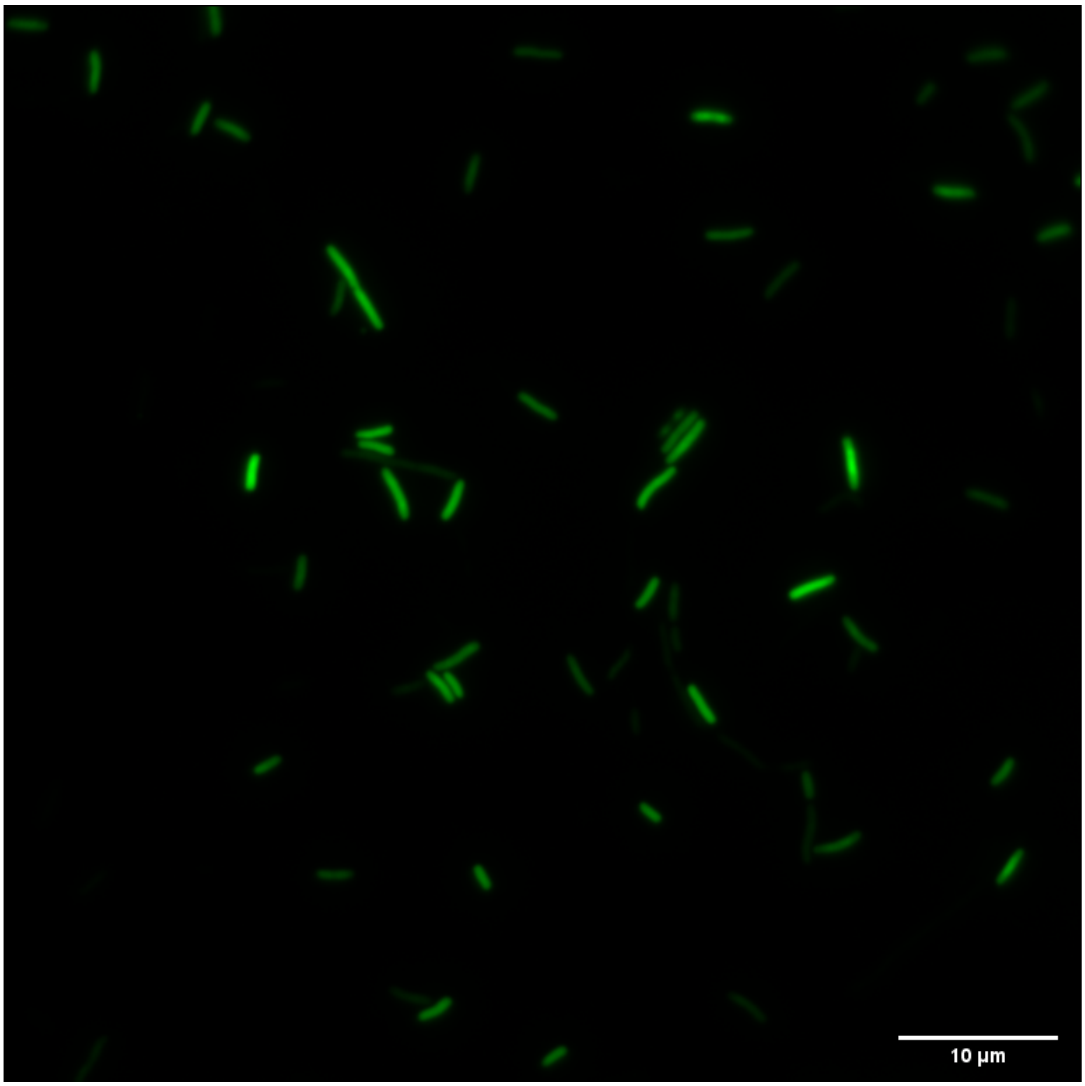

Figure 7.15. Fluorescence image of non-induced *E. coli* CLD1301 on glycerol as the sole carbon source. Mid-exponential growth sample stained with $SYTO_9$ shows "live" cells.

The cells exhibited the following:

	Mean	Median	S.D.	CV	*Figure*
Cell area (μm^2)	1.60 ± 0.06	1.39	0.82	51.07	*7.16 A*
AR	3.35 ± 0.08	3.32	0.95	28.35	*7.16 B*
Circularity	0.55	0.56	0.10	18.37	*7.16 C*

Table 7.1. Shape descriptors of *E. coli* CLD1301 at maximum growth rate on glycerol.

Conversely, at maximal growth rate with un-limited glucose, the cells presented a mean area of 2.03, with a median of 1.78 μm^2, a S.D. of 1.08 and a CV of 53.29 (*Figure 5.16 A*). Whilst the change in substrate hardly seems to influence the cell size variance, larger cells were evident on glucose. This is most probably the result of a higher growth rate on its preferred C source.

7.9.2 Cell morphology in the absence of IPTG

Figure 7.16 shows the *E. coli* CLD1301 cell image challenged with both plasmid maintenance and C source limitation. It should be noted that cells begin to show morphological changes when lowering the growth rate (*Figure 7.16*, compared to *Figure 7.15*). The red arrow (*Figure 7.16*) points to a filamentous cell. Under the double effect of carbon limitation and plasmid maintenance, the cells begin to initiate filamentous growth and thus no division occurs.

a) Cell area

Whilst cells growing at maximum growth rate showed a mean cell area of 1.60 ± 0.06 μm^2 (*Figure 7.17 A*), in glycerol-limited chemostats, this fluctuated from 1.45 to 1.70 at SS3 and SS2, respectively (*Figure 7.17 D*). The median exponential 1.39 μm^2 is included in the chemostat range of 1.2 and 1.54 at SS4 and SS8, respectively. A significant difference was present between area distributions in glycerol-limited growth (Kruskal Wallis, $H = 16.42$, $p < 0.05$), which shows that the cells do not maintain size in chemostat.

b) Aspect ratio

The mean AR at μ_{max} when glycerol is non-limiting was 3.35 (*Figure 7.17 B*), and this increased during glycerol limited growth to values ranging from 3.72 at SS7 and 4.19 at SS1 (*Figure 7.17 E*). The median AR followed the same trend with the exponential value of 3.32 (*Figure 7.17 B*)

smaller than the chemostat range from 3.73 at SS7 and 4.40 at SS1 (*Figure 7.17 E*). This shows that there is an increase in AR during nutrient downshift in the non-induced *E. coli* CLD1301 cells with more elongated cell phenotypes.

There is no conclusive change in the distribution of the data, as the exponential CV of 28.35 is in the chemostat range of 22.58 to 31.83 at SS2 and SS7, respectively. There was, however, a significant difference between AR distributions at steady state (Kruskal-Wallis, $H = 118.64$, $p < 0.001$), showing that the aspect ratios are not maintained. This may be a natural response to nutrient limitation in cells relying on diffusion, in which the cells increase their surface area (and nutrient contact area) without an increase in the surface to volume ratio.

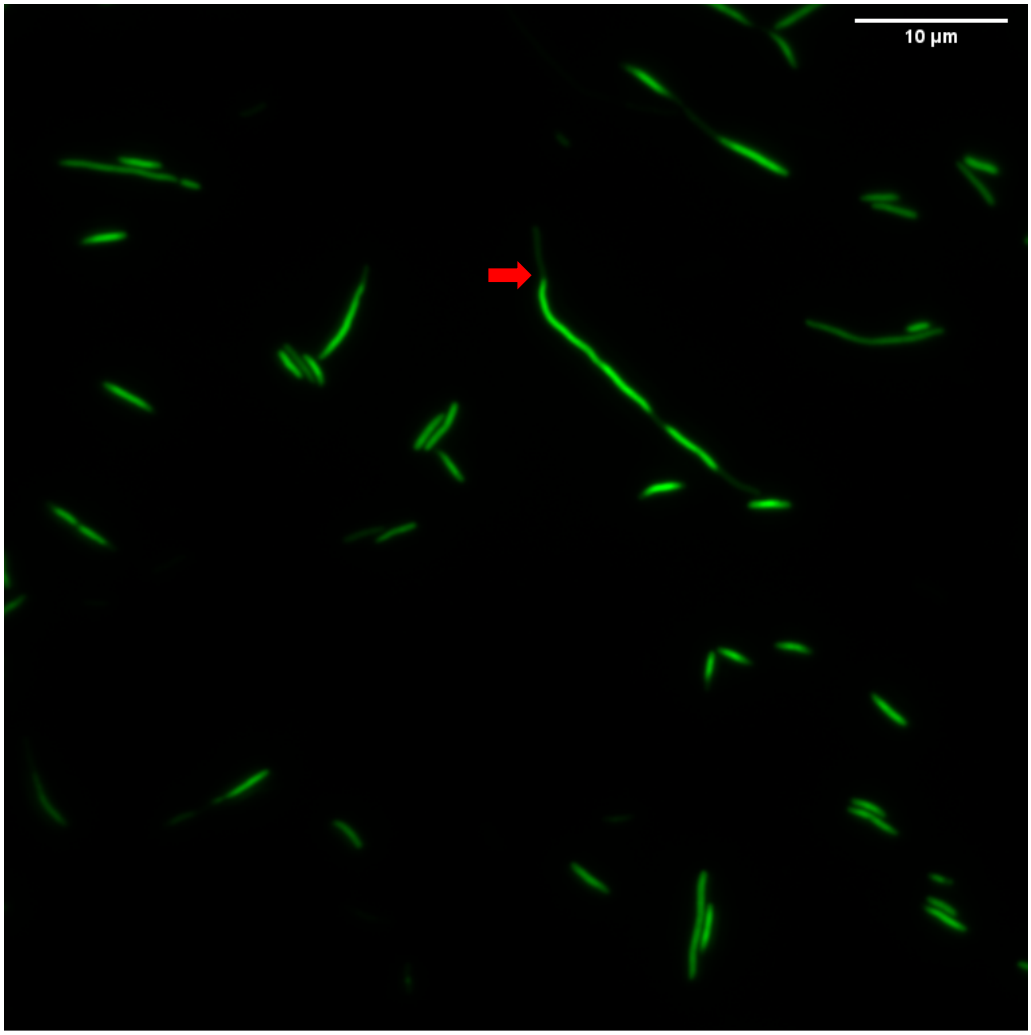

Figure 7.16. Fluorescence image of non-induced *E. coli* CLD1301 on glycerol-limited growth. Steady state sample 2 (SS2) stained with $SYTO_9$. Arrow indicates "live" cell beginning filamentous growth.

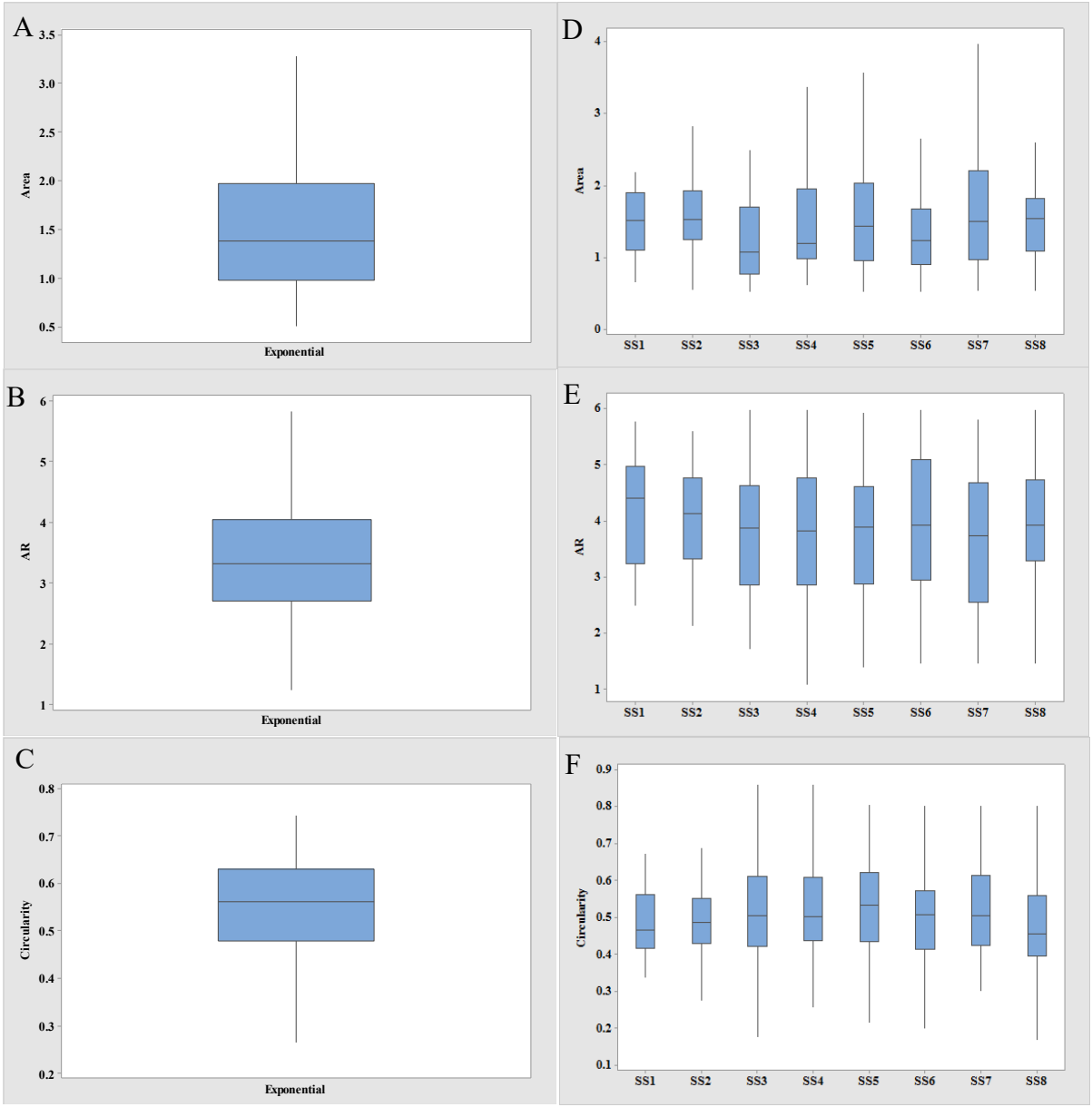

Figure 7.17. Box plots of morphological descriptors of non-induced *E coli* CLD1301 cells at maximum (A, B, C) and submaximal growth rates (D, E, F). Horizontal line within the box shows the median, boundaries of the box plot indicate the 25th and 75th percentile of the distribution, whiskers mark the 5th and 95th percentile of the distribution. Values outside of the 1.5-fold IQR were removed.

The cells in nutrient limitation (*Figures 7.16* and *7.17 E*) are generally longer than the shorter rods observed at maximal growth rate (*Figure 7.15* and *7.17 B*). Consistent with this, filamentous growth occurred in the recombinant CLD1301 under nutrient-limited growth (*Figure 7.16*). This morphology was absent when glycerol was non-limiting (*Figure 7.15*) and was also absent from the host strain W3110 whether glycerol was limiting or not. This suggests filamentous growth is a characteristic of plasmid-based systems under nutrient downshift.

The coupling of cell elongation with the accumulation of division proteins is critical for the maintenance of AR. As cells do not maintain the AR across nutrient downshift, but overall elongate under nutrient limitation, this suggests that the nutrient downshift hampers cells division. This is also indicated by the continuous cytoplasm contour of the filamentous cell, suggesting the inhibition of septation prevents block cell division (red arrow – *Figure 7.16*).

c) Circularity

The maximum cell circularity was identified during maximum growth rate with a mean and a median of 0.56 (*Figure 7.17 C*). Both were lower during nutrient downshift in chemostat. The mean circularity was 0.47 to 0.53, the median being 0.45 to 0.53 at SS8 and SS5, respectively (*Figure 7.17 F*). A reduction in circularity (or form factor) suggests either the cells are elongating and/or they suffer morphological deformities with membrane irregularities, such as twisting, invaginating, a.s.o (see *Figure 2.11*). Changing the growth rate had no effect on data distribution as the exponential CV of 18.37 was within the "steady state" CV of 17.16 to 29.35, at SS2 and SS8 respectively. Moreover, the changes in cell circularity at limited glycerol (SS1 - SS8) were not significant (Kruskal-Wallis, $H = 11.56$, $p > 0.05$).

7.9.3 Cell morphology in the presence of IPTG

Significant area, circularity and aspect ratio changes were observed in the producing *E. coli* CLD1301 cells in *Figure 7.18*. Fluorescence microscopy of induced *E. coli* CLD 1301 detected elongated cells with stable filaments as the dominant cell phenotype at steady state (*Figure 7.18*). These drastic morphological changes, where most of the cells are more than 10 μm occur as a result of significant stress introduced by recombinant protein production. Division in filamentous cells is halted when the cells adopt a productive phenotype and there are not sufficient resources for division.

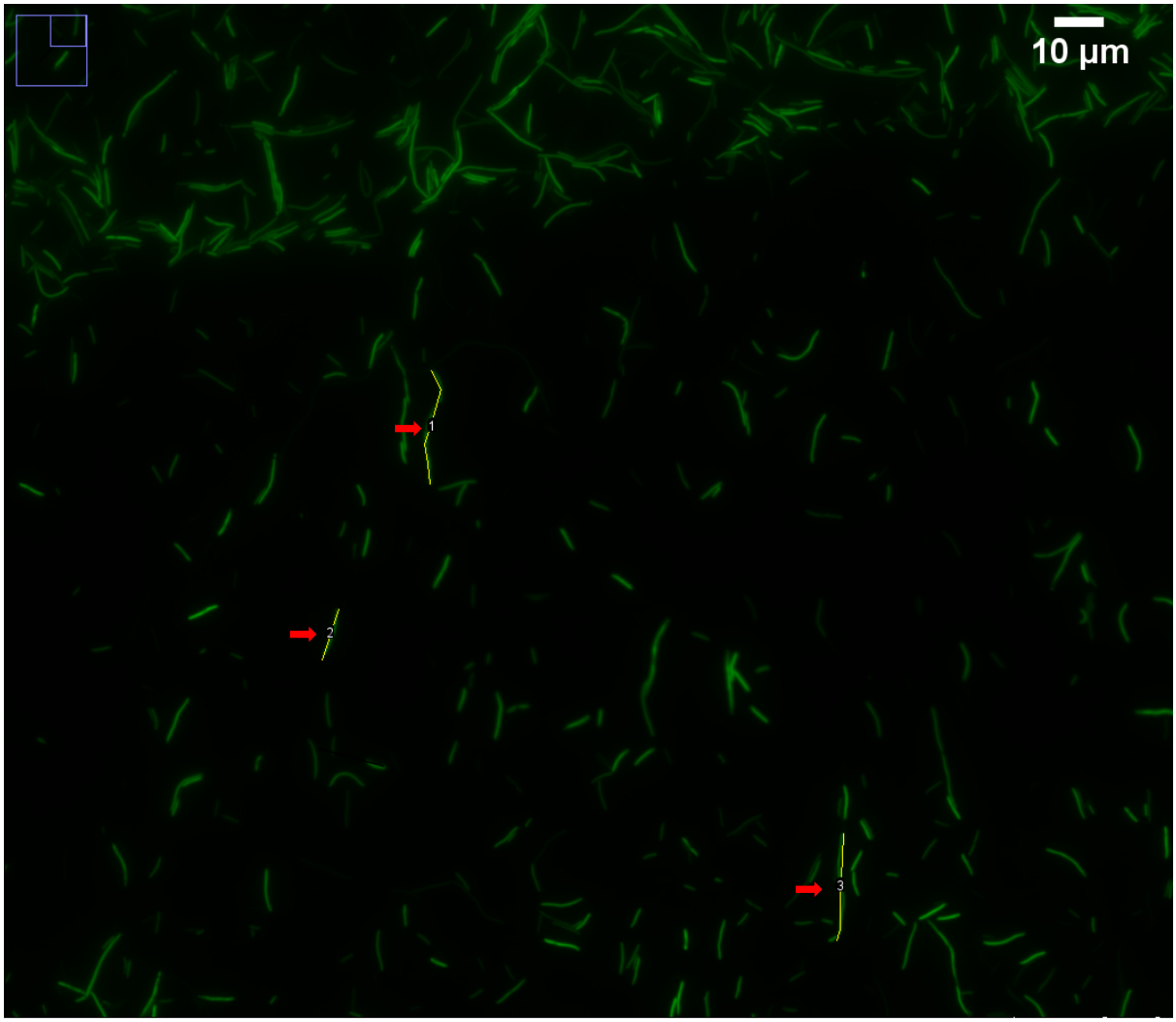

Figure 7.18. Fluorescence microscopy image of GFP mut3*-expressing *E. coli* CLD1301 cells. Steady state sample 7 (SS7) on glycerol-limited growth shows mostly filamentous cells. Indicated by red arrows, cell 1 is 23.38 µm, cell 2 is 10.48 µm and cell 3 is 21.40 µm.

a) Cell area in the presence of IPTG

The plasmid-based system without induction or glycerol limitation exhibits a mean and a median cell area of 1.60 ± 0.06 and 1.39 µm^2 (*Figure 7.17 A*). In the absence of induction, but under glycerol limitation, the mean fluctuated from 1.45 to 1.70 µm^2 and the median from 1.2 to 1.54 µm^2 (*Figure 7.17 D*).

While there was no conclusive correlation, when IPTG was added and the GFP mut3* was produced, an increase in cell area (measuring cell spreading) was observed (*Figure 7.19 A*).

The mean area of GFP-producing cells during glycerol downshift ranged from 1.64 to 2.37 μm^2 at SS2 and SS5, respectively (*Figure 7.19 A*). The median ranged from 1.20 to 2.40 μm^2 at SS1 and SS5 (*Figure 7.19 A*), a range which includes the exponential median of 1.39 μm^2 (*Figure 7.17 A*). A large S.D. ranging from 0.97 to 1.24 at SS3 and SS1/SS8 was observed in cells facing nutrient downshift. These show that cells facing glycerol limitation at high rates of recombinant protein expression led to an increase in cell area and data spreading. The differences in cell area at submaximal growth on glycerol for expressing cells were deemed significant (Kruskal-Wallis, $H = 433.03$, $p < 0.001$). This means that the cells were unable to maintain their size in chemostats when faced with an added carbon-limitation on the top of metabolic burden caused by recombinant expression.

b) Aspect ratio in the presence of IPTG

The mean AR in the presence of plentiful glycerol and without induction was 3.35 ± 0.08, median of 3.32 (S.D. 0.95, CV 28.35) (*Figure 7.17 B*). When the growth rate was lowered by glycerol-limitation without induction, the mean AR increased to a range from 3.72 to SS7 and 4.19 at SS1 (*Figure 7.17 E*). When the growth rate was lowered and the cells were induced to produce the recombinant protein, the mean AR ranged from 3.24 at SS1 to 4.47 at SS7 (*Figure 7.19 B*).

Under glycerol limitation, the median AR fluctuated from 3.73 to 4.40 in the absence of inducer (*Figure 7.17 E*), and from 3.06 to 4.80 in its presence (*Figure 7.19 B*). The lowest S.D. of 0.95 occurred during unlimited glycerol growth in non-producing cells (*Figure 7.17 B*). Changing to glycerol limitation in non-producing cells increased the AR substantially, but not the spread of the data. The further addition of IPTG, with subsequent protein formation in glycerol-limited cultures showed a large variance, with S.D. ranging from 1.06 to 1.33 at SS1 and SS6, respectively (*Figure 7.19 B*).

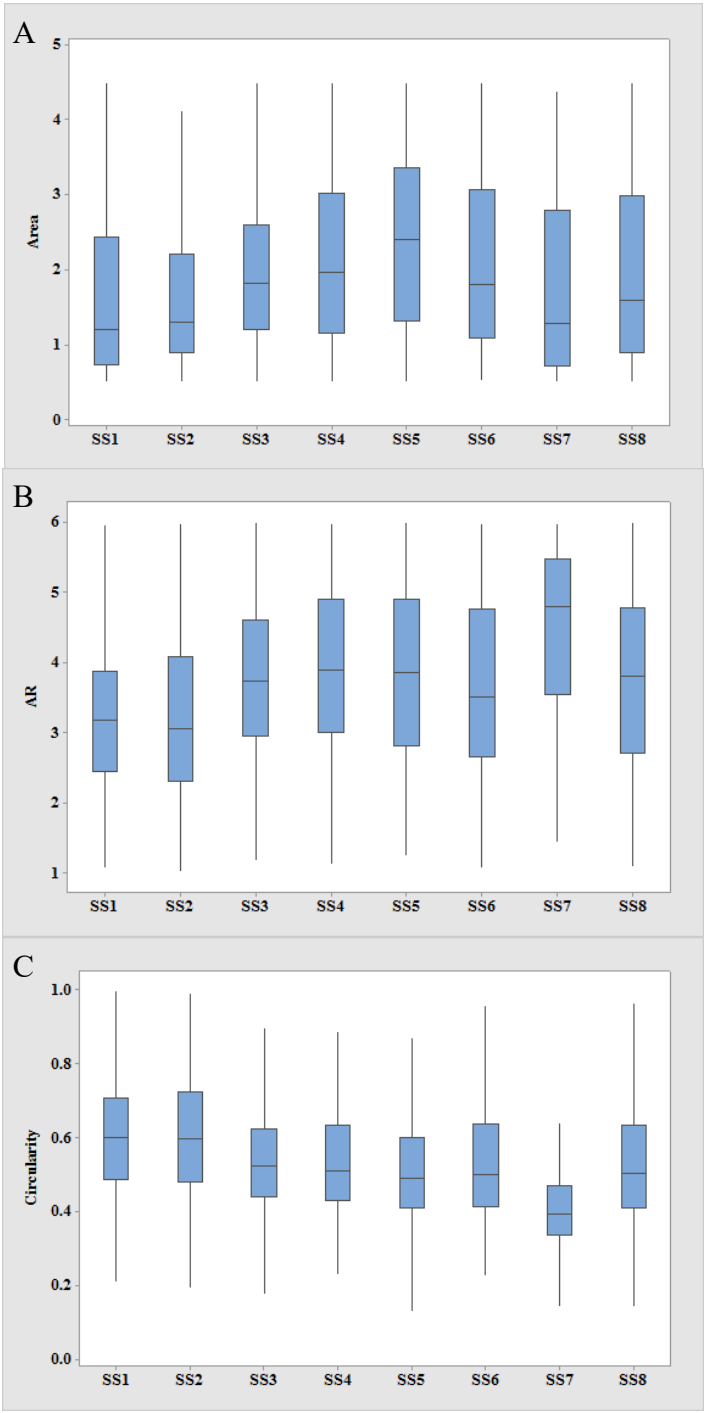

Figure 7.19. Box plots of morphological descriptors of productive *E coli* CLD1301 cells at submaximal growth rates on glycerol. Horizontal line within the box marks the median, boundaries of the box plot indicate the 25th and 75th percentile of the distribution, whiskers mark the 5th and 95th percentile of the distribution.

The aspect ratio of GFP-producing cells changed significantly across the steady state (Kruskal-Wallis, $H = 122.00$, $p < 0.001$).

c) Circularity in the presence of IPTG

With unlimited glycerol in the absence of induction, the mean circularity was 0.56, with a median of 0.56 (*Figure 7.17 C*). Changing to glycerol-limited cultures in the absence of induction led to a decrease in circularity, both as mean (ranging from 0.47 to 0.53) and median (ranging from 0.45 to 0.53) (*Figure 7.17 F*). The addition of 1 mM IPTG in glycerol limited cultures led to significant circularity changes, mostly in terms of data spread.

With glycerol-limited GFP-producing cells, the mean circularity ranged from 0.40 to 0.61 at SS7 and SS1, respectively (*Figure 7.19 C*). The median ranged from 0.39 to 0.60 at SS7 and SS1 respectively (*Figure 7.19 C*). Whilst the exponential sample is more homogenous for cell circularity, illustrated by a lower S.D. (0.10) and CV (18.37), no conclusive change for data spread could be identified under glycerol-limitation, in the absence of induction (*Figure 7.17 C*). Adding the inducer, a more heterogeneous population was observed, in terms of both S.D. and CV (*Figure 7.19 C*). Moreover, the circularity changed significantly during the steady state (Kruskal-Wallis, $H = 172.08$, $p < 0.001$).

Taken together, continuous glycerol-limited cultivations with *E. coli* CLD1301 showed significant cell shape and size changes in all three parameters, in addition to filamentous growth, as the dominant productive phenotype in cells expressing GFP mut3*.

The influence of recombinant protein production on the cell shape was studied by comparing the three morphological descriptors in the absence (SS2) and presence of IPTG (SS2 + IPTG), both under glycerol-limitation (*Figure 7.20*). The mean cell area in the non-induced cells (SS2) was 1.70 and in the induced cells (SS2 + IPTG), 1.64 (*Figure 7.20 A*). The differences in cell areas caused by recombinant protein production were not significant (Mann - Whitney U, $W = 44784.0$, $p > 0.05$). The mean circularity was lower in the non-induced cells (0.48) than in the induced cells (0.61), suggesting increased membrane irregularities induced by recombinant protein expression (*Figure 7.20 C*). The increase in circularity caused by the overproduction of the recombinant product was significant (Mann - Whitney U, $W = 7059.5$, $p < 0.0001$).

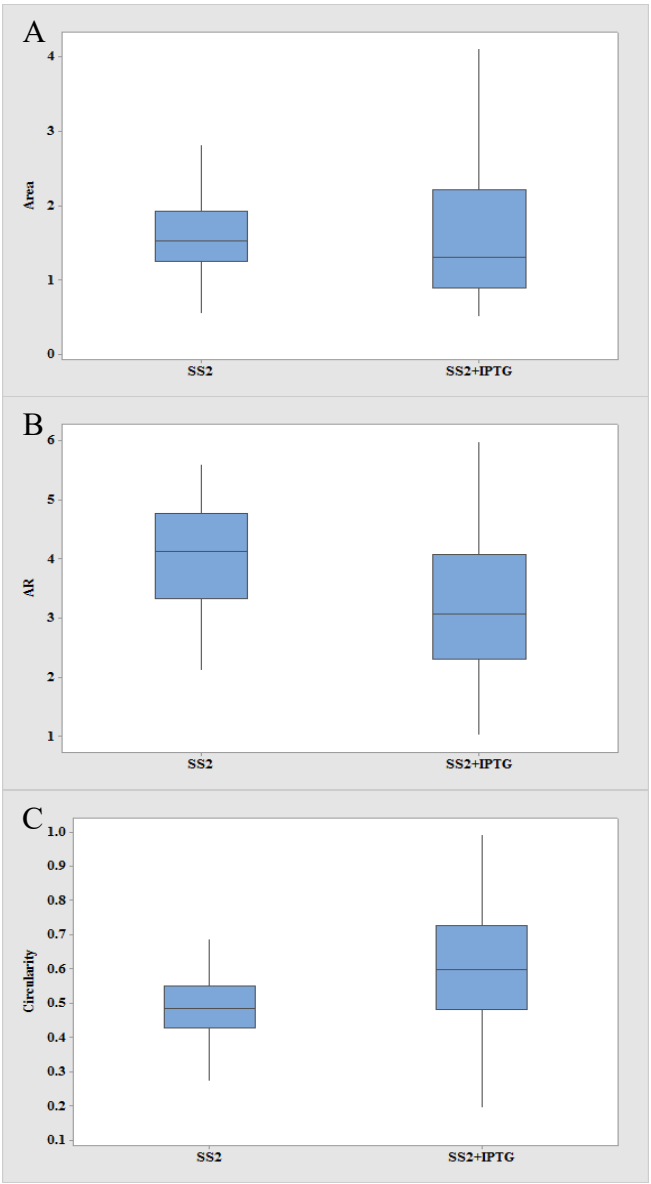

Figure 7.20. Shape descriptors for non-induced (SS2) and induced (SS2 + IPTG) *E. coli* CLD1301 growing under glycerol-limitation. 66 cells were imaged for SS2 and 272 cells for SS2 + IPTG.

Mean cell AR was 3.06 in the producing line and 4.13 in the non-induced cells *(Figure 7.20 B)*. The changes in AR caused by the recombinant product expression were deemed significant (Mann-Whitney U, W = 15033.0, $p < 0.0001$). These changes represent a population whose AR varies from 1 - 6, in line with the applied single cell filters. Thus, although it would seem that the GFP-producing cells are shorter (mean AR 3.06) than their

non-producing counterparts (mean AR 4.13), filamentous growth is probably the dominant cell phenotype (*Figure 7.18*). Given that most filaments have an AR bigger than 10, the only conclusion that can be drawn is that the protein production increases the heterogeneity in cell AR, from smaller cells (with a mean AR of 3.06) that are still able to ensure progeny, to larger filaments (with a minimum AR of 10) that do not, but only consume nutrients.

7.10 Single cell studies of protein production

The heterogeneity in protein production was monitored at single cell level, using fluorescence microscopy (FM) and flow cytometry (FC) and the enhanced GFP mut3* as a reporter for protein expression. *E. coli* CLD1301, described in section *3.1. E. coli strains* contains a pD441- SR: 24046 plasmid expressing the enhanced S2R/S65G/S72A variant of GFP, under the control of a T5 promoter with a kanamycin selection marker.

STR fermentations were carried out using the media described in Section *3.3.2* in a continuous cultivation using glycerol as the sole carbon source. The measurements of fluorescence from IPTG-induced cultures were compared with background fluorescence, resulting from cell auto-fluorescence and leakiness (recombinant protein expression in the absence of inducer).

7.*10.1 Protein production evaluated through flow cytometry*

The heterogeneity in protein production was measured as the CV of the GFP fluorescence as Mean Fluorescence Intensity (MFI) detected in the BL1 channel. The threshold to discriminate between fluorescent and non-fluorescent events was set at an intensity of 10000 A.U. Values above this threshold were considered positive for protein expression, whether it was leakiness or IPTG-induced.

Samples from STR were diluted in DBS buffer to a final OD_{600} ~ 0.25 and analysed immediately using the Attune Nxt Acoustic Focusing Cytometer (Life Technologies, Carlsbad, CA, USA). A "GFP gate" (R4) was set that separated cells with green fluorescence above the threshold. All samples were analysed for fluorescence intensity, total cell counts and % CV in the GFP gate (R4 cell population) (*Figures 7.21* and *7.22).*

Figure 7.21 is the sample at mid-exponential point of growth (S4), which was left unstained and un-induced to test for leakiness.

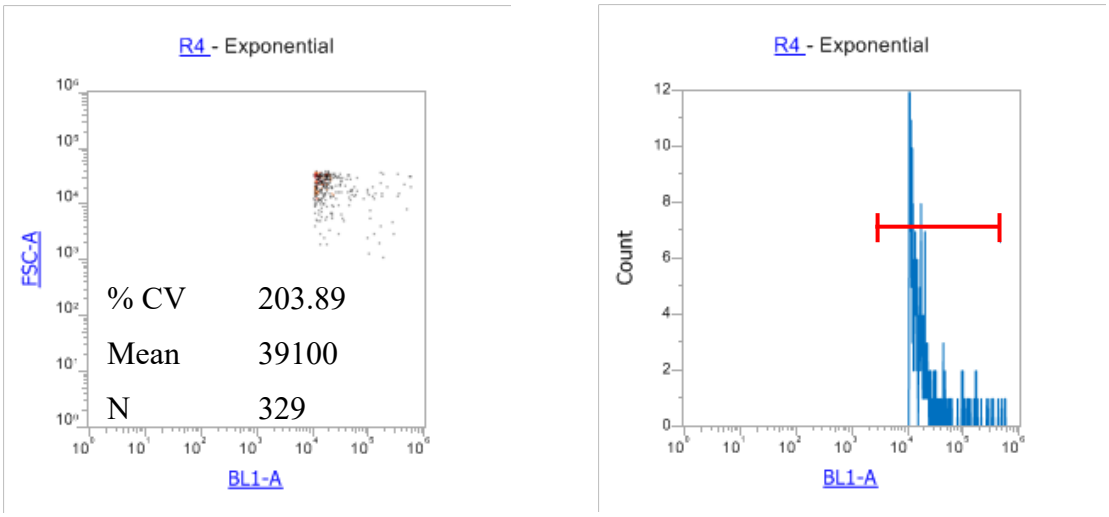

Figure 7.21. Flow cytometry of unstained un-induced exponential sample S4. R4 is the population assigned to the GFP$^+$gate. A) density dotplot of R4 population (n=329 cells) of forward scatter (FSC) versus green fluorescent BL1 channel (530/30 nm) B) florescence intensity (BL1 channel) histogram of mid-exponential phase *E. coli* CLD1301 cells within the GFP$^+$ gate.

A lower MFI (mean 39100) and higher heterogeneity (203.89) compared to induced cells (*Figure 7.22*) shows the exponential sample, left uninduced and unstained exhibits a range of fluorescence intensities from low autofluorescence in a high number of cells to high levels of leakiness in a few cells.

Protein production was induced past the exponential phase of growth and 25 hours were allowed to reach steady state. Protein production was measured as GFP mut3* fluorescence in the GFP$^+$ gate. (*Figure 7.22*).

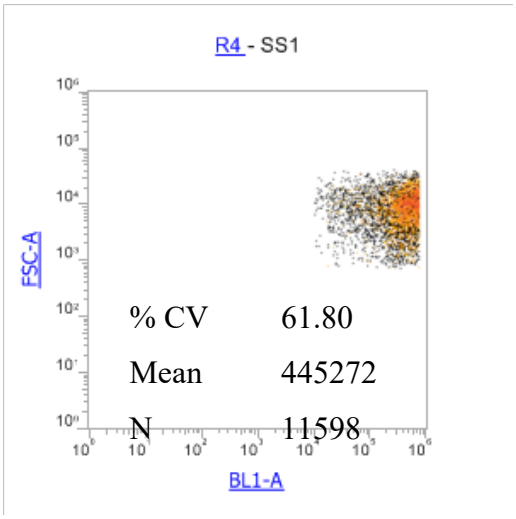
R4 - SS1
FSC-A
BL1-A
% CV 61.80
Mean 445272
N 11598

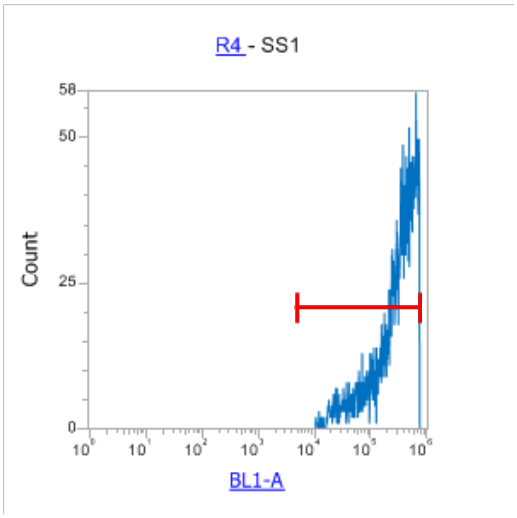
R4 - SS1
Count
BL1-A

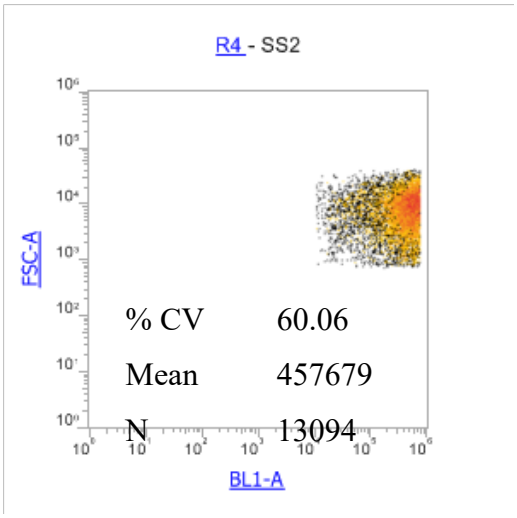
R4 - SS2
FSC-A
BL1-A
% CV 60.06
Mean 457679
N 13094

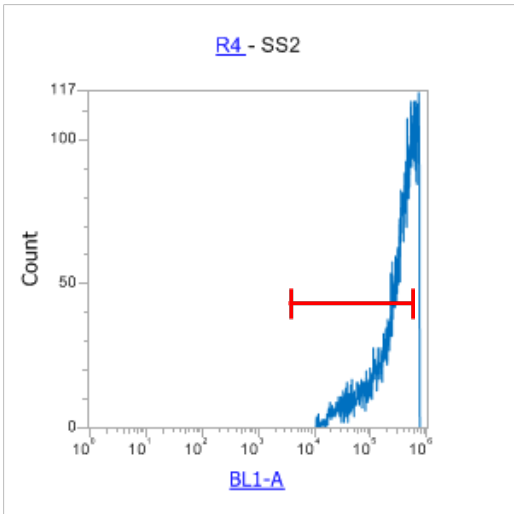
R4 - SS2
Count
BL1-A

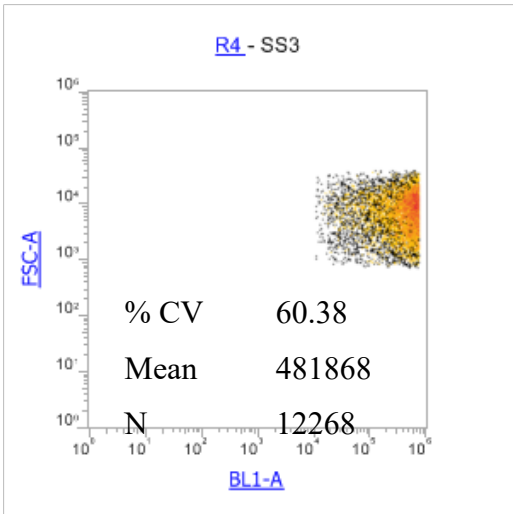
R4 - SS3
FSC-A
BL1-A
% CV 60.38
Mean 481868
N 12268

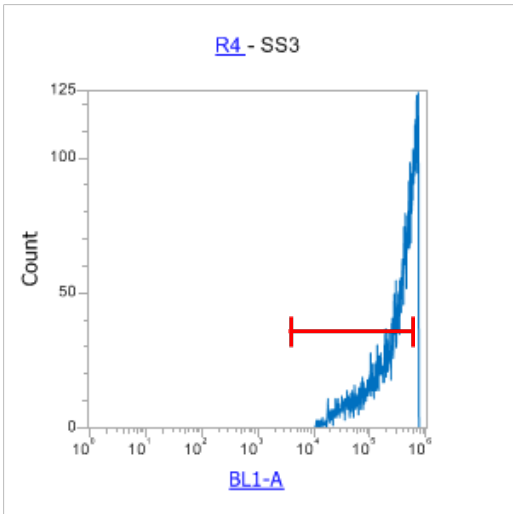
R4 - SS3
Count
BL1-A

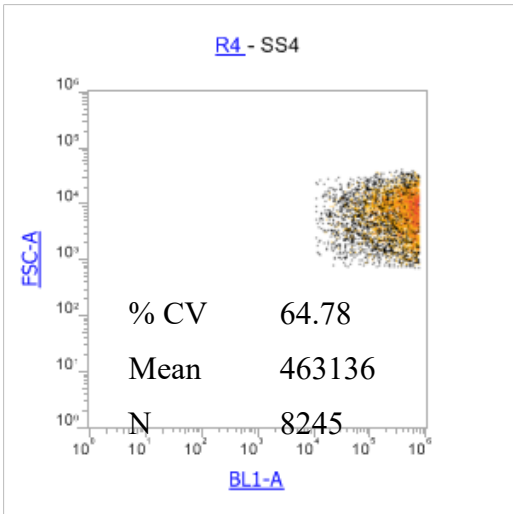
R4 - SS4
FSC-A
BL1-A
% CV 64.78
Mean 463136
N 8245

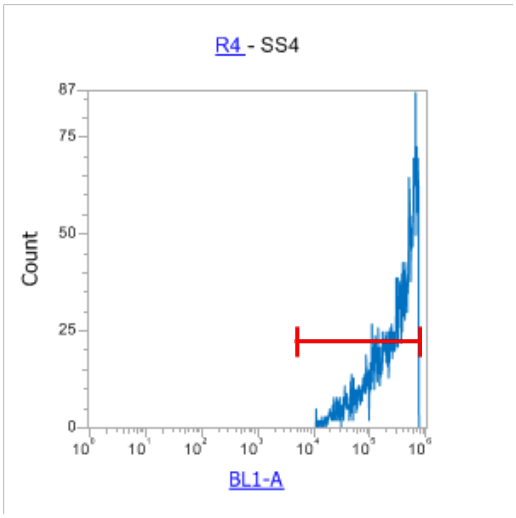
R4 - SS4
Count
BL1-A

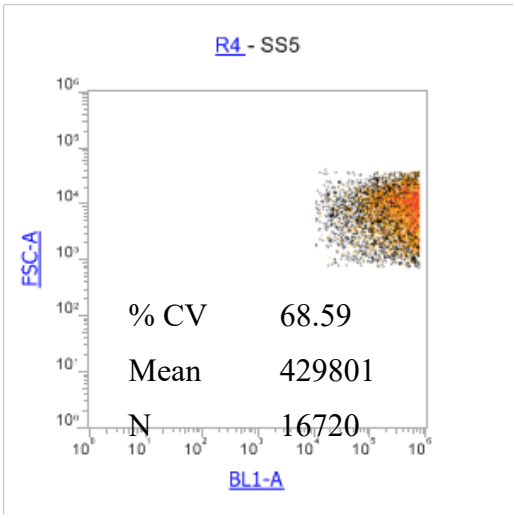
R4 - SS5
FSC-A
BL1-A
% CV 68.59
Mean 429801
N 16720

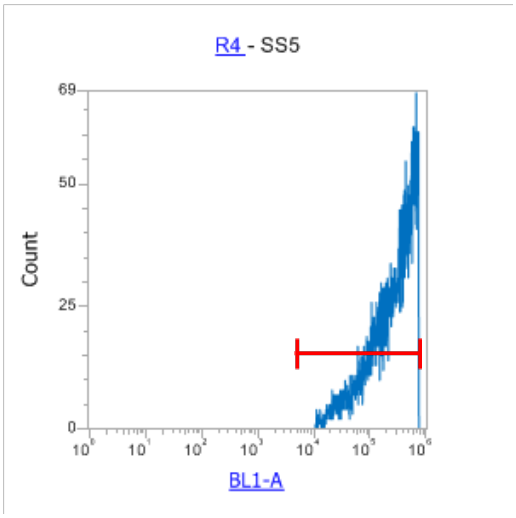
R4 - SS5
Count
BL1-A

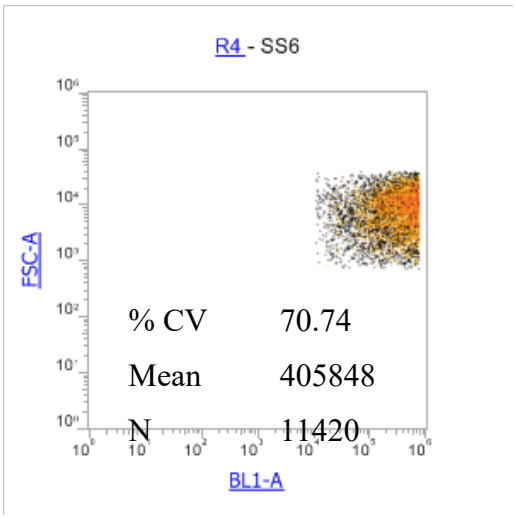
R4 - SS6
FSC-A
BL1-A
% CV 70.74
Mean 405848
N 11420

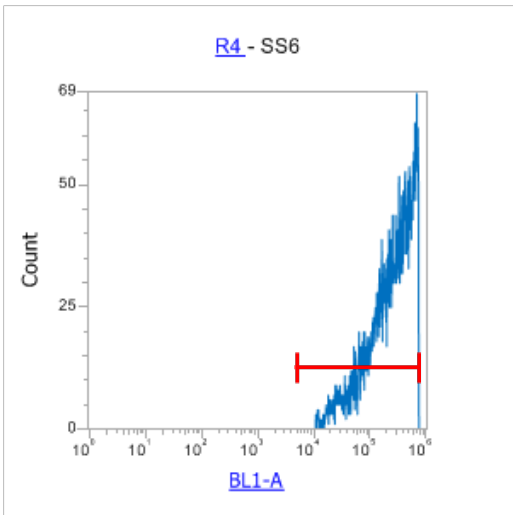
R4 - SS6
Count
BL1-A

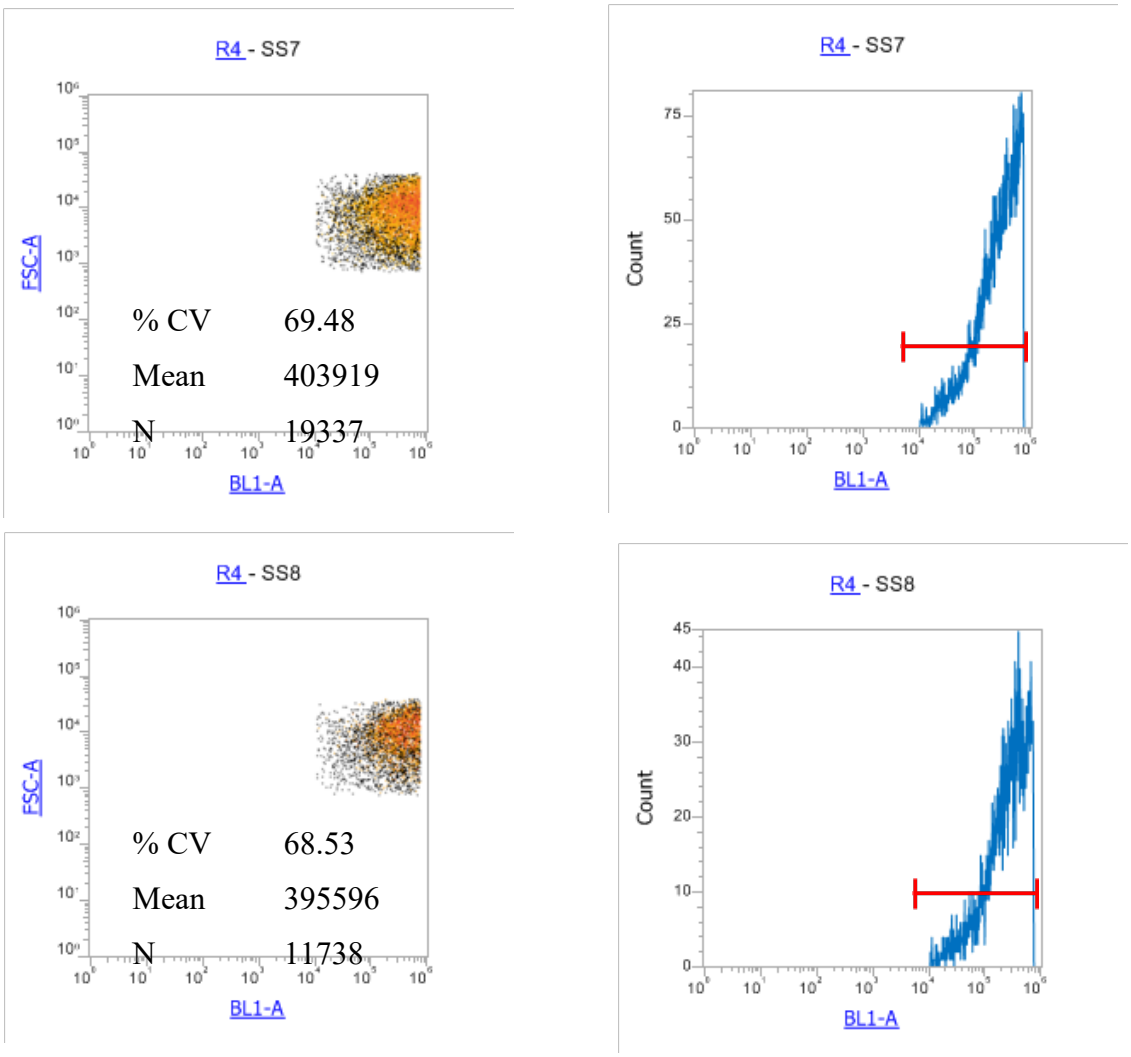

Figure 7.22. Flow cytometry results of steady state glycerol-limited chemostats (SS1-SS8). R4 is the population assigned to the GFP$^+$ gate. A) density dotplot of R4 population of forward scatter (FSC) versus green fluorescent BL1 channel (530/30 nm) B) florescence intensity (BL1 channel) histogram of *E. coli* CLD1301 cells within the GFP$^+$ gate.

The mean intensity, the total number of cells and the CV for glycerol limited chemostats are shown in *Figure 7.22*, for each steady state sample (SS1 - SS8). Considerable variation expressed as CV, ranged from 60.06 to 70.74 and was observed in the GFP intensities of *E. coli* cells grown on glycerol as sole carbon source. The overall mean expression was found to be stable and no non-fluorescent populations were observed, showing that the recombinant protein GFP mut3* was being produced in continuous cultivations (*Figure 7.23*).

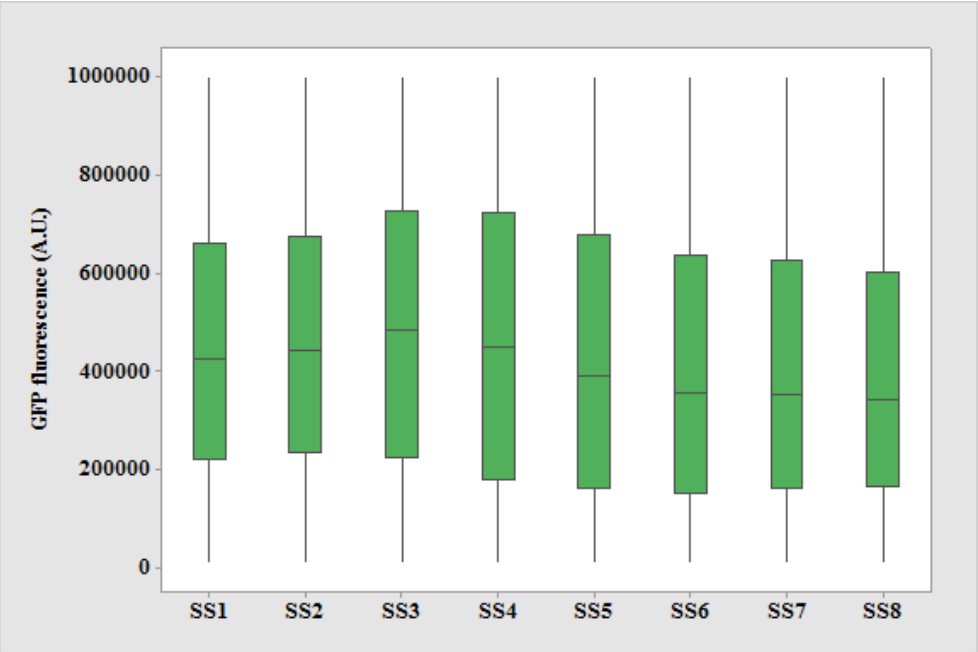

Figure 7.23. GFP protein production at steady state with FC. The green box (IQR) represents 50% of the data, extending from the 1st to 3rd quartile (Q1 to Q3). Number of cells per sample was: SS1 – 11598; SS2 – 13094; SS3 – 12268; SS4 – 8245; SS5 – 16720; SS6 – 11420; SS7 – 19337; SS8 – 11738 cells.

Table 7.2 summarises the fluorescence intensity values (A.U.), representing the recombinant protein being produced. The levels and stability of GFP mut3* in *E coli* CLD1301 cells yielded the CV and 95% confidence intervals for fluorescence intensity (A.U.) shown in *Table 7.3*.

Variable	N	Mean	S.D.	Min	Q1	Median	Q3	Max
SS1	11598	445272	275175	10028	219613	423833	660414	999944
SS2	13094	457679	274880	10003	233611	443312	673435	999933
SS3	12268	481868	290965	10034	224797	483635	726029	999900
SS4	8245	463136	300001	10002	180579	449495	724046	999779
SS5	16720	429801	294809	10018	161240	390236	677995	999954
SS6	11420	405848	287106	10017	150638	355778	636551	999833
SS7	19337	403919	280633	10003	160446	353866	625322	999953
SS8	11738	395596	271094	10025	166637	342208	602162	999814

Table 7.2. Fluorescent protein signal of GFP mut3* in *E. coli* CLD1301 cells at steady state (SS1 - SS8) while growing on glycerol as sole carbon source.

Variable	CV	95% Confidence Interval for mean		95% Confidence Interval for median		95% Confidence Interval for S.D.	
SS1	61.80	440264	450281	416584	430475	271679	278762
SS2	60.06	452971	462388	435750	449987	271591	278251
SS3	60.38	476719	487018	475251	491956	287369	294652
SS4	64.78	456660	469613	436490	461822	295492	304652
SS5	68.59	425332	434269	381622	397780	291683	298003
SS6	70.74	400582	411115	346391	364493	283430	290879
SS7	69.48	399964	407875	347229	360559	277864	283458
SS8	68.53	390692	400501	334554	350909	267670	274607

Table 7.3. CV and confidence intervals for GFP mut3*fluorescence detected by flow cytometry.

The mean expression of GFP mut3* was higher on glucose (*Table 5.3*) than glycerol *(Table 7.2*). The CV (the ratio between standard deviation and the mean) was lower on glucose (*Table 5.4*) than glycerol (*Table 7.3).* This suggests that a higher degree of heterogeneity (a higher CV) is detrimental to bioprocess. However, the production of the recombinant protein comes at a cost of reduced division, therefore other factors must be explored for process optimisation.

7.10.2 Protein production evaluated with fluorescent microscopy

Fluorescence microscopy was performed as previously described (see *3.11 Phase and fluorescence microscopy of E. coli CLD1301*). The acquisition of single cell fluorescence was automated using the ImageJ macro available in *Appendix F*. Cells up to 0.5 μm^2 were filtered out as debris. No upper limit was set because "live" filamentous cells produced recombinant product. GFP mut3* fluorescence showed that the GFP mut3* signal varied across the steady states *(Figure 7.24*). Given the relatively low cell numbers (see below) compared with FC, microscopy proved unsatisfactory in acquiring sufficient data for quantifying the GFP signal distributions.

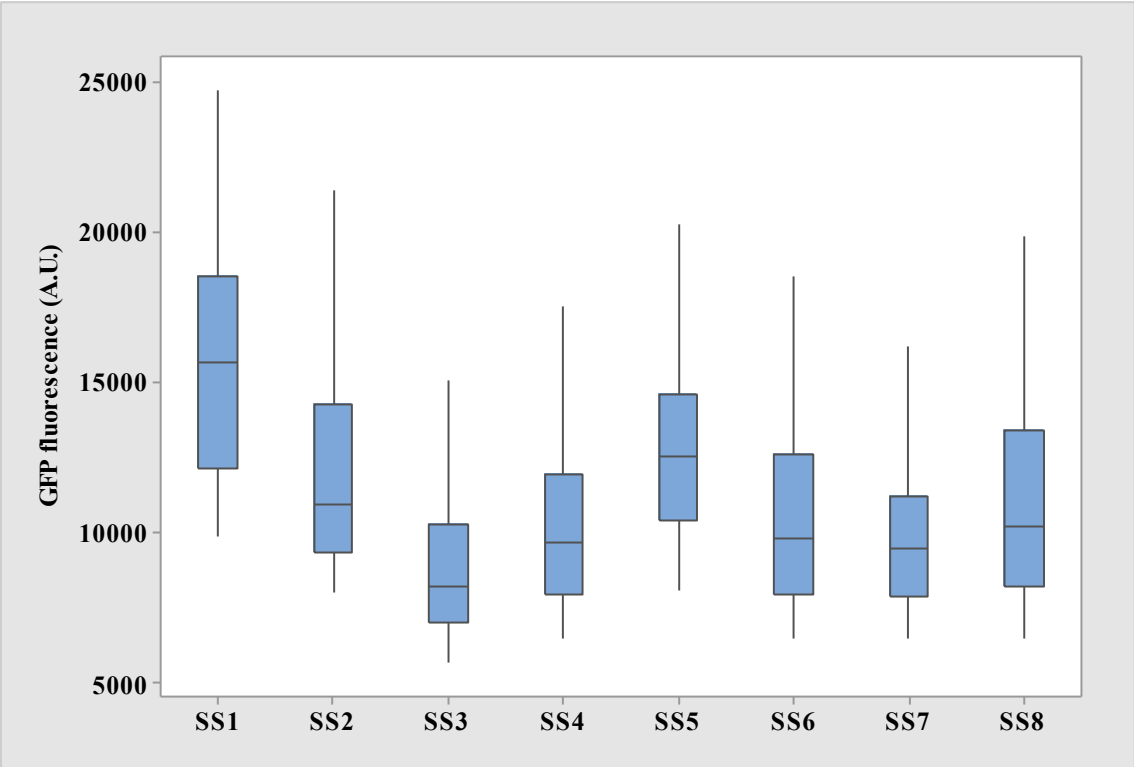

Figure 7.24. GFP mut3* fluorescence (A.U.) at steady state (SS1 - SS8) after induction with 1 mM IPTG maintained constant in the reactor. Number of cells per sample was: SS1– 432; SS2 – 418; SS3 – 749; SS4 – 578; SS5 – 781; SS6 – 685; SS7 – 685; SS8 – 723 cells.

7.11 Discussion and conclusions

This chapter discussed fermentations of *E. coli* CLD1301 with glycerol as the sole carbon source. Cells were subjected to both glycerol excess and limitation to mimic the substrate gradients that exist in large-scale fed-batch reactors. Fermentations were characterised at population level (overall bioprocess monitoring), and at single cell level (cell morphology, total cell counts, membrane integrity and potential).

The results were compared with the host *E. coli* W3110 to show the cost of plasmid maintenance (for non-induced cultures) and protein production (for induced cultures). Protein production in terms of mean GFP-mut3*intensity and CV was compared with fermentations carried out on glucose (discussed in Chapter 5).

The main findings were:

Growth

Recombinant *E. coli* showed an altered growth compared to the host W3110. Firstly, a 19.4 h increase in the lag phase was observed in non-induced cultivations. Secondly, there was a relative decrease of 21.90% in the growth rate caused by plasmid maintenance (*Figure 7.3*). A reduction of "costs" can bring enormous benefits to a bioprocess, in that costs affect the yields. The relative decrease in growth rate for glucose was 61.39% (*Figure 5.3*). This would suggest that plasmid-based systems are best grown on glycerol because the plasmid maintenance cost on the cell is lower.

Biomass

The final biomass determined by BioLector was 96.92 A.U. for un-induced recombinant strain and 78.81 A.U. for the host strain *E. coli* W3110 (*Figure 7.3*). Growth on glucose also recorded a higher biomass of 56.26 for the recombinant strain compared to 48.89 A.U. for the host (*Figure 5.3*). Reducing load from 61.39% on glucose to 21.90% on glycerol led to a 72.26% increase in the final biomass.

Viability

During maximal growth on glycerol there were 85.77% TO^+ cells, but only 14.54% PI^+ cells *(Figure 7.13 A* and *B*). A 99% viability of *E. coli* CLD1301 was detected at maximal growth on glucose (*Figure 5.14).* This shows an increase in cell death when using glycerol as a carbon source, in the absence of carbon limitation (cultures are in exponential phase). This was also noted for the host strain W3110, where the viability of over 97% (*Figure 4.16 A*) was reduced to 94.90% (*Figure 6.13 A*) during exponential growth when replacing glucose with glycerol.

The reduction in growth rate did not lead to a significant decrease in *E. coli* CLD1301 viability, with a mean of 84.77% on glycerol-limited chemostats (*Figure 7.13 C* and *D)*. Nevertheless, the production of a high copy number plasmid further reduced the viability, with the GFP-producing cells at 79.35% viable during submaximal growth on glycerol (*Figure 7.13 C* and *D*).

Florescence microscopy detected significant changes in cell area and aspect ratio in *E. coli* CLD1301 in the absence of inducer (*Figure 7.17 D, E, F*). The circularity changes, associated with membrane protrusions in the absence of IPTG were not significant (*Figure 7.17 F*). All

E. coli CLD1301 morphological parameters in the presence of inducer showed significant changes at "steady state" (*Figure 7.19 A, B, C*). The changes in cell area, circularity and aspect ratio during protein production suggested that for this system, the chemostat cannot be run continuously and indefinitely for protein production.

Fluorescence microscopy also demonstrated the most common phenotype during protein production was the filamentous cell. Filaments started to occur when the cell, challenged with plasmid maintenance, was grown in carbon-limitation, in the absence of induction (*Figure 7.16).*

Protein production

Regardless of these caveats, recombinant protein GFP mut3* was produced in continuous cultivations. The fluorescence acquired with fluorescent microscopy was not robust due to the insufficient number of cells. Flow cytometry gave a more robust signal on a much larger population of cells, showing a decrease in the GFP signal on glycerol (*Table 7.2*) compared to glucose (*Table 5.3*). The CV was higher on glycerol (*Table 7.3*) than on glucose (*Table 5.4)*. This infers that heterogeneity (a higher CV) is detrimental to bioprocess. This is in agreement with initial research by Delvigne's group (Delvigne and Goffin, 2014). No non-productive phenotypes were apparent, however, as previously reported (Delvigne and Goffin, 2014). Cells were found contrastingly that adopted a persistent productive phenotype and that the recombinant protein was produced at many "costs".

At population level, producing a high copy plasmid number reduced the growth rate. At single cell level, it reduced the TCCs, the viability, causing both huge morphological changes and the formation of filaments. These changes were caused by the metabolic load of recombinant protein production on top of plasmid maintenance, on a background of carbon limitation. Further exploration is required for process optimisation. Although bioprocess investigations do not commonly involve changes in morphology, when assessing heterogeneity in protein production through the means of flow cytometry, morphological changes must be considered. This is because flow cytometry measures the amount of a fluorescent molecule in a cell, which depends on the cell size. A bigger cell, such a filamentous cell would display the highest fluorescence of all.

CHAPTER 8

GENERAL CONCLUSIONS AND FURTHER WORK

Chapter 8 General Conclusions and Further Work

8.1 General conclusions

Cellular heterogeneity is an inherent phenomenon in an industrial fed-batch fermenter. For example, cells passing through the top feeding point of a bioreactor, experience a higher level of substrate, while cells opposite the feeding port are exposed to lower levels of substrates. At individual cell level, this results in a different utilisation of substrate, with different growth rates. Heterogeneity at large scale has important implications on process performance, thus needs to be investigated for optimisation and reducing cost. Delvigne has explored the impact of heterogeneity in fermenters used for recombinant protein production (Delvigne and Goffin, 2014), but many questions remain so far, unanswered.

To analyse microbial heterogeneity existing at large scale, lab scale fermentations required single cell analysis of cells exposed to different growth rates. This study explored the dynamics of a host and recombinant *E. coli* strain in a bioreactor in both excess and limitation of carbon, using batch (during exponential phase) and continuous cultivation as methodologies. While neither are standard in bioprocess for RPP, these conditions emulate those encountered at large scale (Section *1.1* and Section *2.6.3*), and thus the information gained is transferable to larger scale. The two techniques used in this work – flow cytometry and fluorescence microscopy complemented each other and helped identify a number of differences with regard to cellular heterogeneity resulting from the growth on either glucose or glycerol as the sole carbon source.

An enhanced model protein GFP mut3* was used as it is easy to detect using flow cytometry and fluorescence microscopy. Single cell parameters were analysed in both batch and continuous cultivations as both methods provide cells in “balanced growth”, a prerequisite for cell physiological studies (Section *2.6.3*). Continuous bioprocessing is particularly important given an ever-increasing need for developing greener bioprocesses. It may be unlikely that the minimal media used during this work would have a large industrial uptake, preference still given to the complex media enabling high cell density cultivations. However, a minimal media is a necessity for physiological studies, assessing the influence of a single chosen component on the individual cells, whilst providing good reproducibility.

The main findings of this work are:

8.1.1 Measurements of viable biomass using flow cytometry with TO/PI

The TO/PI dual combination was used to monitor cell viability in bioreactors for host W3110 and un-induced recombinant CLD1301. The induced recombinant strain used only staining with PI. Flow cytometry methods have been used previously to monitor the membrane integrity of *E. coli* (Richard *et al.*, 2007, Braschi *et al.*, 2018). The following were observed using minimal media with either glucose/glycerol.

Glucose

Both host and recombinant strain showed high levels of viability when grown on glucose at maximum growth rate. *E. coli* W3110 had more than 97% viable biomass, as indicated by the TO/PI staining. Glucose limitation increased the number of dead cells (PI^+) to 12 - 16% during chemostat cultivations. Recombinant *E. coli* CLD1301 maintained a high viability at maximal growth rate on glucose, which did not change significantly when lowering the growth rate in chemostat. However, the viable biomass decreased to 81% in the GFP - producing cells during glucose limitation, showing this is a result of nutrient limitation in cells attempting recombinant protein production.

Glycerol

Viability was maintained for both host and recombinant strain when grown on glycerol. A slight decrease in the amount of TO^+ cells was noted in chemostat compared to maximal growth rate in batch. The recombinant strain exhibited 85.77% viable biomass in the presence of plentiful substrate, and this did not decrease significantly when reducing growth rate in chemostat, but the induction of protein expression lowered the TO^+ cells to 79.35%.

Changing the carbon source from glucose to glycerol decreases slightly the viable biomass, which is of importance for bioprocess industry. The accurate quantification of viable biomass using flow cytometry and PI exclusion is invaluable for process control due to its high throughput and precision (Davey and Kell, 1996, Richard *et al.*, 2007). Yet, a weak point of the PI staining is that it detects cells whose membrane integrity is severely compromised (Stiefel *et al.,* 2015). As such, a promising solution is the use of membrane potential assays, which detect changes in the membrane ion permeability that are sufficient to inhibit or kill bacterial cells by changes in membrane potential.

8.1.2 Measurements of membrane potential using flow cytometry with DIBAC$_{4(3)}$/EB/PI

To overcome the limitation the end-point assay using PI staining in bioprocess optimisation, the triple dye combination DIBAC$_{4(3)}$/EB/PI was used in combination with flow cytometry to distinguish between cell physiological states. Several studies have used DIBAC$_{4(3)}$ to monitor cell physiological states, although the published data for *E. coli* bioprocesses is rare and even then, associated with other stains (Want *et al*., 2009, Wurm *et al*., 2017). Four different phenotypes were identified based on membrane potential, as "active", "depolarised", "deenergised" and "dead" cells.

Glucose

In the presence of plentiful substrate (at μ_{max}), both host W3110 and recombinant CLD1301 show the population is primarily dominated by active cells, with intact cytoplasmic membranes (Section *4.8* and Section *5.8*). Only a small fraction of the population is "dead", and this does not change significantly across experiments (Section *4.8* and Section *5.8*). This was in agreement with TO/PI staining for estimating viability. However, reducing the growth rate in chemostat led to an increase of cell heterogeneity in both strains, with an increase in "depolarised" cells and a simultaneous decrease in "active" cells. An increase in population heterogeneity is a well-known strategy for ensuring population survival and functionality when stressful conditions occur (Van Boxtel et *al.*, 2017). The observed change in the cell energetic status towards depolarisation signifies disrupted cell metabolism with reduced cell functionality. No noticeable change was observed in the "dead" or "deenergised" subpopulations. This shows that depolarisation and increased cell heterogeneity during nutrient limitation is beneficial for the bioprocess, as it protects the cells from death.

Glycerol

During unlimited growth on glycerol, the host W3110 population showed a majority of 70.8% active cells (Section *6.8*). As this was lower than the observed 83.74% on glucose (Section *4.8*) whilst all the other parameters were maintained constant, this showed that the carbon source itself increases the membrane depolarisation. Additionally, an increase in the "dead" subpopulation was observed for glycerol (Section *6.8*) compared to glucose (Section *4.8*), showing that glycerol increases the membrane permeability. The "deenergised" subpopulation

has not changed significantly when reducing the growth rate. The only noticeable change was the increase in the percentage of depolarised host W3110 cells at a reduced growth rate (Section *6.8*).

The trend is maintained for cultivations of recombinant CLD1301 on glycerol, although there are significantly less "active" cells in recombinant strain compared to the host strain (Section *7.8* and Section *6.8*). At maximal growth on glycerol, 31.32% accounted for the "active" subpopulation, and this reduces further with lowering the growth rate (Section *7.8*).This shows a decline in cell functionality for an increasing number of cells. This is not worrying for a standard fed-batch bioprocess where the main concern is the product, but would be detrimental to a long-running continuous fermentation.

8.1.3 Evaluation of protein production

The most important factor defining the success of a bioprocess is the amount of product.

GFP was used as a successful marker for protein production, detected by both flow cytometry and fluorescence microscopy.

Flow cytometry revealed that the heterologous protein was produced during continuous cultivation at a stable near-constant mean level. This is attractive for continuous bioprocessing, although up to date long term stability remained challenging in continuous *E. coli* fermentations (Peebo and Neubaer, 2018). A higher expression of GFP mut3* was observed on glucose over glycerol growth, with 95% confidence intervals of 535277 – 564998 (*Table 5.4*) and 390692 - 487018 (*Table 7.3*), respectively. The population showed a higher heterogeneity when growing on glycerol than glucose, as indicated by a CV of 60.06 – 70.74 (*Table 7.3*) and 47.75 – 51.95 (*Table 5.4*), respectively. This suggests that heterogeneity in protein production is detrimental to bioprocess.

In addition, a decrease in CV for cell area, circularity and aspect ratio, noted on glucose growth for recombinant *E. coli* CLD1301 suggested a more homogeneous population. Given that the expression levels were higher on glucose, this supports the finding that heterogeneity is detrimental to bioprocess. However, in recent years, heterogeneity has been the subject of increasing attention for enhancing the fitness of a population in front of various stressors (Lidstrom and Konopka, 2010, Ryall *et al.*, 2012, Delvigne and Goffin, 2014). Indeed, our results indicate that heterogeneity protects the cells from death, as indicated by the flow

cytometry analysis of membrane potential, but this comes at a cost of a reduced expression, despite a higher biomass (Section *7.3* and Section *7.10.1*). Additionally, a lower biomass was recorded for both strains on glucose than glycerol (Section *4 - 7.3*). This could be addressed at industrial scale by multiple feeding points with a lower concentration of feed, if biomass level is of concern for glucose substrate.

The monitoring of protein production with fluorescence microscopy did not prove reliable because of the low number of cells. In addition, it is time consuming (Frossard *et al*., 2016), which is a limitation in a bioprocess. It did, however, provide information about the state of the cells and identified a multitude of morphological changes in both strains, that would have otherwise been missed out. The contrasting results obtained with microscopy and forward scatter (FSC) in regard to cell size, highlighted the necessity of using complementary techniques for bioprocess understanding. The most striking microscopical feature was cell filamentation, which signifies a highly productive phenotype, previously detected in fed-batch cultivations (Fragoso-Jiménez *et al.,* 2019). While is of no concern in fed-batch reactors, other than an overestimation of the biomass, it has a negative effect on both protein production and viability in long term.

Using this system, successful continuous cultivations in long term would not be feasible. Regulating this system to produce a low but steady recombinant product could lead to feasible approaches for implementing continuous systems. Stress minimising techniques, such as extracellular expression may sound promising, although this approach so far achieved non-feasible titres (Kleiner-Grote, 2018). While the use of GFP is limited at industrial scale, it is as useful as any other protein in wider applications. The burden introduced by the high copy number plasmid (500-700) used during this study, would occur in other proteins produced at industrial scale.

8.2 Future works

Opportunities for future works were identified during this study in regard to the following:

8.2.1 Evaluation of growth

Both strains exhibited a higher biomass when grown on glycerol than cells growing on glucose (*Figure 8.1*) during batch cultivations in BioLector. Given the higher biomass

observed for glycerol than glucose (*Figure 8.1*), one can see the industrial attractiveness of using glycerol for microbial fermentations. A higher affinity for glucose than glycerol, resulting in a higher growth rate, is reported in literature (Betterbrock *et al.*, 2006, Deutscher *et al.*, 2006). This is in accordance with data for host W3110 (μ_{max} = 0.6 h^{-1} on glucose, 0.50 h^{-1} on glycerol), as illustrated in *Figure 8.1 A*.

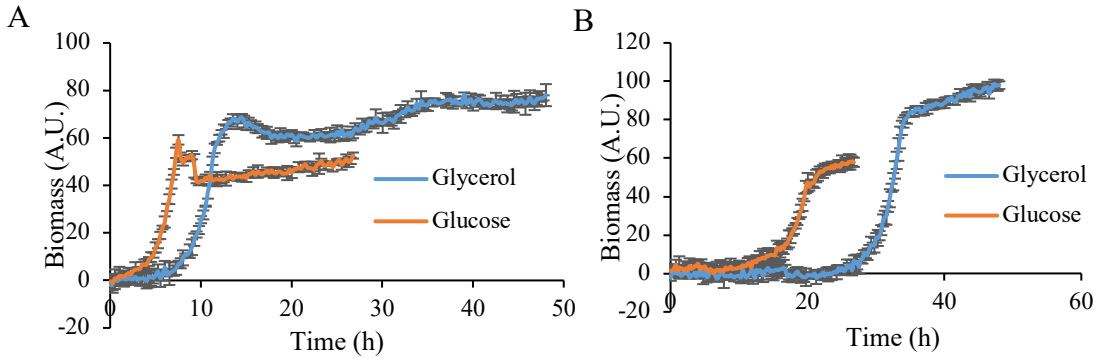

Figure 8.1. *E. coli* W3110 (A) and recombinant *E. coli* CLD1301 (B) growth in glycerol/glucose minimal media (4 g/L).

Batch experiments in STR have shown that the consumption of glucose occurred simultaneously with the dissemination of VFAs through overflow metabolism, indicating a conversion of C in wasteful products instead of biomass at high growth rates on glucose (Section *4.6*, Section *5.6*). This is experienced by cells passing through the top of the industrial fermenter, where a high level of feed adds to the simultaneous relatively low oxygen level and drives cells into overflow metabolism with subsequent by-product formation. This could also be reduced by multiple feeding points with a lower glucose concentration.

The overflow metabolism was not observed on glycerol growth during the batch cultivations. The levels of VFAs at maximum growth rate were 75 times less on glycerol than on glucose for strain W3110 (Section *6.6.3*). Recombinant strain displayed lower levels of VFAs than the host (Section *5.6.5*), as a result of a decreased the growth rate (μ_{max} = 0.37 h^{-1} on glucose). At submaximal growth rate in both glucose and glycerol-limited chemostats, the overflow metabolism was negligible due to the limited C source. This indicated a better conversion of C to biomass synthesis instead of VFAs, showing the potential of continuous cultivations.

A striking fact is that the recombinant strain (*Figure 8.1 B*) displayed a lower growth rate on glucose than glycerol (μ_{max} = 0.37 h^{-1} on glucose, 0.39 h^{-1} on glycerol). In addition to a lower biomass on glucose, this shows that glucose is not the preferential substrate for the recombinant strain. This is relevant in industrial fermentations, and it would be interesting to see whether this suboptimal growth on glucose can be improved by genetic manipulation. Thus, a more in-depth comprehension of the exponentially growing cells is of importance for a better understanding of the bacterial physiology and for bioprocess optimisation.

It is worth mentioning that many *E. coli* studies drew comparisons for glucose/glycerol growth, but experiments were conducted on a different media, and using different methodologies. Korz, for example, conducted experiments in fed-batch (Korz *et al*., 1995), but on a different *E. coli* strain, and did not look at single cell level. Except for the studies of Egli, exclusively using a minimal media with a sole limitation, none of the studies so far provided an in-depth information about the influence of carbon on cell growth. In this context, it should be noted that the experiments were carried out in chemostat in a defined minimal media with glucose (Ihhsen and Egli, 2004). They did not explore the influence of glycerol as sole carbon source, nor used the BioLector for online monitoring of fermentations.

8.2.2. Studies of nitrogen limitation

The media used in this study is single substrate limiting, up to a concentration of 4 g/L carbon source. As illustrated here, the online monitoring of scattered light shows a linear dependency of the biomass on the substrate level up to a concentration of 4 g/L glucose or glycerol (*Figure 8.2*). Studies of nutrient limitation are important to microbial growth and evolution, and may be used in biotechnological contexts. On both substrates (glucose and glycerol), recombinant *E. coli* CLD1301 exhibited a prolonged lag phase compared to host (*Figure 8.2*). The increase in the lag phase arise from the need for plasmid maintenance in the absence of induction.

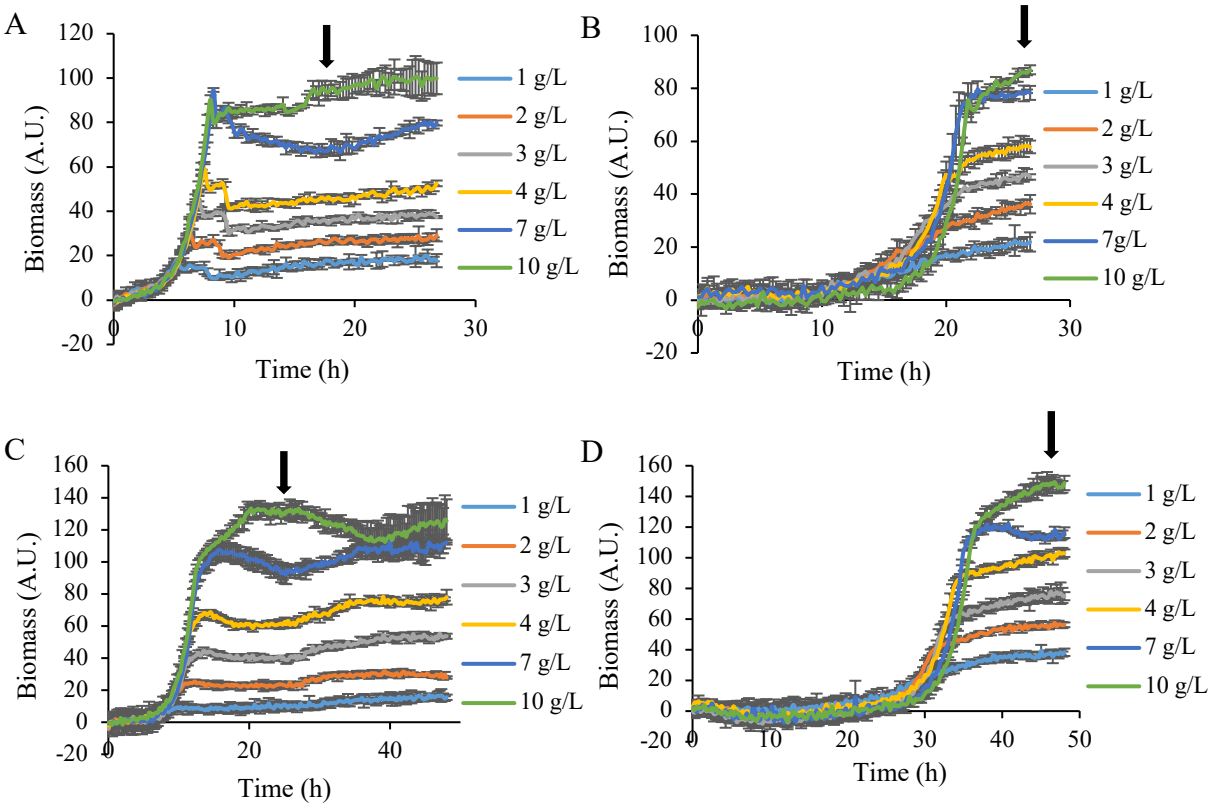

Figure 8.2. Growth on glucose minimal media (4 g/L) of *E. coli* W3110 (A) and recombinant *E. coli* CLD1301 (B). Growth on glycerol minimal media (4 g/L) of *E. coli* W3110 (C) and recombinant *E. coli* CLD1301 (D). Arrows show striking growth patterns on dual carbon-nitrogen limitation.

It is known that the microbial response to nutrient limitation changes in response to the type and degree of scarcity (Maharjan and Ferenci, 2018). Liebig's law of minimum suggests that only a single dominant limitation dictates biological behaviour (Gorban *et al.*, 2011). It has been discussed that the secondary limitation of the media used in this study is nitrogen, detailed further in Appendix A. Our results are not consistent with Liebig's law of minimum as striking growth patterns were identified on both strains during double carbon and nitrogen limitation (*Figure 8.2*). Such patterns differ depending on the carbon source used (glucose-glycerol). The changes in the scatter light signal may identify cell morphological changes and the development of subpopulations (Kottmeier *et al.*, 2009, Kunze *et al.*, 2014). However, occurring in the stationary phase of growth, these patterns have not been explored during this study.

To the best of my knowledge, this is the first work showing biomass development as monitored by BioLector using a single limitation media at different concentrations of substrate (carbon). Further studies exploring these issues may be relevant in biotechnological contexts in which cells are grown under nitrogen limitation. Additionally, mutations could arise in cells challenged with multiple limitations, therefore it is important to include sequencing into future studies regarding microbial heterogeneity.

8.3 Implications for continuous bioprocessing

For continuous bioprocessing to be economically viable, high yields are required. High yields are obtained only if the recombinant plasmid copy number is high and the cells maintain both growth and division, whilst producing the recombinant product.

Although few examples of successful continuous recombinant protein bioprocesses exist in literature (Paulova *et al.*, 2012, Schmideder and Weuster-Botz, 2017), it has not taken over the fed-batch in industry. This study highlighted the complexities of optimising a bioprocess, and will perhaps, in time allow a successful transition to continuous biomanufacturing. The impediments so far have been identified as a lower biomass, reduced total cell numbers, drastic morphological cell changes with cell filamentation as the dominant productive phenotype. For these reasons, fed-batch is preferred over continuous bioprocessing. Finally, a better understanding of the system may allow manipulating the host cell and reducing the metabolic load, so continuous bioprocessing could become a viable alternative to fed-batch.

References:

AAKESSON, M. H., SE), HEITMANN, MARTIN (COPENHAGEN, DK), TIAINEN, PETER (LIMHAMN, SE). 2017. *INTEGRATED CONTINUOUS BIOMANUFACTURING PROCESS*. United States patent application 20170058308.

AIBA, S., HUMPHREY, A. E. & MILLIS, N. F. 1973. *Biochemical engineering,* New York,, Academic Press.

AKAGI, J., KORDON, M., ZHAO, H., MATUSZEK, A., DOBRUCKI, J., ERRINGTON, R., SMITH, P. J., TAKEDA, K., DARZYNKIEWICZ, Z. & WLODKOWIC, D. 2013. Real-time cell viability assays using a new anthracycline derivative DRAQ7 (R). *Cytometry Part A,* 83a**,** 227-234.

ALLDREAD, R. & ROBINSON, J. 2015. Biopharmaceutical factory of the future. *Pharmaceutical Bioprocessing,* 3**,** 293-304.

ALTENBUCHNER, J. & MATTES, R. 2005. *Escherichia coli*. *Production of Recombinant Proteins***,** 7-43.

ANDERSEN, J. B., STERNBERG, C., POULSEN, L. K., BJORN, S. P., GIVSKOV, M. & MOLIN, S. 1998a. New unstable variants of green fluorescent protein for studies of transient gene expression in bacteria. *Applied and Environmental Microbiology,* 64**,** 2240-2246.

ANDERSSON, L., YANG, S. J., NEUBAUER, P. & ENFORS, S. O. 1996. Impact of plasmid presence and induction on cellular responses in fed batch cultures of Escherichia coli. *Journal of Biotechnology,* 46**,** 255-263.

BAERT, J., DELEPIERRE, A., TELEK, S., FICKERS, P., TOYE, D., DELAMOTTE, A., LARA, A. R., JAÉN, K. E., GOSSET, G., JENSEN, P. R. & DELVIGNE, F. 2016. Microbial population heterogeneity versus bioreactor heterogeneity: Evaluation of Redox Sensor Green as an exogenous metabolic biosensor. *Engineering in Life Sciences,* 16**,** 643-651.

BAERT, J., KINET, R., BROGNAUX, A., DELEPIERRE, A., TELEK, S., SORENSEN, S. J., RIBER, L., FICKERS, P. & DELVIGNE, F. 2015. Phenotypic variability in bioprocessing conditions can be tracked on the basis of on-line flow cytometry and fits to a scaling law. *Biotechnology Journal,* 10**,** 1316-1325.

BARER, M. R. & HARWOOD, C. R. 1999. Bacterial viability and culturability. *Advances in Microbial Physiology, Vol 41,* 41**,** 93-137.

BASAN, M., HUI, S., OKANO, H., ZHANG, Z., SHEN, Y., WILLIAMSON, J. R. & HWA, T. 2015. Overflow metabolism in *Escherichia coli* results from efficient proteome allocation. *Nature,* 528**,** 99.

BETTENBROCK, K., FISCHER, S., KREMLING, A., JAHREIS, K., SAUTER, T. and GILLES, E.D., 2006. A quantitative approach to catabolite repression in *Escherichia coli. Journal of Biological Chemistry*, *281*(5), pp.2578-2584.

BILLINTON, N. & KNIGHT, A. W. 2001. Seeing the wood through the trees: A review of techniques for distinguishing green fluorescent protein from endogenous autofluorescence. *Analytical Biochemistry,* 291**,** 175-197.

BINDER, D., DREPPER, T., JAEGER, K. E., DELVIGNE, F., WIECHERT, W., KOHLHEYER, D. & GRUNBERGER, A. 2017. Homogenizing bacterial cell factories: Analysis and engineering of phenotypic heterogeneity. *Metabolic Engineering,* 42**,** 145-156.

BRASCHI, G., PATRIGNANI, F., SIROLI, L., LANCIOTTI, R., SCHLUETER, O. and FROEHLING, A., 2018. Flow cytometric assessment of the morphological and physiological changes of *Listeria monocytogenes* and *Escherichia coli* in response to natural antimicrobial exposure. *Frontiers in microbiology*, *9*, p.2783.

BRIDIER, A., HAMMES, F., CANETTE, A., BOUCHEZ, T. & BRIANDET, R. 2015. Fluorescence-based tools for single-cell approaches in food microbiology. *International Journal of Food Microbiology,* 213**,** 2-16.

BRIDSON, E. Y. & GOULD, G. W. 2000. Quantal microbiology. *Letters in Applied Microbiology,* 30**,** 95-98.

BROGNAUX, A., HAN, S. S., SORENSEN, S. J., LEBEAU, F., THONART, P. & DELVIGNE, F. 2013. A low-cost, multiplexable, automated flow cytometry procedure for the characterization of microbial stress dynamics in bioreactors. *Microbial Cell Factories,* 12.

BRÜCKNER, R. & TITGEMEYER, F. 2002. Carbon catabolite repression in bacteria: choice of the carbon source and autoregulatory limitation of sugar utilization. *FEMS microbiology letters,* 209**,** 141-148.

CAMPBELL, A. 1957. Synchronization of cell division. *Bacteriological reviews,* 21**,** 263-272.

CAMPION, A., MORRISSEY, R., FIELD, D., COTTER, P. D., HILL, C. & ROSS, R. P. 2017. Use of enhanced nisin derivatives in combination with food-grade oils or citric acid to control *Cronobacter sakazakii* and *Escherichia coli* O157:H7. *Food Microbiology,* 65**,** 254-263.

ÇELIK, E. & ÇALıK, P. 2012. Production of recombinant proteins by yeast cells. *Biotechnology Advances,* 30**,** 1108-1118.

CHALFIE, M., TU, Y., EUSKIRCHEN, G., WARD, W. W. & PRASHER, D. C. 1994. Green fluorescent protein as a marker for gene expression. *Science,* 263**,** 802-805.

CHANCE, R. E. & FRANK, B. H. 1993. Research, Development, Production, and Safety of Biosynthetic Human Insulin. *Diabetes Care,* 16**,** 133-142.

CHEN, R. 2012. Bacterial expression systems for recombinant protein production: *E. coli* and beyond. *Biotechnol Adv,* 30.

CHEN, R. H., HUANG, C., JR., NEWTON, B. S., RITTER, G., OLD, L. J. & BATT, C. A. 2009. Factors affecting endotoxin removal from recombinant therapeutic proteins by anion exchange chromatography. *Protein Expression and Purification,* 64**,** 76-81.

CHIRINO, A. J. & MIRE-SLUIS, A. 2004. Characterizing biological products and assessing comparability following manufacturing changes. *Nature biotechnology,* 22**,** 1383.

CONTIERO, J., BEATTY, C., KUMARI, S., DESANTI, C. L., STROHL, W. R. & WOLFE, A. 2000. Effects of mutations in acetate metabolism on high-cell-density growth of *Escherichia coli. Journal of Industrial Microbiology & Biotechnology,* 24**,** 421-430.

COOPER, M. R., FEFER, A., THOMPSON, J., CASE, D. C., KEMPF, R., SACHER, R., NEEFE, J., BICKERS, J., SCARFFE, J. H., SPIEGEL, R. J. & BONNEM, E. M. 1987. Interferon alfa-2b/melphalan/prednisone in previously untreated patients with multiple myeloma: a phase I–II trial. *Investigational New Drugs,* 5**,** S41-S46.

COOPER, S. 2006. Bacterial Growth and Division.

CORMACK, B. P., VALDIVIA, R. H. & FALKOW, S. 1996. FACS-optimized mutants of the green fluorescent protein (GFP). *Gene,* 173**,** 33-8.

CUBITT, A. B., HEIM, R., ADAMS, S. R., BOYD, A. E., GROSS, L. A. & TSIEN, R. Y. 1995. Understanding, Improving and Using Green Fluorescent Proteins. *Trends in Biochemical Sciences,* 20**,** 448-455.

DAVEY, H.M. and KELL, D.B., 1996. Flow cytometry and cell sorting of heterogeneous microbial populations: the importance of single-cell analyses. *Microbiological reviews*, *60*(4), pp.641-696.

DAVEY, H. M. 2011. Life, Death, and In-Between: Meanings and Methods in Microbiology. *Applied and Environmental Microbiology,* 77**,** 5571-5576.

DAVEY, H. M. & HEXLEY, P. 2011. Red but not dead? Membranes of stressed *Saccharomyces cerevisiae* are permeable to propidium iodide. *Environmental Microbiology,* 13**,** 163-171.

DAWSON, P. S. S. 1985. Continuous Cultivation of Microorganisms. *Crc Critical Reviews in Biotechnology,* 2**,** 315-372.

DEMAIN, A. L. & VAISHNAV, P. 2009. Production of recombinant proteins by microbes and higher organisms. Biotechnol. Adv. 27, 297–306.

DE MEY, M., DE MAESENEIRE, S., SOETAERT, W. & VANDAMME, E. 2007. Minimizing acetate formation in *E. coli* fermentations. *Journal of Industrial Microbiology & Biotechnology,* 34**,** 689-700.

DEUTSCHER, J., FRANCKE, C. and POSTMA, P.W., 2006. How phosphotransferase system-related protein phosphorylation regulates carbohydrate metabolism in bacteria. *Microbiology and molecular biology Reviews*, *70*(4), pp.939-1031.

DELAGRAVE, S., HAWTIN, R. E., SILVA, C. M., YANG, M. M. & YOUVAN, D. C. 1995. Red-Shifted Excitation Mutants of the Green Fluorescent Protein. *Bio-Technology,* 13**,** 151-154.

DELVIGNE, F., BOXUS, M., INGELS, S. & THONART, P. 2009. Bioreactor mixing efficiency modulates the activity of a prpoS::GFP reporter gene in *E. coli*. *Microbial Cell Factories,* 8.

DELVIGNE, F. & GOFFIN, P. 2014. Microbial heterogeneity affects bioprocess robustness: Dynamic single-cell analysis contributes to understanding of microbial populations. *Biotechnology Journal,* 9**,** 61-72.

DIAZ, M., HERRERO, M., GARCIA, L. A. & QUIROS, C. 2010. Application of flow cytometry to industrial microbial bioprocesses. *Biochemical Engineering Journal,* 48**,** 385-407.

DING, W. B. 2015. Best Practices in Qualification of Single-Use Systems. *Biopharm International,* 28**,** 32-39.

DOMINGUEZ, D. C. 2004. Calcium signalling in bacteria. *Molecular Microbiology,* 54**,** 291-297.

EGLI, T. 2015. Microbial growth and physiology: a call for better craftsmanship. *Frontiers in Microbiology,* 6.

ERENTAL, A., KALDERON, Z., SAADA, A., SMITH, Y. & ENGELBERG-KULKA, H. 2014. Apoptosis-Like Death, an Extreme SOS Response in *Escherichia coli, MBio,* 5(4).

FARID, S. S., THOMPSON, B. & DAVIDSON, A. 2014. Continuous bioprocessing: The real thing this time? 10th Annual bioProcessUK Conference, December 3-4, 2013, London, UK. *Mabs,* 6**,** 1357-1361.

FELLE, H., PORTER, J. S., SLAYMAN, C. L. & KABACK, H. R. 1980. Quantitative measurements of membrane potential in Escherichia coli. *Biochemistry,* 19**,** 3585-90.

FERENCI, T. 2006. A cultural divide on the use of chemostats. *Microbiology,* 152**,** 1247-8.

FERENCI, T. 2008. Bacterial physiology, regulation and mutational adaptation in a chemostat environment. *Advances in Microbial Physiology, Vol 53,* pp.169-315.

FERRER-MIRALLES, N., DOMINGO-ESPÍN, J., CORCHERO, J. L., VÁZQUEZ, E. & VILLAVERDE, A. 2009. Microbial factories for recombinant pharmaceuticals. *Microbial Cell Factories,* 8**,** 17.

FLORES, S., DE ANDA-HERRERA, R., GOSSET, G. & BOLIVAR, F. G. 2004. Growth-rate recovery of *Escherichia coli* cultures carrying a multicopy plasmid, by engineering of the pentose-phosphate pathway. *Biotechnology and Bioengineering,* 87**,** 485-494.

FRAGOSO-JIMENEZ, J. C., BAERT, J., NGUYEN, T. M., LIU, W. Z., SASSI, H., GOORMAGHTIGH, F., VAN MELDEREN, L., GAYTAN, P., HERNANDEZ-CHAVEZ, G., MARTINEZ, A., DELVIGNE, F. & GOSSET, G. 2019. Growth-dependent recombinant product formation kinetics can be reproduced through engineering of glucose transport and is prone to phenotypic heterogeneity. *Microbial Cell Factories,* 18.

FRANK, B. H. & CHANCE, R. E. 1983. 2 Routes for Producing Human Insulin Utilizing Recombinant DNA Technology. *Munchener Medizinische Wochenschrift,* 125**,** 14-20.

FROSSARD, A., HAMMES, F. and GESSNER, M.O., 2016. Flow cytometric assessment of bacterial abundance in soils, sediments and sludge. *Frontiers in microbiology*, *7*, p.903.

GALBUSERA, L., BELLEMENT-THEROUE, G., URCHUEGUIA, A., JULOU, T. and VAN NIMWEGEN, E., 2019. Using fluorescence flow cytometry data for single-cell gene expression analysis in bacteria. *bioRxiv*, p.793976.

GARCERA, M. J. G., ELFERINK, M. G. L., DRIESSEN, A. J. M. & KONINGS, W. N. 1993. Invitro Pore-Forming Activity of the Lantibiotic Nisin - Role of Protonmotive Force and Lipid-Composition. *European Journal of Biochemistry,* 212**,** 417-422.

GLICK, B. R. 1995. Metabolic Load and Heterologous Gene-Expression. *Biotechnology Advances,* 13**,** 247-261.

GOLDBERG, I. & ROKEM, J. S. 1991. *Biology of methylotrophs,* Boston, Butterworth-Heinemann.

GOMBERT, A. K. & KILIKIAN, B. V. 1998. Recombinant gene expression in *Escherichia coli* cultivation using lactose as inducer. *Journal of Biotechnology,* 60**,** 47-54.

GOORMAGHTIGH, F. and VAN MELDEREN, L., 2019. Single-cell imaging and characterization of *Escherichia coli* persister cells to ofloxacin in exponential cultures. *Science advances*, *5*(6), p.eaav9462.

GORBAN, A.N., POKIDYSHEVA, L.I., SMIRNOVA, E.V. and TYUKINA, T.A., 2011. Law of the minimum paradoxes. *Bulletin of mathematical biology*, *73*(9), pp.2013-2044.

HAGEN, S.J., 2017. The Physical Microbe: An introduction to Noise, Control, and Communication in the Prokaryotic Cell. IOP eBooks, 2017.

HAMORSKY, K., KOUOKAM, J., J BENNETT, L., BALDAUF, K., KAJIURA, H., FUJIYAMA, K. & MATOBA, N. 2013. Rapid and Scalable Plant-based Production of a Cholera Toxin B Subunit Variant to Aid in Mass Vaccination against Cholera Outbreaks. *PLoS neglected tropical diseases,* 7**,** e2046.

HARDER, W. & DIJKHUIZEN, L. 1983. Physiological responses to nutrient limitation. *Annual Review of Microbiology,* 37**,** 1-23.

HARDER, W., KUENEN, J. G. & MATIN, A. 1977. Microbial Selection in Continuous Culture. *Journal of Applied Bacteriology,* 43**,** 1-24.

HELANDER, I. M. & MATTILA-SANDHOLM, T. 2000. Permeability barrier of the Gram-negative bacterial outer membrane with special reference to nisin. *International Journal of Food Microbiology,* 60**,** 153-161.

HENRICI, A. T. 1928. Morphologic Variation and the Rate of Cjrowth of Bacteria.

HERBERT, D. 1961. The chemical composition of microorganisms as a function of their environment.

HEWITT, C. J. & NEBE-VON-CARON, G. 2001. An industrial application of multiparameter flow cytometry: Assessment of cell physiological state and its application to the study of microbial fermentations. *Cytometry,* 44**,** 179-187.

HEWITT, C. J., ONYEAKA, H., LEWIS, G., TAYLOR, I. W. & NIENOW, A. W. 2007. A comparison of high cell density fed-batch fermentations involving both induced and non-induced recombinant *Escherichia coli* under well-mixed small-scale and simulated poorly mixed large-scale conditions. *Biotechnology and Bioengineering,* 96**,** 495-505.

HEYLAND, J., BLANK, L. M. & SCHMID, A. 2011. Quantification of metabolic limitations during recombinant protein production in *Escherichia coli. Journal of Biotechnology,* 155**,** 178-184.

HILL, N., BUSKE, P. J., SHI, Y. & LEVIN, P. 2013. A Moonlighting Enzyme Links Escherichia coli Cell Size with Central Metabolism. *PLoS genetics,* 9**,** e1003663.

HOLLYWOOD, N. & DOELLE, H. W. 1976. Effect of specific growth rate and glucose concentration on growth and glucose metabolism of *Escherichia coli* K-12. *Microbios,* 17**,** 23-33.

HOLME, S., HEATON, A., KONCHUBA, A. & HARTMAN, P. 1988. Light Scatter and Total Protein Signal Distribution of Platelets by Flow Cytometry as Parameters of Size. *Journal of Laboratory and Clinical Medicine,* 112**,** 223-231.

HOLMS, W. H. & BENNETT, P. M. 1971. Regulation of Isocitrate Dehydrogenase Activity in *Escherichia coli* on Adaptation to Acetate. *Journal of General Microbiology,* 65**,** 57-+.

HU, Z. S., YE, C., MI, W., ZHAO, Y., QUAN, C., LI, W. W., LI, H. M. & HANG, H. Y. 2018. Light-scattering detection within the difficult size range of protein particle measurement using flow cytometry. *Nanoscale,* 10**,** 19277-19285.

HUDSON, B., UPHOLT, W. B., DEVINNY, J. & VINOGRAD, J. 1969. The use of an ethidium analogue in the dye-buoyant density procedure for the isolation of closed circular DNA: the variation of the superhelix density of mitochondrial DNA. *Proc Natl Acad Sci U S A,* 62**,** 813-20.

IHSSEN, J. & EGLI, T. 2004. Specific growth rate and not cell density controls the general stress response in *Escherichia coli*. *Microbiology-Sgm,* 150**,** 1637-1648.

JAGSCHIES, G. 2018. Chapter 3 - Selected Biotherapeutics Overview. *In:* JAGSCHIES, G., LINDSKOG, E., ŁĄCKI, K. & GALLIHER, P. (eds.) *Biopharmaceutical Processing.* Elsevier.

JAGSCHIES, G. N., LINDSKOG, E., ¿*A**CKI, K. & GALLIHER, P. 2018. *Biopharmaceutical processing : development, design, and implementation of manufacturing processes,* Amsterdam, Netherlands, Elsevier.

JAHN, M., VORPAHL, C., HUBSCHMANN, T., HARMS, H. & MULLER, S. 2016. Copy number variability of expression plasmids determined by cell sorting and Droplet Digital PCR. *Microbial Cell Factories,* 15.

JERNAES, M.W. and STEEN, H.B., 1994. Staining of *Escherichia coli* for flow cytometry: influx and efflux of ethidium bromide. *Cytometry: The Journal of the International Society for Analytical Cytology*, *17*(4), pp.302-309.

JÓDAR-GIMENO, E. 2007. Full length parathyroid hormone (1-84) in the treatment of osteoporosis in postmenopausal women. *Clinical interventions in aging,* 2**,** 163-174.

JOUAULT, H., LOUFRANI, J., BLANC, C., HENTGES, L. & IMBERT, M. 1994. Automated Reticulocyte Count Using New Methylene-Blue - Evaluation in 143 Samples and Comparison with Flow Cytometry Technique Using Thiazole Orange and Microscopic Method. *Blood,* 84**,** A548-A548.

JONES, L.J., CARBALLIDO-LOPEZ, R. and ERRINGTON, J., 2001. Control of cell shape in bacteria: helical, actin-like filaments in *Bacillus subtilis*. *Cell*, *104*(6), pp.913-922.

K. LINDSKOG, E. 2018. The Upstream Process: Principal Modes of Operation.

KACHEL, V., FELLNER-FELDEGG, H. & MENKE, E. 1990. Flow cytometry and sorting. Wiley, New York.

KAISER, C., KNIGHT, A., NORDSTROM, D., PETTERSSON, T., FRANSSON, J., FLORIN-ROBERTSSON, E. & PILSTROM, B. 2012. Injection-site reactions upon Kineret (anakinra) administration: experiences and explanations. *Rheumatology International,* 32**,** 295-299.

KARIM, A. S., CURRAN, K. A. & ALPER, H. S. 2013. Characterization of plasmid burden and copy number in *Saccharomyces cerevisiae* for optimization of metabolic engineering applications. *Fems Yeast Research,* 13**,** 107-116.

KATZ, A., ALIMOVA, A., XU, M., RUDOLPH, E., SHAH, M.K., SAVAGE, H.E., ROSEN, R.B., McCORMICK, S.A. and ALFANO, R.R., 2003. Bacteria size determination by

elastic light scattering. *IEEE Journal of Selected Topics in Quantum Electronics*, *9*(2), pp.277-287.

KÄß, F., JUNNE, S., NEUBAUER, P., WIECHERT, W. & OLDIGES, M. 2014. Process inhomogeneity leads to rapid side product turnover in cultivation of *Corynebacterium glutamicum. Microbial cell factories,* 13**,** 6-6.

KELLY, C. J. & MIR, F. A. 2009. Economics of biological therapies. *Bmj,* 339**,** b3276.

KENSY, F., ZANG, E., FAULHAMMER, C., TAN, R. K. & BUCHS, J. 2009. Validation of a high-throughput fermentation system based on online monitoring of biomass and fluorescence in continuously shaken microtiter plates. *Microbial Cell Factories,* 8.

KERKER, M., CHEW, H., MCNULTY, P. J., KRATOHVIL, J. P., COOKE, D. D., SCULLEY, M. & LEE, M. P. 1979. Light scattering and fluorescence by small particles having internal structure. *J Histochem Cytochem,* 27**,** 250-63.

KERR, R. A., LEVINE, H., SEJNOWSKI, T. J. & RAPPEL, W.-J. 2006. Division accuracy in a stochastic model of Min oscillations in *Escherichia coli. Proceedings of the National Academy of Sciences,* 103**,** 347-352.

KIM, H. T., CHOI, H. J. & KIM, K. H. 2009. Flow cytometric analysis of *Salmonella enterica* serotype Typhimurium inactivated with supercritical carbon dioxide. *Journal of microbiological methods,* 78**,** 155-160.

KIMURA, K., MORIMATSU, K., INAOKA, T. & YAMAMOTO, K. 2017. Injury and recovery of *Escherichia coli* ATCC25922 cells treated by high hydrostatic pressure at 400-600 MPa. *Journal of Bioscience and Bioengineering,* 123**,** 698-706.

KIPRIYANOV, S. M., MOLDENHAUER, G. & LITTLE, M. 1997. High level production of soluble single chain antibodies in small-scale *Escherichia coli* cultures. *Journal of immunological methods,* 200**,** 69-77.

KLEINER-GROTE, G. R. M., RISSE, J. M. & FRIEHS, K. 2018. Secretion of recombinant proteins from E. coli. *Engineering in Life Sciences,* 18**,** 532-550.

KOCH, A. L., ROBERTSON, B. R. & BUTTON, D. K. 1996. Deduction of the cell volume and mass from forward scatter intensity of bacteria analyzed by flow cytometry. *Journal of Microbiological Methods,* 27**,** 49-61.

KOH, B. T., NAKASHIMADA, U., PFEIFFER, M. & YAP, M. G. S. 1992. Comparison of acetate inhibition on growth of host and recombinant *E. coli* K12 strains. *Biotechnology letters,* 14**,** 1115-1118.

KONSTANTINOV, K. B. & COONEY, C. L. 2015. White Paper on Continuous Bioprocessing May 20-21, 2014 Continuous Manufacturing Symposium. *Journal of Pharmaceutical Sciences,* 104**,** 813-820.

KORDEL, M., SCHULLER, F. & SAHL, H. G. 1989. Interaction of the pore forming-peptide antibiotics Pep 5, nisin and subtilin with non-energized liposomes. *FEBS Lett,* 244**,** 99-102.

KORZ, D.J., RINAS, U., HELLMUTH, K., SANDERS, E.A. and DECKWER, W.D., 1995. Simple fed-batch technique for high cell density cultivation of *Escherichia coli. Journal of biotechnology*, *39*(1), pp.59-65.

KOTTMEIER, K., WEBER, J., MULLER, C., BLEY, T. and BUCHS, J., 2009. Asymmetric division of *Hansenula polymorpha* reflected by a drop of light scatter intensity measured in batch microtiter plate cultivations at phosphate limitation. *Biotechnology and bioengineering*, *104*(3), pp.554-561.

KOZIEL, D., MICHAELIS, U. & KRUSE, T. 2018. Broad application and optimization of a single wash-step for integrated endotoxin depletion during protein purification. *Journal of Chromatography B-Analytical Technologies in the Biomedical and Life Sciences,* 1091**,** 101-107.

KRAMER, B. & THIELMANN, J. 2016. Monitoring the live to dead transition of bacteria during thermal stress by a multi-method approach. *Journal of Microbiological Methods,* 123**,** 24-30.

KRAMER, C. E. M., WIECHERT, W. & KOHLHEYER, D. 2016. Time-resolved, single-cell analysis of induced and programmed cell death via non-invasive propidium iodide and counterstain perfusion. *Scientific Reports,* 6.

KROGH, T.J., MOLLER-JENSEN, J. and KALETA, C., 2018. Impact of chromosomal architecture on the function and evolution of bacterial genomes. *Frontiers in microbiology*, *9*, p.2019.

KRZESLAK, J., BRAUN, P., VOULHOUX, R., COOL, R. H. & QUAX, W. J. 2009. Heterologous production of *Escherichia coli* penicillin G acylase in Pseudomonas aeruginosa. *Journal of Biotechnology,* 142**,** 250-258.

KUHN, A. & KELLENBERGER, E. 1985. Productive phage infection in *Escherichia coli* with reduced internal levels of the major cations. *Journal of bacteriology,* 163**,** 906-912.

KUNZE, M., ROTH, S., GARTZ, E. and BUCHS, J., 2014. Pitfalls in optical on-line monitoring for high-throughput screening of microbial systems. *Microbial Cell Factories*, *13*(1), p.53.

KUMAR, P. K. R., MASCHKE, H. E., FRIEHS, K. & SCHUGERL, K. 1991. Strategies for Improving Plasmid Stability in Genetically Modified Bacteria in Bioreactors. *Trends in Biotechnology,* 9**,** 279-284.

KYSLIK, P., DOBISOVA, M., MARESOVA, H. & SOBOTKOVA, L. 1993. Plasmid Burden in Chemostat Culture of Escherichia coli - Its Effect on the Selection for Overproducers of Host Enzymes. *Biotechnology and Bioengineering,* 41**,** 325-329.

LANE-CLAYPON, J. E. 1909. Multiplication of Bacteria and the Influence of Temperature and some other Conditions thereon. *J Hyg (Lond),* 9**,** 239-48.

LANGER, E. 2019.

LARSSON, G., TÖRNKVIST, M., WERNERSSON, E. S., TRÄGÅRDH, C., NOORMAN, H. & ENFORS, S. O. 1996. Substrate gradients in bioreactors: origin and consequences. *Bioprocess Engineering,* 14**,** 281-289.

LEE, L. G., CHEN, C. H. & CHIU, L. A. 1986. Thiazole Orange - a New Dye for Reticulocyte Analysis. *Cytometry,* 7**,** 508-517.

LEE, M. E., DELOACHE, W. C., CERVANTES, B. & DUEBER, J. E. 2015. A Highly Characterized Yeast Toolkit for Modular, Multipart Assembly. *Acs Synthetic Biology,* 4**,** 975-986.

LENDENMANN, U. & EGLI, T. 1995. Is *Escherichia coli* Growing in Glucose-Limited Chemostat Culture Able to Utilize Other Sugars without Lag. *Microbiology-Sgm,* 141**,** 71-78.

LEWIS, G., TAYLOR, I. W., NIENOW, A. W. & HEWITT, C. J. 2004. The application of multi-parameter flow cytometry to the study of recombinant *Escherichia coli* batch fermentation processes. *Journal of Industrial Microbiology & Biotechnology,* 31**,** 311-322.

LI, B. & YOU, L. 2013. Predictive power of cell-to-cell variability.

LIDSTROM, M.E. and KONOPKA, M.C., 2010. The role of physiological heterogeneity in microbial population behavior. *Nature chemical biology*, *6*(10), pp.705-712.

LOKEN, M. R., SWEET, R. G. & HERZENBERG, L. A. 1976. Cell discrimination by multiangle light scattering. *J Histochem Cytochem. Journal of Histochemistry & Cytochemistry,* 24**,** 284-291.

LUO, Q., SHEN, Y.-L., WEI, D.-Z. & CAO, W. 2006. Optimization of culture on the overproduction of TRAIL in high-cell-density culture by recombinant *Escherichia coli. Applied Microbiology and Biotechnology,* 71**,** 184-191.

MAHARJAN, R.P. and FERENCI, T., 2018. *Escherichia coli* mutation rates and spectra with combinations of environmental limitations. *Microbiology*, *164*(12), pp.1491-1502.

MARBA-ARDEBOR, A. M., TURON, X., NEUBAUER, P. & JUNNE, S. 2016. Application of flow cytometry analysis to elucidate the impact of scale-down conditions in *Escherichia coli* cultivations. *Afinidad,* 73**,** 7-15.

MARCH, J. C., RAO, G. & BENTLEY, W. E. 2003. Biotechnological applications of green fluorescent protein. *Applied Microbiology and Biotechnology,* 62**,** 303-315.

MARR, A. G., HARVEY, R. J. & TRENTINI, W. C. 1966. Growth and division of *Escherichia coli. Journal of bacteriology,* 91**,** 2388.

MARTICH, G. D., BOUJOUKOS, A. J. & SUFFREDINI, A. F. 1993. Response of Man to Endotoxin. *Immunobiology,* 187**,** 403-416.

MASON, D., ALLMAN, R. & LLOYD, D. 1993. Uses of Membrane Potential Sensitive Dyes with Bacteria. *In:* LLOYD, D. (ed.) *Flow Cytometry in Microbiology.* London: Springer London.

MATZ, M. V., LUKYANOV, K. A. & LUKYANOV, S. A. 2002. Family of the green fluorescent protein: journey to the end of the rainbow. *Bioessays,* 24**,** 953-959.

MELAMED, M. R., MULLANEY, P. F. & MENDELSOHN, M. L. 1979. Flow cytometry and sorting.

MIDGLEY, M. 1986. The Phosphonium Ion Efflux System of *Escherichia coli* - Relationship to the Ethidium Efflux System and Energetic Studies. *Journal of General Microbiology,* 132**,** 3187-3193.

MIKHALEVA, N. I., GOLOVASTOV, V. V., ZOLOV, S. N., BOGDANOV, M. V., DOWHAN, W. & NESMEYANOVA, M. A. 2001. Depletion of phosphatidylethanolamine affects secretion of *Escherichia coli* alkaline phosphatase and its transcriptional expression. *FEBS Letters,* 493**,** 85-90.

MILLS, T. Y., SANDOVAL, N. R. & GILL, R. T. 2009. Cellulosic hydrolysate toxicity and tolerance mechanisms in *Escherichia coli. Biotechnology for Biofuels,* 2.

MINIHANE, B. J. & BROWN, D. E. 1986. Fed-Batch Culture Technology. *Biotechnology Advances,* 4**,** 207-218.

MIYASHIRO, T. and GOULIAN, M., 2007. Single-cell analysis of gene expression by fluorescence microscopy. In *Methods in enzymology* (Vol. 423, pp. 458-475). Academic Press.

MONEM, A. A. E-commerce in Healthcare: A Case Study on Promoting the Therapeutic Hardware. MATEC Web of Conferences, 2016. EDP Sciences, 04018.

MORIN, J. G. & HASTINGS, J. W. 1971. Energy Transfer in a Bioluminescent System. *Journal of Cellular Physiology,* 77**,** 313-318.

MSADEK, T. 1999. When the going gets tough: survival strategies and environmental signaling networks in *Bacillus subtilis. Trends in Microbiology,* 7**,** 201-207.

MUTHUKRISHNAN, T., GOVENDER, A., DOBRETSOV, S. and ABED, R.M., 2017. Evaluating the reliability of counting bacteria using epifluorescence microscopy. *Journal of Marine Science and Engineering*, *5*(1), p.4.

NAKANO, K., RISCHKE, M., SATO, S. & MÄRKL, H. 1997. Influence of acetic acid on the growth of *Escherichia coli* K12 during high-cell-density cultivation in a dialysis reactor. *Applied microbiology and biotechnology,* 48**,** 597-601.

NEBE-VON-CARON, G., STEPHENS, P. J., HEWITT, C. J., POWELL, J. R. & BADLEY, R. A. 2000. Analysis of bacterial function by multi-colour fluorescence flow cytometry and single cell sorting. *J Microbiol Methods,* 42**,** 97-114.

NEIDHARDT, F. C. 1987. *Escherichia coli* and *Salmonella typhimurium*: cellular and molecular biology, American Society for Microbiology.

NEUBAUER, P., LIN, H. Y. & MATHISZIK, B. 2003. Metabolic load of recombinant protein production: Inhibition of cellular capacities for glucose uptake and respiration after induction of a heterologous gene in *Escherichia coli*. *Biotechnology and Bioengineering,* 83**,** 53-64.

NORRIS, V., CHEN, M., GOLDBERG, M., VOSKUIL, J., MCGURK, G. & HOLLAND, I. B. 1991. Calcium in Bacteria - a Solution to Which Problem. *Molecular Microbiology,* 5**,** 775-778.

NORRIS, V., GRANT, S., FREESTONE, P., CANVIN, J., SHEIKH, F. N., TOTH, I., TRINEI, M., MODHA, K. & NORMAN, R. I. 1996. Calcium signalling in bacteria. *Journal of Bacteriology,* 178**,** 3677-3682.

NOVO, D., PERLMUTTER, N. G., HUNT, R. H. & SHAPIRO, H. M. 1999. Accurate flow cytometric membrane potential measurement in bacteria using diethyloxacarbocyanine and a ratiometric technique. *Cytometry,* 35**,** 55-63.

NOVO, D. J., PERLMUTTER, N. G., HUNT, R. H. & SHAPIRO, H. M. 2000. Multiparameter flow cytometric analysis of antibiotic effects on membrane potential, membrane permeability, and bacterial counts of *Staphylococcus aureus* and *Micrococcus luteus*. *Antimicrobial Agents and Chemotherapy,* 44**,** 827-834.

O'BEIRNE, D. & HAMER, G. 2000. The utilisation of glucose/acetate mixtures by *Escherichia coli* W3110 under aerobic growth conditions. *Bioprocess Engineering,* 23**,** 375-380.

O'BRIEN-SIMPSON, N. M., PANTARAT, N., ATTARD, T. J., WALSH, K. A. & REYNOLDS, E. C. 2016. A Rapid and Quantitative Flow Cytometry Method for the Analysis of Membrane Disruptive Antimicrobial Activity. *Plos One,* 11.

OLIVER, J. D. 2010. Recent findings on the viable but nonculturable state in pathogenic bacteria. *Fems Microbiology Reviews,* 34**,** 415-425.

OMASA, T., CAO, Y., PARK, J.Y., TAKAGI, Y., KIMURA, S., YANO, H., HONDA, K., ASAKAWA, S., SHIMIZU, N. and OHTAKE, H., 2009. Bacterial artificial chromosome library for genome-wide analysis of Chinese hamster ovary cells. *Biotechnology and bioengineering*, *104*(5), pp.986-994.

PELEG, A., SHIFRIN, Y., ILAN, O., NADLER-YONA, C., NOV, S., KOBY, S., BARUCH, K., ALTUVIA, S., ELGRABLY-WEISS, M., ABE, C. M., KNUTTON, S., SAPER, M. A. & ROSENSHINE, I. 2005. Identification of an *Escherichia coli* operon required for formation of the O-antigen capsule. *Journal of bacteriology,* 187**,** 5259-5266.

PAULOVA, L., HYKA, P., BRANSKA, B., MELZOCH, K. and KOVAR, K., 2012. Use of a mixture of glucose and methanol as substrates for the production of recombinant trypsinogen in continuous cultures with *Pichia pastoris* Mut+. *Journal of biotechnology*, *157*(1), pp.180-188.

PEEBO, K. and NEUBAUER, P., 2018. Application of continuous culture methods to recombinant protein production in microorganisms. *Microorganisms*, *6*(3), p.56.

PIERCE, A., GILLETTE, D. & JONES, P. G. 2011. *Escherichia coli* cold shock protein CsdA effects an increase in septation and the resultant formation of coccobacilli at low temperature. *Archives of Microbiology,* 193**,** 373-384.

PIRT, S. J. 1975. *Principles of microbe and cell cultivation,* Oxford, Blackwell Scientific.

POSTGATE, J. R. 1969. Chapter XVIII Viable counts and Viability. *In:* NORRIS, J. R. & RIBBONS, D. W. (eds.) *Methods in Microbiology.* Academic Press.

PRASHER, D. C. 1995. Using GFP to see the light. *Trends in Genetics,* 11**,** 320-323.

QUIANZON, C. C. & CHEIKH, I. 2012. History of insulin. *J Community Hosp Intern Med Perspect,* 2.

R. O'KEEFE, B. 2005. *Biotechnology and Biopharmaceuticals: Transforming Proteins and Genes into Drugs Edited by R. J. Y. Ho and M. Gibaldi (University of Washington). Wiley-LISS, New York. 2003.*

REZAEINEJAD, S. & IVANOV, V. 2011. Heterogeneity of *Escherichia coli* population by respiratory activity and membrane potential of cells during growth and long-term starvation. *Microbiological Research,* 166**,** 129-135.

RICHARD, D. M., LARA, K. & SHELLIE, W. 2007. Evaluation of *Escherichia coli* cell disruption and inclusion body release using nucleic acid binding fluorochromes and flow cytometry. *BioTechniques,* 43**,** 777-782.

ROBERTSON, J., McGOVERIN, C., VANHOLSBEECK, F. and SWIFT, S., 2019. Optimisation of the protocol for the LIVE/DEAD® BacLightTM bacterial viability kit for rapid determination of bacterial load. *Frontiers in microbiology*, *10*, p.801.

RODRIGUEZ, V., ASENJO, J. A. & ANDREWS, B. A. 2014. Design and implementation of a high yield production system for recombinant expression of peptides. *Microbial Cell Factories,* 13.

ROE, A. J., O'BYRNE, C., MCLAGGAN, D. & BOOTH, I. R. 2002. Inhibition of *Escherichia coli* growth by acetic acid: a problem with methionine biosynthesis and homocysteine toxicity. *Microbiology-Sgm,* 148**,** 2215-2222.

ROSENBERG, M., AZEVEDO, N. F. & IVASK, A. 2019. Propidium iodide staining underestimates viability of adherent bacterial cells. *Scientific Reports,* 9.

RUSS, J. & RUSS, C. 2017. How Not to be a Circle: Dimensionless Ratios as Shape Descriptors. *infocus Magazine***,** 58-72.

RUSSO, E. 2003. Special Report: The birth of biotechnology. *Nature,* 421**,** 456.

RYALL, B., EYDALLIN, G. and FERENCI, T. 2012. Culture history and population heterogeneity as determinants of bacterial adaptation: the adaptomics of a single environmental transition. *Microbiology and Molecular Biology Reviews*, *76*(3), pp.597-625.

SAHDEV, S., KHATTAR, S. K. & SAINI, K. S. 2008. Production of active eukaryotic proteins through bacterial expression systems: a review of the existing biotechnology strategies. *Molecular and Cellular Biochemistry,* 307**,** 249-264.

SAMBROOK, J. 2001. *Molecular cloning : a laboratory manual / Joseph Sambrook, David W. Russell,* Cold Spring Harbor, N.Y, Cold Spring Harbor Laboratory.

SANDERS, J. K. M. & JACKSON, S. E. 2009. The discovery and development of the green fluorescent protein, GFP. *Chemical Society Reviews,* 38**,** 2821-2822.

SARPATWARI, A., AVORN, J. & KESSELHEIM, A. S. 2015. Progress and hurdles for follow-on biologics. *New England Journal of Medicine,* 372**,** 2380-2382.

SCHAEPE, S., KUPRIJANOV, A., SIMUTIS, R. & LUBBERT, A. 2014. Avoiding overfeeding in high cell density fed-batch cultures of *E. coli* during the production of heterologous proteins. *Journal of Biotechnology,* 192**,** 146-153.

SCHMIDEDER, A. and Weuster-Botz, D., 2017. High-performance recombinant protein production with *Escherichia* coli in continuously operated cascades of stirred-tank reactors. *Journal of Industrial Microbiology & Biotechnology*, *44*(7), pp.1021-1029.

SCHOLZ, O., THIEL, A., HILLEN, W. & NIEDERWEIS, M. 2000. Quantitative analysis of gene expression with an improved green fluorescent protein. *European journal of biochemistry,* 267**,** 1565-1570.

SENN, H., LENDENMANN, U., SNOZZI, M., HAMER, G. & EGLI, T. 1994. The Growth of *Escherichia coli* in Glucose-Limited Chemostat Cultures - a Reexamination of the Kinetics. *Biochimica Et Biophysica Acta-General Subjects,* 1201**,** 424-436.

SHAPIRO, H. H. 2000. Microbial analysis at the single-cell level: tasks and techniques. *Journal of Microbiological Methods,* 42**,** 3-16.

SHAPIRO, H. M. 1977. Fluorescent dyes for differential counts by flow cytometry: does histochemistry tell us much more than cell geometry? *J Histochem Cytochem. Journal of Histochemistry & Cytochemistry,* 25**,** 976-989.

SHAPIRO, H. M. 2002. *Practical flow cytometry,* Chichester, Wiley.

SHAPIRO, H. M. 2005. *Practical Flow Cytometry*, Wiley.

SHARPLESS, T. K., BARTHOLDI, M. & MELAMED, M. R. 1977. Size and Refractive-Index Dependence of Simple Forward Angle Scattering Measurements in a Flow System Using Sharply-Focused Illumination. *Journal of Histochemistry & Cytochemistry,* 25**,** 845-856.

SHIMIZU, N., FUKUZONO, S., FUJIMORI, K., NISHIMURA, N. & ODAWARA, Y. 1988. Fed-Batch Cultures of Recombinant *Escherichia coli* with Inhibitory Substance Concentration Monitoring. *Journal of Fermentation Technology,* 66**,** 187-191.

SHIMOMURA, O. 2005. The discovery of aequorin and green fluorescent protein. *Journal of Microscopy-Oxford,* 217**,** 3-15.

SILVA, F., QUEIROZ, J. A. & DOMINGUES, F. C. 2012. Plasmid DNA fermentation strategies: influence on plasmid stability and cell physiology. *Applied Microbiology and Biotechnology,* 93**,** 2571-2580.

SMITH, R. J. 1995. Calcium and bacteria. *Adv Microb Physiol,* 37**,** 83-133.

SNIJDER, B., SACHER, R., RAMO, P., LIBERALI, P., MENCH, K., WOLFRUM, N., BURLEIGH, L., SCOTT, C. C., VERHEIJE, M. H., MERCER, J., MOESE, S., HEGER, T., THEUSNER, K., JURGEIT, A., LAMPARTER, D., BALISTRERI, G., SCHELHAAS, M., DE HAAN, C. A. M., MARJOMAKI, V., HYYPIA, T., ROTTIER, P. J. M., SODEIK, B., MARSH, M., GRUENBERG, J., AMARA, A., GREBER, U., HELENIUS, A. & PELKMANS, L. 2012. Single-cell analysis of population context advances RNAi screening at multiple levels. *Molecular Systems Biology,* 8.

STIEFEL, P., SCHMIDT-EMRICH, S., MANIURA-WEBER, K. and REN, Q., 2015. Critical aspects of using bacterial cell viability assays with the fluorophores SYTO9 and propidium iodide. *BMC microbiology*, *15*(1), p.36.

STOCKS, S. M. 2004. Mechanism and use of the commercially available viability stain, BacLight. *Cytometry Part A,* 61a**,** 189-195.

STRÄUBER, H. & MÜLLER, S. 2010. Viability states of bacteria - Specific mechanisms of selected probes Cytometry Part A Volume 77A, Issue 7.

STUDIER, F. W. 2005. Protein production by auto-induction in high density shaking cultures. *Protein Expr Purif,* 41**,** 207-34.

TOPLEY, W. W., AYRTON, J. & LEWIS, E. R. 1924. The Spread of Bacterial Infection: Further Studies on an Experimental Epidemic of Mouse-Typhoid. *The Journal of hygiene,* 23**,** 223-239.

TSIEN, R. Y. 1998. The green fluorescent protein. *Annual Review of Biochemistry,* 67**,** 509-544.

TSUJI, F. I. 2010. Early History, Discovery, and Expression of Aequorea Green Fluorescent Protein, With a Note on an Unfinished Experiment. *Microscopy Research and Technique,* 73**,** 785-796.

VALDEZ-CRUZ, N. A., CASPETA, L., PÉREZ, N. O., RAMÍREZ, O. T. & TRUJILLO-ROLDÁN, M. A. 2010. Production of recombinant proteins in E. coli by the heat

inducible expression system based on the phage lambda pL and/or pR promoters. *Microbial Cell Factories,* 9**,** 18.

VAN BOXTEL, C., VAN HEERDEN, J.H., NORDHOLT, N., SCHMIDT, P. and BRUGGEMAN, F.J., 2017. Taking chances and making mistakes: non-genetic phenotypic heterogeneity and its consequences for surviving in dynamic environments. *Journal of The Royal Society Interface*, *14*(132), p.20170141.

VAN RENSBURG, E., DEN HAAN, R., SMITH, J., VAN ZYL, W. H. & GORGENS, J. F. 2012. The metabolic burden of cellulase expression by recombinant *Saccharomyces cerevisiae* Y294 in aerobic batch culture. *Appl Microbiol Biotechnol,* 96**,** 197-209.

VANDERMIES, M. & FICKERS, P. 2019. Bioreactor-Scale Strategies for the Production of Recombinant Protein in the Yeast *Yarrowia lipolytica*. *Microorganisms,* 7.

VANHOVE, L., GOOSSENS, W., VANDUPPEN, V. & VERWILGHEN, R. L. 1990. Reticulocyte Count Using Thiazole Orange - a Flow-Cytometry Method. *Clinical and Laboratory Haematology,* 12**,** 287-299.

VASDEKIS, A. E. & STEPHANOPOULOS, G. 2015. Review of methods to probe single cell metabolism and bioenergetics. *Metabolic Engineering,* 27**,** 115-135.

VOSTIAR, I., TKAC, J. & MANDENIUS, C. F. 2004. Off-line monitoring of bacterial stress response during recombinant protein production using an optical biosensor. *Journal of Biotechnology,* 111**,** 191-201.

WANT, A., THOMAS, O.R., KARA, B., LIDDELL, J. and HEWITT, C.J., 2009. Studies related to antibody fragment (Fab) production in *Escherichia coli* W3110 fed-batch fermentation processes using multiparameter flow cytometry. *Cytometry Part A: The Journal of the International Society for Analytical Cytology*, *75*(2), pp.148-154.

WARD, M., TURNER, P., DEJOHN, M. & KADUCHAK, G. 2009. Fundamentals of Acoustic Cytometry.

WARD, W. W., CODY, C. W., HART, R. C. & CORMIER, M. J. 1980. Spectrophotometric Identity of the Energy-Transfer Chromophores in Renilla and Aequorea Green-Fluorescent Proteins. *Photochemistry and Photobiology,* 31**,** 611-615.

WEGRZYN, G. & WEGRZYN, A. 2002. Stress responses and replication of plasmids in bacterial cells. *Microbial Cell Factories,* 1**,** 2.

WELCH, R.L., SLADEK, R., DEWAR, K. and REISNER, W.W., 2012. Denaturation mapping of *Saccharomyces cerevisiae. Lab on a Chip*, *12*(18), pp.3314-3321.

WHATMORE, A. M., CHUDEK, J. A. & REED, R. H. 1990. The effects of osmotic upshock on the intracellular solute pools of *Bacillus subtilis. Microbiology,* 136**,** 2527-2535.

WLODKOWIC, D., SKOMMER, J., FALEY, S., DARZYNKIEWICZ, Z. & COOPER, J. M. 2009. Dynamic analysis of apoptosis using cyanine SYTO probes: From classical to microfluidic cytometry. *Experimental Cell Research,* 315**,** 1706-1714.

WURM, D.J., MARSCHALL, L., SAGMEISTER, P., HERWIG, C. and SPADIUT, O., 2017. Simple monitoring of cell leakiness and viability in *Escherichia coli* bioprocesses—a case study. *Engineering in Life Sciences*, *17*(6), pp.598-604.

YANG, F., HANNA, M. A. & SUN, R. 2012. Value-added uses for crude glycerol--a byproduct of biodiesel production. *Biotechnology for Biofuels,* 5**,** 13.

YOON, J. H., MOON, S. K., CHOI, C., RYU, B. Y. & LEE, S. Y. 2019. Detection of viable but nonculturable Vibrio parahaemolyticus induced by prolonged cold-starvation using propidium monoazide real-time polymerase chain reaction. *Letters in Applied Microbiology,* 68**,** 537-545.

ZARITSKY, A. 1975. On dimensional determination of rod-shaped bacteria. *J Theor Biol,* 54**,** 243-8.

ZARITSKY, A., KIHARA, M. & MACNAB, R. M. 1981. Measurement of membrane potential in *Bacillus subtilis*: A comparison of lipophilic cations, rubidium ion, and a cyanine dye as probes. *The Journal of Membrane Biology,* 63**,** 215-231.

ZHAO, H., OCZOS, J., JANOWSKI, P., TREMBECKA, D., DOBRUCKI, J., DARZYNKIEWICZ, Z. & WLODKOWIC, D. 2010. Rationale for the Real-Time and Dynamic Cell Death Assays Using Propidium Iodide. *Cytometry Part A,* 77a**,** 399-405.

Appendix

Appendix A - Assessment of widely used "Green and Sambrook" minimal media in terms of growth yields

Appendix B - Model of the Flow Cytometer

Appendix C - Model of experimental set-up

Appendix D - Plasmid description

Appendix E - MP calibration

Appendix F - ImageJ macro

Appendix A – Assessment of widely used "Green and Sambrook" minimal media in terms of growth yields

The most common defined media originates from Sambrook (Sambrook et al, 1989). This is not suitable for physiological studies because it does not have a single limitation. The growth yield, as expressed by Monod equals the weight of the cells produced in grams dry weight/grams of substrate in media. The growth yields factors for each constituent $Y_{X/E}$ were derived from the composition of the biomass (*Table A.1*). Theoretical excess factors in respect to carbon were calculated for different individual elements, using the following equation:

$$F_C = \frac{Y_{\frac{X}{E}} x\ c_E}{C_C \times Y_C^X} \qquad \text{(A.1)}$$

where:

F_C = theoretical excess factor in respect to carbon;

$Y_{X/E}$ = average growth yield for element E, expressed as g cell dry weight x (g element)$^{-1}$;

$Y_{X/C}$ = average growth yield for Carbon, expressed as g cell dry weight x (g element)$^{-1}$;

c_E = concentration of element E, expressed as g element liter^{-1};

c_C = concentration of carbon, expressed as g carbon liter^{-1}.

For example, when the media is C limited, bacteria produce 8 g dry biomass from 1 g Nitrogen and 33 g of dry biomass from 1g Phosphorus (*Table A.1*).

The most common media in research is limited in nitrogen, calcium, iron, manganese and not in carbon (*Table A.2*). A deficiency of iron, for example inhibits bacterial growth as the iron links to many cell functions, in particular aerobic metabolism. The growth curves of *E. coli* W3110 in Sambrook media with different concentrations of glucose are shown in *Figure A.1*. The concentrations (w/v) of glucose used were 0.1, 0.4, 0.7, 1, 1.5 and 2% (*Figure A.1*).

The defined media used during this work has a single limitation, specifically the carbon source, up to 0.4% or 4g/L (*Figure A.2*).

Element	Average (% of CDW)	Average $Yx_{/E}$ for C-limited growth	Excess factors F_C recommended for C-limited growth
C	50	1	Limiting
O	21	-	Not limiting
N	12	8	3-5
P	3	33	5-10
S	1	100	5-10
K	1	100	5-10
Mg	0.5	200	5-10
Fe	0.5	200	10-20

Table A. 1. Average elemental composition of dry biomass in Gram-negative bacteria growing at μ_{max} in batch culture, adapted from Egli (Egli, 2015a). CDW (cell dry weight); growth yield factor ($Yx/_E$) in g CDW/g element.

Element	Media component	C_C in g/L	C_E in g/L	$Y_{\frac{X}{E}}$	Fc	Predicted CDW (g/L)	Excess Factor over C CDW predicted/CDW from C
C	Glucose ($C_6H_{12}O_6$) Mr = 180 ArC = 12	4 g/L or 22.22 mM	1.6	1	1	1.6	1 (as limiting factor)
O							not limiting (aerobic)
N	NH_4Cl Mr = 53.5 ArN = 14	0.5 g/L or 9.35 mM	1.31 x 10^{-1}	8	3	1.05	0.65 (limiting)
P	Na_2HPO_4-$2H_2O$ Mr = 178 ArP =31	7.52 g/L or 6 g/L anhydrous or 33.70 mM anhydrous	1.31	33	5	65.78	41.11
	KH_2PO_4 Mr = 136 ArP = 31	3 g/L or 22.05 mM	0.68				

S	$MgSO_4$-$7H_2O$ Mr = 246.47 ArS = 32	0.25 g/L 1 mM	3.2×10^{-2}	100	5	3.19	1.99
K	KH_2PO_4 Mr = 136 ArK =39	3 g/L or 22.05 mM	8.60×10^{-1}	100	5	86.02	53.76
Mg	$MgSO_4$-$7H_2O$ Mr = 246.47 ArMg = 24	0.2464 g/L 1 mM	2.39×10^{-2}	200	5	4.78	2.98
Ca	$CaCl_2$-$2H_20$ Mr = 147 ArCa = 40	4.41×10^{-2} g/L 0.3 mM	1.2×10^{-2}	100	10	1.2	0.75 (limiting)
Fe	FeCl3-$6H_20$ Mr = 270.30 ArFe = 56	8.3 mg/L or 8.3×10^{-3} g/L or 3.07×10^{-2} mM	1.7×10^{-3}	200	10	0.34	0.21 (limiting)
Mn	$MnCl_2$-$4H_2O$ Mr = 197.91 ArMn = 55	1.6×10^{-2} mg/L or 1.6×10^{-5} g/L or 8.08×10^{-2} µM	4.45×10^{-6}	10^4	20	0.04	0.028 (limiting)

Zn	$ZnCl_2$ Mr = 136.30 ArZn =65	0.84 mg/L or 8.4 x 10^{-4} g/L or 6.16 x 10^{-3} mM	4.01 x 10^{-4}	10^4	20	4	2.5
Cu	$CuCl_2$- $2H_2O$ Mr = 170.48 ArCu = 63.55	0.13 mg/L or 1.3 x 10^{-4} g/L or 7.6 x 10^{-4} mM	4.85 x 10^{-5}	10^5	20	4.85	3.03
Co	$CoCl_2$ -$6H_2O$ Mr = 238 ArCo=59	0.1 mg/L or 1 x 10^{-4} g/L	2.48 x 10^{-4}	10^5	20	24.79	15.49

Table A.2. Assessment of Sambrook minimal media in terms of growth yields.

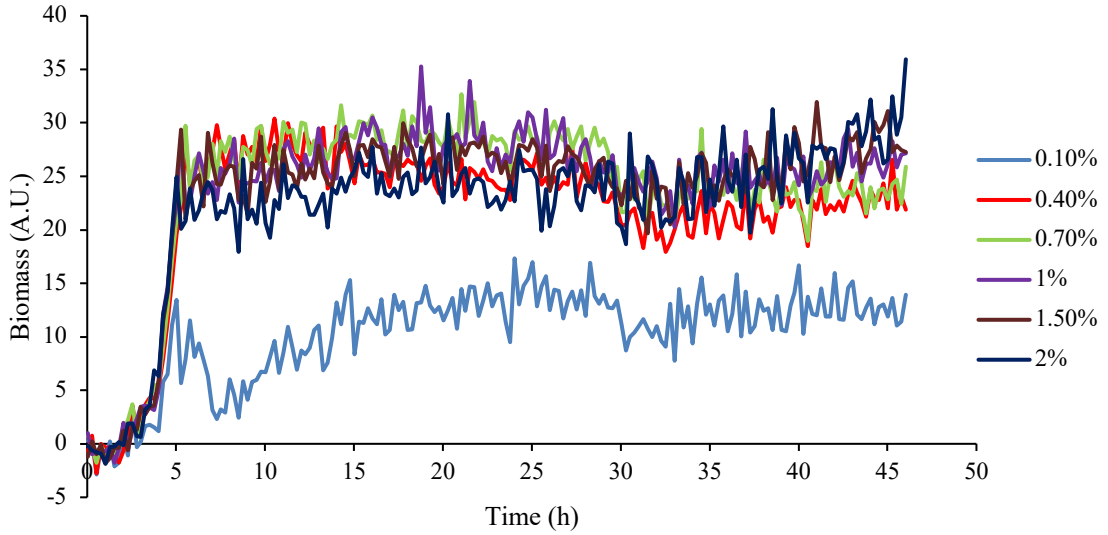

Figure A.1. Growth of *E. coli* W3110 in Sambrook media with different concentrations of glucose. Online monitoring of biomass (scattered light). Conditions: minimal media with up to 20 g/L of glucose, T = 37^{0}C, V_L = 800 µL, n = 1500, d_0 = 3 mm.

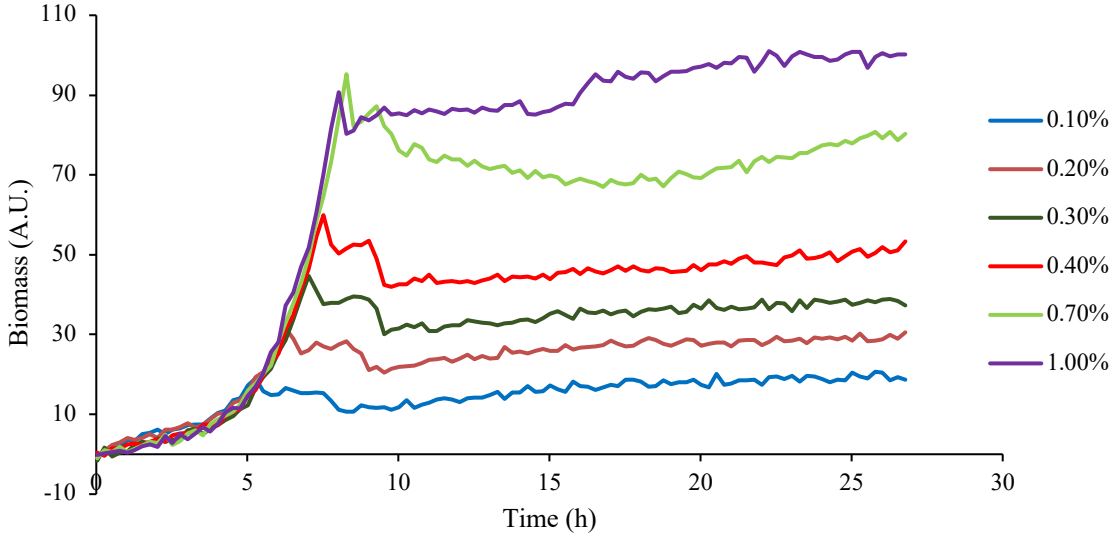

Figure A. 2. Growth of *E. coli* W3110 in media used in this work. Online monitoring of biomass (scattered light). Conditions: minimal media with up to 10 g/L of glucose, T = 37^{0}C, V_L = 800 µL, n = 1500, d_0 = 3 mm. Media is limited in carbon up to 4 g/ glucose.

Appendix B – Model of Flow Cytometer

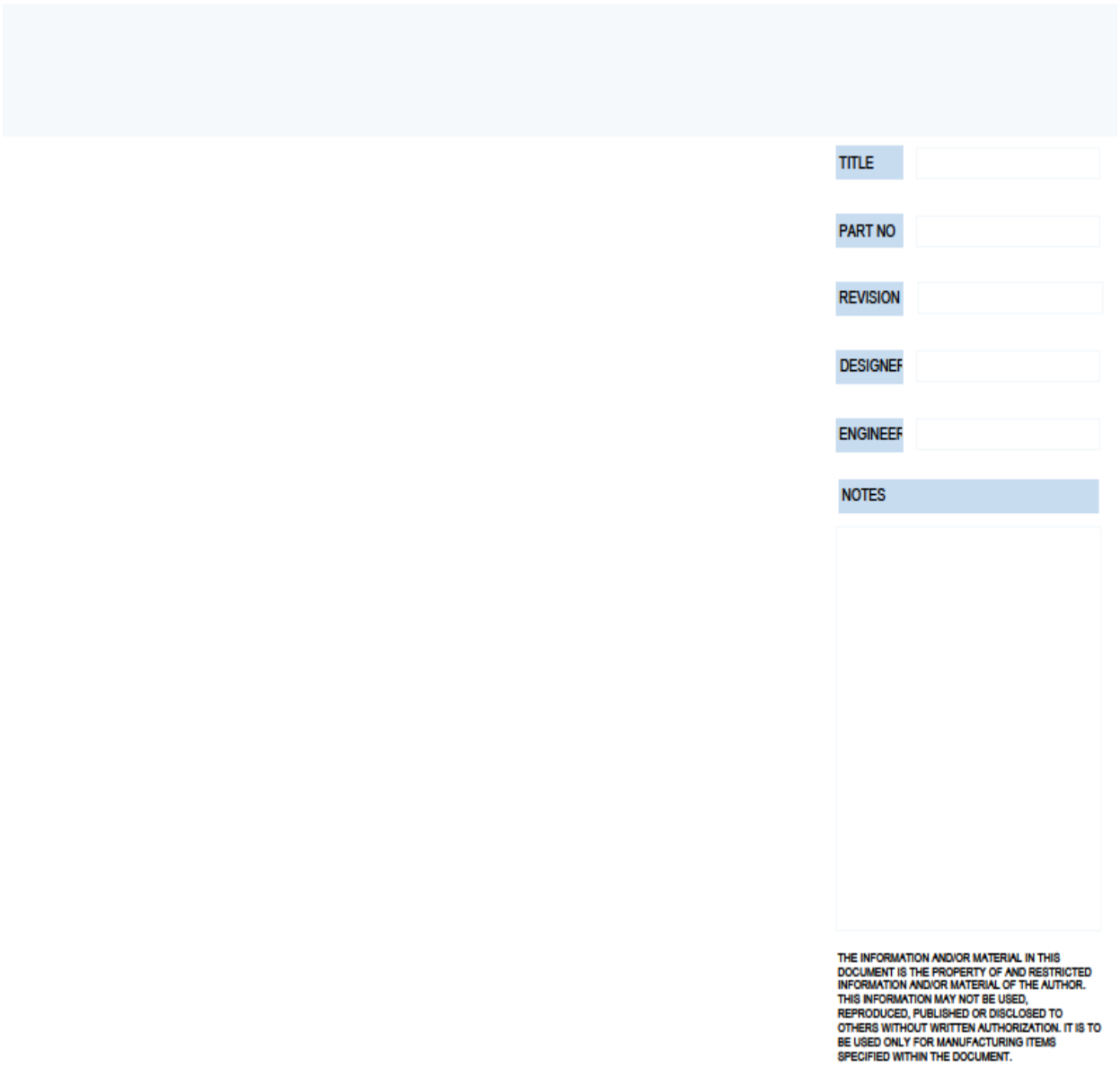

Appendix C – Model of experimental set-up

Appendix D – Plasmid description

DNA 2.0

Plasmid Map

pD441-SR:240460

Only single and double cutters are shown in the map.

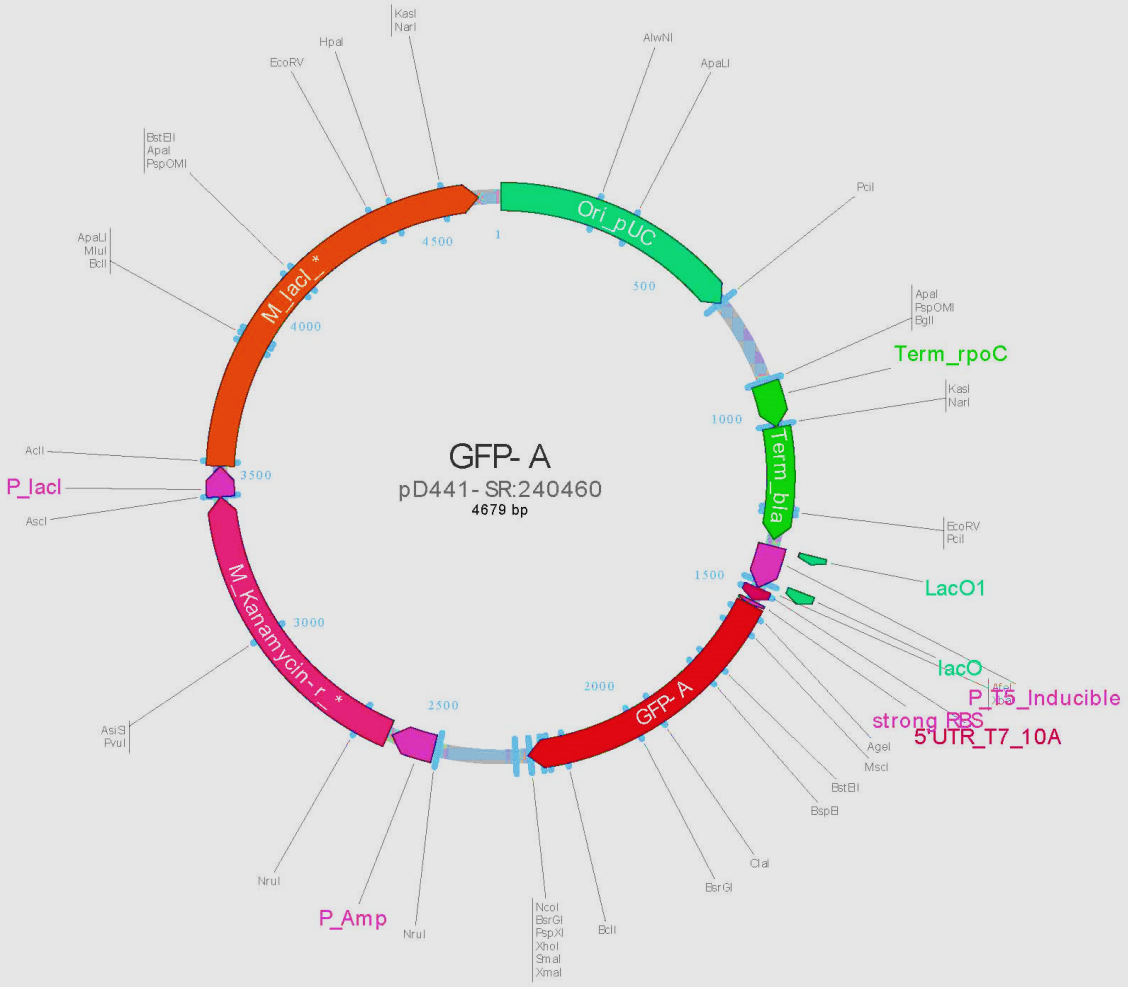

Appendix E – MP calibration

The values for potassium equilibrium potential were calculated using the measured values of extracellular potassium as follows:

$$V_{Eq} = \frac{RT}{zF} \ln \frac{K_{out}}{K_{in}}$$

where

R = Gas constant, 8.134 J K^{-1} mol^{-1}

T = temperature in K (273.17 + temp in ^{o}C)

z = valency of ion (K^{+} is +1)

F = Faraday's constant, 9.6485 x 10^{4} C mol^{-1}

K_{out} = the concentration of K in the extracellular media

K_{in} = the concentration of K in the cell

1 J = 1 V x 1 C = 1000 mV x 1 C

Shown above, Nernst equation defines the relationship between the concentration of an ion (K) on either side of a membrane that is perfectly selective for that ion. V_{Eq} is the difference in voltage measured across that membrane under equilibrium conditions. It dictates the membrane potential that must exist across that membrane in order to balance a chemical gradient for the respective ion.

At growth temperature of 37°C,

$$V_{Eq} = \frac{(8.314\ \text{J K}^{-1}\ \text{mol}^{-1})(310.17\ \text{K})}{(1)(96{,}485\ \text{C mol}^{-1})} \ln \frac{K_{out}}{K_{in}},$$

$$V_{Eq} = \frac{(8.314 \times 1000\ \text{mV C K}^{-1}\ \text{mol}^{-1})(310.17\ \text{K})}{(1)(96{,}485\ \text{C mol}^{-1})} \ln \frac{K_{out}}{K_{in}},$$

$$V_{Eq} = 26.7269\ \ln \frac{K_{out}}{K_{in}}$$

Where V_{Eq} is in mV

Therefore $\frac{V_{Eq}}{26.7269} = \ln K_{out} - \ln K_{in}$

The K_{in} = 300 mM in bacterial cells, so $\frac{V_{Eq}}{26.7269} = \ln K_{out} - 5.7$

If $V_{Eq} = 26.7269 \ ln \frac{K_{out}}{K_{in}}$, this is $V_{Eq} = 26.7269 \times 2.303 \ log \frac{K_{out}}{K_{in}}$, so $V_{Eq} = 61.5522 \ log \frac{K_{out}}{K_{in}}$

2.303 is a conversion factor from ln to $\log_{10}$.

When membrane potential V_{Eq} is plotted on y-axis against a log of K concentration on the x axis, at 37°C, the slope of the line (linear function) is 61.5522 mV. This means that the difference between two timepoints at ten-fold K concentration is 61.5522.

$$ln \ K_{out} = \frac{V_{Eq}}{26.7269} + 5.7$$

The M_9 media formulation contains 22 mM of K outside the cell and 300 mM inside the cell. Therefore, V_{Eq} for Potassium in the growth media is -69.8306 mV, or -70 mV as a close approximation. This is the potential necessary to keep the K from diffusing out of the cells, down its concentration gradient.

V_{Eq} (mV)	K_{out} (mM)
0	300
-20	141.9500
-40	67.1661
-60	31.7807
-69.8306	22 (media)
-80	15.0375
-100	7.1153

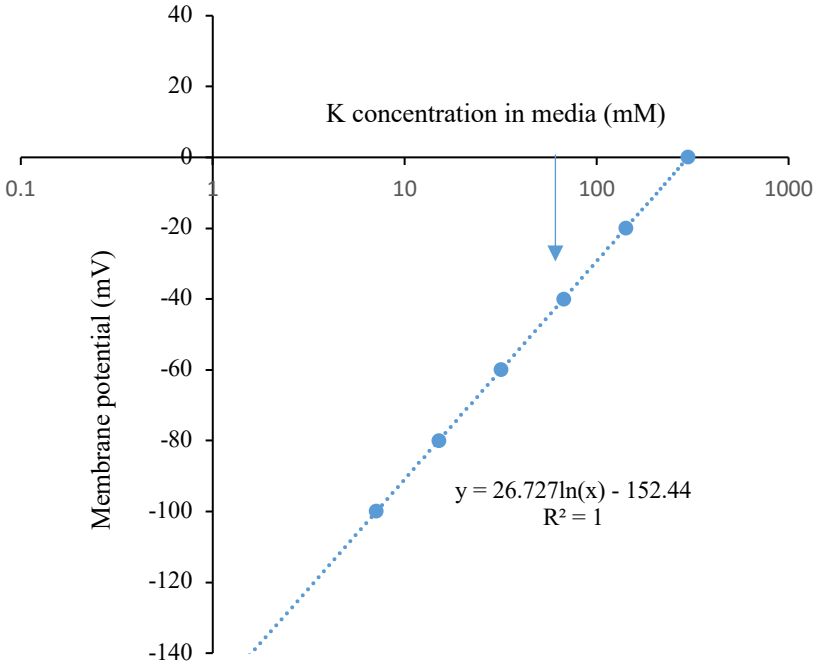

Figure E.1. Plot of transmembrane potential difference for Potassium used for calibration in the presence of valinomycin.

Appendix F – ImageJ macro

```
title = getTitle();

run("Duplicate...", " ");

setAutoThreshold("Otsu dark");

//run("Threshold...");

setOption("BlackBackground", false);

run("Convert to Mask");

run("Set Measurements...", "area mean min shape feret's integrated redirect=None
decimal=3");

run("Analyze Particles...", "exclude add");

selectWindow(title);

roiManager("Show All without labels");

roiManager("Show None");

roiManager("Show All");

roiManager("Measure");
```